Hollow-Core 3D Printing
for Facades

Diss. ETH No. 30062

Matthias Leschok

ETH zürich

Diss. ETH No. 30062

Hollow-Core 3D Printing for Facades

A thesis submitted to attain the degree of

Doctor of Sciences

(Dr. sc. ETH Zurich)

presented by

Matthias Leschok

Dipl. Ing. Architecture, Karlsruhe Institute of Technology

born on January 12, 1989

Accepted on the recommendation of

Prof. Dr. Benjamin Dillenburger (Supervisor)

Prof. Dr. Roland Snooks (Co-Examiner)

2024

Acknowledgements

I would like to express my deepest gratitude to my supervisor, Prof. Benjamin Dillenburger, for his exceptional guidance, unwavering support, and insightful advice throughout my PhD journey. His expertise and encouragement have been instrumental in shaping this research, and I am incredibly fortunate to have had the opportunity to work under his mentorship. I would like to express my gratitude also to Prof. Roland Snooks for his support as co-supervisor, his valuable input during our discussions, and the manuscript editing process.

I would like to extend my heartfelt thanks to the entire NCCR Facade stream. Especially Prof. Fabio Gramazio, Prof. Matthias Kohler, and Prof. Arno Schlüter for their invaluable guidance and mentorship throughout my PhD journey. I am deeply grateful to Dr. Valeria Piccioni for being a fantastic research partner and providing invaluable feedback and encouragement throughout our collaborative work. Not to forget the colleagues at HSLU and their support and testing campaigns we run on our facade prototypes. Let the beams explode! Thank you Thomas Wuest and Ringo Perez Gamote.

I want to thank all my fellow colleagues at ETH and beyond for sharing, shaping, and easing my way through the PhD, namely Andrei Jipa, Nik Eftekhar, Hyunchul Kwon, Ioanna Mitropoulou, Pietro Odaglia, Yael Ifrah, Georgia Chousou, Yen Fen Chan, Eleni Skevaki, Mathias Bernhard, Yvonne Moosmann, Thodoris Kyttas, René Jähne. And not to forget the endless hours in the workshop supported by Tobias Hartmann, Michael Lyrenmann, Philippe Fleischmann, Andi Reusser, and Heinz Richner, besten Dank!

I also want to thank my fellow founders of SAEKI Robotics, Andrea Perissinotto and Oliver Harley for their help and dedication starting large-scale polymer 3D printing with me at ETH Zurich. It has been a wild ride and it continues to be!

I want to thank my family for supporting me throughout the years, enabling me to chase my dreams. Many thanks to my dad, who showed me how to build nearly anything, and to my mum for always lending me an ear whenever I needed it. Many thanks also to my brother Thomas, who showed me more than once how to calculate the gaussian normal distribution.

Lastly I want to express my sincere gratitude to my mental ping pong partner Marirena Kladeftira without whom I would have not been able to get where I am today. Thank you for teaching me how to structure my thoughts and write coherent sentences, and not to forget, being my IT mastermind, I love you.

Matthias Leschok

Abstract

The use of 3D printing in the fabrication of building facades enables the creation of site-specific and climate-adaptive envelopes, optimised to their unique environmental conditions. Over the past decade, large-scale 3D printing (3DP) of thermoplastic materials, specifically Material Extrusion (ME), has advanced significantly in terms of maximum extrusion rate and build volume and, as such, facilitates the fabrication of large-scale translucent building components. Presently, it is feasible to 3DP elements several metres in size using large-scale extruders fed by granular feedstock. However, this increase is facilitated by the extrusion of thick, massive, beads which result in heavy and material inefficient components. Furthermore, the maximum print speed is constrained by the need for the extruded material to cool down before adding the subsequent layer, and is delayed for large extrusion sizes significantly. Consequently, today's large-scale ME stands in stark contrast to the potential of synthetic materials in architecture, particularly regarding attributes such as lightness, transparency, and the ability to achieve large-spanning structures at affordable costs.

Therefore, this thesis investigates Hollow-Core 3D printing (HC3DP), a novel polymer 3DP method for large-scale and lightweight elements. This approach is based on the idea of 3D printing with hollow sections; as known from industrial plastic extrusion processes as die-extrusion. HC3DP advances ME to achieve extrusion rates comparable to those of high-resolution 3D concrete printing. This thesis presents for the first time tubular large-scale 3D printing with a bead cross-section of 24mm and beyond and, therefore, provides new design opportunities for large-scale additive manufacturing. HC3DP enables the extrusion of hollow, tubular beads and therefore results in significant material savings (50-85%). Additionally, the tubular bead structure substantially enhances the material cool-down during the printing process, thereby increasing the printing speed by a factor of 3-8.

HC3DP is specifically developed for improving the performance of ME in the use-case of 3DP facades and is the core contribution of this thesis. This development entails research on several extrusion geometries at different scales, including small and large-scale ME, and finally HC3DP. Furthermore, different cross-sections, die geometries, and materials are investigated for HC3DP, showcasing the versatility of the printing process. After the implementation of HC3DP, several small-scale prototypes are printed and on larger prototypes, physical experiments are conducted. A large-scale demonstrator explores the design space of HC3DP and 2.1m tall elements are 3DP to act a as quasi load bearing structure. In collaboration with researchers from multiple disciplines, the performance of HC3DP is investigated, and aspects like thermal, structural, and acoustics are compared to state-of-the-art large-scale ME methods. It is shown that all aforementioned performances are significantly improved by HC3DP; a thermal resistance of triple-glazed windows can be achieved, with high airborne sound insulation, and large span widths can be achieved due to the optimised strength to weight ratio. Finally, based on these experimentally validated findings the production viability of HC3DP for facade application is presented, with a facade fabrication speed of up to 1.5h/m2.

With the presented developments in HC3DP, the vision of customised, free-form designs and performative facade elements is becoming more attainable. This represents a significant step towards reducing both the primary and operational energy requirements of buildings. Additionally, it paves the way for an architecture characterised by more diverse and spatially complex building envelopes.

Zusammenfassung

Der Einsatz des 3D-Drucks bei der Herstellung von Gebäudefassaden ermöglicht die Schaffung standortspezifischer und klimaangepasster Gebäudehüllen, die für die jeweiligen Umweltbedingungen optimiert sind. In den letzten zehn Jahren hat sich der großformatige 3D-Druck (3DP) von thermoplastischen Materialien, insbesondere die Material Extrusion (ME), hinsichtlich der maximalen Extrusionsrate und des Bauvolumens erheblich weiterentwickelt und erlaubt somit die Herstellung großformatiger, lichtdurchlässiger Gebäudekomponenten. Gegenwärtig ist es möglich, 3DP-Elemente mit einer Größe von mehreren Metern mit Hilfe von großen Extrudern herzustellen, die mit Granulat beschickt werden. Diese Skalierung wird jedoch durch die Extrusion dicker, massiver Stränge erreicht, die zu schweren und material-ineffizienten Bauteilen führen. Darüber hinaus wird die maximale Druckgeschwindigkeit dadurch eingeschränkt, dass das extrudierte Material vor dem Auftragen der nächsten Schicht abkühlen muss. Bei großen Querschnittsflächen ist die Abkühlrate deutlich verlangsamt. Folglich steht das heutige großformatige ME in klarem Gegensatz zum Potenzial synthetischer Materialien in der Architektur, insbesondere im Hinblick auf Eigenschaften wie Leichtigkeit, Transparenz und die Fähigkeit, großflächige Strukturen zu erschwinglichen Kosten zu realisieren.

Daher wird in dieser Arbeit der 3D-Druck mit Hohlprofilen (HC3DP) untersucht, einer neuartigen Polymer-3D-Druck-Methode für großformatige Leichtbauelemente. Dieser Ansatz basiert auf der Idee des Extrudierens von Hohlprofilen, wie sie aus der industriellen Kunststoffextrusion als Die-Extrusion bekannt ist. Mit HC3DP erreicht ME Extrusionsraten, die mit denen des hochauflösenden 3D-Betondrucks vergleichbar sind. In dieser Arbeit wird zum ersten Mal ein Hohlprofil 3D-Druck in großem Maßstab mit einem Querschnitt von 24 mm und mehr vorgestellt, wodurch sich neue Designmöglichkeiten für die additive Fertigung ergeben. HC3DP ermöglicht die Extrusion hohler, röhrenförmiger Stränge und führt daher zu erheblichen Materialeinsparungen (50-85%). Darüber hinaus verbessert dies die Abkühlung des Materials während des Druckvorgangs erheblich, wodurch sich die Druckgeschwindigkeit um den Faktor 3-8 erhöht

HC3DP wurde speziell für die Optimierung der Leistung von ME im Anwendungsfall von 3DP-Fassaden entwickelt und ist der Hauptbeitrag dieser Arbeit. Diese Entwicklung umfasst die Erforschung mehrerer Extrusionsgeometrien in verschiedenen Maßstäben, einschließlich kleiner und großer ME und schließlich HC3DP. Darüber hinaus werden verschiedene Querschnitte, Matrizengeometrien und Materialien für HC3DP untersucht, um die Vielseitigkeit des Druckverfahrens zu demonstrieren. Nach der Implementierung von HC3DP werden mehrere Prototypen in kleinem Maßstab gedruckt und für größere Prototypen werden physikalische Experimente durchgeführt. Ein großformatiger Demonstrator erforscht den Gestaltungsspielraum von HC3DP und 2,1 m hohe 3DP-Elemente werden fabriziert, die als praktisch tragende Struktur dienen. In Zusammenarbeit mit multidisziplinären Forschungspartnern wird die Performance von HC3DP untersucht und Aspekte wie thermische, strukturelle und akustische Aspekte werden mit state-of-the-art ME-Methoden im großen Maßstab verglichen. Es wird gezeigt, dass alle oben genannten Eigenschaften durch HC3DP erheblich verbessert werden; es kann ein Wärmewiderstand von dreifach verglasten Fenstern mit hoher Luftschalldämmung erreicht werden, und aufgrund des optimierten Verhältnisses von Festigkeit zu Gewicht können große Spannweiten erzielt werden. Abschließend wird auf der Grundlage dieser experimentell validierten Ergebnisse die Produktionstauglichkeit von HC3DP für die Fassadenanwendung mit einer Herstellungsgeschwindigkeit von bis zu 1,5h/m2 vorgestellt.

Mit den vorgestellten Entwicklungen des HC3DP wird die Vision von maßgeschneiderten, frei gestaltbaren Designs und performativen Fassadenelementen immer greifbarer. Dies kann ein wichtiger Schritt zur Senkung des Primärenergie- und des operativen Energiebedarfs von Gebäuden sein. Zudem ebnet es den Weg für eine Architektur, die sich durch vielfältigere und räumlich komplexere Gebäudehüllen auszeichnet.

Contents

Acknowledgements iii

Abstract v

Contents ix

INTRODUCTION AND MOTIVATION 1

1 Introduction 3
- 1.1 Motivation . . . 3
- 1.2 Research questions . . . 13
- 1.3 Methodology . . . 14
- 1.4 Structure of the thesis . . . 16

MANUSCRIPTS RELATED TO CURRENT METHODS 19

2 3D printing facades: Design, fabrication, and assessment methods 21
- 2.1 Overview of Paper A . . . 21
- 2.2 Introduction . . . 24
- 2.3 Design for 3DP facade . . . 27
- 2.4 Fabrication, Materials, and Applications . . . 32
- 2.5 Performance Assessment for 3DP Facades . . . 49
- 2.6 Discussion and Conclusion . . . 52

3 Printing thermal performance: ME for 3DP facades 57
- 3.1 Overview of Paper B . . . 57
- 3.2 Introduction . . . 59
- 3.3 Methods . . . 60
- 3.4 Results . . . 66
- 3.5 Conclusions . . . 68

MANUSCRIPTS RELATED TO THE DEVELOPMENT OF HC3DP 71

4 Large-scale HC3DP for ultralightweight components 73
- 4.1 Overview of Paper C . . . 73
- 4.2 Introduction . . . 76
- 4.3 Method and Materials . . . 79
- 4.4 Results . . . 84
- 4.5 Discussion . . . 94
- 4.6 Conclusion . . . 97

5 HC3DP: Cross-section and printing features 101
- 5.1 Overview of Paper A . . . 101
- 5.2 Introduction . . . 103
- 5.3 Materials and methods . . . 105

5.4 Results 111
5.5 Discussion 115
5.6 Conclusions 116

6 Prōtóplasto: a discrete roof-column system 119
6.1 Overview of Paper E 119
6.2 Plastic Architecture in the Digital Age 121
6.3 Towards Discrete Prefabricated Architecture 122
6.4 Constructive System and Digital Workflow 123
6.5 A Plastic Future? 128

Manuscripts related to HC3DP facades 129

7 HC3DP for highly insulated facades 131
7.1 Overview of Paper F 131
7.2 Introduction 134
7.3 Methods and materials 138
7.4 Results 149
7.5 Discussion 153
7.6 Outlook 154
7.7 Conclusion 155
7.8 Appendix A - Print time calculations 157
7.9 Appendix B 159

8 HC3DP for large-spanning facades 161
8.1 Overview of Paper G 161
8.2 Introduction 164
8.3 Methods and materials 165
8.4 Results 171
8.5 Discussion 177
8.6 Conclusion 178

Conclusions and future work 181

9 Contribution and discussion 183
9.1 Potentials of 3DP facades 183
9.2 ME and HC3DP for facade application 186

10 Future work 191
10.1 Category 1 191
10.2 Category 2 193
10.3 Category 3 194
10.4 Category 4 195

Appendix 197

A Sound insulation of HC3DP and ME 199
A.1 Method 200
A.2 Results 200
A.3 Discussion 201

B Filament-based HC3DP **203**

C HC3DP formwork for concrete **205**
C.1 Results 206
C.2 Next steps 207

Bibliography **209**

List of Figures **228**

List of Tables **234**

CURRICULUM VITAE **237**

Introduction and motivation

1 Introduction

1.1 Motivation 3
1.2 Research questions 13
1.3 Methodology 14
1.4 Structure of the thesis . . . 16

This thesis presents the development and scale-up of Hollow-Core 3D printing (HC3DP), a novel polymer 3D printing (3DP) method for large-scale and lightweight elements. HC3DP advances Material Extrusion (ME) to achieve extrusion rates comparable to those of high-resolution 3D concrete printing. HC3DP facilitates the extrusion of hollow, tubular, large-scale beads instead of solid ones and therefore allows for extreme material savings (50-85%). Furthermore, the tubular bead structures increases the material cool-down during printing process significantly, and therefore, increases the printing speed by factor 3-6. HC3DP is specifically developed for improving the performance of ME in the use-case of 3DP facades and is the core contribution of this thesis. Together with multidisciplinary research partners the performance of HC3DP are investigated, and aspects like thermal, structural and acoustics are compared to state-of-the-art large-scale ME methods. Finally, based on these experimentally validated findings the production viability of HC3DP for facade application is presented.

1.1 Motivation

This thesis is motivated by the significant challenges the construction industry is currently facing, including environmental and sustainability concerns, particularly in the context of the climate crisis. In combination with rising costs of materials, compounded by a shortage of skilled labor, and an increasing demand for more affordable housing. The urgency of these issues is highlighted by the immediate needs to build more with less, to construct high-performance structures, to focus on mono-material building methods, and to achieve material efficiency in construction. These challenges collectively emphasize the necessity to enhance the efficiency of construction processes and innovate through technological advancements. Therefore, there is a strong trend towards new, automated, and flexible fabrication methods.

The current trends in the construction industry are characterized by an increased use of technology and automation. This encompasses the implementation of Building Information Modeling (BIM) and robotic

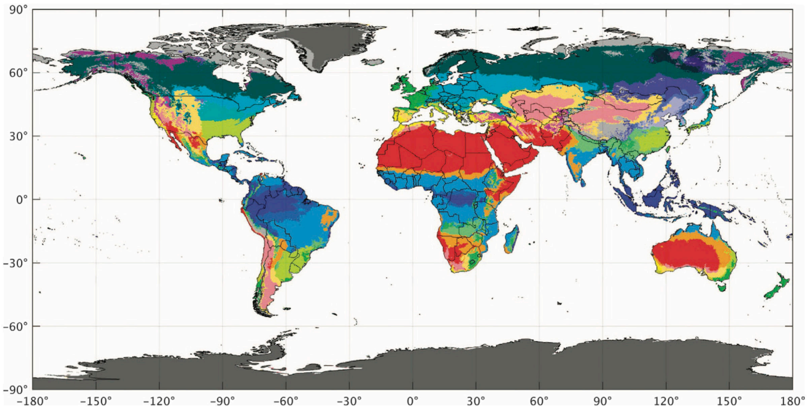

Figure 1.1: Predicted changed in climate zones due to climate change. (a) shows the present-day map (1980–2016) and (b) the future map (2071–2100). Figure adapted from ”Present and future Köppen-Geiger climate classification maps at 1-km resolution" [1].

manufacturing, which are pivotal in enhancing efficiency and accuracy in construction processes. Furthermore, there is a greater focus on sustainability and attention to the life-cycle of buildings. This aspect involves the use of materials that have a lower environmental impact and emphasizes the importance of reuse, recycle, and repurposing over creating new developments. In addition, there is a rising demand for adaptability, and prefabrication in construction projects. These approaches are aimed at speeding up the building process while simultaneously reducing costs, labor, and material requirements. Collectively, these trends reflect a significant shift in the construction industry towards more sustainable, efficient, and technologically advanced methods of building.

Alongside these trends, there is a growing interest in robotic 3DP, also known as additive manufacturing (AM), in construction. This method allows for greater automation in production and increases efficiency. 3DP is a fabrication technology that creates parts by adding material, typically layer by layer. This quasi waste-free fabrication method not only offers material savings during production but also allows for the customization of parts to specific needs. 3DP has been scaled up to create large-scale elements relevant to architectural practices and when those large objects can be tailored to a local construction site, they become multifunctional. Such parts have the potential to reduce the variety of materials used and eventually evolve into mono-material components, which can enhance sustainability and recyclability. Alongside the trend of large-scale AM, there is extensive research into the use of recycled materials, which can improve the environmental impact of such designs. For ME, a thermoplastic polymer is melted and deposited by a nozzle in consecutive beads that solidify, usually into a disco rectangular section. This process promises the efficient, waste-free fabrication of highly complex individualized parts without custom molds or expensive tooling. Furthermore, buildings typically consist of many non-repetitive, custom parts, in addition to a limited number of repetitive elements. Optimized building elements often result in complex, differentiated geometries, which are expensive or impossible to fabricate with traditional means. Additionally, building elements often benefit from an internal differentiation of their structure, especially the integration of functional voids at different scales. Voids can be devised to distribute material more efficiently, reduce weight, integrate building services, or improve certain functional aspects, such as acoustics and thermal insulation. For such complex geometries with non-solid sections, AM is a promising fabrication strategy.

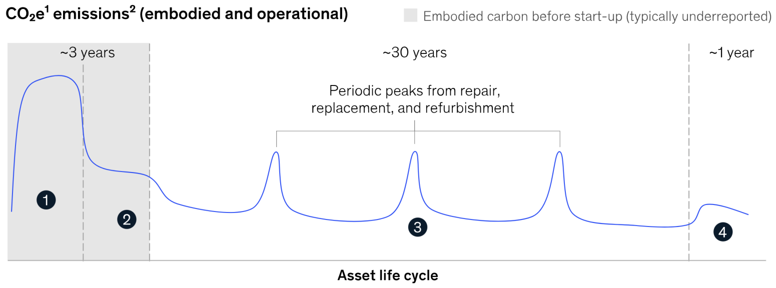

Figure 1.2: (1) Construction material procurement. Driven by carbon-intensive manufacturing processes for materials such as steel, concrete, aluminum, copper, and plastic. (2) On-site construction. Driven by fuel consumed by heavy construction vehicles and other emissions. (3) Operations. Driven by heating and water utilities and electricity consumption. (4) End of life. Driven by demolition, waste processing; can gain credits for reuse and recycling [2].

3DP can benefit greatly facade construction as a site-specific design can become a climate-specific design. The Köppen-Geiger map in Figure 1.1 provides an overview of the different climate zones, each representing different boundary conditions in regard thermal, structural, or acoustic requirements. For facade design and fabrication, the ability to adapt to climate conditions (global), and site specific circumstances (local) are of great importance. There are various ways in which a 3D printed (3DP) facade can tailor its performance to specific sites or climates. For example, in colder climates, a facade might have increased depth for better thermal insulation; conversely, in hotter climates, it might incorporate self-shading geometries to reduce the risk of overheating. However, these functional adaptations need not be uniformly applied across a building. They can vary depending on the orientation of the facades. For instance, in colder climates, facades facing the sun can be designed to maximize solar gains, while others focus on enhanced thermal insulation. HC3DP not only facilitates the aforementioned strategies but also introduces an expanded design space, extending adaptability beyond the geometric articulation of the element. In HC3DP, the size, shape, and wall thicknesses of the 3D printed bead can be varied. This variation offers the opportunity to approach the topic of adaptation with greater precision and resolution. To revisit the previous example, in order to enhance solar gains, a layer height of 25mm could be employed instead of the standard 2.5mm. This increase in layer-height results in fewer layer interfaces, thereby effectively increasing solar gain.

The construction sector is a significant contributor to global greenhouse gas emissions, primarily through energy consumption during the operational phase of buildings. By focusing on designs that are tailored to the specific climate and site, buildings can achieve higher energy efficiency. This leads to reduced reliance on fossil fuels, lower carbon emissions, and overall a smaller ecological footprint.

Climate-specific designs allow for the utilization of natural environmental conditions to optimize heating, cooling, and lighting within a building. For instance, in warmer climates, designing for natural ventilation and shading can significantly reduce the need for climate control. Similarly, in colder climates, maximizing solar gain and using thermal mass can decrease heating requirements. These strategies not only cut down on energy consumption but also lead to substantial operational cost savings over the building's lifecycle.

1.1.1 Site-specific, high Performance Building Envelopes

Site-specific, high performance facades are a key factor to reach Net Zero Emissions by 2050 [3]. Over the life-time of a building two drivers of CO_2 emissions are the most prominent: grey energy, the sum of all energy used to produce the materials for the building, and operational energy, which is related to energy consumed during the use of use of the building (Fig. 1.2). Today, the design and fabrication of high-performance facade systems is being re-evaluated. Current methods rely on different material systems assembled in a layered fashion. This increases complexity and poses a challenge to circularity and positive end-of-life if multi-material systems are connected or assembled in a non-reversible manner [4].

[3]: Delmastro et al. (2022), *Building Envelopes – Technology deep dive*

[4]: Hartwell et al. (2021), 'Circular economy of façades'

Multifunctional facades systems have been envisioned by architects since the late 1970s, with an example being the *polyvalent wall* by the british Architect Mike Davies [5]. The polyvalent wall exhibits multiple performances in a single element and draws inspiration from nature and process regulation in biological form. Recent advancements in 3D printing enable the fabrication of large-scale bespoke elements at no extra cost. Those elements hold the potential to increase functional integration within one single component, which is found to be one of the key benefits of digital fabrication [6]. Today, with AM technology the fabrication of elements such as the poylvalent wall seem in reach, as mono-material, multi-functional elements can now be 3D printed at large dimensions.

[5]: Davies et al. (1981), 'A wall for all seasons'

[6]: Agustí-Juan et al. (2017), 'Environmental design guidelines for digital fabrication'

[8]: Crump (1994), 'Modeling apparatus for three-dimensional objects'

In this thesis, the chosen 3D printing method is Material Extrusion (ME) [7], as this AM method allows to fabricate translucent, nearly transparent, elements at large dimensions. ME uses thermoplastic feedstock for 3D printing, and after patents have expired in 2011 [8], ME has become one of the most used 3D printing methods entering the consumer market. It has also received increasing research interest, focusing on providing large-scale 3D printing systems. The aspect of CO2 reduction can be addressed by ME using two strategies. To reduce the grey energy of the 3D printed element, either the material consumption is reduced significantly, or recycled feedstock can be used as the largest amount of energy is spent on creating virgin materials. To address the operational energy of buildings, 3D printing allows for the design and fabrication of site-specific and high-performance facade solutions with its positive implications mentioned above.

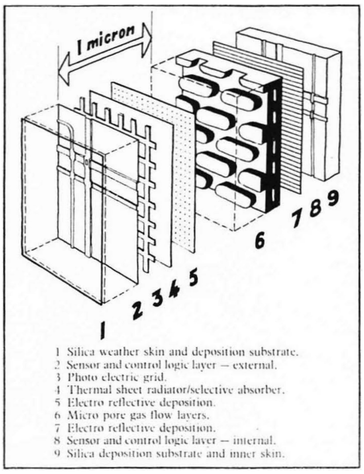
I micron
1
2
3
4
5
6
7
8
9
1 Silica weather skin and deposition substrate.
2 Sensor and control logic layer — external.
3 Photo electric grid.
4 Thermal sheet radiator/selective absorber.
5 Electro reflective deposition.
6 Micro pore gas flow layers.
7 Electro reflective deposition.
8 Sensor and control logic layer — internal.
9 Silica deposition substrate and inner skin.

Figure 1.3: Polyvalent wall 1981, Mike Davies and Richard Rogers [5]

1.1.2 Plastic in Architecture and Buildings

Plastics have become an integral part of the construction industry, revolutionizing various aspects of building design, materials, and processes. Plastic materials offer numerous advantages such as durability, versatility, and cost-effectiveness, making them highly desirable in construction applications. Since their invention, different applications of plastic for construction have been envisioned [9] and are still applicable today [10].

[9]: Koehler (1955), *Plastics in Building*

[10]: Häkkinen et al. (2018), *Plastic in Buildings, A Study of Finnish Blocks of Flats and Daycare Centers*

The following section distinguishes the topic of plastic in architecture and buildings. The first section discusses the developments of plastic architecture and provides a concise history of synthetic materials, along with their implications on design and fabrication in architecture. The latter section offers a more pragmatic approach to synthetic materials, highlighting their common use-cases within buildings.

Synthetic Materials in Architecture

The utilisation of synthetic materials in construction presents a diverse array of architectural possibilities. These innovative materials, capable of being shaped through processes such as forming, moulding, extrusion, or winding, have significantly expanded the architectural vocabulary. The advent of synthetic materials like plastic sheets, membranes, or fibre-reinforced plastic shells has catalysed the development of a novel architectural lexicon ranging from modular components that seamlessly merge roof, wall, and slab elements to large-spanning organically shaped roof structures. After their invention these materials displayed qualities reminiscent of futuristic innovations, blending strength, transparency, thermal insulation, and lightness. Finally leading to a new set of architectural language and innovative construction schemes. One of the first examples of using synthetic materials in architectures is the *Dymaxion Dwelling Machines* from Buckminster Fuller in 1927, promoting a prefabricated, lightweight and easy to transport housing unit, drawing inspiration from the car and aviation industry [11].

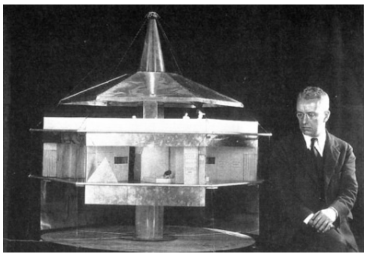

Figure 1.4: Dymaxion Dwelling model, with Buckminster Fuller.

[11]: Baldwin et al. (1996), *Bucky works : Buckminster Fuller's ideas for today*

30 years later the Monsanto House of the Future, by the American architects Hamilton and Goody, was conceived as four prefabricated curved plastic shells exhibiting a seamless transition between roof, wall, and floor. In 1956, Alison and Peter Smithson envisioned an introverted, glossy looking interior, not constrained by right angles, but seamlessly created by glassfibre reinforced elements, also titled *House of the Future*. End of the 1960s the technological advances ended the constraint of designing and fabricating predefined/confined modules and allowed for open and flexible floor plan arrangements. The FG2000 system was certified for residential and commercial building in the US. The trend to create large structures, and move away from small scale prefabricated modules continued in the 1950s and onwards, plastic sheets and membranes became a solution to cover large-spanning structures, such as the geodesic domes of Buckminster Fuller. The 1970 World Expo in Osaka is often understood as the zenith of plastic architecture. The Fuji pavilion was made from inflatable arches, similar to the US pavilion featuring a large-spanning cable roof with inflated air cushions, or the Floating Theater[12]. The oil crisis in 1973 ended the popularity of synthetic materials in architecture abruptly, but only temporarily[13].

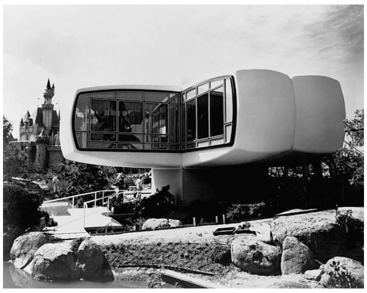

Figure 1.5: Monsanto House of the Future, 1957.

[12]: Chi (2014), 'An outline of the evolution of pneumatic structures'

[13]: Simone Jeska (2008), 'A Brief History of Plastic Buildings'

With the introduction of modern CAD software and the digitization of the construction industry in the 1990s, synthetic materials and their flexibility, efficiency and malleability became, once again, part of the architectural discussion. Today, the most common use of synthetic materials is large-spanning membranes, with examples such as the *Olympic Stadium* by Frei Otto in Munich (1972), or the *Rocket Tower*, for the National Space Center in London, by Nicholas Grimshaw and Partners from 2001, or as a last example, the *Allianz Arena* from Herzo de Meuron from 2005 in Munich. These membranes are often used in combination with pneumatic actuation, as for the Festo headquarters in Germany, where the triple leaf

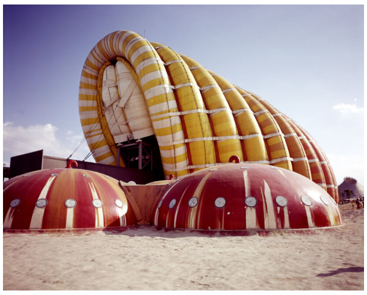

Figure 1.6: Fuji Group pavilion, osaka, 1970, Yutaka Murata. © yutaka murata. © photo courtesy of Osaka prefectural government.

assembly allows to actively control the climate within the atrium of the building.

With the advent of large-scale 3D printing technologies, only recently, additive manufacturing of thermoplastic materials has become a field of interest for architecture. With a few pioneering architects and built projects, presented later in section 1.1.4.

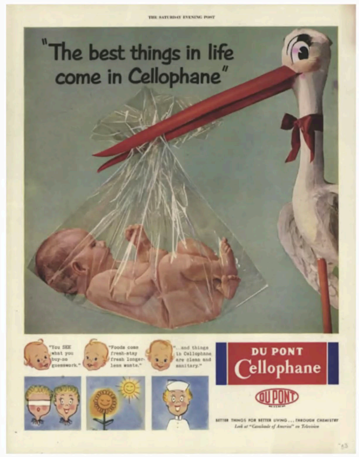
"The best things in life come in Cellophane"
DU PONT
Cellophane
DU PONT

Figure 1.7: Cellophane advertisement 1950s. "Better things for better living... though chemistry", Du Pont.

Synthetic Materials in Buildings

One prominent use of plastics in construction is in the form of polymer-based building materials such as PVC (polyvinyl chloride), HDPE (high-density polyethylene), PC (polycarbonate), and composite plastics, among others. They are lightweight, strong, and resistant to corrosion, moisture, and chemicals, making them suitable for a wide range of construction applications. Plastic pipes and fittings have therefore gained immense popularity in plumbing and drainage systems. Plastic pipes are also widely used for gas distribution and electrical conduit systems due to their safety, insulation properties, and cost-effectiveness.

Plastics in construction are also used for insulation purposes. Plastic foam boards, such as expanded polystyrene (EPS) and extruded polystyrene (XPS), provide excellent thermal insulation and are commonly used in roofs, walls, and foundations at a low price. The affordability of cheap insulation materials enables wider application in the mass market, offering significant potential for sustainability benefits by enhancing energy efficiency in more buildings. Besides insulation, recycled plastics materials can be utilized in various construction products, reducing waste and minimizing the environmental impact. Depending on the application, plastics have a lower greenhouse gas impact than non-plastic alternatives [14]. Plastics can therefore potentially play a crucial role in sustainable construction practices.

[14]: Helmcke et al. (2022), *Climate impact of plastics*

1.1.3 The Perception and Problems of Synthetic Materials

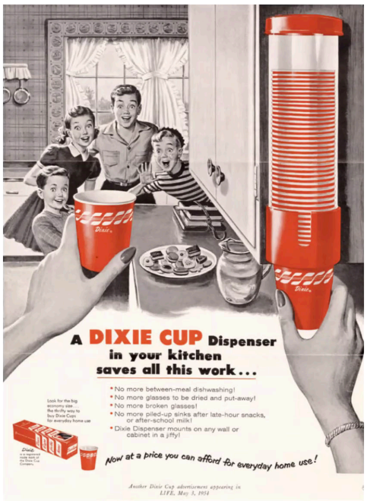
A DIXIE CUP Dispenser
in your kitchen
saves all this work...
No more between-meal dishwashing!
No more glasses to be dried and put-away!
No more broken glasses!
No more piled-up sinks after late-hour snacks, or after-school milk!
Dixie Dispenser mounts on any wall or cabinet in a jiffy!
Now at a price you can afford for everyday home use!

Figure 1.8: Dixie Cup advertisement, 1954. Single-use paper cups with polyethylene coating.

The perception of plastic has undergone a significant transformation since its invention to the present day. In the early 20th century, the advent of plastics was hailed as a revolutionary development, promising a new era of convenience and innovation. Initially, plastics were celebrated for their durability, versatility, and the ease with which they could be molded into a vast array of products, Figure 1.7, Figure 1.8. This novel material symbolized modernity and progress, finding applications in everything from household items to critical components in the aerospace and automotive industries. However, over the past decades the challenges related to increasing plastic consumption are becoming apparent. The very durability that made it successfully also meant that most polymers today are non-biodegradable, leading to high levels of environmental pollution [15, p. 1.3cm], Figure 1.9. In the 21st century, the narrative around plastic had shifted dramatically. Plastics became synonymous with environmental crisis, particularly ocean pollution and their impact on wildlife. Public awareness and scientific research have highlighted the threats posed by plastic waste, leading to a growing movement towards sustainable alternatives and increased recycling efforts. Today, the perception of plastic is that of a double-edged sword, a material that has been central to technological advancement and everyday convenience, yet poses significant challenges for environmental sustainability and global ecological health.

Figure 1.9: Plastic pollution in the ocean and mountains. Source: www.circular-solutions.eu, unsplash.com

The construction industry is actively exploring ways to reduce plastic waste, promote recycling, and develop eco-friendly alternatives [16–18]. Efforts are underway to find innovative solutions such as biodegradable plastics, bio-based polymers, and improved recycling processes to mitigate the environmental impact of plastics in construction [19, 20]. However, the way plastic is treated at the end of life is what is causing the most negative impact on our environment. Plastic pollution is a imminent problem since its invention and is becoming more significant with the increasing yearly production volumes, [21, 22]. Today, however, stricter regulations on recycling, the banning of land-filling, and biodegradable bio-plastics as a alternative to petrol-chemicals provide hope to overcoming today's challenges. Nevertheless, it should be noted that mechanical recycling usually goes in hand with a reduction of material properties [23, 24]. However, studies show that the material is not severely affected of up to 5 cycles [25], which would already improve the sustainability of such 3DP materials. Once the material properties are not sufficient anymore, the polymers must undergo tertiary recycling, which can include chemical, or energy recovery processes to transform them into basic chemicals, fuels, or energy.

The construction sector is, after the packing industry, the second largest market for plastic materials, 1.10.a . Figure 1.10.b compares the lifetime of plastic elements for different industries, and displays for construction the highest average lifespan of over 35 years. This stands in strong contrast to the short life span of single-use plastic items, which accumulated to 139 million tons of waste in 2021 [22].

[16]: Goli et al. (2020), 'Application of Municipal Plastic Waste as a Manmade Neo-construction Material'

[17]: Rebeiz et al. (1995), 'Plastic waste management in construction'

[18]: Zulkernain et al. (2021), 'Utilisation of plastic waste as aggregate in construction materials'

[19]: Gökçe (2018), 'Rethinking sustainability'

[20]: Oberti et al. (2022), 'Bioplastic as a Substitute for Plastic in Construction Industry'

[21]: Center for International Environmental Law (2017), *Fueling Plastics: Plastic Industry Awareness of the Ocean Plastics Problem*

[22]: Charles et al. (2023), *Plastic Waste Makers Index 2023*

[23]: Latko-Durałek et al. (2019), 'Thermal, Rheological and Mechanical Properties of PETG/rPETG Blends'

[24]: Anderson (2017), 'Mechanical Properties of Specimens 3D Printed with Virgin and Recycled Polylactic Acid'

[25]: Vidakis et al. (2021), 'Sustainable Additive Manufacturing'

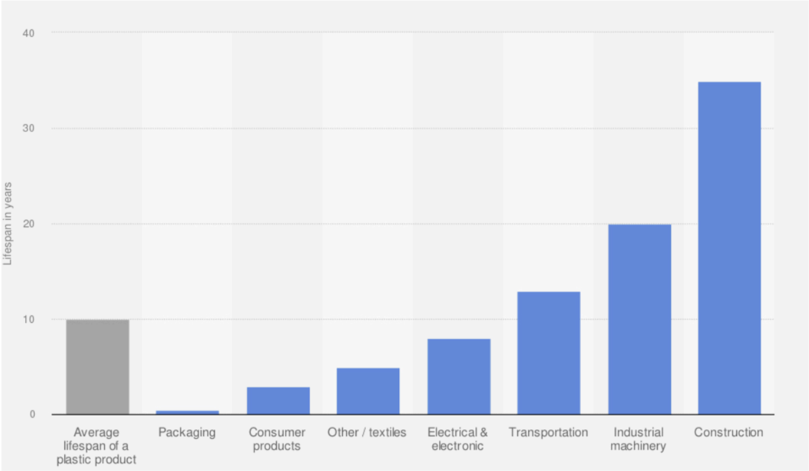

Figure 1.10: Average lifespan of plastic elements per sector. Source: OECD Statista 2023.

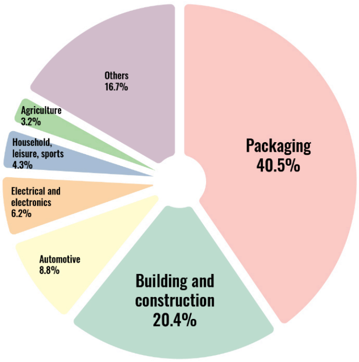

Figure 1.11: Plastic consumption per sector. Building and construction is the second largest customer of plastic products. Source: plasticeurope.com .

Nevertheless, to provide meaningful applications of 3D printed plastics in the construction sector several aspects must be considered. Monomateriality, and if not achievable, design for disassembly are key factors to consider during the conception phase. If composites are fabricated that cannot be separated at the end of life, the barrier for recycling rises and plastic looses its value and turns from a material-feedstock to material-waste. It could be argued that the issue with using plastics in architecture and construction is not strictly related to the material itself or its typical lifespan. Instead, the problem is more related to the end of life scenario, such as the low rates of recycling and the uncontrolled disposal of waste.

1.1.4 Large-Scale Material Extrusion

Large-scale 3D printing with plastics in construction is a relatively new and emerging technology that has the potential to revolutionize the way buildings and structures are designed and constructed. It offers unique opportunities to manufacture complex and custom building elements. The key benefits of large-scale 3D printing with plastics in construction can be summarized as follows. 3DP offers the ability to produce elements with high precision and minimal waste, marking a significant advancement in building efficiency. This technology also enables the creation of unique and complex designs, which would be challenging or even impossible to achieve using traditional construction methods. When it comes to sustainability, 3D printing with plastics presents an opportunity, especially when using biodegradable plastics derived from renewable resources. This approach not only contributes to sustainability and provides a cradle to cradle construction scheme but also allows for the creation of material-efficient or multifunctional components from a mono-material. In terms of speed and cost-effectiveness, large-scale 3D printing can significantly reduce labor costs in construction projects, as it eliminates the need for formwork or molds, streamlining the building process and tackling skilled labour shortage.

One of the first times Material Extrusion (ME) using granular feedstock was presented was during the production of the endless chair by the artist Dirk van der Kooji [26]. In parallel DUS Architects started the

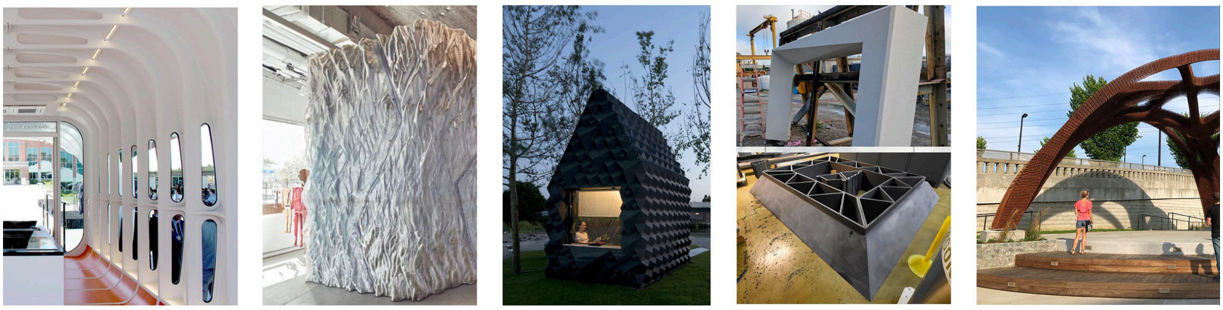

Figure 1.12: Example of large-scale thermoplastic extrusion in construction, 3D printed building envelope, interior wall elements , “urban cabin” from DUS architects , concrete formwork for facades, oneC1TY Pavilion Branch Technologies.

development of a thermoplastic extrusion 3D printer for architectural application at a large dimension [27]. Both introduced pellet extruders that don’t rely on pre-manufactured filaments, but directly use granular (pellet) feedstock, similar to injection molding machines. By using these extruders, the output of printed material (kg/h) could be increased dramatically. These large tool heads are mounted on either a robotic arm with a high payload and long reach or on modified gantry systems, as found in large-scale CNC milling. A 3DP setup usually consists also of a pellet drying/storing system, including a material conveying system. Since 2015 the Oak Ridge Laboratory has been researching ME with a focus on maximizing material output, increasing the dimension of the printed object [28], overcoming weak layer bonds [29], or material characterization [30].

Fused granular manufacturing (FGM), large format additive manufacturing (LFAM), or Big Area Additive Manufacturing (BAAM) all describe the same ME process of using a granular (thermoplastic) feedstock to 3D print objects at a large dimension. This technique is due to the possible size of printed objects and material properties, most often used for automotive, naval, aerospace, and architectural applications [31]. Irrespective of the printing method, the application of 3DP polymers ranges from 3DP molds for concrete [32], 3DP of facades [33], or wall elements [34], temporary structures [35], or furniture [36]. A more detailed review of large-scale polymer extrusion can be found here [37].

The growing interest in polymer 3D printing for architectural applications is reflected in the increasing number of commercially available printing systems (e.g. thermwood, ingersoll), pellet extruders providers (e.g. CEAD, Massiv Dimensions, Dyse Design), and companies/startups that focus on providing products or services for large-scale 3D printing (e.g. Nagami, AI build, The New Raw).

[28]: Love et al. (2015), ‘Breaking barriers in polymer additive manufacturing’

[29]: Kishore et al. (2017), ‘Infrared preheating to improve interlayer strength of big area additive manufacturing (BAAM) components’

[30]: Duty et al. (2017), ‘Structure and mechanical behavior of Big Area Additive Manufacturing (BAAM) materials’

[31]: Pignatelli et al. (2022), ‘An application- and market-oriented review on large format additive manufacturing, focusing on polymer pellet-based 3D printing’

[32]: Jipa et al. (2022), ‘3D Printed Formwork for Concrete’

[33]: Naboni et al. (2022), ‘Additive manufacturing in skin systems’

[34]: Branch Technology (2022), *Branch Technology*

[36]: The New Raw (2015), *Crafting plasitc waste with robots*

[37]: Moreno Nieto et al. (2020), ‘Large-format fused deposition additive manufacturing’

1.1.5 Towards 3DP facades, a Novel Vernacular Architecture of the Digital Age?

Overcoming challenges in ME for 3DPF

To 3D print high-performance, and material efficient facades using polymers, current ME methods must be critically examined. Recent developments in ME have focused on scale-up of the fabrication method by using large-scale pellet extruders, printing thicker beads at larger layer heights [30]. This approach shifts the problem of the print speed

[30]: Duty et al. (2017), ‘Structure and mechanical behavior of Big Area Additive Manufacturing (BAAM) materials’

[38]: Roschli et al. (2019), 'Designing for Big Area Additive Manufacturing'

limitations from the extrusion rate of the hardware (kg/h), to the minimal layer-time for the extrudate to cool down enough for the consecutive layer to be printed on top [38]. Furthermore, this 3DP approach results in heavy, material-intensive, components where thicknesses are not determined by functional requirements like the strength of the element, but are dictated by the fabrication constraints of large-scale 3D printing. This renders the large-scale 3D printed elements not material-efficient and brings into the question aspects of material consumption and sustainability. Therefore, this thesis proposes to 3D print using non-solid sections that allow the scaling and speeding up of the printing process through increased layer heights and increased cooling rates.

Combining the benefits of large-scale ME with tubular extrusion is a promising research avenue, especially with the focus on facade construction, that has not been investigated yet. HC3DP overcomes the downside of current large-scale ME approaches, limited printed speed due to slow cool-down [38], material in-efficient structures, while maintaining the potential benefits of 3DP for facades, namely site specific-design, high-performance, and functional integration in a, potentially, mono-material construction scheme [39, 40].

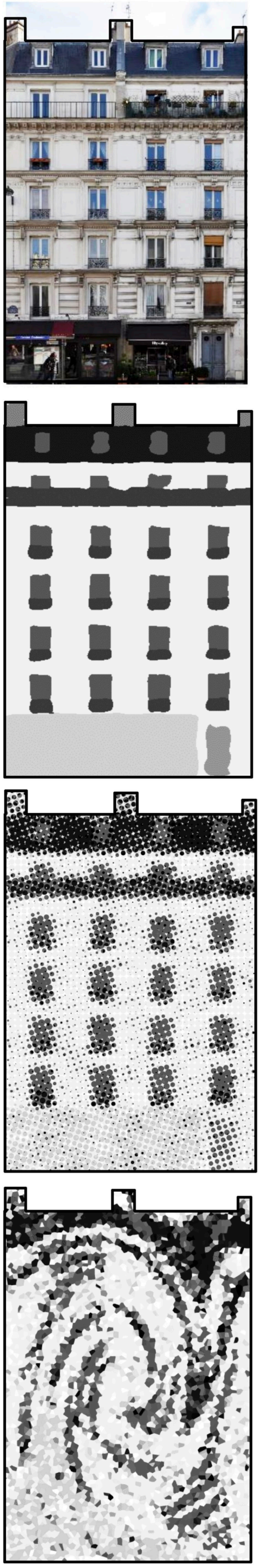

Figure 1.13: Diagram: From discrete building elements towards mono-material multi-functional elements, designed at millimetre scale.

Site-specific, high-performance facades

Vernacular architecture, deeply rooted in local traditions, materials, and needs, offers a unique view into the cultural and environmental context of a region [41]. The facades of vernacular buildings are often crafted from locally-sourced materials and designed to naturally regulate climate conditions. For instance, thick stone walls in mountainous areas provide insulation against cold, while light, airy structures in tropical regions allow for ventilation and cooling. These facades not only exhibit a harmonious blend with the surrounding landscape but also reflect the ingenuity and adaptability of local building practices. Emphasizing functionality and sustainability, vernacular facades stand as build examples of a deep understanding of the local environment and climate.

With industrialized products the way buildings are designed and fabricated changed. Now, float glass is one of the most prominent facade types in modern architecture with the need of additional functionalities added to them in a layered fashion. For each functionality a new set of products is added to the layered construction scheme of facade architecture. Increased performance comes today with increased complexity, as multiple stakeholders, companies, products, and the interfaces between those require meticulous coordination and integration, demanding advanced project management and clear communication strategies to ensure all components work synergistically. Multicomponent facades often face challenges in being reused or recycled because they frequently use permanent adhesive connections. These adhesives, such as silicone and epoxy used for structural and weather-proofing, along with laminated glass, hinder the ability to disassemble these components [42].

Standardized elements work effectively in new developments with uniform and straight facades, but they encounter difficulties when the consistent pattern they are intended for is disrupted. Each building consists of non-regular elements, such as connection to the ground, the attic, and corner elements. Those rely on non-catalogue items and take up significant manual labour and come at an increasing price.

Computational design paired with additive manufacturing technologies will not only change the way architectural elements are designed, but will also allow adjusting the material properties of those, all within one process. This brings into question how facades will be designed in the future and materialised with 3D printing. 3DP will cause a shift from discrete building blocks towards a multi performance mono-material construction, where the fabrication of facades can be changed at a millimetre scale. Building blocks can be as small as droplets of material, having different properties, gradients or blend functionalities. Can ME become the future vernacular construction method for 3DP facades, in a time where abundant polymer waste can be potentially turned into high-performance, and site specific facade?

1.2 Research questions

This thesis investigates the potential benefits of 3D printing for building envelopes and proposes a novel AM method for high-performance, lightweight, and fast to fabricate 3DP facades. In order to prove that Hollow-Core 3D Printing can be used to fabricate high-performance 3DP facades, the following research questions are posed:

Potential and challenges of 3DP ME building envelopes

RQ1

Facades are understood, due to their numerous requirements, as one of the most complex building components. It is therefore important to provide a hollistic understanding of state of the art of 3DP facades, their design, fabrication, and assessment methods to identify research gaps and future research trajectories. This will lay the foundation to understand why and how 3D printed facades can be used in the future and where their true benefits lies.

How can existing 3DP methods be altered for facade applications?

RQ2

Different 3D printing methods have been developed for certain use-cases. There are AM methods such as ME that cover a broader range of applications, and there are highly specialized AM methods such as 3D concrete printing. For facade 3D printing no specific AM method exist yet. Based on the findings of RQ1, ME has been identified as one of the promising AM methods for facade application, as it allows to 3DP large-scale translucent elements. The goal of RQ2 is to develop a new method for large-scale 3D printing, specifically designed for facade applications, improving the performance of the printed element while allowing for fast fabrication times. Key investigations are the hardware (nozzles) and process (peripherals and software) developments, material investigations and printing experiments.

Which facade relevant performances can be achieved with HC3DP?

RQ3

After the successful development of the novel 3DP approach, it is important to answer how HC3DP performs in comparison to state of the art ME techniques. Facade related performances investigated in this thesis are structural, thermal, as well as acoustics. Futhermore, as 3DP facades must cover numerous square meters of built volume, it is of great importance to understand the fabrication viability of HC3DP in regards to fabrication time, costs, and material consumption. These complex research questions are therefore best addressed within an interdisciplinary research team.

1.3 Methodology

To answer the research questions experimental research was conducted with the goal to develop a novel 3D printing method, based on tubular extrusion. In parallel to the process development, the principal applicability of HC3DP for facade construction is evaluated for functional goals, such as strength-to-weight ratio, fabrication time, thermal, and acoustic performance. These aspects are investigated using quantitative experimental methods within an interdisciplinary research team, combining expertise from different disciplines. Finally, an architectural demonstrator explores qualitatively the design space of the novel AM method and its architectural expression. In addition, this demonstrator pushes the development of the process in regard to technological readiness and results in quasi load-bearing components of 2.1m height.

1.3.1 HC3DP process development

The development of HC3DP contains several steps which can be categorized as follows. Those steps are not linear and often involve revisiting earlier steps based on new findings or challenges. The goal of this methodology is not to create a ready-made product, but to contribute to the broader scientific understanding of HC3DP and its potential applications.

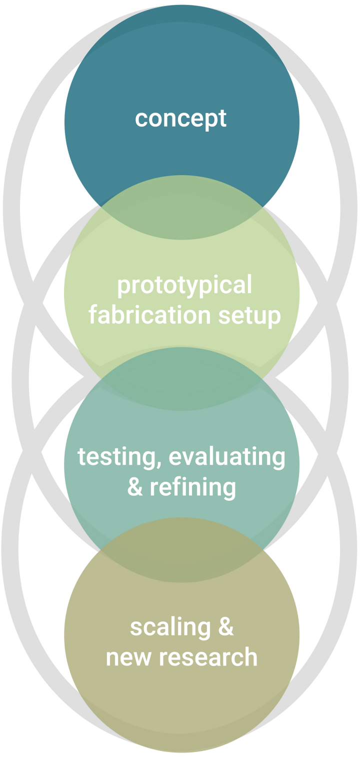
concept
prototypical fabrication setup
testing, evaluating & refining
scaling & new research

Figure 1.14: Interdependencies in the methodology.

Conceptualization and Research Phase: The process starts by identifying limitations or potential improvements of current 3DP systems for the application of facades. The main limitations identified in current ME methods, are speed, material consumption, and critical performances for facades, such as thermal resistance. Based on these findings new concepts and underlying principles are investigated and conceptualized.

Fabrication Setup: After the ideation, it is essential to establish a prototypical fabrication setup. This includes the mechanical design hardware, the software interface, and the printing process itself. Building prototypes in a laboratory setting is essential for validating theoretical concepts. This hands-on phase allows for the observation of how new materials and processes behave under real world conditions. For HC3DP, the prototypical fabrication setup was installed on an ABB IRB1600 industrial robot with a reach of approx. 1.5m. The system furthermore consists of a pellet extruder with a maximum extrusion rate of 1 kg/h and a nozzle with a hollow-mandrel supported by spider vanes.

Testing and Refinement: This prototypical fabrication setup was used for rigorous testing to assess initial material behaviour, and to develop an understanding of the correct process parameters. The testing revealed issues with the inflation of the bead, and print path limitations. Based on the testing results, the design of the system is iteratively refined. First, by implementing peripheral hardware that increases the control over the printing process (controllable pressure valve). Second, the nozzle was redesigned and a different material was chosen to improve the heat transfer to the plastic. Third, a revision opening was introduced, allowing to unclog the nozzle in case of a failed print.

Scaling and New research: As a final step in the developed, the system is transferred to a 6-axis robotic arm with a reach of 3 meters (ABB IRB 6700) equipped with a pellet extruder with an extrusion rate of max. 10kg/h, for the given material. The scaled fabrication setup allows for the production of large-scale elements at a fast pace, such as 2 m tall cylinders under 2h, and was used for the demonstrator in chapter 6. The increased fabrication scale and speed was then tested for different thermoplastic materials to investigate the versatility of the process. Furthermore, this scale-up triggered the development of a theoretical thermal cool-down model, to understand the implications of the thin-wall extrudate on the cooling rate of the polymer. Finally, the increased scale of the hollow-bead allows for the introduction of bespoke cross-sections, such as reinforcement crosses or tube in tubes.

1.3.2 Interdisciplinary collaboration - performance assesment

This thesis is part of a wider interdisciplinary research project within the NCCR in Digital Fabrication in Architecture; and together the performance of the HC3DP elements is investigated at different scales. In addition the improvements are quantified against other, off-the-shelf ME methods and 1:1 demonstrators are printed. The interdisciplinary research stream contains internal and external collaborators. Together with external collaborators the acoustic dampening effects of the HC3DP elements is investigated (EMPA), and structural tests of ME and HC3DP specimen are conducted (HSLU). With internal collaborators the thermal resistance of ME and HC3DP elements is evaluated, and a first large-scale ME facade prototype is 3D printed (GKR and A/S).

1.3.3 Demonstrators

Two large-scale demonstrators are collaboratively designed to evaluate the architectural potential of ME for facade application and HC3DP for large-scale architectural application. An initial facade prototype was fabricated within the interdisciplinary research stream as a 1:1 demonstrator [43]. Although successfully printed, the demonstrator brings into question the applicability of ME for facade architecture, as material consumption and print time are too high (approx. 10-12 h/m^2 at 50-70kg/m^2) and therefore render this process economically not viable. These early findings were key motivators for the development of HC3DP.

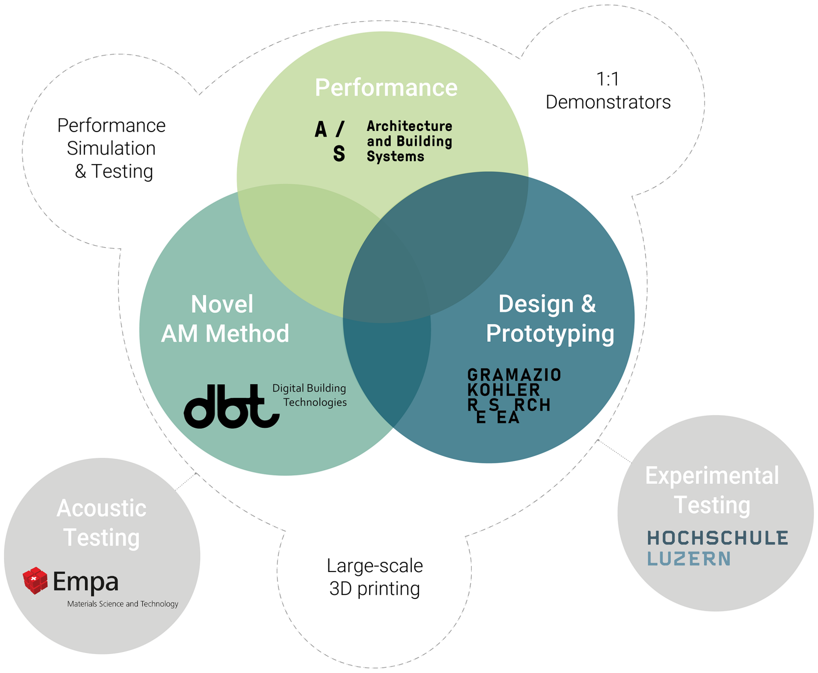
Performance
A / S Architecture and Building Systems
1:1 Demonstrators
Performance Simulation & Testing
Novel AM Method
dbt Digital Building Technologies
Design & Prototyping
GRAMAZIO KOHLER RESEARCH
Experimental Testing
HOCHSCHULE LUZERN
Acoustic Testing
Empa Materials Science and Technology
Large-scale 3D printing

Figure 1.15: NCCR Facade research stream, internal and external collaborators and their function.

After an initial developement phase of HC3DP a second demonstrator is formulated as a design brief for students of the MAS DFAB program 2023. "Protoplasto" pushes the development of HC3DP to a large-scale and acts as a stress-test for the prototypical fabrication setup. For the first time large-scale HC3DP elements, with a height of over 2m, are fabricated to act as quasi-load-bearing columns.

1.4 Structure of the thesis

This thesis is a cumulative dissertation and contains seven manuscripts. In addition, this introduction contextualizes the research, presents motivation, as well as research questions, and finally introduces the methods used. An overview of content, methods, and results precedes each individual manuscript and is followed by the manuscript in an adapted layout. The chapter contribution and discussion summarizes the contribution of this manuscript to the state of the art of large-scale ME and the field of 3D printed facades. It also discusses the current status of HC3DP for 3DPF and provides a comparison matrix based on the findings of the individual peer-reviewed manuscripts. Finally, future research trajectories are suggested.

Paper A

is a review article published in the peer-reviewed journal *Automation in Construction* and presents a holistic perspective on state-of-the-art design, 3D printing, and assessment methods for 3DP facades [44]. It lays the foundation for the thesis and the collaboratively conducted research. –status: published

Paper B

is a peer-reviewed conference publication in *IOP Conference Series: Earth and Environmental Science* and focuses on the thermal performance of regular large-scale ME elements [45]. The findings of poor thermal performance, high fabrication, and high material consumption bring into question the production viability of regular ME for facade application. It became apparent that there is a need of change the 3D printing approach fundamentally to increase performance while reducing fabrication time. –status: published

Paper C

is a peer-reviewed journal article in *Additive Manufacturing* and describes the fundamentels of the HC3DP process [46]. It highlights benefits compared to off-the-shelf ME regarding material consumption, increasing print speed, and maximum extrusion rate. It showcases that different materials can be used for HC3DP and, finally, provides a simplified cool-down model that is essential for understanding the constraints of layer times for large-scale AM that define the fabriction speed. –status: published

Paper D

is a peer-reviewed journal article in *3D Printing and Additive Manufacturing* and focuses on the increased cross-section of HC3DP [47]. First, it proves that the extrudates' cross-section can be varied significantly without changing the hardware. Then bespoke die geometries are introduced that create non-tubular cross-sections. Finally, design experiments provide fundamental understanding on 3D printing features like bridging or non-planar printing. –status: published

Paper E

is a peer-reviewed conference article in *Fabricate 2024* and provides the first large-scale 3D printed HC elements in a quasi-structural application [48]. 2.1m tall columms are 3D printed using HC3DP, resting on bespoke concrete feet, cast into HC3DP formwork. The columns host large-spanning space-frame roofs made from glass fibre tubes and 3D printed connections. –status: published

Paper F

is a peer-reviewed journal article in *Building and Environment* and it investigates the increased thermal performance of HC3DP elements and compares the findings to Paper B [49]. Furthermore, the introduction of a high-performance composite, made from HC3DP and aerogel, enables minimal fabrication time and offers superior insulation performance. These materials are not permanently bonded, allowing for the polymer to be recycled and the aerogel to be reused. Finally, different ME approaches (FDM, ME, HC3DP) are compared to each other in regards to thermal performance, fabrication time, and costs. –status: published

Paper G

is a peer-reviewed journal article in *Journal of Building Engineering* and summarizes the investigation of the structural performance of HC3DP. First, tensile testing of off-the-shell large-scale ME is characterizing the material. Then, 3PT bending tests of high-resolution HC3DP and ME are compared to each other, having the same extrusion width. Followed by 3PT bending test of large-scale HC3DP, with and without internal reinforcement ribs. Then, the facade relevant scale is investigated by 3D printing a series of different facade sections, providing fundamental understanding on the behaviour or large-scale elements. Finally, these findings are used to estimate the maximum spanning distance (maximum height) of a 3DP facade. –status: internal review process NCCR-Facade stream

Appendix A

presents investigations on the airborne sound insulation of ME and HC3DP elements and compares the results to established glazing products. –status: experiments concluded, conception paper

Appendix B complements the HC3DP experiments at large-dimensions by presenting a series of design experiments, fabricated using a small-scale HC3DP filament-based printing setup. The experiments were conducted by students of the Master of Advanced Studies in Architecture and Digital Fabrication program 2023.

Appendix C presents an alternative use-case of HC3DP as formwork for concrete. A 2.1 m tall column of 500 kg is cast into a single outline HC print of 9.5 kg.

MANUSCRIPTS RELATED TO CURRENT METHODS

3D printing facades:
Design, fabrication, and assessment methods
2

2.1 Overview of Paper A 21
2.2 Introduction 24
2.3 Design for 3DP facade . . . 27
2.4 Fabrication, Materials, and Applications 32
2.5 Performance Assessment for 3DP Facades 49
2.6 Discussion and Conclusion 52

2.1 Overview of Paper A

2.1.1 Content

This review paper explores various AM methods specifically applied in facade construction. It covers various aspects, including computational design strategies, fabrication processes and materials, and performance assessment for 3DP facades. It delves into the use of diverse materials like Thermoplastics, Clay-based materials, Concrete, and Metals in 3D printing processes. Additionally, the paper examines alternative or non-established 3DP techniques, offering insights into emerging trends and innovations in the field. For each AM method the manuscript provides an extensive table, summarizing research and applied projects. These tables are a concise visual database for the state of the art. Furthermore, the manuscript presents and discusses computational design and assessment methods, showcasing how these approaches can enhance the efficiency, accuracy, and sustainability of facade design and production.

2.1.2 Method

The review process consists of four steps. The first step is a comprehensive literature search based on the combination of keywords referring to the facade domain and 3DP domain. The second step entails a check on the title and abstracts of the selected articles to exclude irrelevant material. The third step is an extensive analysis of the selected articles in order to develop a meaningful categorization system. The literature is categorized into three main groups focusing on 1) the design of 3DP facades, 2) fabrication processes, materials, and applications 3) the performance assessment of 3DP facades. The fourth and last step consists of an extension and refinement of the literature search based on the identified categories. The corpus of reviewed studies covers approximately 180 items, the majority being peer-reviewed journal articles, book chapters, and a few conference contributions.

2.1.3 Results

The review provides insights into the potential and limitations of 3DP facades for different materials, while identifying future research in this emerging field.

Design methods: The review emphasizes the importance of computational design in the 3D printing of facades, highlighting the complexity of integrating fabrication and environmental parameters into the design process. It discusses the use of parametric design and performance optimization tools to facilitate the exploration of optimized 3D printed facade designs. The review also underscores the unique feature of 3D printing to design and fabricate infill structures, which can be optimized and customized for specific boundary conditions and environmental performance requirements.

Thermoplastics: The review highlights the potential of thermoplastics in 3D printed facades, as they allow for mono-material, translucent facade solutions that can have a positive impact on sustainability. The review discusses the successful scaling up of thermoplastic 3D printing to facade applications, with examples of real-scale projects. However, the review also emphasizes the need for further research in areas such as thermal insulation, reaction to fire and fire propagation, UV resistance, optical properties, and connection details

Clay-based: The review states that 3D printing of clay-based materials can be used for specific applications to achieve environmentally friendly facade systems. The review discusses the challenges in 3D printing clay-based materials, such as high deformation due to water content and high post-processing firing temperatures, which can lead to sample deformation and cracking. The response to harsh weather conditions, for non-fired clay, requires further explorations and constructive measures to protect the 3DP facade.

Concrete: Increased attention has been given to 3D printing of concrete over the past two decades, with the maturity of this method demonstrated by the presence of numerous start-ups and construction companies focusing on concrete 3D printing. Various approaches for 3D printing concrete, such as extrusion-based 3D printing, shotcreting, casting concrete in 3D printed formwork, selected cement activation, and 3D printing of foamed concrete, have been explored. Additionally, the environmental impact of concrete 3D printing, including the use of alternative binding agents and recycled aggregates, has been become an important research topic. Facade-related topics, such as thermal and acoustic comfort, have not been sufficiently investigated in the context of 3D printed concrete.

Metal 3DP: The review discusses the potential of metal 3D printing in facade applications, particularly for the fabrication of small-scale elements and nodes of bespoke curtain walls. It highlights the advantages of metal 3D printing, such as the free-form design potential of complex geometries with superior mechanical strength, resistance to fatigue, and fracture toughness. The review also outlines several challenges for metal 3D printing processes, including limited component size, slow fabrication time, high material prices, and the need for post-optimization steps.

Alternative AM methods: The manuscript also discusses alternative 3D printing processes for facade applications. These processes include 3DP of glass, self-healing, self-cleaning, CO2 capturing, and shape-memory materials (SMM). SMM processes have been investigated for facade applications due to their responsive behavior, which can modify the facade response to the environment in real-time. The chapter highlights the potential of SMM for active climate-specific facades, but also notes the challenges associated with their durability and material degradation. The chapter also discusses the use of 3DP for creating active membrane elements and structures, as well as dynamic shading for facades using 4D-printed actuators that respond to various humidity levels.

Performance Assessement: Paper A provides a comprehensive summary of the challenges and advancements in evaluating the performance metrics of 3DP facades. It highlights the difficulties in integrating and measuring the thermo-optical behavior, weather resistance, and durability of 3DP facades. The section emphasizes the challenges in obtaining consistent performance results over a batch of 3D printed components, as well as the limited predictability of the final outcome due to factors such as material properties and printing parameters. Additionally, it discusses the need for a better understanding of the effects of fabrication parameters on optical properties and the interaction of thermal and optical domains.

2.1.4 Authors contribution to the paper

Matthias Leschok* Conceptualization, Investigation, Writing—original draft preparation, Writing—review and editing, Visualization.
Ina Cheibas* Conceptualization, Investigation, Writing—original draft preparation, Writing—review and editing, Visualization.
Valeria Piccioni* Conceptualization, Investigation, Writing—original draft preparation, Writing—review and editing, Visualization.
Bharath Seshadri Writing—review and editing.
Arno Schlüter Supervised the project and manuscript conception.
Fabio Gramazio Supervised the project and manuscript conception.
Matthias Kohler Supervised the project and manuscript conception.
Benjamin Dillenburger Supervised the project and manuscript conception.

*contributed equally to this paper

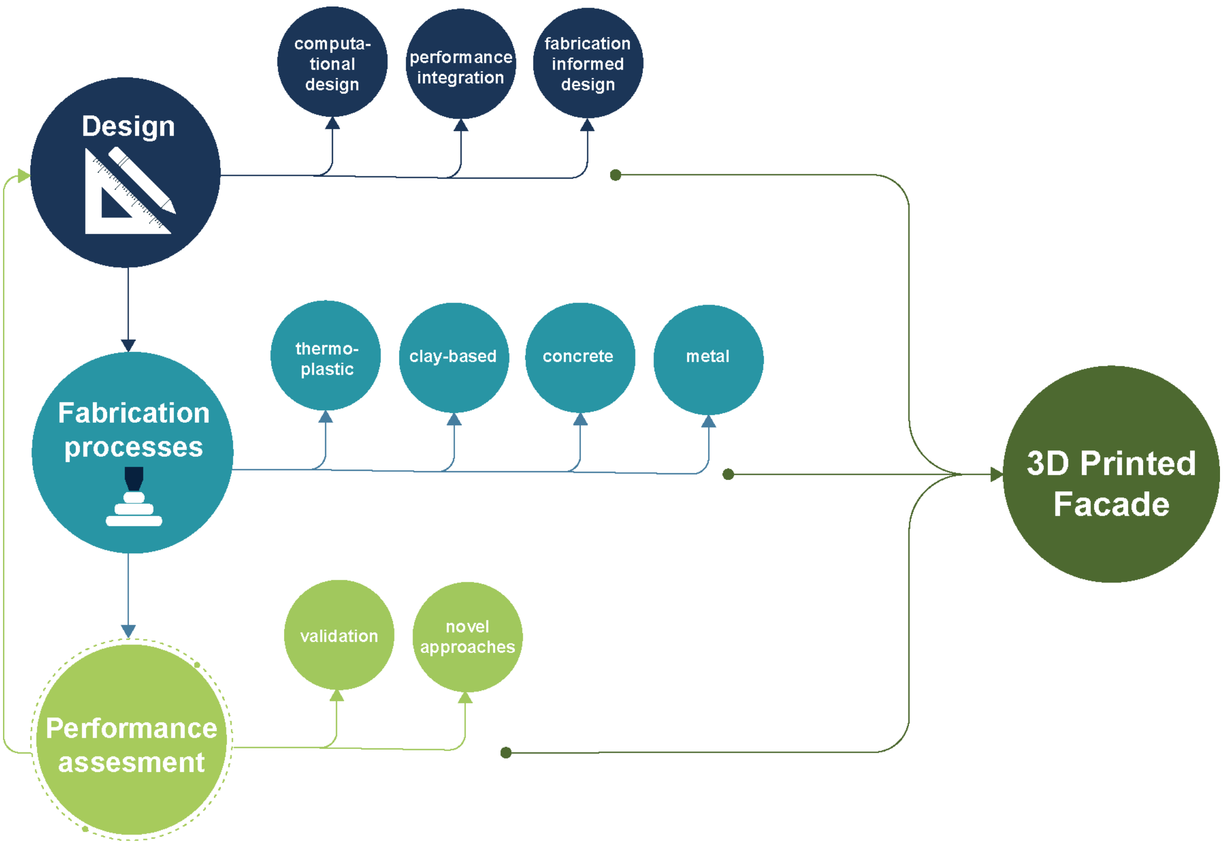
computa-
tional
design
performance
integration
fabrication
informed
design
Design
thermo-
plastic
clay-based
concrete
metal
Fabrication
processes
3D Printed
Facade
validation
novel
approaches
Performance
assesment

Figure 2.1: Conceptual diagram of manuscript strucutre, investigating different aspects of 3DP facades.

Abstract This paper presents a state of the art review for 3D printed facades. In the review, three main topics are identified: (i) computational design strategies for 3D printed facades, (ii) fabrication processes and materials, and (iii) performance assessment. The design section displays computational tools and methods for design to production of 3D printed facades. The chapter fabrication processes, materials, and applications illustrates the technology potential for facade application sorted by material groups. The performance assessment section presents current approaches to evaluating and validating the performance of 3DP facades. Finally, knowledge gaps, challenges, and future trends are discussed to offer insights into leading-edge solutions for facade design and fabrication.

2.2 Introduction

Facades are among the most complex elements in a building. Besides defining the architectural expression of a building, they represent the boundary between the external and internal environment, controlling the energy flow and matter from the outside to the indoor space. For this reason, they have a considerable impact on the user's comfort, indoor spaces' environmental conditions, and the buildings' energy performance [50]. Therefore, improvements in the performance of facades are essential to meet the goals of Net Zero Emissions by 2050 [3].

To reach high levels of efficiency and functionality, current facades are be-

[50]: GhaffarianHoseini et al. (2013), 'Intelligent Facades in Low-Energy Buildings'

[3]: Delmastro et al. (2022), *Building Envelopes – Technology deep dive*

ing reevaluated. The focus is to develop integrated building components tailored to the building's use, services, location, and orientation [39]. Conventional facades typically have standardized and homogeneous properties as they are assembled using multiple standardized, mass-produced components. This fact limits their ability to be tailored to their specific environmental conditions and their recyclability. A fundamental shift towards site-specific facades would offer novel opportunities for air tempering, improving indoor air quality, and electrical energy production [51]. Moreover, it holds great potential for reducing the energy demand, up to 30% (depending on specific climate and building type [52, 53]) and improving indoor comfort. 3DP printing has the potential to propel this development as it allows for the creation of multifunctional, bespoke elements in a mono-material construction.

[39]: Aelenei et al. (2016), 'Adaptive Façade'

[51]: Juaristi et al. (2018), 'Qualitative analysis of promising materials and technologies for the design and evaluation of Climate Adaptive Opaque Façades'

[52]: Favoino et al. (2015), 'The optimal thermo-optical properties and energy saving potential of adaptive glazing technologies'

[53]: Sheikh et al. (2019), 'Adaptive biomimetic facades'

2.2.1 Site-Specific Facades

Site-specific facades are high-performance systems that can improve the overall building performance. These improvements can be achieved by site-specific construction or using active adaptive facade systems [54, 55]. Compared to traditional systems, they require advanced control over their design, engineering, fabrication, and operations. Often, their multiple performances and operating mechanisms are facilitated by several functional layers [56], with increased complexity and sophistication of the facade systems [57]. Moreover, it poses a challenge to circularity and positive end-of-life of the components if multi-material systems are connected/assembled in a non-reversible manner. For this reason, next-generation facades are required to integrate the multiple performative aspects with a clear design-to-disassembly strategy or create mono-material elements to reach a sustainable outcome.

[54]: Loonen et al. (2013), 'Climate adaptive building shells'

[55]: Romano et al. (2018), 'What is an adaptive façade?'

[56]: Zhao et al. (2019), 'Shape and Performance Controlled Advanced Design for Additive Manufacturing'

[57]: Rosen et al. (2015), 'Special Issue'

2.2.2 3D Printed Facades

The idea of adding multiple performances in a facade is far from new to architecture. Vernacular examples of traditional architectural types show a deep understanding of the role of facades as mediators between the interior and the exterior. More recently, in 1978, British Architect Mike Davies proposed the innovative concept of an integrated polyvalent wall, which has multiple performances in a single element [5]. This facade draws inspiration from nature and process regulation in biological forms. For many years, however, technological gaps have prevented integrated climate-specific facades from being considered a viable alternative for the construction industry. This is because such facades were difficult to manufacture, maintain, repair, and recycle [58, 59].

[5]: Davies et al. (1981), 'A wall for all seasons'

Only recently, advancements in material sciences, manufacturing, and computational methods opened up a new set of opportunities to build integrative climate-specific facades. Among these, 3D printing (3DP) is an emerging fabrication technique that enables the production of customizable components. The free-form design combined with the efficient and optimized placement of material through 3DP opens up the possibility for integrating multiple functionalities/performances in a single element [60, 61]. Additionally, design freedom fosters the use of integra-

[58]: Attia et al. (2018), 'Current trends and future challenges in the performance assessment of adaptive façade systems'

[59]: Loonen et al. (2017), 'Review of current status, requirements and opportunities for building performance simulation of adaptive facades'

[60]: Strauß (2013), 'AM Envelope: The potential of Additive Manufacturing for façade construction'

[61]: Leung et al. (2019), 'Challenges and Status on Design and Computation for Emerging Additive Manufacturing Technologies'

tive design approaches with a closer interdependency between design, material, performance, and fabrication. Consequently, a customizable performative geometry can be 3DP from a mono-material, which is easier to disassemble and recycle at the end of its life cycle. Moreover, seamless design-to-fabrication workflows provide new opportunities for reducing development time and cost, and increasing performance and profitability [62]. Mass customization can be potentially achieved at no additional cost, contrary to most traditional manufacturing techniques, for which economic feasibility relies on large batch production [63]. Therefore, 3DP offers the potential to materialize context-specific and high-performance facades with novel aesthetics [64]. Material efficiency, low waste in additive manufacturing, and the availability of low-embodied-energy materials are promising solutions from a sustainability perspective [6, 65]. Moreover, the performance integration into a mono-material component can overcome the recycling challenges, common to conventional facades.

[62]: Seepersad (2014), 'Challenges and Opportunities in Design for Additive Manufacturing'

[63]: Hauschild et al. (2011), *Digital Processes Planning, Designing, Production*

[64]: Paoletti (2017), 'Mass Customization with Additive Manufacturing'

[6]: Agustí-Juan et al. (2017), 'Environmental design guidelines for digital fabrication'

[65]: Agustí-Juan et al. (2017), 'Integration of environmental criteria in early stages of digital fabrication'

2.2.3 Scope and Methodology

We define the scope of this review paper considering a broad meaning of the term facade. Facades are those vertical construction elements that form the division between inside and outside environments. This includes large-scale facade systems, such as concrete 3DP walls, single facade panels, like in polymer 3DP, up to small-scale elements, like bespoke metal connections and ceramic tiles, tackling either one or multiple functional requirements of building facades on different scales. After defining the scope, the review process consisted of four steps. The first step was a comprehensive literature search based on the combination of keywords referring to the facade domain, such as "facade", "building envelope", "cladding", "wall" and "enclosure", and to the 3DP domain, such as "3D printing", "additive manufacturing" and "digital fabrication". Scopus was used as the main search database. The second step entailed a check on the title and abstracts of the selected articles to exclude irrelevant material. The third step was an extensive analysis of the selected articles in order to develop a meaningful categorization system. As a result of this step, the literature was categorized into three main groups focusing on 1) the design of 3DP facades, 2) fabrication processes, materials, and applications 3) the performance assessment of 3DP facades. The fourth and last step consisted of an extension and refinement of the literature search based on the identified categories.

The corpus of reviewed studies covers approximately 200 items, the majority being peer-reviewed journal articles, book chapters, and a few conference contributions. Given the novelty of the research field, the review search was not limited to scientific articles but also included websites, web articles, and architecture magazines. The reviewed contributions belong to the domains of architecture, engineering, and material science (see fig. 2.2.a.), and the average year of publication is 2019 (see fig. 2.2.b.). Apart from a few old publications, the majority of articles date to the last four years, and the highest number of publications is from 2020, demonstrating growing research interest in 3DP of building facades.

To the present day, comprehensive summaries of 3DP for the construction sector exist [66–68]. However, these publications evolve mostly around the

[66]: Delgado Camacho et al. (2018), 'Applications of additive manufacturing in the construction industry – A forward-looking review'

[67]: Ngo et al. (2018), 'Additive manufacturing (3D printing)'

[68]: Labonnote et al. (2016), 'Additive construction'

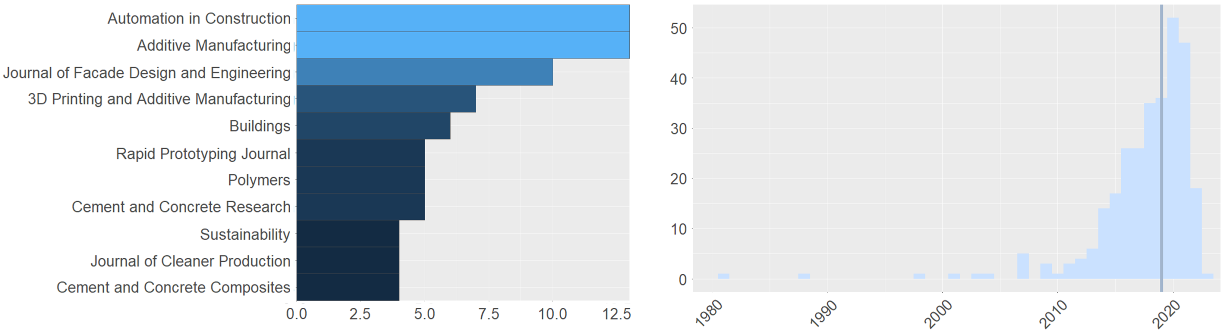

Figure 2.2: Bibliometric analysis on reviewed literature. a) Most sidecited journals: the reviewed articles cover a variety of disciplines from construction, to manufacturing up to specific material system (concrete and polymers). b) Publication year: the majority of reviewed articles were published in the last four years and represent a growing research interest.

topic of fabricating free-form design, large-scale structural components, or in-depth technological details, without offering a comprehensive overview of 3DP facades. Only one facade-specific review paper exists [33]. None of these reviews, however, encompasses the entire process chain from design to production, to performance evaluation of 3DP facades, explores the relationship between these aspects and critically evaluates them. This review paper closes this gap by providing an extensive overview of the latest developments in the design, fabrication, and assessment methodologies of 3DP facades. We present the state-of-the-art and highlight the key challenges, research gaps, and future opportunities. Different 3DP methods are categorized by material group, with the aim of identifying the most relevant for the facade application. The manuscript is structured as follows:

[33]: Naboni et al. (2022), 'Additive manufacturing in skin systems'

- Section 1 introduces the research motivation and relevance for the construction industry.
- Section 2 presents the most prominent design approaches for 3DP facades, by elaborating on the topic of computational design and performance integration.
- Section 3 focuses on material and fabrication processes. For each material group, the latest developments in regard to fabrication and performance integration are presented. Each subchapter is concluded with knowledge gaps, future opportunities, and research trajectories.
- Section 4 presents the performance assessment strategies for 3DP facades. Simulation and life cycle analysis are identified as essential elements when designing and building 3DP facades. Additionally, the challenges of performance validation for 3DP facades through experimental prototyping are listed.
- Section 5 concludes the presented sections highlighting challenges, limitations, and future opportunities.

2.3 Design for 3DP facade

3DP or additive manufacturing (AM) offers novel opportunities in terms of geometrical freedom and complexity. Along with these opportunities,

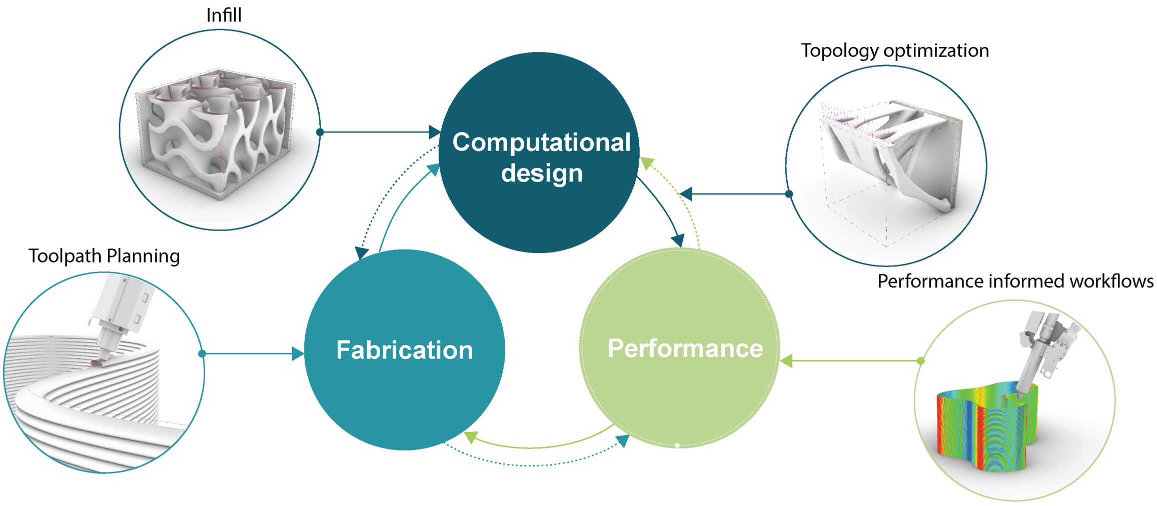

Figure 2.3: DFAM methodologies for 3D printed facades. Topology Optimization, Infill Design, Toolpath Planning, and Performance informed workflows.

comes also the challenges of designing for 3DP processes. Traditional design tools and methods are not adequate for such complex production processes [62]. Therefore, novel design methodologies are required for 3DP facades. Such methodologies have to consider a seamless integration of 3D printing parameters and performative aspects of the facades in the design process. These performances can be structural, thermal, acoustic, and daylighting. Then, to fabricate these performance-informed designs, the computational tools have to incorporate the material and fabrication processes. Therefore, designing for additive manufacturing (DFAM) of 3DP facades is a novel methodology, which requires an integrative process between the computational design, material and fabrication, and environmental performance integration, see Figure 2.3 [57].

[62]: Seepersad (2014), 'Challenges and Opportunities in Design for Additive Manufacturing'

[57]: Rosen et al. (2015), 'Special Issue'

2.3.1 Computational design

The design of a 3DP facade is a complex task due to the multitude of fabrication and environmental parameters required to be integrated into the process. For this reason, computational tools are imperative for accommodating the increased complexity. Such tools should account for the relations between multiple design variables, such as environmental performances in an iterative generation of design alternatives [69]. Parametric design can offer iterative solutions by employing computational tools such as Grasshopper (GH) [70], and Dynamo [71], which are directly integrated into a 3D modeling software. Furthermore, parametric design is often coupled with performance optimization tools that facilitate the exploration of optimized 3DP facade designs. Moreover, with the increased computational experience of architects and engineers, engaging with

[69]: García-Dominguez et al. (2020), 'Integration of Additive Manufacturing, Parametric Design, and Optimization of Parts Obtained by Fused Deposition Modeling (FDM). A Methodological Approach'

[70]: McNeel (2021), *Grasshopper, Algorithmic Modeling for Rhino*

[71]: (2021), *Dynamo*

Application Programming Interfaces (APIs) and Software Development Kits (SDKs) has brought new flexibility to modeling software.

One of the most unique features of AM is the possibility to design and fabricate infill. Parts can be designed as a combination of a solid outer shell and a porous internal articulation, as opposed to fully solid parts (Figure 2.3.b.) [69]. Infill structures can be designed to decrease the weight of 3DP parts and improve their performance by enhancing the material's base properties [72]. For application in facades, these infills have the potential to be optimized and customized for specific boundary conditions and environmental performance requirements [73]. Some of the methods of modeling them are through cellular geometries or lattice structures [74]. These geometries are often defined by periodic repetition of unit cells or interconnected networks of struts, see Figure 2.3 [75, 76]. A major design challenge of these infill structures is their digital representation. Most commercial CAD software tools for AEC are based on boundary representation (BRep). BRep is defined by a solid shape, as a collection of connected surface elements [77].

[69]: García-Dominguez et al. (2020), 'Integration of Additive Manufacturing, Parametric Design, and Optimization of Parts Obtained by Fused Deposition Modeling (FDM). A Methodological Approach'

[72]: Gibson (2003), 'Cellular Solids'

[73]: Craveiro et al. (2020), 'An automated system for 3D printing functionally graded concrete-based materials'

[74]: Tao et al. (2016), 'Design of lattice structure for additive manufacturing'

[75]: Naboni et al. (2019), 'Bone-inspired 3D printed structures for construction applications'

[76]: Materialise et al. (2021), *The Spider Bracket*

[77]: Mäntylä (1988), *An introduction to solid modeling*

While BRep representation is advantageous for subtractive manufactured objects, it comes short for 3DP applications, particularly, for cellular structures, due to their shape complexity [78]. This is because, BRep are defined as collections of surfaces that can end up with mismatches, discontinuities, self-intersections, and non-orientable faces in complex designs [79]. Therefore, a solution for building complex cellular geometries is implicit or volumetric modeling (VM). In VM, geometries are built by function representation (FRep) instead of BReps. Geometric operations and transformations are defined mathematically, and objects are only generated in the final step, for rendering or export [80]. This approach results in a faster computational process and minimal requirement for post-processing. Commercial software packages such as Ntopology [81] or spherene [82] have been developed to specifically aid the design of 3DP cellular and lattice structures. Additionally, open-source plug-ins such as Axolotl [83] are integrated in the Grasshopper parametric modeling environment, which makes the process available to a wider public.

[78]: Gibson et al. (2021), 'Design for Additive Manufacturing'

[79]: Bernhard et al. (2018), 'Volumetric modelling for 3D printed architecture'

[80]: Kladeftira et al. (2020), 'Redefining Polyhedral Space Through 3D Printing'

[81]: ntopology (2021), *nTopology. Next-Generation Engineering Design Software*

[82]: (2022), *Spherene AG.*

[83]: DBT (2021), *Axolotl*

2.3.2 Performance integration

Integrating performance indicators in the computational design is essential to building a site-specific, sustainable, and cost-efficient 3DP facade. These performance indicators can be integrated with optimization tools that incorporate environmental parameters, such as daylight, as well as structural strength, thermal, and acoustic parameters. To integrate environmental performance aspects in the design process, several climate-specific factors have to be considered. For example, Craveiro et al. [73] displayed how 3DP fabrication parameters of concrete walls can include a material design module with different types of cork-concrete aggregates. The aggregate has thermo-mechanical performance assigned to discrete parts of the geometry. Additionally to thermal performance, cost and fabrication efficiency can also be included as performance indicators in the design process [84]. Mostafavi et al. [85] presented a design workflow for optimized material distribution in a robotic fabrication process. Similarly, Naboni et al. [86] developed an algorithmic design workflow for mate-

[73]: Craveiro et al. (2020), 'An automated system for 3D printing functionally graded concrete-based materials'

[84]: Kontovourkis et al. (2020), 'Robotic additive manufacturing (RAM) with clay using topology optimization principles for toolpath planning'

[85]: Mostafavi et al. (2016), 'Materially Informed Design to Robotic Production'

[86]: Naboni et al. (2019), 'Multi-scale design and fabrication of the Trabeculae Pavilion'

rial and structural topological optimization on multiple interdependent scales in the Trabeculae Pavilion.

To optimize the 3DP facade design, material efficiency is a fundamental feature in the fabrication process. Together with the use of low-embodied energy materials, the optimization of material distribution is a major design direction in the challenge of the building sector decarbonization. Topology optimization (TO) is an optimization method that combines a numerical solution method, such as Finite Element Analysis (FEA), with an optimization algorithm that iteratively improves the material distribution within the design space, given a set of boundary conditions and loads [87] (Figure 2.3). Several studies demonstrated the synergies between TO and material design as 3DP allows the fabrication of components with intermediate densities and material properties [88, 89]. Application of TO to the design of facade components can be found in metal 3D printed connections with optimized material use and wall components where structural optimization results in voids and cavities. Those can integrate additional environmental performances such as thermal insulation, soundproofing, and embedded utilities [90, 91]. Moreover, Kontovourkis et al. [84] explored topology optimization principles for toolpath planning in robotic additive manufacturing (RAM) of clay walls.

Nevertheless, there is a lack of complete software packages that combine DFAM features with TO methodologies [88]. Manufacturing constraints and parameters such as dimensional accuracy, printable overhang, need for support material, and printing time are often accounted for at a later stage of the design as a rationalization process of the initial optimized design [92]. Such solutions are often application-specific and lack generalizability. A few commercial software options, such as Optistruct [93] incorporate 3DP constraints, lattice designs, and TO procedures. However, the geometry complexity of these parts is often such that an intermediate step of simplification and smoothening is needed before the geometry can be transformed into a mesh for fabrication, as for the Spider Bracket [76] or the Acoustic Mirrors [94]. Another challenge of TO is the material properties description and validation of the entire topologically optimized part and the 3D printed material. Additional efforts towards the establishment of standard testing protocols and material property databases are needed, along with real-time monitoring of the production processes to correlate printing factors and part properties [66]. These aspects are especially crucial for facade application as behaviors observed on a smaller scale need to be validated for large-scale components. Yet, the advantage of TO is that it could potentially scale up from the design of structural nodes to that of entire facade panels. Paoletti et al. [95] describes the possibility of generative TO for the optimal material organization according to wind load compliance and stiffness. Moreover, since building facades are inherently multi-functional components, the multi-objective TO, combining structure with thermal control and daylighting, represents a promising design approach. Finally, for application in facades, TO should embed additional safety levels or redundancies to make the optimized design robust to disturbance events such as unanticipated or exceptional loading cases and human factors [96].

TO can work synergistically with infill design to materialize variable-

[87]: Munk et al. (2015), 'Topology and shape optimization methods using evolutionary algorithms'

[88]: Panesar et al. (2018), 'Strategies for functionally graded lattice structures derived using topology optimisation for Additive Manufacturing'

[89]: Laghi et al. (2020), 'Computational design and manufacturing of a half-scaled 3D-printed stainless steel diagrid column'

[90]: Gosselin et al. (2016), 'Large-scale 3D printing of ultra-high performance concrete – a new processing route for architects and builders'

[91]: Buswell et al. (2007), 'Freeform Construction'

[84]: Kontovourkis et al. (2020), 'Robotic additive manufacturing (RAM) with clay using topology optimization principles for toolpath planning'

[88]: Panesar et al. (2018), 'Strategies for functionally graded lattice structures derived using topology optimisation for Additive Manufacturing'

[92]: Hassani et al. (2020), 'Rationalization algorithm for a topologically-optimized multi-branch node for manufacturing by metal printing'

[93]: (2021), *Optimization-enabled Structural Analysis - Altair OptiStruct*

[76]: Materialise et al. (2021), *The Spider Bracket*

[94]: Kladeftira et al. (2018), 'Printing Whisper Dishes. Large-scale binder jetting for outdoor installations'

[66]: Delgado Camacho et al. (2018), 'Applications of additive manufacturing in the construction industry – A forward-looking review'

[95]: Paoletti et al. (2018), 'Adaptive Façades and Topology Optimization'

[96]: Rodrigues da Silva et al. (2023), 'Hyperstatic and redundancy thresholds in truss topology optimization considering progressive collapse due to aleatory and epistemic uncertainties'

density components. A common approach is to design infill structures with a chosen base shape to periodically fill the component's volume following a density map derived by TO [97]. For example, Naboni and Kunic [75] propose a computational approach to design nature-inspired cellular structures for materially efficient facade components. They also show how to use TO and porous structures to design structurally efficient objects that meet the 3DP constraints. The Spider Bracket features a topologically optimized overall shape consisting of solid parts and variable density lattice structures for reduced compliance and improved thermal behavior [76].

[97]: Liu et al. (2018), 'Current and future trends in topology optimization for additive manufacturing'

[75]: Naboni et al. (2019), 'Bone-inspired 3D printed structures for construction applications'

[76]: Materialise et al. (2021), *The Spider Bracket*

Along with performance indicators, economy, printing time, and process efficiency are also relevant criteria for displaying the full potential of 3DP facades [75],[85]. Sustainability aspects, such as the components' life-cycle energy and carbon intensity, must also be included in DFAM.

[75]: Naboni et al. (2019), 'Bone-inspired 3D printed structures for construction applications'

[85]: Mostafavi et al. (2016), 'Materially Informed Design to Robotic Production'

2.3.3 Fabrication informed design

Material and fabrication methods are essential parameters for fabricating a 3DP facade from a virtual design into a physical prototype. The process by which material behavior, fabrication parameters, and geometry are integrated into the computational design method is known as toolpath planning, or slicing (see Figure 2.3). Slicing is the process of contouring a 3D model of the final object (e.g., STL file format) into its individual layers [68]. From this layer-based information, the final tool path, such as a G-Code, is created. Mature 3DP processes create fabrication data and toolpaths using proprietary slicing software. Some slicing software supports a novel data format, called Additive Manufacturing File (AMF). AMF contains additional information compared to a standard-triangulation file format. Print paths are often created based on customized computational tools for novel processes, such as concrete 3DP or large-scale polymer extrusion. The toolpath can be defined with a Robot Code, such as RapidCode or KRL, that contains the print path, tool orientation, speed, and acceleration.

[68]: Labonnote et al. (2016), 'Additive construction'

For facade elements, toolpath planning plays a key role in environmental performance. This is because performance is highly dependent on the layer-to-layer bonding, irrespective of the 3DP method, [30, 56]. Ashrafi et al. [98] investigated the effect of layer properties, number of contours, and printing time on the deformation of large 3D-printed concrete elements. By testing different samples, material behavior, such as geometry deformation and accuracy, was strongly correlated to the toolpath design. Although slicing plug-ins such as Silkworm [99] exist, in most applications, custom-made scripts are created to tune printing parameters and robotic motion. Kontovourkis et al. [84] developed a parametric-integrated algorithm to generate contour polylines by slicing any geometry and offsetting them according to the printing parameters (layer height and width). Their algorithm generates different infill geometries, based on the required density, and sorts the resulting polylines to minimize the robotic movement during printing and non-printing motions. Molloy and Miller [100] explored the potential of freeform 3DP through direct toolpath planning and not relying on layer-based slicing software. Their direct toolpath planning allowed them to print spatially, overcoming the traditional 2.5D printing approach. While planar slicing

[30]: Duty et al. (2017), 'Structure and mechanical behavior of Big Area Additive Manufacturing (BAAM) materials'

[56]: Zhao et al. (2019), 'Shape and Performance Controlled Advanced Design for Additive Manufacturing'

[98]: Ashrafi et al. (2021), 'Experimental prediction of material deformation in large-scale additive manufacturing of concrete'

[99]: (2012), *Silkworm*

[84]: Kontovourkis et al. (2020), 'Robotic additive manufacturing (RAM) with clay using topology optimization principles for toolpath planning'

[100]: Molloy et al. (2018), 'Digital Dexterity. Freeform 3D Printing through Direct Toolpath Manipulation for Crafted Artifacts'

is a robust and simple technique, more advanced slicing methodologies such as multi-axis, multi-directional, and adaptive slicing are being investigated to mitigate the stair-step effect and minimize the need for support structures [56, 101].

[56]: Zhao et al. (2019), 'Shape and Performance Controlled Advanced Design for Additive Manufacturing'
[101]: Mitropoulou et al. (2020), 'Print Paths Key-framing'

To summarize, the method of designing and building a 3DP facade has to consider an interlinked process of computational design, performance integration, and fabrication constraints. However, such methodologies need a large number of iterations and evaluations in the design process to identify optimized solutions. Complete software packages, such as Ansys and 3D Experience, provide tools for geometry preparation, TO procedures, FEA, validation, and printing process simulation. However, these packages are not yet designed for large-scale applications; therefore, custom software needs to be further developed for the application of 3DP facades. Such workflows are usually project-specific, and the AEC sector would benefit from the establishment of informed design approaches with general applicability. Essential in this approach is also to provide open access to tools and design methodologies to propel knowledge and methods transfer between different disciplines within and outside the AEC sector [61], [102]. Finally, a database of fabrication processes and material properties would allow a comprehensive overview of the 3DP facade design potential.

[61]: Leung et al. (2019), 'Challenges and Status on Design and Computation for Emerging Additive Manufacturing Technologies'

[102]: Lopez Taborda et al. (2021), 'Design for additive manufacturing'

2.4 Fabrication, Materials, and Applications

The following chapter presents a state-of-the-art of 3DP technologies for facade application, sorted by material groups. This section displays studies and projects which aim to manufacture performative facade components with varying degrees of complexity. The focus of this section is to identify the implications of fabrication technology and material on the design and manufacturing of 3DP facades. We discuss the benefits and challenges connected to each technique and highlight their potential for creating performative facade components.

2.4.1 Thermoplastics

Polymers can be 3D printed with a wide variety of processes, such as material extrusion, Stereolithography, Multi Jet Fusion, PolyJet, Selective Laser Sintering, and Digital Light Processing. These processes use different polymer base materials to create 3D geometry, ranging from small to large-scale applications. This paragraph focuses on material extrusion processes that use thermoplastic polymers to create three-dimensional objects. The major benefit of this technology is that it is the only 3DP technology that can create translucent, nearly transparent components at a large scale. For a more detailed review of other AM methods of polymers, please refer to [103]. Thermoplastic extrusion uses filaments or granular polymer materials as feedstock for 3D printing. The largest thermoplastic extrusion setup can be currently found at Thermwood (30 x 6.7 x 3 m) [104]. Those systems are relevant for architecture, because of

[103]: Arefin et al. (2021), 'Polymer 3D Printing Review'

[104]: Thermwood (2023), *Thermwood LSAM - Large Scale Additive Manufacturing*

their fabrication size, material output (up to 68.0 kg/hr), and competitive pricing. Furthermore, an increasing number of pellet extruder providers, such as CEAD, MassivDimension, and Pulsar, offer easier access at a competitive cost to large-scale thermoplastic 3D printing.

Table 2.1: Thermoplastic 3DP for facade application.

Description	Image
Research projects	
3DP shading devices. 2016 *Additive Manufacturing for daylight. Towards a customized shading device* [105]. Delft University of Technology. Digital framework for the design of 3d printed daylighting and shading devices.	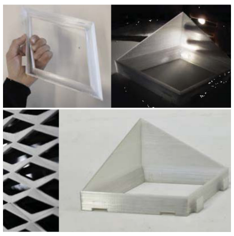
Fluid Morphology. 2017. *Fluid Morphology – 3D-printed functional integrated facade* [40]. Technical University of Munich (TUM). Research on monomaterial functional integrated facade with a large-scale outdoor prototype.	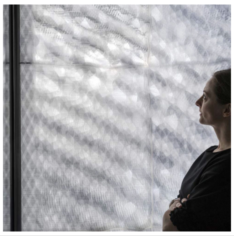
Sponge 3D. 2017. *Developing an integrated 3D-printed facade with complex geometries for active temperature control* [106]. Delft University of Technology. Investigations on closed cellular structures for thermal insulation in a thermoplastic 3D printed facade.	
Double Face 2.0. 2018. *Double Face 2.0 A lightweight translucent adaptable Trombe wall* [107]. Delft University of Technology. 3D printed Trombe wall for passively reducing the energy demands of buildings. Combining polymer 3D printing with phase changing materials (PCM).	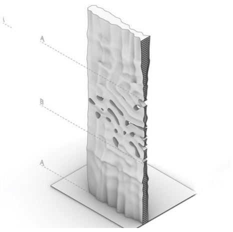
Artificial aging tests of 3DP shading elements. 2019. *Fabrication and durability testing of a 3D printed facade for desert climates* [108]. Politecnico di Milano. Artificial aging tests of thermoplastic 3D printed shading elements. Testing different materials and objects of different size.	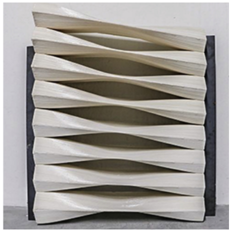

Description	Image
Digital Composites. 2019. *Digital Composites: Robotic 3D Printing of Continuous Carbon Fiber-Reinforced Plastics for Functionally-Graded Building Components* [109]. ETH Zurich. Addon 3D printing of continuous carbon fibers on polymer 3D printed elements.	
Infill design for insulating facade. 2020. *Performance-Driven Approach for the design of cellular geometries with low thermal conductivity for application in 3D-printed facade components* [110]. Delft University of Technology. Development of a digital workflow to design to optimize thermal insulation of 3DP facades.	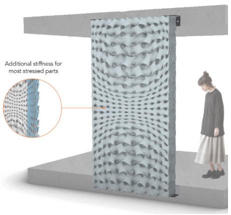
Facade prototype. 2020. *Large-scale 3D Printing for Functionally-Graded Facade* [111]. ETH Zurich. Research on connections, infill design and prototyping using different large-scale 3D printing setups.	
Super Composite. 2021. *Super Composite: Carbon Fibre Infused 3D Printed Tectonics* [112]. Royal Melbourne Institute of Technology. Centre for Innovative Structures and Materials, RMIT University. Carbon reinforced components to overcome weak layer-bonding.	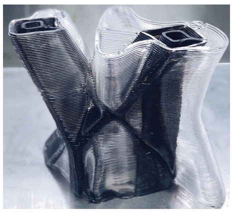
Applied research projects	
Europe Building. 2015. *Europe Building*, 300m2 3DP facade for mobile event/-conference space [113]. DUS Architects, Netherlands.	
Urban Cabin. 2015. *Urban Cabin.* Polymer 3D printed facade in combination with cast concrete [114]. DUS Architects, Netherlands.	

Description	Image
AMIE. 2016. *Additive Manufacturing Integrated Energy—Enabling Innovative Solutions for Buildings of the Future* [115]. Oak Ridge National Laboratory, The University of Tennessee, Skidmore, Owings & Merrill LLP. Development and fabrication of a compact housing using large-scale polymer extrusion.	
Sensilab Studio. 2020. *Printed Assemblages, a Co-Evolution of Composite Tectonics and Additive Manufacturing Techniques* [116]. RMIT University, Studio Roland Snooks. Large-scale polymer 3D printing for indoor application.	

One of the main challenges of thermoplastic 3DP is the anisotropic mechanical behavior [30, 117]. The printing direction has a large impact on the structural properties and, therefore, its final use case. In order to overcome weak layer bonding, the project Cloud Effects from Studio Roland Snooks [112] integrates channels in the 3DP elements that are infused with continuous carbon fiber, after assembly into a larger structure. Other projects rely on a substructure to take all critical loads or are not intended for outdoor applications. Post-tensioning of elements as shown by Biswas et al. [115] as a viable method of reinforcing the final geometry. A more speculative approach has been investigated by Kwon et al. by addon-3D printing continuous carbon fiber strands onto thermoplastic 3DP components [109].

Researchers have been increasingly investigating thermoplastic 3DP for functional facade applications in the past decade. Researchers from TU Delft developed a digital workflow in the Rhinoceros-Grasshopper environment to design 3DP thermoplastic facades with internal cellular structures to optimize thermal insulation [110]. Results were generated using FEA simulations and calibrated by empirical data from standardized heat flow meter tests. It was shown that a mono-material 3D printed facade can be created with a 29 cm thick panel complying with the thermal insulation requirements of the Dutch building code. ETH Zurich researchers showed how a computational design tool can be used to manipulate the infill structure of 3DP facades [111]. Furthermore, they provided initial investigations on how a 3DP facade can be discretized and assembled using 3DP connection details. Sarakinioti et al. investigated closed cellular structures for thermal insulation in a thermoplastic 3DP facade using an experimental 'hot-box' set-up [106]. The authors showed that by using a low-conductivity (PETG) material and specific cellular structures, high-performance thermal insulation could be achieved.

Researchers focus also on using translucent/transparent thermoplastic materials for creating functional prototypes at an architectural relevant scale, see Table 2.1. A study at TU Delft investigated a multifunctional 3DP facade to account for annual seasonal variations in temperature

[30]: Duty et al. (2017), 'Structure and mechanical behavior of Big Area Additive Manufacturing (BAAM) materials'

[117]: Torrado et al. (2015), 'Characterizing the effect of additives to ABS on the mechanical property anisotropy of specimens fabricated by material extrusion 3D printing'

[112]: Mohamed et al. (2021), 'Super Composite'

[115]: Biswas et al. (2017), 'Additive Manufacturing Integrated Energy - Enabling Innovative Solutions for Buildings of the Future'

[109]: Kwon et al. (2019), 'Digital Composites'

[110]: Piccioni et al. (2020), 'A Performance-Driven Approach for the Design of Cellular Geometries with Low Thermal Conductivity for Application in 3D-Printed Façade Components'

[111]: Taseva et al. (2020), 'Large-Scale 3D Printing for Functionally-Graded Facade'

[106]: Sarakinioti et al. (2018), 'Developing an integrated 3D-printed façade with complex geometries for active temperature control'

[106]. The concept uses air cavities and a water-based working fluid to insulate and regulate heat flows through the facade. Tenpierik et al. investigate the possibility of combining phase-changing materials (PCM) with thermoplastic 3DP elements to create a Trombe wall [107]. They used computational fluid dynamics (CFD) models to simulate phase change materials encapsulated in 3d printed thermoplastic facades for thermal control. However, the challenge of using phase changing materials in combination with currently available 3DP thermoplastics is two-fold: a) the 3DP parts might not always be watertight and therefore the liquid PCM can escape the object, and b) the heat released from the PCMs might deform the thermoplastic shell due to the material's low glass-transition temperature. The authors concluded that creating smaller, stacked, PCM modules ensured less convective heat transfer in the vertical direction. The authors concluded that creating smaller, stacked, PCM modules ensured less convective heat transfer in the vertical direction.

[106]: Sarakinioti et al. (2018), 'Developing an integrated 3D-printed façade with complex geometries for active temperature control'

[107]: Tenpierik et al. (2018), 'Double Face 2.0'

A multi-performative approach was investigated by Mungenast on 3D printed, mono-material (PETG), and multifunctional facade prototypes [40]. Mungenast concluded the following: (i) layer alignment and inner 'infill' structures heavily influence structural failure; (ii) self-shading geometries and internal cellular structures should be simulated and designed to avoid facade overheating, to optimize daylight transmission, and thermal insulation; (iii) UV testing resulted in discoloration; (iv) lack of water tightness and presence of dust during the printing process led to condensation and algae formation. Grassi et al. prototyped a facade shading system for hot-dry climate conditions using high-temperature resistant thermoplastic (Polylactic acid, PLA) with additives [108]. They performed accelerated aging for durability testing (Temperature, UV resistance) using the Reference Service Life method and concluded that pure PLA shows better durability than fiber-reinforced (delamination) and metal-colored PLA. Karagianni et al. developed a performance-informed digital framework for the design of 3DP daylighting and shading devices. These are fabricated using small-scale thermoplastic 3D printers and snap-fit connection allows for an easy assembly [105]. With "SensiLab Studio"(2017) and the project at "RMIT school of design" (2020) [116] Studio Roland Snooks showcased large-scale thermoplastic 3DP for indoor applications, passing indoor fire and building regulations in Australia. DUS architects created the facade for a temporary pavilion for the European Union using bioplastics [113]. The printed elements were partly used as a lost formwork for concrete. A similar approach was taken for the Urban Cabin, a 25 cubic meter large cabin that was entirely 3D printed out of biodegradable thermoplastics [114]. In a collaborative research project, the Oak Ridge National Laboratory (ORNL) has created the AMIE, the Additively Manufactured Integrated Energy project [115]. The facade prototype (10.9m x 3.6m x 4.2m) is constructed from multiple thermoplastic 3DP structural elements, which are insulated using low-cost vacuum insulation pads. In another project, the ORNL used thermoplastic 3DP formwork for casting bespoke concrete facade panels [118].

[40]: Moritz Basil Mungenast (2019), '3D-Printed Future Facade'

[108]: Grassi et al. (2019), 'Fabrication and durability testing of a 3D printed façade for desert climates'

[105]: Karagianni et al. (2016), 'Additive Manufacturing for daylight: Towards a customized shading device'

[116]: Snooks et al. (2020), 'Fabricate 2020'

[113]: DUS (2015), *Europe Building – DUS Architects*

[114]: DUS Architects (2015), *Urban Cabin*

[115]: Biswas et al. (2017), 'Additive Manufacturing Integrated Energy - Enabling Innovative Solutions for Buildings of the Future'

[118]: Burke (2019), *3D printing shapes building industry, creates rapid construction potential | ORNL*

Thermoplastic 3DP has been successfully scaled up to facade application. Furthermore, they allow for mono-material facade solutions which can have a positive impact on their sustainability. Although thermoplastics has been recently used for real-scale projects, further research needs to tackle topics such as thermal insulation, the reaction to fire and fire propagation, UV resistance, optical properties, and connection details. Additionally, thermoplastic 3DP facades' transmissive properties and their potential solar gains require further investigation. The argument for mono-material, multifunctional 3DP polymer facades need to be further strengthened by investigations on sustainability aspects. It has been shown that, depending on the method of recycling, thermoplastics can be recycled up to 5 times without severely affecting the thermomechanical properties [25]. Other studies show that recycling always goes in hand with the degradation of material characteristics [23, 24]. However, these studies directly recycle the specimens after testing them and do not consider the lifecycle of a facade, or the aging behavior due to UV radiation. Only by understanding the material lifecycle and the facades' environmental and performative aspects, can holistic design approaches toward mono-material 3DP thermoplastic facades be formulated.

[25]: Vidakis et al. (2021), 'Sustainable Additive Manufacturing'

[23]: Latko-Durałek et al. (2019), 'Thermal, Rheological and Mechanical Properties of PETG/rPETG Blends'

[24]: Anderson (2017), 'Mechanical Properties of Specimens 3D Printed with Virgin and Recycled Polylactic Acid'

2.4.2 Clay-based materials

3DP of clay-based materials contains a wide variety of approaches to building environmentally friendly facades. Clay-based materials refer to clay, adobe, cob, and rammed clay [119]. These materials are generally composed of clay, gravel, sand, silt, and water, with sometimes additional fibers and stabilizers. The fabrication technique of these materials is dependent on the material type, and post-processing demands [120]. Adobe and green body clays can use material extrusion, compaction, and molding [121]. Ceramics can be manufactured in a two-step process: initially, a clay green body is digitally fabricated and then is fired in a second step for hardening. Because ceramics require a sintering process, they can be manufactured with binder jetting, digital light processing, powder bed fusion, and sheet lamination. In facade applications, 3DP of clay-based materials is advantageous because local materials can be used. These can vary from small-scale elements such as tiles or bricks to large-scale exterior walls [122]. Research on clay-based 3DP facades focuses on using local clay materials to explore novel methods for ecological wall construction, see Table 2.2 [123]. Facade elements have been investigated for several performances, such as thermal insulation, vapor permeability, mechanical strength, and construction efficiency. For example, Dubor et al. and Wasp identified how such walls can be optimized for thermal, ventilation, daylight, or structural performances [124]. Gomaa et al. concluded that the integration of air cavities and soil-straw elements in the fabrication process improved the thermal insulation of brick elements [125]. Kontovourkis et al. [84] demonstrated that toolpath planning control parameters such as 12 mm versus 4 mm layer width results in optimized settings for 3DP wall components. These researchers concluded that the printing time of bespoke wall elements with complex shapes was similar to conventional ones.

[119]: Gomaa et al. (2022), 'Digital manufacturing for earth construction'

[120]: Perrot et al. (2018), '3D printing of earth-based materials'

[121]: Wolf et al. (2022), 'Additive manufacturing of clay and ceramic building components'

[122]: Abdallah et al. (2021), '3D-Printed Biodigital Clay Bricks'

[123]: Fratello et al. (2020), 'Innovating materials for large scale additive manufacturing'

[124]: Dubor et al. (2018), 'Energy Efficient Design for 3D Printed Earth Architecture'

[125]: Gomaa et al. (2021), '3D printing system for earth-based construction'

[84]: Kontovourkis et al. (2020), 'Robotic additive manufacturing (RAM) with clay using topology optimization principles for toolpath planning'

The reasons for using adobe or clay for 3DP facade walls is because of their beneficial mechanical strength, low material costs, and low environmental impact [121]. Additionally, raw clay can be easily recyclable if they do not contain limestone and cement. Nevertheless, 3DP of adobe and clay is relevant for climates with lower relative humidity changes. This is because certain 3DP clay-based materials require additional stabilizers

[121]: Wolf et al. (2022), 'Additive manufacturing of clay and ceramic building components'

or protection to prevent material degradation from precipitation, mold, and high-temperature fluctuations in specific environments. A way to mitigate these challenges is by using ceramics as a 3DP material [126]. Ceramics, compared to clay, have appealing physical and mechanical properties, such as high-temperature strength, corrosion resistance, water tightness, high hardness, superior mechanical properties, and electrical and thermal conductivities [127]. For this reason, 3DP ceramics have been implemented for facade application in the form of modular components, such as bricks, tiles, or cladding [128]. Nevertheless, the disadvantages of these materials is that they require additional fabrication energy due to the sintering step, and they cannot be recycled and reused. Therefore, ceramics are not considered a viable solution from a sustainability perspective. An essential part of the 3DP process of clay-based materials is the computational framework. Recent research in computational design has focused on non-conventional form-finding [84]. AlOthman et al. displayed how to 3DP spatial toolpaths compared to layered deposition techniques to optimize fabrication time potentially and material use [129]. At the same time, Friedman et al. and Rosenwasser et al. incorporated weaving techniques in the 3DP process. They proved the 3DP clay potential on non-flat surfaces to reduce fabrication time [130, 131].

[126]: Travitzky et al. (2014), 'Additive Manufacturing of Ceramic-Based Materials'

[127]: Lakhdar et al. (2021), 'Additive manufacturing of advanced ceramic materials'

[128]: Cruz et al. (2020), 'Additive Manufacturing of Ceramic Components for Façade Construction'

[84]: Kontovourkis et al. (2020), 'Robotic additive manufacturing (RAM) with clay using topology optimization principles for toolpath planning'

[129]: AlOthman et al. (2019), 'Spatial Print Trajectory'

[130]: Friedman et al. (2014), 'Experiments in Additive Clay Depositions'

[131]: Rosenwasser et al. (2017), 'Clay Non-Wovens: Robotic Fabrication and Digital Ceramics'

Table 2.2: Clay-based 3DP for facade application.

Description	Image
Research projects	
Clay Non-Wovens. 2017. *Clay Non-Wovens* [131]. Cornell University, Sabin Design Lab. Woven system of porous cladding panels for natural daylighting performances.	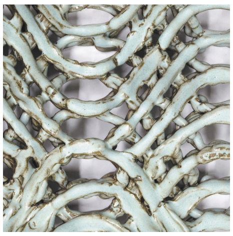
3DP earth architecture. 2017. *Energy Efficient Design for 3D Printed Earth Architecture* [124]. Institute for Advanced Architecture of Catalonia. Analysis of 3D printed mud performance and simulation for the optimization of a wall prototype.	
Spatial Print Trajectory. 2018. *old, Spatial Print Trajectory: Controlling Material Behavior with Print Speed, Feed Rate, and Complex Print Path* [129]. Harvard University. Controlling clay material behavior with 3D print speed, extrusion rate, and complex print path.	

Description	Image
Biodigital Clay Bricks. 2021. *3D-Printed Biodigital Clay Bricks* [122]. Universitat Internacional de Catalunya, Helwan University. 3D printed clay bricks.	
CO-MIDA. 2022. *CO-MIDA : Biophotovoltaic Vertical Gardens 3D Printed With Clay* [132]. Institute for Advanced Architecture of Catalonia. Ceramic modular tiles made of 3D printed clay, for growing edible plants in built environments.	
Applied research projects	
Cabin of 3D printed curiosities. 2018. *Innovating materials for large scale additive manufacturing: Salt, soil, cement and chardonnay* [123]. Emerging objects. Glazed 3D-printed ceramic cladding system that serves as a rain screen.	
New Delft Blue. 2019. *New Delft Blue* [133]. Studio Rap. Glazed ceramic tiles manufactured with material extrusion.	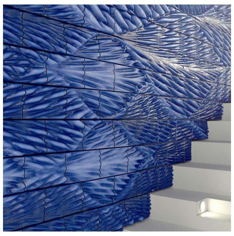
TECLA. 2021. *TECLA Technology and Clay 3D Printed House* [134]. Mario Cucinella Architects, WASP. House built with raw earth in a material extrusion process.	

Nevertheless, 3DP of clay-based materials is confronted with several fabrication challenges. High deformation is a predominant issue because of the water content and post-processing firing temperatures. For instance, shrinkage of the elements is a challenge due to water evaporation during material drying or sintering, which in turn leads to sample deformation and even cracking. The cracking of non-sintered clay constructions can be solved by filling the gaps; however, this process requires post-processing.

For facade application, water-tightness is required in specific climates, which limits the use of clay-based materials. Additionally, printing-induced defects, such as air inclusions in printed beads, reduce the structural performance of the printed object compared to conventional (e.g.rammed) elements. However, controlled air inclusions potentially have a positive impact on the thermal resistance of the printed component. 3DP of clay-based materials can be used for specific applications, to achieve environmentally friendly facade systems. Sustainability plays a key role in building 3DP clay-based facades. These materials are advantageous due to their recyclability and minor negative environmental impact. However, the challenges in the fabrication process require further exploration that can be overcome by investigations on deformation control, tensile strength optimization, and material response to the environment. Future possibilities can rely on using multiple clay body types, on making functionally-graded materials with a dual-material nozzle and adding a fourth axis to the 3DP setup [135].

[135]: Seibold et al. (2019), 'Janus Printing: Coextrusion based Multi-material Additive Manufacturing for Ceramics'

2.4.3 Concrete

In the past two decades, 3DP of concrete has gained increased attention from the research community as well as industry. The maturity of this 3DP method is showcased by the high number of start-ups (e.g., Xtree, Aeditve, COBOD, WASP) and construction companies focusing on this specific part of 3DP for AEC, such as PERI, and SIKA. Concrete can be 3DP using different approaches like extrusion-based 3DP, shotcreting, casting concrete in 3DP formwork, selected cement activation, or 3DP of foamed concrete [136]. A comprehensive overview of different fabrication methods of concrete 3DP can be found here [137]. The environmental impact of concrete 3DP is largely defined by its binding agent [138] and the construction scheme used [139]. High cement contents in 3DP concrete increase the embodied energy of the printed object, and therefore, alternative binding agents are investigated [138]. In parallel, the potential of recycled aggregates is explored [140, 141]. Major research topics of 3DP concrete, like reinforcement and challenges in regards to scaling up the process, have been investigated in depth by [142–144]. Over the past years, different trajectories for reinforcing 3DP concrete structures have been investigated. For extrusion-based concrete printing, those range from embedding a metal wire within the bead while printing [145], or shooting metal clamps through printed layers [146]. As an alternative way to 3DP concrete, shotcrete has proven to incorporate regular rebar and create load-bearing elements in an automated manner [142]. However, its application compared to extrusion-based processes is low. Bos et al. have concluded that the structural application of extrusion-based 3DCP elements is still limited due to the lack of regulatory and limited options for reinforcements [147]. Therefore contemporary projects mainly focus on either, using 3DCP elements as lost formwork for regular reinforcing and casting, or creating unreinforced masonry structures.

[136]: Furet et al. (2019), '3D printing for construction based on a complex wall of polymer-foam and concrete'

[137]: Wangler et al. (2019), 'Digital Concrete'

[138]: Bhattacherjee et al. (2021), 'Sustainable materials for 3D concrete printing'

[139]: Mohammad et al. (2020), '3D Concrete Printing Sustainability'

[138]: Bhattacherjee et al. (2021), 'Sustainable materials for 3D concrete printing'

[140]: Xiao et al. (2020), '3D recycled mortar printing'

[141]: Xiao et al. (2021), 'Fiber-reinforced mortar with 100% recycled fine aggregates'

[142]: Kloft et al. (2020), 'Reinforcement strategies for 3D-concrete-printing'

[143]: Asprone et al. (2018), 'Rethinking reinforcement for digital fabrication with concrete'

[144]: Mechtcherine et al. (2021), 'Integrating reinforcement in digital fabrication with concrete'

[145]: Bos et al. (2017), 'Experimental Exploration of Metal Cable as Reinforcement in 3D Printed Concrete'

[146]: Geneidy et al. (2020), 'Simultaneous Reinforcement of Concrete While 3D Printing'

[142]: Kloft et al. (2020), 'Reinforcement strategies for 3D-concrete-printing'

[147]: Bos et al. (2022), 'The realities of additively manufactured concrete structures in practice'

As concrete 3DP technology becomes more mature, the control over fabrication parameters is improving, researchers recently investigated topics that go beyond the free-form design and structural integrity of the facade component, see Table 2.3. For facades application, thermal resistance, sound insulation, and absorption are performances of great relevance. Research on these topics is summarized in the following paragraphs.

Table 2.3: Concrete 3DP for facade application.

Description	Image
Research projects	
3DP foam for cast concrete. 2017. *Toward site-specific and self-sufficient robotic fabrication on architectural scales* [148]. Mediated Matter Group, MIT Media Lab, Massachusetts Institute of Technology. Robotic on-site 3D printed foam as lost-formwork for concrete.	
Robotic concrete surface finishing. 2018. *Robotic concrete surface finishing: a moldless approach to creating thermally tuned surface geometry for architectural building components using Profile-3D-Printing* [149]. Carnegie Mellon University. Prototyping concrete surfaces to tune heat absorption, storage, and dissipation.	
Foamed 3DP Concrete. 2019. Ultra-lightweight foamed concrete for an automated facade application [150]. RWTH Aachen. Development of ultra lightweight foamed concrete (150kg/m3) for spraying/extruding onto vertical walls.	
3DP of lightweight concrete. 2020. *Additive Manufacturing by Extrusion of Lightweight Concrete - Strand Geometry, Nozzle Design and Layer Layout* [151]. Technical University of Munich. Investigations of nozzle design, layer layout for lightweight concrete extrusion. Addition of perlite and wood particles to improve thermal resistance.	
Thermal and sounds isolation of 3DPC. 2020. *Thermal and Sound Insulation of Large-Scale 3D Extrusion Printing Wall Panels* [152]. SCG Cement, Bangkok. Investigation on thermal and acoustic insulation of 3D concrete printed wall elements.	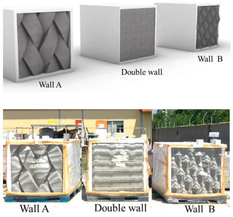 Wall A Double wall Wall B Wall A Double wall Wall B

Description	Image
Shotcrete 3D Printing. 2020. *Shotcrete 3D Printing Technology for the Fabrication of Slender Fully Reinforced Freeform Concrete Elements with High Surface Quality: A Real-Scale Demonstrator* [153]. Technical University of Braunschweig. Fully reinforced, large-scale demonstrator created using shotcrete 3D printing.	
Thermally enhanced lightweight concrete wall. 2021. *Additive Manufacturing of Thermally Enhanced Lightweight Concrete Wall Elements with Closed Cellular Structures* [154]. Technical University of Munich. Closed cellular infill structures for a thermal performant 3DP concrete facade. Customization with 2D thermal performance simulation.	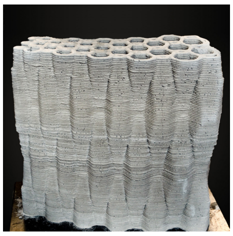
Applied research projects	
3DP foam for cast concrete. 2019. *3D printing for construction based on a complex wall of polymer-foam and concrete* [136]. University of Nantes. Robotic foam 3D printed formwork. Deviation measurement and real-world demonstrator.	
On-site concrete 3DP. 2020. *3D Concrete Printing on Site: A Novel Way of Building Houses* [155] Ghent University, Beneens Construction & Interior, Saint-Gobain Weber Beamix. 3D printed house with different insulation strategies.	

Different research trajectories have been investigating the thermal performance of 3DP concrete or how to thermally insulate the 3DP building component. For extrusion-based 3DP concrete, two main strategies are identified: i) cladding the finished component with insulation material, and ii) filling up the internal cavities with insulation material. The KampC-House showcases both examples in a real-world application [155]. In addition to that, Bard et al. [149] introduced 'thermal design' within the robotic construction of building components by connecting the behavior of airflow and heat transfer with robotic tool-path planning. The researchers used the process to prototype the surface geometry of concrete facades to tune heat absorption, storage, and dissipation. The process combined measured thermal data and simulated input with robotic manufacturing techniques. 3DP polymer foam can be used as a lost formwork for cast concrete, as a load-bearing approach for in-

[155]: Van Der Putten et al. (2020), '3D Concrete Printing on Site'

[149]: Bard et al. (2018), 'Robotic concrete surface finishing'

sulating facades [148]. A similar approach is used by Furet et al. and the company Batiprint3d where a mobile robotic arm sprays foam as a lost formwork on the construction site [136]. However, the potential health risks connected to the organic foam of these methods require an investigation of alternative solutions, such as inorganic foams [156]. Adams et al. demonstrated how concrete can be foamed in a shotcrete-3D printing approach. The research successfully identified that a concrete foam with a density of only 150 kg/m3 can be applied to vertical surfaces [150]. Although this ultra-lightweight foamed concrete mix displays good thermal performance and fire resistance, the material strength is very low and thus not suitable for facade application. Another approach to increase the thermal resistance of 3D-printed concrete is the use of lightweight additives. The research from Liu et al. used expanded perlite to replace sand in the dry mix shotcrete [157]. They proved that 75% sand substituted with expanded perlite aggregate offers superior thermal properties without compromising its mechanical performance. Additionally, Henke et al. used perlite or wood aggregates to create lightweight mixes for extrusion-based concrete 3D printing [151]. Dielemans et al. investigated cellular geometries as thermal insulation for 3D-printed concrete structures by using a design workflow that includes geometric, material, and fabrication parameters. The authors used 2d (conduction and radiation) heat transfer models and concluded that cell partitioning along the heat transfer direction improves thermal insulation by limiting convection even if the air-solid ratio decreases [154]. Similar to this research, on how the geometrical features of 3DP concrete can increase thermal resistance, Prasittisopin et al. investigate how geometrical differentiation improves acoustic properties [152]. However, this research trajectory seems to offer only limited applicability, as sound absorption can only be achieved for specific frequencies. Further research is needed to understand and improve the acoustic properties of 3DP concrete.

To conclude, concrete 3DP has the potential to create bespoke facade components. Major improvements in process and material development have made it possible to create components at an architectural scale. Nevertheless, facade-relevant topics, such as thermal and acoustics comfort, have not yet been sufficiently investigated. The manufacturing parameters of the printed component, as well as the assembly details, have a great impact on acoustics performance. The physical separation of single 3DP components needs to be investigated to holistically tackle this topic. For this reason, the topic of connections and how to accommodate thermal expansion and air-water permeability requires further investigation [158]. Nevertheless, the potential 3DP concrete for facade applications confines in successfully combining the displayed research examples. For example, a fully reinforced shotcrete wall element [153] can be combined with lightweight, thermally insulated shotcrete layers [157] that not only increase the thermal performance but have the potential to increase sound absorption and improve indoor comfort. Additionally, the fabricated geometry can be designed to enhance the thermal performance [154] to create a high-performance bespoke facade element.

2.4.4 Metal

Metal 3DP has been progressively adopted in the construction, biomedical, aerospace, automotive, and marine industries [159]. For this technique,

[148]: Keating et al. (2017), 'Toward site-specific and self-sufficient robotic fabrication on architectural scales'

[136]: Furet et al. (2019), '3D printing for construction based on a complex wall of polymer-foam and concrete'

[156]: Bedarf et al. (2021), 'Foam 3D printing for construction'

[150]: Adams et al. (2019), 'Ultra-lightweight foamed concrete for an automated facade application'

[157]: Liu et al. (2014), 'Thermal properties of lightweight dry-mix shotcrete containing expanded perlite aggregate'

[151]: Henke et al. (2020), 'Additive Manufacturing by Extrusion of Lightweight Concrete - Strand Geometry, Nozzle Design and Layer Layout'

[154]: Dielemans et al. (2021), 'Additive Manufacturing of Thermally Enhanced Lightweight Concrete Wall Elements with Closed Cellular Structures'

[152]: Prasittisopin et al. (2020), 'Thermal and Sound Insulation of Large-Scale 3D Extrusion Printing Wall Panel'

[158]: Pessoa et al. (2021), '3D printing in the construction industry - A systematic review of the thermal performance in buildings'

[153]: Hack et al. (2020), 'Shotcrete 3D Printing Technology for the Fabrication of Slender Fully Reinforced Freeform Concrete Elements with High Surface Quality'

[157]: Liu et al. (2014), 'Thermal properties of lightweight dry-mix shotcrete containing expanded perlite aggregate'

[154]: Dielemans et al. (2021), 'Additive Manufacturing of Thermally Enhanced Lightweight Concrete Wall Elements with Closed Cellular Structures'

[159]: Buchanan et al. (2019), 'Metal 3D printing in construction'

metal and alloys are usually used in powder or wire form [67, 160]. These materials are melted by a high-energy source in a layer-by-layer deposition to form a solid part. For Metal 3DP different processes can be used. The most notable techniques are powder bed fusion, direct energy deposition (DED), binder jetting, sheet lamination, material extrusion, and stereolithography [161]. For large-scale fabrication, several projects have displayed the potential of metal 3DP, with DED as one of the widest-used techniques. For example, NASA 3DP with DED, a rocket thrust chamber, as part of the Rapid Analysis and Manufacturing Propulsion Technology project [162]. MX3D manufactured a metal bridge with wire arc additive manufacturing (WAAM), which is also a DED technique [163]. Similarly, Roland Snooks, together with RMIT Architecture Tectonic Formation Lab and FormX Technology, fabricated with WAAM a large-scale metal installation [164]. Nevertheless, these AM large-scale developments have not yet been used to fabricate facades.

For facade application, metal 3DP has been mostly investigated for the fabrication of small-scale elements and nodes of bespoke curtain walls, see Table 2.4. Nodes are essential facade elements with high structural demands. The metal 3DP process is advantageous for node manufacturing because of the free-form design potential of complex geometries with superior mechanical strength, resistance to fatigue and fracture toughness [165]. For this reason, in the last decade, metal 3DP nodes have been of particular interest to industry and academia [166, 167]. For example, the Nematox node has been designed for critical zones of bespoke facade geometries where high mechanical strength is required [60]. Li3 Lithium Designers GmbH has been developing topologically optimized 3DP metal nodes for custom facade-systems designs [168]. These nodes have been augmented through topology optimization by distributing the material where it is required and creating lightweight parts. Others also used topology optimization by enabling a free-form design that responds to structural loads [76, 169].

However, there are multiple challenges for metal 3DP processes. For example, powder-based 3DP techniques suffer from limited component size, a slow fabrication time, and high material prices [170]. Although stereolithography or digital light processing are high-precision techniques, they require post-processing and have a small build volume [171]. Direct energy deposition, such as wire arc-based technique, can potentially facilitate large-scale components [172]. For the application of facades, metal large-scale manufacturing is challenging and relies heavily on material properties and fabrication constraints. For this reason, there have been scarce investigations on large-scale Metal 3DP facades. A cost-effective material with lower porosity would be advantageous with a deposition strategy to prevent cracking, delamination, swelling, and warping [161]. Additionally, the post-optimization steps of facade nodes require high-level and time-consuming computational skills [169]. This is because the optimization process is not entirely automated. A human operator usually investigates the quality control of these metal parts and modifies them accordingly throughout the entire design-to-fabrication process. The Bespoke Cast Facade is a rare example of a large-scale cast aluminum structure in a 3DP sand mold [171]. Current investigations of metal 3DP facades are still in development and require quality control. The lack of standardized guidelines and practices limits the validation

[67]: Ngo et al. (2018), 'Additive manufacturing (3D printing)'

[160]: Das et al. (2016), 'Metallic materials for 3D printing'

[161]: Duda et al. (2016), '3D Metal Printing Technology'

[162]: Vitug (2020), *Rapid Analysis and Manufacturing Propulsion Technology (RAMPT)*

[163]: Gardner et al. (2020), 'Testing and initial verification of the world's first metal 3D printed bridge'

[164]: Shakeri (2022), *Remnants of a Future Architecture, by Roland Snooks*

[165]: Frazier (2014), 'Metal Additive Manufacturing'

[166]: Raspall et al. (2018), 'International Association for Shell and Spatial Structures (IASS)'

[167]: Kassabian et al. (2017), '3D Metal Printing as Structure for Architectural and Sculptural Projects'

[60]: Strauß (2013), 'AM Envelope: The potential of Additive Manufacturing for façade construction'

[168]: Mohsen (2020), *Li3-Method*

[76]: Materialise et al. (2021), *The Spider Bracket*

[169]: Galjaard et al. (2015), 'New Opportunities to Optimize Structural Designs in Metal by Using Additive Manufacturing'

[170]: Bandyopadhyay et al. (2020), 'Recent developments in metal additive manufacturing'

[171]: Aghaei Meibodi et al. (2019), 'Bespoke Cast Facade'

[172]: Attaran (2017), 'The rise of 3-D printing'

[161]: Duda et al. (2016), '3D Metal Printing Technology'

[169]: Galjaard et al. (2015), 'New Opportunities to Optimize Structural Designs in Metal by Using Additive Manufacturing'

[171]: Aghaei Meibodi et al. (2019), 'Bespoke Cast Facade'

and reliability of these results.

Table 2.4: Metal 3DP for facade application.

Description	Image
Research projects	
Tensegrity node. 2015. *New Opportunities to Optimize Structural Designs in Metal by Using Additive Manufacturing* [169]. Arup. Comparison between a traditional node in galvanized steel, and a 3DP one made from maraging steel.	
Nematox II. 2016. *AM Envelope: The potential of Additive Manufacturing for facade construction, Architecture and the Built environment* [60]. Delft University of Technology. Printed nodal point in aluminum for bespoke glass windows.	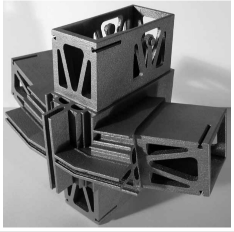
The Spider Bracket. 2016. *39] The Spider Bracket: A Topology Optimization Project by Altair, Materialise and Renishaw* [76]. Topologically optimized bracket manufactured with laser melting process.	
Bespoke node. 2017. *3D metal printing as structure for architectural and sculptural projects* [167]. 3DP connectors for articulated glass panels in a facade.	
3D Printed Space Frames. 2018. *3D Printed Space Frames* [166]. Singapore University of Technology and Design, Massachusetts Institute of Technology. 3DP nodes with tags to facilitate an easy assembly process.	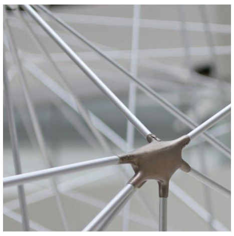

Description	Image
Cast Alu in 3DP mold. 2019. *Bespoke Cast Facade: Design and Additive Manufacturing for Aluminum Facade Elements* [171]. ETH Zurich. Aluminum poured in a 3D printed sand mold for facades.	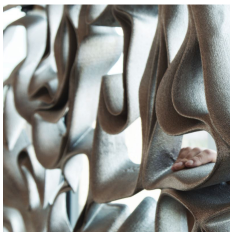
Applied research projects	
Facade inserts. 2019. *3D-Printed bespoke facade* [173]. FIT Additive Manufacturing Group. Facade panel inserts customized by 3DP.	
Alu 3DP nodes. 2020. *Design to Manufacture of Complex facades* [168]. Lithium Architects GmbH. N-AM Li3 project component test – Steel construction connected to the N-AM Li3 node.	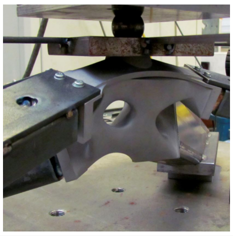

To summarize, metal 3DP has been mostly investigated for bespoke nodes, as it offers excellent opportunities for structural elements. These materials have a high degree of recyclability, compared to polymers, concrete, and ceramics [174]. Additionally, free-form design and topology optimization facilitate the fabrication of efficient and custom-tailored features. Nevertheless, 3DP of large-scale facade components are still in its infancy. Further investigation is required to implement large-scale 3DP nodes in real-world case scenarios. Such as building elements that integrate well with 3DP facade nodes and would create added value in terms of environmental performance and CO2 footprint. However, as the commercialization of WAAM advances, the authors see the potential for durable and bespoke large-scale metal facades

[174]: Colorado et al. (2020), 'Sustainability of additive manufacturing'

2.4.5 Alternative Processes

This section presents experimental materials and fabrication techniques that, although relevant for facade application, are still in an early stage of development and have not reached an architecture-relevant scale. Such limitations indicate that these processes fall in the category of future potential rather than an applied facade fabrication technique. The alternative methods of this section include glass 3D printing, self-healing [175], self-cleaning [176], CO2 capturing [177], and shape-memory materials (SMM), see Table 2.5. Generally, SMM, also known as smart materials,

[175]: Gomez et al. (2021), '3D-Printed Self-Healing Elastomers for Modular Soft Robotics'

[176]: Behera et al. (2022), 'Chapter 19 - Fabrication of nanostructures with excellent self-cleaning properties'

[177]: Gutierrez et al. (2021), 'The potential of additively manufactured membranes for selective separation and capture of CO2'

are the materials investigated the most and have been classified as 4D printing processes. SMMs respond to various actuation mechanisms, such as pre-tension [178], or changes to moisture, temperature, light, current, or pH level [179–181].

[178]: Agkathidis et al. (2019), 'Active membranes'

[179]: Vazquez et al. (2019), 'Designing for shape change'

[180]: Abdel-Rahman et al. (2018), 'Heat-actuated auxetic facades'

[181]: Ahmed et al. (2021), '4D printing'

Shape Memory Materials

SMM processes have been investigated for facade applications due to their responsive behavior. It has been theorized that climate actuators can modify in real time the facade response to the environment, such as sun, humidity, wind, and temperature fluctuations, see 2.5. The manufacturing principles include design strategies towards material modification, and geometry amplification [182]. For example, Yi et al. investigated 4D printing for a climate-specific building skin. A two-way shape memory effect of the 3DP polymer was analyzed in a small-scale prototype, which demonstrated reliable reversibility of the shapeshift [183]. Another design potential for facade application is the 3D printing of polymers on textiles, creating active membrane elements and structures [178]. Dynamic shading for facades has been investigated using 4D-printed actuators that respond to various humidity levels [184, 185]. The results prove the potential of self-actuated mechanisms for responsive facade designs.

[182]: Vazquez et al. (2019), 'Shape-changing architectural skins'

[183]: Yi et al. (2021), 'Prototyping of 4D-printed self-shaping building skin in architecture'

[178]: Agkathidis et al. (2019), 'Active membranes'

[184]: El-Dabaa et al. (2021), '4D printing of wooden actuators'

[185]: Correa et al. (2015), '3D-Printed Wood'

SMM showcases a great potential for active climate-specific facades. However, there are significant challenges in regard to facade application, as SMM are typically less durable and relatively fragile [186]. Additionally, material reversibility to the original configuration becomes challenging after repetitive use. For this reason, future developments require a multidisciplinary approach to achieve the technological transfer from material science to architecture. Furthermore, advancements in materials and fabrication processes are essential to solve the issue of material degradation [187].

[186]: Mallakpour et al. (2021), '3D and 4D printing'

[187]: Alshahrani (2021), 'Review of 4D printing materials and reinforced composites'

3D Printing of glass

Despite the notorious difficulties in shaping glass due to the high temperatures required, it has been investigated as a material for 3DP [188]. 3D printing of glass comprises a variety of techniques: Stereolithography (SLA) and digital light processing (DLP), Selective laser sintering/melting, direct ink writing, and vat photopolymerization [189]. These techniques allow high-resolution fabrication of complex components for optical and microfluidic applications. Only recently, extrusion-based processes have been investigated to scale up to an architecturally relevant scale. Researchers from MIT, demonstrated the capability of large-scale glass 3D printing through the fabrication of three-meter tall columns assembled out of multiple large-scale components [190]. Maple Glass Printing [191] is an Australian company that also focuses on scaling up this technique and its commercialization. Their current 3D printer offers a build volume of 170 x 200 x 300 mm.

[188]: Kotz et al. (2017), 'Three-dimensional printing of transparent fused silica glass'

[189]: Zhang et al. (2021), '3D printing of glass by additive manufacturing techniques'

[190]: Inamura et al. (2018), 'Additive Manufacturing of Transparent Glass Structures'

[191]: Maple Glass Printing Ltd. (2021),

In the future, 3DP glass will hold great potential for the application of facades due to its mechanical strength and optical transparency. Still in its infancy, further research needs to investigate performance characteristics as well as improvements in the fabrication process to fully harvest its potential.

Table 2.5: Alternative 3DP processes for facade application.

Description	Image
Heat-actuated auxetic facades. 2018. *Heat-Actuated Auxetic Facades* [180]. Autodesk, Steinberg Architects. Auxetic patterns for reconfigurable shading elements in a facade.	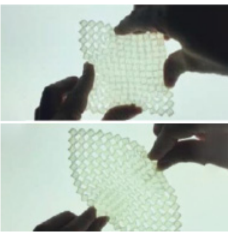
4DP hygroscopic actuators. 2018. *4D printing of wooden actuators: encoding FDM wooden filaments for architectural responsive skins* [184]. Arab Academy for Science, Technology and Maritime Transport. 3DP wooden responsive actuators for adaptive facades with dynamic shading configurations.	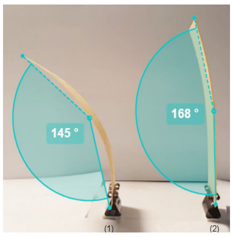
3DP glass. 2018. *Additive Manufacturing of Transparent Glass Structures* [190]. Massachusetts Institute of Technology. Demonstration of novel large-scale glass 3D printing technology through the design of 3-m tall columns.	
Thermoresponsive facade elements. 2019. *SMP Prototype Design and Fabrication for Thermoresponsive Facade Elements* [192]. University of Seoul. Shape Memory Polymers prototypes are proposed in cell types for facade shading.	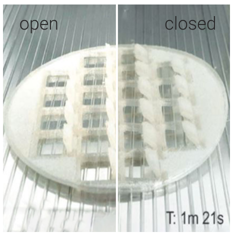
4D-printed self-shaping building skin. 2021. *Prototyping of 4D-printed self-shaping building skin in architecture: Design, fabrication, and investigation of a two-way shape memory composite* [183]. Ajou University. Design, fabrication, and investigation of a two-way shape memory composite facade panel.	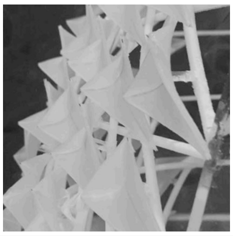

Description	Image
Hygroscopic actuators. 2021. *3D-Printed Wood: Programming Hygroscopic Material Transformations* [185]. University of Stuttgart, Massachusetts Institute of Technology. 3DP custom wood grain structures to promote tunable self transformation.	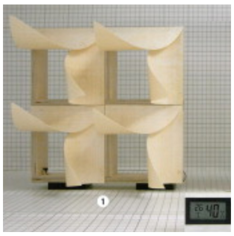
3DP glass. 2022. *Glass 3D Printing, Maple Glass Printing Ltd* [191]. Maple Glass Printing. Demonstration of commercializing recycled glass 3D printing technology.	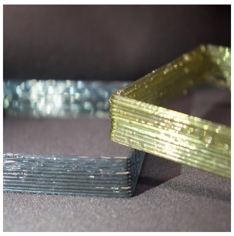

2.5 Performance Assessment for 3DP Facades

State-of-the-art research in 3D printing in architecture and construction demonstrates iterative workflows that integrate essential facade performances in the design process. The reviewed studies highlight the difficulties connected to integrating and measuring the performance metrics of 3DP facades. Irrespective of the material-technology combination, researchers and designers face similar challenges when it comes to quantifying the thermo-optical behavior, weather resistance, and durability of 3DP facades.

First of all, obtaining consistent performance results over a batch of 3DP components is usually a challenging task [64], for the difficulty in maintaining continuity and quality in the extrusion process [125]. Moreover, insufficient control over the rheological and hardening properties of the printing materials poses a challenge to the achievement of high performances [84]. This is even more crucial in ceramic manufacturing, as the sintering or curing process contributes to uneven shrinkage and microcracking of the elements. This brings limited predictability of the final outcome, contributing to challenges in standardizing 3DP ceramic parts for performance assessment. Moreover, the material type and mix play an essential role in thermal conductivity characterization. Thermal performance simulation of 3DP cellular structures requires an understanding of the multiple heat transfer modes within porous geometries. It needs to include the modeling of 3-dimensional buoyancy-driven heat transfer and its validation through experiments [154]. In the study of insulation and thermal bridging, the effect of printing parameters, such as layer thickness and height, has not been sufficiently researched [154, 193]. Regarding solar and daylighting properties, specifically thermoplastics, the relation between printing settings, geometry, and performance needs

[64]: Paoletti (2017), 'Mass Customization with Additive Manufacturing'

[125]: Gomaa et al. (2021), '3D printing system for earth-based construction'

[84]: Kontovourkis et al. (2020), 'Robotic additive manufacturing (RAM) with clay using topology optimization principles for toolpath planning'

[154]: Dielemans et al. (2021), 'Additive Manufacturing of Thermally Enhanced Lightweight Concrete Wall Elements with Closed Cellular Structures'

[154]: Dielemans et al. (2021), 'Additive Manufacturing of Thermally Enhanced Lightweight Concrete Wall Elements with Closed Cellular Structures'

[193]: De Witte et al. (2017), 'Convective Concrete'

[40]: Moritz Basil Mungenast (2019), '3D-Printed Future Facade'

[105]: Karagianni et al. (2016), 'Additive Manufacturing for daylight: Towards a customized shading device'

[106]: Sarakinioti et al. (2018), 'Developing an integrated 3D-printed façade with complex geometries for active temperature control'

[194]: Seshadri et al. (2021), 'Parametric design of an additively manufactured building facade for bespoke response to solar radiation'

to be investigated [40, 105, 106]. In this direction, Seshadri et al. [194] propose a data-driven characterization of the optical performance of 3DP facades to be embedded in a parametric design tool for building facades. However, there is still a lack of understanding of the effects of fabrication parameters on optical properties and the interaction of thermal and optical domains.

The application of standardized durability and weather-tightness testing procedures to 3DP facades is in its infancy. Preliminary and short-term accelerated testing has been performed, and observed UV degradation of 3DP polymer samples[40, 108]. Due to the lack of built examples, however, standardized testing of full-scale prototypes is also required to obtain representative results for the expected service life of 3DP facade components. In general, the effects of coating and post-processing to achieve weather resistance have not been sufficiently addressed [106, 108].

[40]: Moritz Basil Mungenast (2019), '3D-Printed Future Facade'
[108]: Grassi et al. (2019), 'Fabrication and durability testing of a 3D printed façade for desert climates'

[106]: Sarakinioti et al. (2018), 'Developing an integrated 3D-printed façade with complex geometries for active temperature control'
[108]: Grassi et al. (2019), 'Fabrication and durability testing of a 3D printed façade for desert climates'

2.5.1 Performance indicators and standards

The performance characterization of digitally fabricated facade components poses a series of challenges. First, the simplified models prescribed by facade standards (e.g., ISO 6946, ISO 10077-12, and ISO 15099) can not fully be applied to complex and bespoke geometries [195, 196]. Furthermore, the standard averaged performance indicators, such as u-value or solar heat gain coefficient (SHGC), are not able to capture the heterogeneous and site-specific properties that 3DP facades can exhibit [197]. Secondly, as no specific fabrication standard has been established for 3DP facades, complying with existing norms is a challenge, and extensive testing is required [158]. This can mean a huge effort when bespoke geometries are involved, and it is often not feasible to test all the different specimens. Therefore, a combination of analytical, computational, and experimental methods should be used for effective performance assessment. Such an approach has not been found in most of the reviewed studies, and the development of general methodologies of performance assessment of non-standard facades [198] holds great potential for 3DP components.

[195]: Briels et al. (2022), 'Thermal Optimization of Additively Manufactured Lightweight Concrete Wall Elements with Internal Cellular Structure through Simulations and Measurements'
[196]: De Michele et al. (2018), 'Opportunities and Challenges for Performance Prediction of Dynamic Complex Fenestration Systems (CFS)'

[197]: Piccioni et al. (2023), 'Tuning the Solar Performance of Building Facades through Polymer 3D Printing'

[158]: Pessoa et al. (2021), '3D printing in the construction industry - A systematic review of the thermal performance in buildings'

[198]: Favoino et al. (2018), *Building Performance Simulation and Characterisation of Adaptive Facades - Adaptive Facade Network*

Besides performance capabilities, environmental impact is becoming a crucial aspect in facade design [68, 199]. The application of LCA to 3DP building components is currently at an early stage. However, some studies reveal that the fabrication process itself contributes minimally to the overall environmental impact of the components [6]. Material production has the highest environmental impact and, therefore, reduction in the amount of material use and embedding multiple functionalities in a single component are critical strategies [6, 200]. In light of this, there have been efforts towards 3DP of recycled polymers with built examples relevant to the building scale [36, 201]. However, none of the reviewed studies addresses the assessment of operational emissions of spaces or buildings equipped with such components, which would clarify the impact of hybrid and tailored performances in the use phase of these components [65]. A comprehensive assessment of building facades, and 3DP ones, should include environmental impact indicators. Additionally, there is a growing research interest in the social and economic implications of 3DP

[68]: Labonnote et al. (2016), 'Additive construction'
[199]: Wiberg et al. (2019), 'Design for additive manufacturing – a review of available design methods and software'

[6]: Agustí-Juan et al. (2017), 'Environmental design guidelines for digital fabrication'

[6]: Agustí-Juan et al. (2017), 'Environmental design guidelines for digital fabrication'
[200]: Shah et al. (2023), 'Environmental life cycle assessment of wire arc additively manufactured steel structural components'

[36]: The New Raw (2015), *Crafting plasitc waste with robots*

[201]: ArchiTech (2021), *R-Iglo workspace. Rotterdam*

[65]: Agustí-Juan et al. (2017), 'Integration of environmental criteria in early stages of digital fabrication'

in relation to business models, labor market, and working conditions [202].

2.5.2 Need for new modeling approaches

As presented in the previous section, the challenges of performance assessment of 3DP parts connect to the complex interactions between material, geometry, and fabrication. On the first level, the properties of the 3DP materials are affected by the fabrication process. The extrusion and subsequent layered deposition of material cause changes in material properties and anisotropy, so the thermal, mechanical, electrical, and optical behaviors of the 3DP material differ from those of the solid one [203, 204]. Furthermore, AM-induced geometrical irregularity can have important effects on their mechanical behavior [205, 206]. For 3DP facades, structural anisotropy has been widely investigated, and different studies show how to account for this in the design of the components [56, 117, 207, 208]. The effect of fabrication parameters on other properties such as thermal conductivity [209], optical properties [210], and electrical insulation [211] is mainly under investigation outside the building domain. Performance modeling of 3DP facade components could greatly benefit from the adoption of well-established methods from other fields, such as automotive, aerospace, and material engineering. Fabrication-induced material behaviors and properties are often investigated through experimental campaigns. Small-scale material samples are fabricated and tested to obtain material properties databases [207, 212]. Moreover, experimental data can be used to train generative statistical models allowing for structural performance predictions for AM steel, at higher dimensional scales [213]. Another approach is the simulation of the 3DP process by means of computational fluid dynamics (CFD) and finite element (FE) simulation. It was shown that the numerical study of the rheological behavior of the printing material and its hardening is key to understanding the properties of 3DP parts [214, 215]. At the component level, the 3DP material behavior and the geometry-dependent properties need to be simulated. This is a common challenge when designing infill porous structures, and TO components (Section 2.4.4) [73, 76]. In contrast to traditional standardized facade components, 3DP ones often exhibit heterogenous properties [110, 111]. Therefore, the validation of numerical models is done through testing of large-scale components [152, 195].

Multiscale modeling is a commonly used approach in engineering to bring together the physical phenomena that occur at various dimensional scales in 3DP components, and enable the designer's control over the entire process [216]. This approach is based on the simultaneous modeling of the physical phenomena occurring at the material and component level and bridging between the scale by means of homogenization, averaging techniques, and statistical analysis, among others [217]. Over the last decade, multiscale approaches to modeling have reached maturity for 3DP metal parts [218] and accelerated the establishment of metal 3DP for fabricating functional parts. The authors believe that this approach would be beneficial to improve the fundamental understanding of the behavior of 3DP components for facade applications and enhance their performance. Because of this new level of complexity, there has been little attempt at investigating the behavior of 3DP facades once applied

[202]: Ribeiro et al. (2020), 'Framework for Life Cycle Sustainability Assessment of Additive Manufacturing'

[203]: Zohdi et al. (2021), 'Material Anisotropy in Additively Manufactured Polymers and Polymer Composites'

[204]: Tonelli et al. (2021), 'Influence of Interlayer Forced Air Cooling on Microstructure and Mechanical Properties of Wire Arc Additively Manufactured 304L Austenitic Stainless Steel'

[205]: Laghi et al. (2022), 'Mechanical response of dot-by-dot wire-and-arc additively manufactured 304L stainless steel bars under tensile loading'

[206]: Laghi et al. (2021), 'On the influence of the geometrical irregularities in the mechanical response of Wire-and-Arc Additively Manufactured planar elements'

[56]: Zhao et al. (2019), 'Shape and Performance Controlled Advanced Design for Additive Manufacturing'

[117]: Torrado et al. (2015), 'Characterizing the effect of additives to ABS on the mechanical property anisotropy of specimens fabricated by material extrusion 3D printing'

[207]: Zouaoui et al. (2019), 'Numerical Prediction of 3D Printed Specimens Based on a Strengthening Method of Fracture Toughness'

[208]: Kyvelou et al. (2020), 'Mechanical and microstructural testing of wire and arc additively manufactured sheet material'

[209]: Yuk et al. (2020), '3D printing of conducting polymers'

[210]: Amendola et al. (2021), 'Optical characterization of 3D printed PLA and ABS filaments for diffuse optics applications'

[211]: Li et al. (2017), 'Anisotropy on electrical insulation performance of 3D printed nylon 12'

[207]: Zouaoui et al. (2019), 'Numerical Prediction of 3D Printed Specimens Based on a Strengthening Method of Fracture Toughness'

[212]: Auffray et al. (2022), 'Design of experiment analysis on tensile properties of PLA samples produced by fused filament fabrication'

[213]: Dodwell et al. (2021), 'A data-centric approach to generative modelling for 3D-printed steel'

[214]: Pandit et al. (2017), 'Simulation Mechanism Development for Additive Manufacturing'

[215]: Reinold et al. (2022), 'Extrusion process simulation and layer shape prediction during 3D-concrete-printing using the Particle Finite Element Method'

to buildings. The lack of built examples and post-occupancy data makes it imperative to investigate each project's performance and durability aspects. At the same time, current building performance simulation (BPS) tools often lack the ability to account for interactions between physical domains, and spatial and time scales [59]. Building-scale performance assessment could be done in living labs where research buildings are used as a test-bed for the performance monitoring of innovative components [219–221].

2.6 Discussion and Conclusion

In this chapter, we reflect on and discuss the different aspects of 3DP of facades reviewed in this paper. Over the last decade, research has focused on establishing large-scale 3DP processes in the AEC sector using different technologies, resulting in general public awareness, investments of established construction companies in 3DP technologies, as well as the creation of start-ups. However, research related to 3DP facades is a novel topic, which has gained increased visibility in the past decade. To this date, few fundamental studies have tackled this topic, as most reviewed articles focused on demonstrating the 3DP facade fabrication potential. The performance aspects of these facades, like thermo-optical properties, need more in-depth, incremental research efforts. With similar effort, assembly details and installation requirements, such as panel-to-panel and panel-to-structure connections, need to be investigated. Therefore, this review provides a comprehensive overview of 3DP facades to guide novel research and identify future trends.

2.6.1 Design and performance assessment

We have identified that most reviewed articles tend to establish project-specific workflows and methodologies, as no comprehensive standardized design software, printing, or assessment tool exists to this date. Most of the research is conducted with in-house developed processes, including hardware, printing material, and software. This process results in a lack of a generalized database for researchers to compare material properties, printing settings, or performance measurements. With open-access databases, as for instances established for metal forming and composite materials, a closer collaboration between industry, academia, and regulatory authorities can be achieved towards the development of new building components. In line with this observation, none of the reviewed articles described the modification of the 3D printing process, or hardware, as well as material, for improving the performance of a 3DP facade and designers' control over it.

So far, performance-informed computational strategies, like topology optimization, are mainly found in the application of metal 3D printing for bespoke connections. Other facade-relevant attributes like thermal resistance and optical properties are not yet fully integrated into the design process considering environmental boundary conditions. Moreover, the

[73]: Craveiro et al. (2020), 'An automated system for 3D printing functionally graded concrete-based materials'
[76]: Materialise et al. (2021), *The Spider Bracket*
[110]: Piccioni et al. (2020), 'A Performance-Driven Approach for the Design of Cellular Geometries with Low Thermal Conductivity for Application in 3D-Printed Façade Components'
[111]: Taseva et al. (2020), 'Large-Scale 3D Printing for Functionally-Graded Facade'
[152]: Prasittisopin et al. (2020), 'Thermal and Sound Insulation of Large-Scale 3D Extrusion Printing Wall Panel'
[195]: Briels et al. (2022), 'Thermal Optimization of Additively Manufactured Lightweight Concrete Wall Elements with Internal Cellular Structure through Simulations and Measurements'
[216]: Lavery et al. (2014), 'A Review of Computational Modelling of Additive Layer, Manufacturing - Multi-Scale and Multi-Physics'
[217]: Horstemeyer (2009), 'Multiscale Modeling'
[218]: Francois et al. (2017), 'Modeling of additive manufacturing processes for metals'
[59]: Loonen et al. (2017), 'Review of current status, requirements and opportunities for building performance simulation of adaptive facades'
[219]: MIT (2021), *Office of Sustainability - Living Labs | MIT Sustainability*
[220]: NEST (2021), *Next Evolution in Sustainable Building Technologies - HiLo*
[221]: The Green Village - TU Delft (2022), *The Green Village - Field lab for sustainable innovation*

use of infill structures and their influence on fabrication (e.g., printing time, weight) and performative aspects (e.g., U-value, SHGC, optical and acoustic properties) are not investigated sufficiently yet.

2.6.2 Fabrication maturity and potential commercialization

Over the last few years, 3DP technologies have become more mature and commercially available. There is a tendency to move away from in-house developed 3D printing equipment towards commercially available systems, which was until now hindering the reproducibility and comparability of experimental results. Research can now focus on more facades-related research like material development, testing of weather resistance, or the aging behavior of 3DP objects. Additionally, the commoditization of large-scale 3DP equipment will allow for easier access and more research activities, which finally increase comparative studies and data sharing. The authors believe that this development will propel the research and commercialization of 3DP facade systems. 3D concrete printing is, until now, the only process that has successfully moved from academia to industry, which is reflected in the high number of companies and startups focusing on different aspects of 3DP concrete. Although researchers describe in detail the material characteristics and printing parameters for other 3DP methods, there is a lack of knowledge transfer from academia to the industry of those. In general, only a few companies provide general price market information and estimation of costs per square meter of 3D printed facade elements, or how many printers it would take to 3D print the entire facades of a building in a reasonable cost and time frame. The question of logistics or in-situ printing against pre-fabrication for the use-case of 3DP facades is not been sufficiently addressed yet.

The authors identified that the selected 3DP material defines the application scale and functionality of the 3DP facade, see Table 6. Polymers display ease of integrating multiple functionalities in a translucent element. Non-fired clay-based materials are low-embodied energy alternatives for 3DP facades. Concrete shows great potential for large-scale in-situ fabrication. Metal 3D printing is mainly used for high-precision joining elements requiring mechanical strength.

2.6.3 Sustainability and impact

The urgent challenge of decarbonization of the building sector is leading the construction industry towards more performative and sustainable building components and systems. The authors believe that 3DP can contribute to this transition by enabling site-specific, high-performance facade components with low environmental impact. Although the life expectancy of 3DP facades still needs to be assessed, several studies highlight the positive impact of mono-material components, which can be easily replaced and recycled at the end of their life cycle. Moreover, as the 3DP construction sector develops, consolidation of recycling schemes and growing implementation of recycled material 3DP is expected. Comprehensive sustainability assessment methods should be applied to the 3DP components, combining environmental impact with economic and social sustainability. This would unveil the socio-economic aspects connected to a shift to 3DP building components in the construction industry, in relation to working conditions, safety, employment patterns, and the role of users.

2.6.4 Conclusion

To conclude, although 3DP provides the opportunity to create site-specific designs, the review revealed that, to the present date, this potential mainly remains untouched. The question of true added value of 3DP for the application of facades remains open, as the potential benefits need to face the challenges in regards to scalability and economic viability. The authors believe that this lack of development is due to the fact that large-scale 3DP methods only recently became available to a broader audience. Furthermore, facades are among the most complex building components, and, thus, difficult to be extensively investigated within single research projects. Therefore, the authors identify the need for a multidisciplinary research approach and collaborations, as well as large-scale demonstrators that bring together expertise on computational design, digital fabrication, material development, and performance assessment. More fundamental research is required to understand the relationship between fabrication constraints, material behavior, and computational design. A thorough understanding of these aspects will allow 3DP facades to move from prototypical demonstrators to viable solutions for the building industry.

Author Contributions

M.L., I.C., and V.P. contributed equally to this paper. Conceptualization, M.L., I.C., and V.P.; investigation, M.L., I.C., and V.P.; writing—original draft preparation, M.L., I.C., and V.P., and B.S.; writing—review and editing, M.L. and V.P.; visualization, M.L., I.C., and V.P.; B.D., F.G., M.K., and A.S. supervised the project and manuscript conception. All authors have read and agreed to the published version of the manuscript.

Acknowledgement

This research is financially supported by the National Centre for Competence in Research in Digital Fabrication, funded by the Swiss National Science Foundation (NCCR Digital Fabrication Agreement number 51NF40141853).

Table 6: 3DP Facades Advantages and Challenges.

Material/ Application		**Advantages**	**Challenges**
Thermoplastics Facade elements/Panels non-structural transparent/ opaque insulating monomaterial multifunctional		**Fabrication** ● adjustable resolution & high design freedom ● high buildup rate **Performance** ● good thermal resistance ● low density/ lightweight ● recyclable ● diverse materials: translucent, opaque, reflective	**Fabrication** ● high shrinkage during fabrication ● overhangs need support **Performance** ● low acceptance as a building material ● low fire resistance ● weather resistance needs testing; ● unknown long term material behavior
Clay-based materials Walls/ Cladding/ Tiles	**Un-fired** Structural/non-structural opaque insulating	**Fabrication** ● suitable for large scale ● in-situ fabrication ● affordable ● sourced local **Performance** ● reusable ● low environmental impact	**Fabrication** ● high crack sensitivity ● heavy equipment needed ● high deformation after curing **Performance** ● low toughness ● brittle ● low weather resistance
	Fired weathering layer non-structural non-insulating	**Fabrication** ● suitable for small to mid scale **Performance** ● good weather resistance ● good compressive strength ● durable	**Fabrication** ● additional firing process ● high deformation after firing **Performance** ● difficult to recycle ● no structural applications
Concrete in-situ 3DP walls stay-in place formwork structural/ non-structural opaque non-insulating multifunctional		**Fabrication** ● large-scale components ● high industry adaptation ● high buildup rate ● different approaches for 3DCP available **Performance** ● fire resistant ● good compressive strength ● durable	**Fabrication** ● low resolution limits design freedom ● postprocessing to meet surface finish standards ● heavy equipment needed **Performance** ● low thermal resistance ● additional reinforcement needed ● high cement content increases CO2 footprint ● high density /heavy weight
Metal structural nodes structural monomaterial		**Fabrication** ● standard: high resolution, detailed and complex geometry ● WAAM: low resolution for mid to large-scale parts **Performance** ● structural strength and ductility ● recyclable	**Fabrication** ● standard: small build size, high costs & fabrication time ● limited resolution (WAAM) **Performance** ● high density /Heavy weight ● high thermal conductivity

Printing thermal performance:
an experimental exploration of 3DP polymers for facade applications

3

3.1 Overview of Paper B 57
3.2 Introduction 59
3.3 Methods 60
3.4 Results 66
3.5 Conclusions 68

3.1 Overview of Paper B

3.1.1 Content

This study investigates the potential of ME for the fabrication of mono-material translucent facade components, tailored according to climatic conditions and functional requirements. The study aims to develop building components that provide energy efficiency while producing minimal environmental impact. The research investigates the effect of component geometry on the thermal insulation properties of 3DP objects with bespoke internal structures. Different prototypes are fabricated using a robotic polymer extruder, and their thermal properties are being measured following a hot-box test method. The experimental results are then used to calibrate a heat transfer simulation model describing the joint effects of conduction, natural convection, and infrared radiation through the components.

3.1.2 Method

A combination of experimental and numerical simulation methods is used to investigate the thermal insulation properties of 3D printed objects with bespoke internal structures. The study involves the fabrication of three different specimens of size 500x500x150mm using a large-scale polymer extruder mounted on a 6-axis robot. The material chosen for the experiments is PETG, a glycol-modified PET thermoplastic. The thermal properties of the specimens are measured following a hot-box test method, and the experimental results are used to calibrate a heat transfer simulation model describing the joint effects of conduction, natural convection, and infrared radiation through the components. The effective thermal conductivity is derived from the heat flow throughout the sample per unit area, and the sample's total thermal resistance and U-value are calculated. The experimental setup includes a metering chamber consisting of a box of dimensions 1 x 1 x 1m approximately, with a total of 35 sensors measuring the state of the chamber. The data acquisition is made through a NI cDAQ-9133, and LabView collects and records data with a one-second resolution.

3.1.3 Results

The study demonstrates the possibility of fabricating facade components through 3D printing of polymers and provides insights into the thermal behavior of polymer 3DP facades on a large scale. The findings suggest that tailored 3DP components can be designed according to climate-specific insulation requirements, and the orientation of the cavities does not significantly affect the thermal properties of the components. The research also provides guidelines for designing thermally insulating 3D printed facade elements that offer a low environmental impact yet performant alternative to traditional components. Although U-values of 1.0 W/m^2K are achieved, these elements take a significant time to print. In hand with the long print time, the weight per m^2 of these elements is as high as 50 kg/m^2. This brings into question the production viability of off-the-shelf ME for the application of facades and is one of the drivers for the development of a novel approach to large-scale ME.

3.1.4 Authors contribution to the paper

Valeria Piccioni* - Conceptualization, Methodology, Formal Analysis, Writing – Original Draft Preparation, Visualization
Matthias Leschok* - Conceptualization, Methodology, Investigation, Writing – Original Draft Preparation, Visualization
Gearoid Lydon - Methodology, Writing – Review & Editing
Matthias Kohler - Supervision, Writing – Review & Editing
Fabio Gramazio - Supervision, Writing – Review & Editing
Arno Schlueter - Supervision, Writing – Review & Editing
Benjamin Dillenburger - Supervision, Writing – Review & Editing
* M Leschok and V Piccioni contributed equally to this work.

Abstract The decarbonisation of the building sector requires the development of building components that provide energy efficiency while producing minimal environmental impact. We investigate the potential of polymer 3D printing (3DP) for the fabrication of mono-material translucent facade components, whose properties can be tailored according to climatic conditions and functional requirements. These components bear the potential to reduce energy consumption in buildings and, at the same time, can be fabricated with minimal environmental impact thanks to the recyclability of the feedstock material. In this study, we explore the effect of component geometry on the thermal insulation properties of 3DP objects with bespoke internal structures. Different prototypes are fabricated using a robotic polymer extruder, and their thermal properties are measured following a hot-box test method. The experimental results are then used to calibrate a heat transfer simulation model describing the joint effects of conduction, natural convection and infrared radiation through the components. We show that it is possible to fabricate insulating polymer components providing thermal transmittance ranging from 1.7 to 1 W/m^2K only by changing the internal cavity distribution and size. This proves the possibility of designing 3DP thermally-insulating components for different climatic conditions and requirements. This study provides the first insights into the thermal behaviour of polymer 3DP facades on a large scale. The results suggest that this innovative manufacturing technique is promising for application in facades and encourages further research toward performant and low-embodied energy 3DP building components.

3.2 Introduction

Achieving energy efficiency while minimising environmental impact is a stringent requirement for the decarbonisation of the building sector [222]. In this context, the building facade plays a key role as it greatly impacts the amount of energy needed to provide comfort in buildings. Moreover, the way facades are constructed significantly contributes to the embodied emission impact of buildings [3]. Therefore, creating high-performance facades is imperative to achieve the Net-zero by 2050 goals.

Advancements in large-scale 3D printing (3DP), in combination with computational design, have shown that it is possible to fabricate building components with embedded performances that can be tuned for their specific application [223, 224]. Thanks to 3DP, designers can not only control the shape of an object but can also define its internal articulation using infill structures to ensure structural integrity during printing and reduce material use [84, 147, 225]. Recent studies have focused on the design of infill structures to achieve thermal performance in 3DP wall components, out of earth-based materials [124, 226] and concrete [154, 227, 228]. To improve the thermal performance of 3DP concrete elements, concrete mixtures with air inclusions or low conductivity materials can be used [195], and insulating materials can be simultaneously extruded along the concrete layer or fill the infill cavities [136, 158]. However, the inclusion of additional materials compromises the ease of fabrication and assembly, and recyclability.

[222]: Too et al. (2022), ‘Framework for standardising carbon neutrality in building projects’

[3]: Delmastro et al. (2022), *Building Envelopes – Technology deep dive*

[223]: Bischof et al. (2022), ‘Fostering innovative and sustainable mass-market construction using digital fabrication with concrete’

[224]: Jipa et al. (2019), ‘3D-Printed Formwork for Integrated Funicular Concrete Slabs’

[84]: Kontovourkis et al. (2020), ‘Robotic additive manufacturing (RAM) with clay using topology optimization principles for toolpath planning’

[147]: Bos et al. (2022), ‘The realities of additively manufactured concrete structures in practice’

[225]: Kontovourkis et al. (2020), ‘Robotic 3D clay printing of prefabricated non-conventional wall components based on a parametric-integrated design’

[124]: Dubor et al. (2018), ‘Energy Efficient Design for 3D Printed Earth Architecture’

[226]: Gomaa et al. (2019), ‘Thermal performance exploration of 3D printed cob’

[154]: Dielemans et al. (2021), ‘Additive Manufacturing of Thermally Enhanced Lightweight Concrete Wall Elements with Closed Cellular Structures’

[227]: Marais et al. (2021), ‘Computational assessment of thermal performance of 3D printed concrete wall structures with cavities’

[228]: Sun et al. (2021), ‘Experimental study on the thermal performance of a 3D printed concrete prototype building’

[195]: Briels et al. (2022), ‘Thermal Optimization of Additively Manufactured Lightweight Concrete Wall Elements with Internal Cellular Structure through Simulations and Measurements’

[136]: Furet et al. (2019), ‘3D printing for construction based on a complex wall of polymer-foam and concrete’

[158]: Pessoa et al. (2021), ‘3D printing in the construction industry - A systematic review of the thermal performance in buildings’

As an alternative, thermoplastic polymers have also been proposed for the fabrication of facade components, taking advantage of their translucency, light weight and low thermal conductivity. Monomaterial components that integrate thermal insulation and seasonal thermal control have been designed in [40, 106, 107, 110]. Most thermal insulation studies investigate millimetre-scale geometrical articulations fabricated using off-the-shelf desktop 3D printers. These infill designs are based on periodic porous structures [229, 230], with limited scalability potential. Recently, large-scale polymer extruders have been used to improve scalability and material output. Those can print polymers with a material output up to 225Kg/h [104], and a generally lower print resolution. To this date, there is little to no research on how the internal articulation of polymer 3DP components influences thermal performance at an architectural scale. This knowledge is required to fabricate thermally insulating 3DP facade elements efficiently.

[40]: Moritz Basil Mungenast (2019), '3D-Printed Future Facade'
[106]: Sarakinioti et al. (2018), 'Developing an integrated 3D-printed façade with complex geometries for active temperature control'
[107]: Tenpierik et al. (2018), 'Double Face 2.0'
[110]: Piccioni et al. (2020), 'A Performance-Driven Approach for the Design of Cellular Geometries with Low Thermal Conductivity for Application in 3D-Printed Façade Components'
[229]: Alqahtani et al. (2021), 'Thermal performance of additively manufactured polymer lattices'
[230]: Grabowska et al. (2020), 'The Thermal Conductivity of 3D Printed Plastic Insulation Materials—The Effect of Optimizing the Regular Structure of Closures'
[104]: Thermwood (2023), *Thermwood LSAM - Large Scale Additive Manufacturing*

This study investigates the integration of thermal insulation performance in 3D-printed polymer facades by exploring the interplay of geometry and performance in infill structures. Combining experiments and numerical simulations, we retrieve guidelines for designing thermally insulating 3DP facade elements that provide a low environmental impact yet performant alternative to traditional components.

3.3 Methods

The following chapter presents the robotic 3DP setup for the creating of bespoke, large-scale prototypes and the design intent for the specimens. After that, we introduce the testing apparatus used for the heat flow experiments and the steady-state method for the thermal characterisation of building components. Finally, we present the experimental procedure, along with the numerical simulation models used for the validation.

3.3.1 Samples design and 3D printing

To conduct the thermal experiments, we print three different specimens of size 500x500x150mm. These large dimensions are chosen to allow for a 1:1 scale testing scenario. The large area reduces edge effects during the measurements, as sensors can be placed in the centre and far away from the borders/border conditions. The thickness of 150mm results from preliminary studies conducted by the authors. In particular, this thickness is identified to withstand the structural loads considered for application as a 3DP facade.

The specimens are 3D printed using a large-scale polymer extruder mounted on a 6-axis robot (fig.3.1). The material chosen for these experiments is PETG, a glycol-modified PET thermoplastic [231]. PETG is a well-known polymer, most often used for medical products or food applications due to its transparency, chemical, and structural resistance [232]. Extrusion-based polymer 3D printing (also referred to as BAAM

[231]: Sepahi et al. (2021), 'Mechanical Properties of 3D-Printed Parts Made of Polyethylene Terephthalate Glycol'
[232]: Petrov et al. (2021), 'Research into the effect of the 3D-printing mode on changing the properties of PETG transparent plastic'

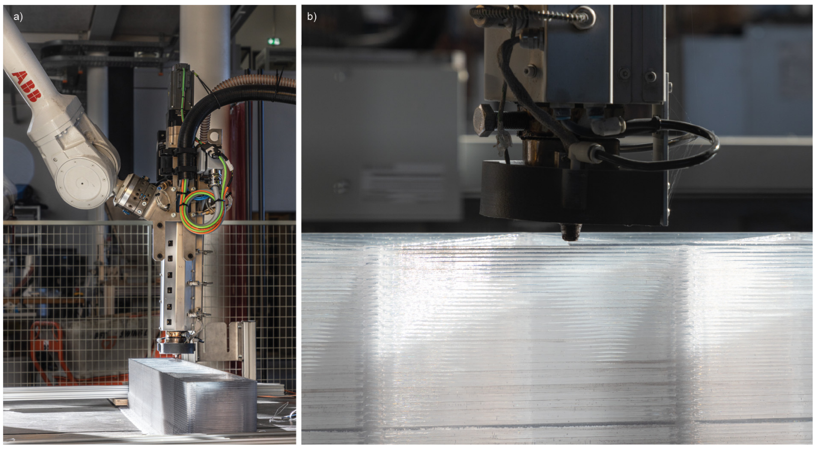

Figure 3.1: a. Robotic 3D printing setup, comprising a CEAD E25 extruder mounted on an ABB IRB4600. **b.** Close-up of the polymer printing process: PETG printed with 2.5mm layer height and 6mm layer width.

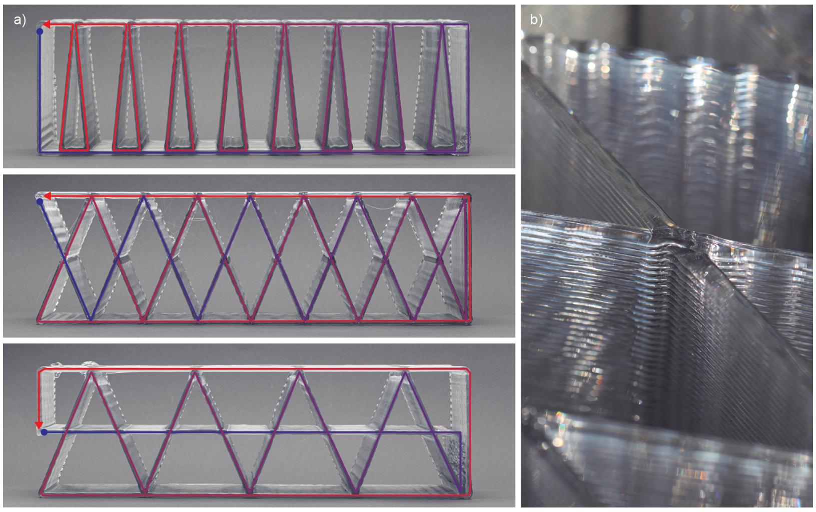

Figure 3.2: a. Studies on continuous print paths. Different arrangements of infill lines allow for differentiation within the 3DP component. **b.** Close-up of self-intersecting print path, crossing within the same layer forces the material to dwell and form a knot.

- Big Area Additive Manufacturing or LSAM - Large Scale Additive Manufacturing) is a process where feedstock material is heated up in an extruder and deposited successively line by line, layer by layer. The extruder used has three different heating zones and a maximum output of 12 kg/h [233]. A 5mm nozzle was used for the fabrication of the specimens. Considering the challenge of creating horizontal surfaces with large-scale polymer 3DP by simple bridging [234], the authors decided to seal the top and bottom surfaces of the specimens by gluing a 3mm polystyrene sheet onto them. The samples are printed with a layer height of 2.5mm and a line thickness of 6mm, resulting in samples between 8.75 and 12.6kg.

[233]: CEAD (2022), *E25 printing head. for large-scale additive manufacturing*

[234]: Eyercioglu et al. (2019), ‘Determination of the Maximum Bridging Distance in Large Scale Additive Manufacturing’

The specimens are designed to form a continuous 3D printing path, resulting in a continuous extrusion of material with no start/stop. Intersections can be printed by simple crossing; this way, the material just “dwells” on top of the previous layer, forming a small knot, see Figure 3.2.b. A continuous print path was chosen due to a lack of a proprietary start/stop mechanism for the printing setup. Compared to continuous print paths, start/stop ones might result in local discontinuities and voids in the printed object. These compromise the parts’ air-tightness and therefore have a negative impact on the thermal performance of the object. Figure 3.2.a shows 3DP studies on continuous infill patterns. The chosen pattern is able to control the dimension of air cavities along the thickness of the element without significantly increasing the amount

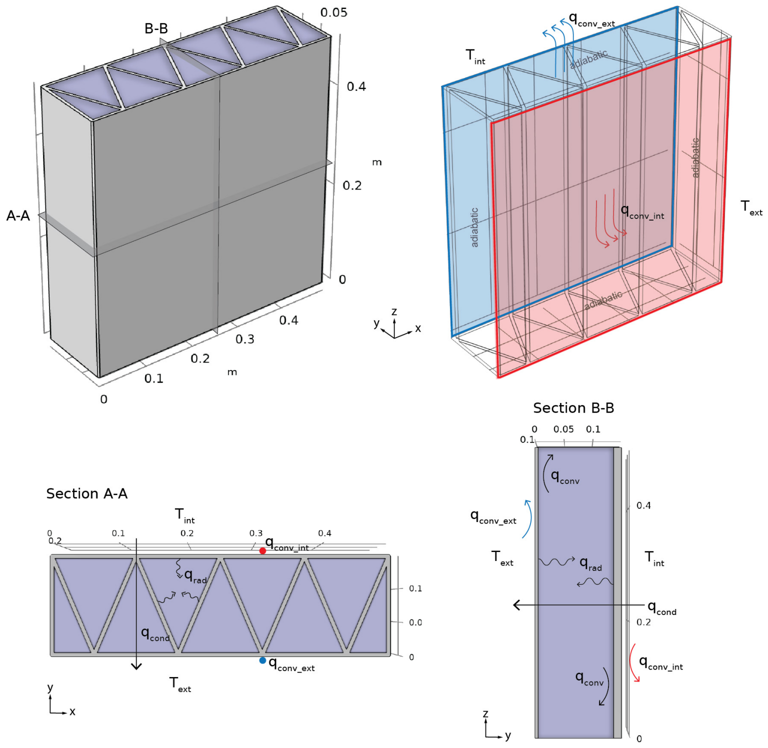

Figure 3.3: Boundary conditions for the numerical models. **a.** 3D model of sample R1 for the FE simulation. From this, 2D representation are derived based on the cross-section **b.** and the longitudinal section

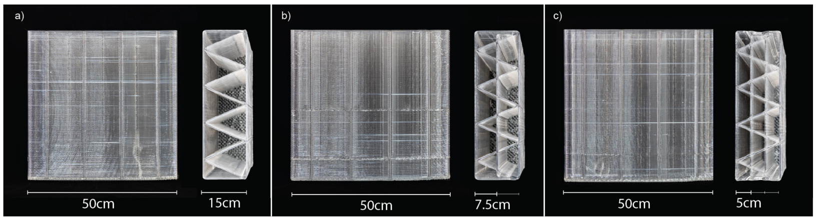

Figure 3.4: 3DP specimens for the experimental campaign. **a.** R1, one cavity approx. 15cm. Weight: 8.8kg. **b.** R2, two cavities approx. 7.5cm. Weight: 10.5kg. **c.** R3, three cavities approx. 5cm. Weight: 12.5kg.

of material used (Figure 3.4). It consists of a zig-zag pattern (primary lines) and a separator between the inner and the outer wall of the object (secondary lines). The pattern is kept as simple as possible to ensure good printing quality and ease of study. The distance between the base triangles (primary lines) is kept constant at 125mm, which results, depending on the amount of separator (secondary lines), in a 10 -18% infill percentage. The separator lines divide the air domain within the panel, creating smaller cavities to potentially increase the thermal insulation of the component.

3.3.2 Hot-Box Apparatus

The tests are conducted using a hot-box apparatus, according to the hot-box heat flux meter approach (HB-HFM) [235–237]. The HB-HFM approach is based on the steady-state method for the thermal characterisation of building materials and envelope assemblies [238, 239]. The method measures the heat flux through the component to be studied and the temperature profile across it [240]. The hot-box apparatus comprises a cold chamber kept at a constant low temperature, containing a metering chamber kept at a higher temperature. The specimen to be tested is placed on a mounting ring at the interface between the two chambers.

[235]: Amaral et al. (2017), 'Polyurethane foams with microencapsulated phase change material'
[236]: Meng et al. (2015), 'Feasibility experiment on the simple hot box-heat flow meter method and the optimization based on simulation reproduction'
[237]: Buratti et al. (2016), 'Thermal Conductivity Measurements By Means of a New 'Small Hot-Box' Apparatus'

[238]: C16 Committee ASTM International (2019), *Practice for Calculating Thermal Transmission Properties Under Steady-State Conditions*

[239]: C16 Committee ASTM International (2019), *Test Method for Thermal Performance of Building Materials and Envelope Assemblies by Means of a Hot Box Apparatus*

[240]: Soares et al. (2019), 'Laboratory and in-situ non-destructive methods to evaluate the thermal transmittance and behavior of walls, windows, and construction elements with innovative materials'

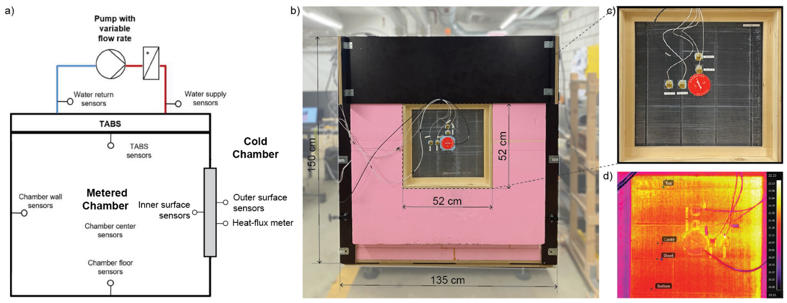

Figure 3.5: a. Schematics of the hot-box setup. **b.** Front view of the experimental chamber with testing specimen. **c.** Example of RTD and heat-flux sensor placement on testing specimen. **d.** Thermographic images of a tested sample, guiding the sensors placement.

The air temperature inside the metering chamber and in the cold chamber is monitored using platinum resistance thermometers (PT100) and the specimen wall temperatures. The heat fluxes through the specimens are measured using a heat flux transducer.

The experimental setup is in an underground laboratory room enclosed by concrete walls and slabs, ensuring stable temperature conditions and minimal thermal disturbances. The metering chamber consists of a box of dimensions 1 x 1 x 1m approximately (Fig 3.5. The chamber's walls are made of a thick insulation layer of two XPS panels (2 x 8 cm) and a plywood sheet (2 cm) to ensure minimal heat losses through the structure. The top side of the box consists of a 3.5 cm concrete slab and an outer insulation layer of XPS (8 cm). The concrete slab is the prototype of a thermally active building system (TABS), as described in [241]. It embeds water pipes for cooling and heating through water and takes advantage of the high thermal storage of concrete to dampen temperature peaks. Finally, the front panel comprises a double layer of XPS insulation (22 cm) and accommodates a wooden frame to mount the testing specimen.

[241]: Lydon et al. (2019), 'Coupled simulation of thermally active building systems to support a digital twin'

A total number of 35 sensors measures the state of the metering chamber (Fig 3.5.a). Most sensors are placed on the floor and wall surfaces of the metering chamber and on the TABS. Pairs of resistance temperature detectors (RTDs) of type PT100 (Omega Engineering) are placed on each side to measure the specimen's surface temperatures (Fig 3.5.b,c). Moreover, a heat flux plate of type HFP01 (Hukseflux) is placed in the centre of the specimen's outer surface to measure normal one-dimensional heat flux. Infrared thermography was used to guide the correct placement of thermocouples and heat flux transducer, minimising inaccuracies due to specimen heterogeneity and edge effects (Fig 3.5.d). The data acquisition is made through a NI cDAQ-9133, and LabView collects and records data with a one-second resolution.

3.3.3 Experimental Procedure

To better understand the relative effect of air buoyancy on the overall heat transfer, each sample was measured for two different cavity orientations. One measurement is done for the configuration with the cavities running parallel to the ground (along the x-axis, 3.6.b) and then rotated by 90 degrees (along the z-axis, 3.6.a) so the internal cavities allow for air movement from top to bottom. To minimise possible air leakages and to accommodate fabrication tolerances, the specimens are installed in the box by placing a rubber gasket around them. A total of seven RTDs were placed on the specimen: four on the surface exposed to the room and three

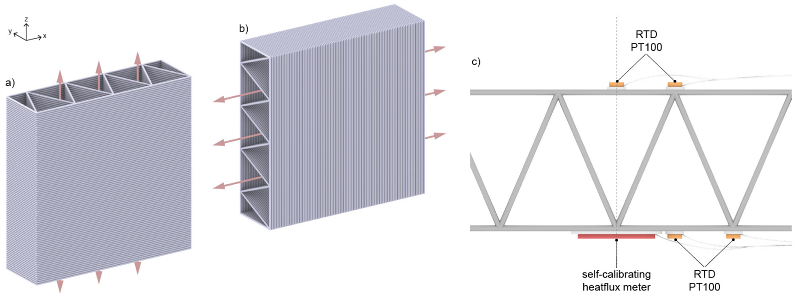

Figure 3.6: a,b. Schematics showing different testing directions for the 3DP samples. **c.** Schematics of thermal sensor placement, measuring the sample's surface temperatures at the connection of contour and infill and at the middle of an air cavity.

on the surface exposed to the metering chamber. The sensors are placed in this way to measure the expected extreme surface temperature conditions due to the cavities, either at a full-depth cavity or the connection point of the primary infill lines with the contour of the specimen (3.6.c).

Experiments start with placing the sample in the metering chamber and activating the pump for water circulation in the TABS at 40 °C. Measurements were performed for a minimum of 72 h to ensure steady-state conditions. For the termination of the test, it was verified that the results obtained at the end of the test do not differ by more than ± 5% compared to the previous 24h [242]. Recorded data show that steady-state conditions are met a few hours after the test initiation due to the elements' low thermal mass; in most cases, the results converge before 24h, as in Figure 3.7. This suggests that the duration of the experiments could be greatly reduced.

[242]: Secretary (2014), *ISO 9869-1:2014(en), Thermal insulation — Building elements — In-situ measurement of thermal resistance and thermal transmittance — Part 1: Heat flow meter method*

Data are analysed using the average method [242]. Mean values for heat flow density rate and temperature difference between the two sample's surfaces are obtained by averaging over the last 10h of measurement. As in [243] a value of effective thermal conductivity (λ_{eff}) is derived following the one-dimensional solution of Fourier's law [244]:

[242]: Secretary (2014), *ISO 9869-1:2014(en), Thermal insulation — Building elements — In-situ measurement of thermal resistance and thermal transmittance — Part 1: Heat flow meter method*

[243]: Sánchez-Calderón et al. (2022), 'Methodology for measuring the thermal conductivity of insulating samples with small dimensions by heat flow meter technique'

[244]: Çengel (2003), *Heat Transfer*

$$q = -\lambda_{eff}\frac{dT}{dx} \longrightarrow \lambda_{eff} = \frac{qd}{T1 - T2}\,[W/mK] \tag{3.1}$$

where q is the heat flow throughout the sample per unit area in $\mathrm{W/m^2}$, d is the sample's thickness in m, $T2$ is the temperature of the cold source, $T1$ is the temperature of the hot source, and ΔT is the temperature difference across the sample in K. In order to retrieve standard thermal performance indicator for building elements [242], from the effective thermal conductivity we derive the sample's total thermal resistance (R) and the u-value (U):

[242]: Secretary (2014), *ISO 9869-1:2014(en), Thermal insulation — Building elements — In-situ measurement of thermal resistance and thermal transmittance — Part 1: Heat flow meter method*

$$R_{tot} = R_{si} + \frac{d}{\lambda_{eff}} + R_{se}\left[m^2K/W\right] \tag{3.2}$$

$$U = \frac{1}{R_{tot}}\left[W/m^2K\right] \tag{3.3}$$

where R_{si} and R_{se} are the resistance of the air boundary layers at the internal and external surface of the component, equal to 8 $\mathrm{W/m^2K}$ and 25 $\mathrm{W/m^2K}$ respectively. To reach appropriate confidence, the experimental results of the testing apparatus were benchmarked by performing measurements on a specimen with known thermal characteristics. The

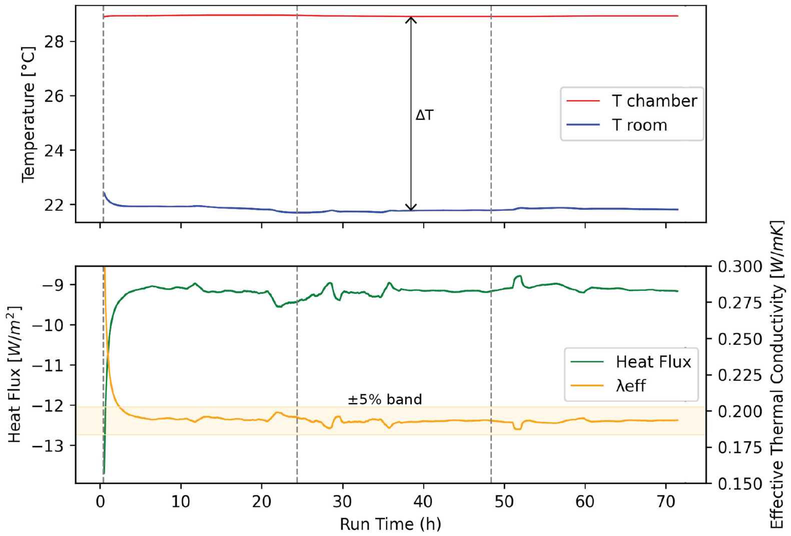

Figure 3.7: Recorded data during the 72h experiments. **a.** Measured temperatures inside the hot-box (red) and room temperature (blue); **b.** Measured heat flux (green) and calculated effective thermal conductivity (yellow).

experimental procedure was performed on an XPS panel of known thermal properties (λ= 0.035 W/mK). Results from the experiment differ by less than 3% from the nominal properties of the product, which is considered an acceptable accuracy for the experiment.

3.3.4 Numerical Study

Experimental results were validated against FE simulations simulating the heat transfer through the 3DP samples under experimental conditions. The heat transfer and fluid flow modules of COMSOL Multiphysics® [245] were used for the simulations. Conductive heat transfer happens through the solid thermoplastic domain, with thermal conductivity λ_{petg} equal to 0.2 W/mK [246] and, less significantly, through the fluid domain of the air cavities (λ_{air}= 0.025 W/mK). Convective heat transfer occurs in the cavity and is driven by buoyancy effects originating from air density difference due to the temperature gradient. Radiative heat transfer between the infill walls with emissivity ϵ equal to 0.9, as reported in [247]. Radiation enhances air circulation [248] and strongly depends on the walls surface temperatures. Two heat fluxes are imposed at the two sides of the sample, with a cold temperature (T_{ext}) of 22 °C and a hot temperature (T_{int}) of 35°C, to match the experimental conditions. The boundary conditions are summarised in Figure 3.3. From the 3D representations, simplified models were created to reduce the computational effort. The models are based on a 2D representation of the samples' geometry. They are modelled using the *heat transfer in solids and fluids* module, coupled with the *surface-to-surface radiation* interface. Two 2D simplifications can be derived from the model by choosing a longitudinal (Figure 3.3.b) or cross-section (Figure 3.3.a), section A-A and B-B respectively. The cross section allows the modelling of the triangular-trapezoidal cavities, while the longitudinal section reduces the cavity to two facing walls. For geometries with cavity orientation along the x-axis, air convection is simulated explicitly using the *laminar flow* interface and the Boussinesq approximation [249]. For geometries with cavities along the z-axis, convection is modelled implicitly [250]. The fluid domain is still modelled for conduction, but airflow fields and velocity are not computed. Instead, convection is

[245]: COMSOL (), *COMSOL*

[246]: MatWeb, LLC (), *MatWeb: Material Property Data. Overview of materials for PETG Copolyester*

[247]: Badarinath et al. (2022), 'Real-Time Sensing of Output Polymer Flow Temperature and Volumetric Flowrate in Fused Filament Fabrication Process'

[248]: Mezrhab et al. (2006), 'Computation of combined natural-convection and radiation heat-transfer in a cavity having a square body at its center'

[249]: Kleinstreuer (), 'Engineering Fluid Dynamics: An Interdisciplinary Systems Approach'

[250]: COMSOL (), *Modeling Natural and Forced Convection in COMSOL Multiphysics®*

accounted for by defining an increased thermal conductivity based on an empirical correlation factor that depends on the cavity dimensions and the temperature variation across the cavity. This correlation factor is based on rectangular cavities; therefore, the triangular and trapezoidal cavities are transformed into rectangular air cavities with the same area and aspect ratio, as explained in ISO 10077-2 [242].

[242]: Secretary (2014), *ISO 9869-1:2014(en), Thermal insulation — Building elements — In-situ measurement of thermal resistance and thermal transmittance — Part 1: Heat flow meter method*

3.4 Results

3.4.1 Experimental results

The results of the experiments are summarized in Figure 3.8. An effective thermal conductivity in the range of 0.19 - 0.36 W/mK was observed, corresponding to a U-values from 1 to 1.7 W/m^{2}K. These results confirm the significant effect of geometry on the heat transfer in 3DP components with bespoke cavities. Repetition of the experiments for sample R1 in the two-cavity alignment showed good accordance of results, with an error below 2%. Similarly to porous media, an increase in the number of air cavities inhibits heat transfer and hence positively correlates with thermal insulation [106, 110, 229]. In porous media, however, an increase in air cavity numbers usually results from higher porosity and lower relative density; in our sample, the relative density increases with the number of air cavities due to the additional separating layers. This shows that, for large-scale cavity structures, there is a trade-off between the increase in thermal insulation due to the introduction of air layers and the decrease of insulation due to the enhanced buoyancy-driven effects in wider cavities [251]. Therefore, adding additional cavities in the geometry while keeping the component's width constant correlated to a decrease in effective thermal conductivity, as also reported by [252]. Moreover, it was found that orientation does not affect thermal conductivity significantly for this cavity dimensions. A slightly lower thermal insulation is observed in R1 for the horizontal cavity arrangement, but this effect is not visible in the other samples.

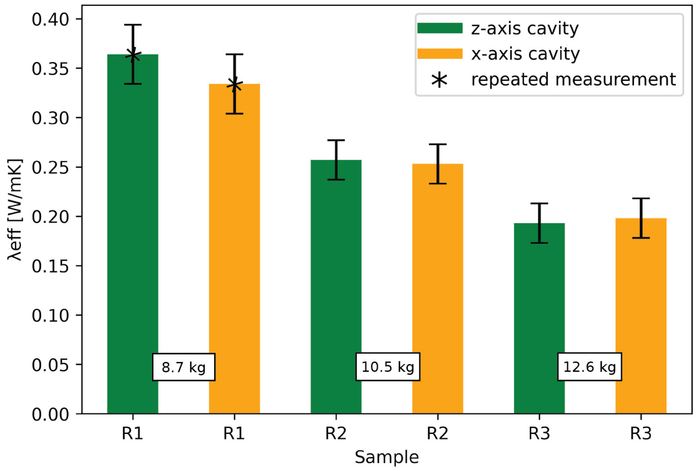

Figure 3.8: Overview of experimental results: effective thermal conductivity for the six tested samples. Error bars represent the uncertainties of the measurements.

3.4.2 Numerical results

The 3D FE model allowed observation of the three heat transfer modes through the 3DP component, as shown in Figure 3.9. The results confirm the presence of a radiative heat exchange between the cavity walls. Moreover, buoyancy-driven air flows develop with the cavities and ultimately affect the thermal stratification in the components. Results from the 3D and 2D numerical models were compared with the experimental results. Figure 3.10 shows there is generally good accordance between simulations and experiments, with deviations between 4 - 15%. Furthermore, the trends observed in the experimental study are also confirmed in the simulation results. A more significant deviation is found for the 2D model representing section B-B. Compared to the experiments, this model overestimates the thermal transmittance of the component R1 by 35%, assumably due to the impossibility of modelling surface-to-surface radiation between all the cavity walls. The difference between simulated and measured values increases with the number of cavities, which could indicate inaccuracies in the description of the heat transfer mechanisms of multiple cavities in series. Nevertheless, the 2D models based on section A-A can describe the physical behaviour of the system and, thanks to the fast computation time (<1 min), can be effectively used to support the component's design.

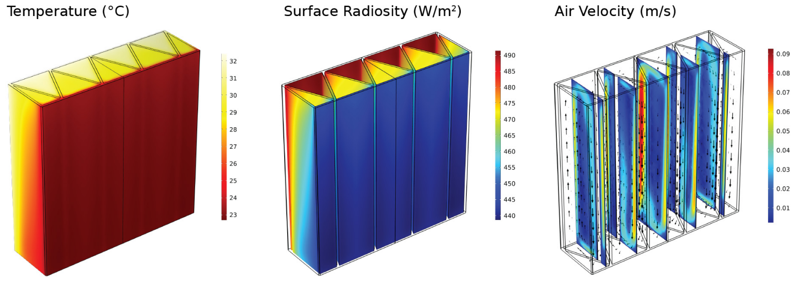

Figure 3.9: FE simulation results for sample R1. The joint effects of radiative, convective and conductive heat transfer influence the thermal stratification in the sample.

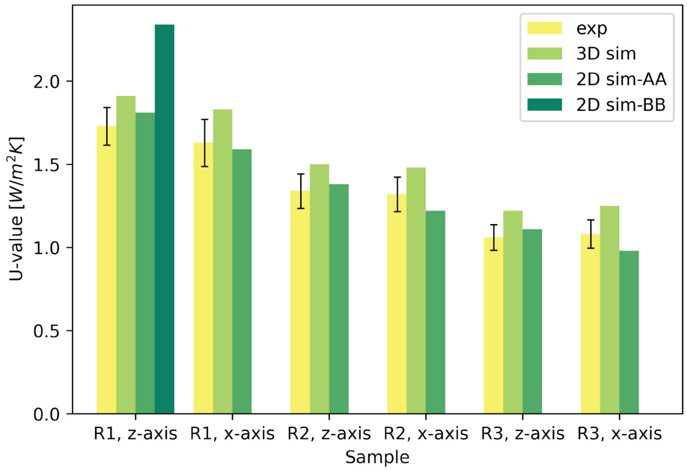

Figure 3.10: Comparison of results for experiments, 3D and 2D simulations. The error bars represent the measurement uncertainties.

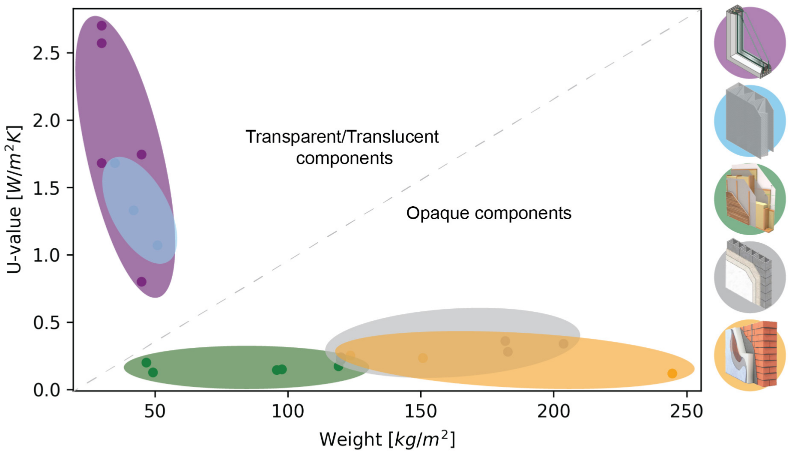

Figure 3.11: Comparison of thermal performance of 3DP facade and traditional facade components.

3.5 Conclusions

3.5.1 Design Guidelines

This study demonstrated the possibility of fabricating facade components through large-scale 3D printing of polymers. It was shown that by managing the cavities' size and arrangement, a reduction in thermal insulation could be achieved by up to 60%. This suggests that tailored 3DP components can be designed according to climate-specific insulation requirements. The combination of experimental and simulation analysis enabled a first understanding of heat transfer mechanisms into 3DP components with internal cavity structures. We observed a trade-off between the increase in thermal insulation due to the air layers and the decrease in insulation due to the enhanced convection effects. Therefore, partitioning the air layers into smaller cavities has proved to decrease thermal transmittance. Moreover, the orientation (x-axis, z-axis) of the cavities does not significantly affect the thermal properties of the components, irrespective of the number of cavities.

3.5.2 Outlook

The tested prototypes revealed good insulation properties comparable to high-performance triple glazing (Figure 3.11). Compared with standard facade components, the 3DP components provide such insulation at a relatively low weight, making them promising for application in buildings (e.g. for retrofits with weight constraints and buildings with lightweight bearing structures). Considerations of the life-cycle environmental impact of 3DP components could further highlight their potential. Compared to standard facade systems, the proposed mono-material 3DP components would be easy to replace and recycle, while the use of recycled polymers would significantly lower their embodied emissions [253].

[253]: Zhou Shengrong (2021), *An Environmental Perspective on 3DPrinted Facade with Plastics*

Building upon this study, the thermal insulation properties of 3DP facades can be further improved by introducing additional cavities within the element thickness. However, creating additional cavities comes with higher weight, printing time and cost, and reduced light transmission, and a trade-off needs to be identified. Using different layer thicknesses for the element, thicker for the outline and thinner for the infill, could help reduce the part's weight while ensuring structural stability. Moreover, polymers with lower thermal conductivity could be investigated such as ABS (λ=0.14-0.21 W/mK) and PP (λ=0.12-0.22 W/mK). Alternatively, the cavities could be filled with a low-conductivity material reducing convective heat transfer. However, this could significantly compromise the component's optical transmission properties and ease of disassembly. Low-emissivity materials/coatings could also be applied to reduce radiative heat transfer in the cavities.

Finally, to fully characterize the performance of translucent 3DP facades, the influence of solar radiation on the heat transfer needs to be investigated, considering the geometrical complexity of the elements. 3D printing creates anisotropic elements with layered resolutions, resulting in angle-dependent, directional transmission of solar radiation [197]. By coupling thermal and optical domains, we can define seasonal/temperature-dependent solar heat gain coefficients (SHGC) and U-values, which would better capture the component behaviour.

[197]: Piccioni et al. (2023), 'Tuning the Solar Performance of Building Facades through Polymer 3D Printing'

Acknowledgements

V Piccioni and M Leschok contributed equally to this work and jointly worked on paper conceptualization, experimental testing and writing.

MANUSCRIPTS RELATED TO THE DEVELOPMENT OF HC3DP

Large-scale Hollow-Core 3D-Printing (HC3DP): a polymer 3D printing technology for large-scale ultralightweight components

4

4.1 Overview of Paper C 73
4.2 Introduction 76
4.3 Method and Materials . . . 79
4.4 Results 84
4.5 Discussion 94
4.6 Conclusion 97

4.1 Overview of Paper C

4.1.1 Content

The manuscript discusses the development and application of hollow-core 3D printing (HC3DP) technology for large-scale 3D printing. For the first time, large-scale (>20mm) hollow beads are used for ME. The content of this paper includes the challenges of current pellet extrusion methods, the impact of material properties on the 3D printed parts, and highlights the need for alternative approaches to large-scale 3D printing processes. HC3DP focuses on minimizing the environmental impact, improving material efficiency, and increasing the printing speed by using hollow, tubular beads. Additionally, the document presents key parameters for successful HC3DP and states HC3DP guidelines. The study also quantifies material savings and print speed compared to ME and presents internal subdivisions for hollow 3D-printed beads.

4.1.2 Method

Process Development: The methods in the study involve the development and implementation of Hollow-Core 3D Printing (HC3DP) technology for large-scale thermoplastic extrusion. This includes the design and fabrication of bespoke nozzles with different cross-sections (6 and 24mm), with and without internal reinforcements. Printing experiments are conducted using different nozzles with and without internal air supply.

Printing experiments and thermal cooldown: The method for the thermal cooldown analysis involves conducting thermal imaging of the printed polymer samples to assess the cooldown rate of the material. The study uses a thermal camera (B1L - Hikmicro) to capture thermal images of the printed samples at specific time intervals after the completion of the printing process. The thermal images are taken at the end of the print, as well as 5 and 20 minutes after the print is finished. This allows for the measurement of the temperature distribution and cooldown characteristics of the printed polymer samples over time. The comparison of the cooldown rates between regular material extrusion (ME) and HC3DP provides the data to develop a simplified cool-down model to describe the thermal behavior of the two printing methods. Additionally, the authors conduct initial material experiments using four different compounds. Printing parameters such as temperature, extrusion rate, and internal air-pressure are adjusted to facilitate the successful printing of a cylinder of 40cm diameter. To successfully HC3DP with internally reinforced beads, printing experiments are conducted and the concept of differentiated air-pressure values per print point is introduced.

Extrusion-rate and print time comparison: The print time comparison for different 3DP technologies describes the fabrication time required for a 2m-tall cylinder with a diameter of 40cm. For large-scale HC3DP, this involves the fabrication of 2m-tall cylinders printed using HC3DP at a layer height of 19mm. This print time is then compared to the average fabrication speeds of other 3D printing technologies. For ME and small-scale HC3DP, the maximum extrusion rate for the given geometry determined in this manuscript is used to calculate the print time. For commercial 3DP methods, the calculations are based on data provided by the manufacturer, and for concrete 3DP, the calculations are based on published data.

3PT bending tests: 3PT bending tests are conducted using a Zwick 1484 with specimens of 270 mm support span. The bending tests aim to assess the mechanical behavior and performance of the 3D-printed hollow beads, with and without internal reinforcement inside the bead. The study utilizes two models for calculating bending stress: one for rectangular hollow beams and another for elliptical hollow beams, as detailed in appendix 4.6. The results of the bending tests are used to compare the different die geometries and evaluate their impact on the mechanical properties of the 3D-printed hollow beads.

4.1.3 Results

The study investigates the use of hollow-core 3D printing (HC3DP) for large-scale applications and evaluates its potential benefits in terms of extrusion rate, printing speed, material savings, and mechanical properties. The study finds that HC3DP can produce large-scale, lightweight elements using different materials and internal subdivisions for large-scale HC3DP beads. The 3PT bending tests provide valuable insights into the mechanical behavior of the 3D-printed hollow beads with different die geometries, contributing to a better understanding of their structural performance. Additionally, the study highlights the superior cooldown rate of HC3DP compared to regular material extrusion, emphasizing its potential benefits for large-scale 3D printing applications.

4.1.4 Authors contribution to the paper

Matthias Leschok: Visualization, Methodology, Investigation, Data curation, Conceptualization, Formal analysis, Writing - original draft, Writing - review & editing.
Lex Reiter: Formal analysis, Investigation, Validation, Writing – review & editing.
Benjamin Dillenburger: Writing – review & editing, Writing – original draft, Supervision, Project administration, Methodology, Conceptualization.

Abstract Material extrusion (ME) has become a popular 3D printing method for large-scale applications such as in the automotive, naval, aerospace, and architecture sectors. It allows the production of complex, customized parts without the need of labour-intensive molds. The increasing need to produce larger and larger parts has been addressed with the introduction of large pellet extrusion systems to increase the extrusion rate. With these extruders the production time is not limited by the extrusion rate of the extruder (kg/h) but by the time the material needs to cool down before the next layer can be printed consecutively. Furthermore, larger bead dimensions result in increased material usage and, therefore, might affect the environmental impact of the printed element. In this study, a method for large extrusion 3D printing based on hollow beads is proposed, to address the limitations of speed, cooldown and maximize the extrusion rate of thermoplastic 3D printing. This paper introduces Hollow-Core 3D printing (HC3DP) and compares it to off-the shelf large-scale pellet extruders and their maximum achievable extrusion rate for a given geometry. A comparative analysis of cooldown characteristics between conventional thermoplastic extrusion 3D printing and HC3DP validates that the latter increases the maximum possible extrusion rate. Additionally, the successful 3D printing of large-scale beads with multiple polymer feedstocks is demonstrated. Then the data associated with printing speed and material usage is presented and discussed in comparison with thermoplastic and other large-scale 3D printing methods. The fabrication of large-scale hollow-core beads at a dimension of 24×20mm is showcased with an extrusion rate of 7250 mm3/s (1308 material, 5941 air). HC3DP for large-scale applications is validated through the production of 2-meter tall cylinders with a diameter of 400 mm in less than two hours. Furthermore, bespoke die geometries that subdivide the inside of hollow 3D-printed beads are presented. To successfully print those, the concept of differentiated internal air pressure per print point is introduced. Finally, 3PT bending tests are conducted to compare different die geometries. In conclusion, this study presents a printing method that highlights the benefits of hollow core 3D printing for large-scale applications, showcasing its positive impact on both the printing process and resulting part properties. By addressing the limitations of traditional approaches, HC3DP pushes polymer 3D printing into a scale relevant for architecture and construction, offering similar extrusion rates as concrete 3DP.

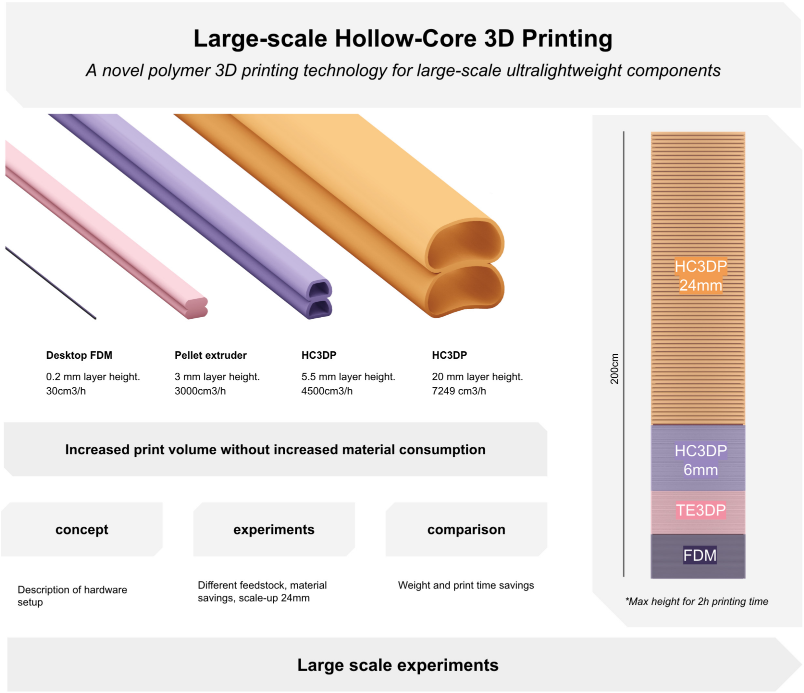
Large-scale Hollow-Core 3D Printing
A novel polymer 3D printing technology for large-scale ultralightweight components
Desktop FDM
0.2 mm layer height.
30cm3/h
Pellet extruder
3 mm layer height.
3000cm3/h
HC3DP
5.5 mm layer height.
4500cm3/h
HC3DP
20 mm layer height.
7249 cm3/h
Increased print volume without increased material consumption
concept
Description of hardware setup
experiments
Different feedstock, material savings, scale-up 24mm
comparison
Weight and print time savings
200cm
HC3DP 24mm
HC3DP 6mm
TE3DP
FDM
*Max height for 2h printing time
Large scale experiments

Figure 4.1: Summary of printing strategies investigated.

4.2 Introduction

Material extrusion (ME) is gaining popularity for large-scale applications such as automotive, naval, aerospace, and architecture [31]. It allows the production of complex, customized parts without the need of labor intense molds. Over the last few years, there has been a tendency to scale up the volumetric output of this printing process by introducing large pellet extrusion systems. These extruders use granular feedstock and extrude beads of approx. 10 mm width [30]. With these extruders, new fabrication constraints arise as the production time is not limited by the extrusion rate of the extruder (kg/h), but by the time the material needs to cool down before the next layer can be printed consecutively [254]. The larger the bead cross-section, the longer the material takes to cool down (surface-to-volume ratio). Furthermore, larger bead dimensions result in increased material usage and, therefore, might affect the environmental impact of the printed element. There is a need to find alternative approaches for large-scale 3D printing processes to keep its ecological footprint as small as possible. One way to address this challenge is to find alternatives to petroleum-based polymers [255], or to establish cradle-to-cradle production schemes. A fundamental shift in the 3D printing process is not yet investigated.

[31]: Pignatelli et al. (2022), 'An application- and market-oriented review on large format additive manufacturing, focusing on polymer pellet-based 3D printing'

[30]: Duty et al. (2017), 'Structure and mechanical behavior of Big Area Additive Manufacturing (BAAM) materials'

[254]: Go et al. (2017), 'Rate limits of additive manufacturing by fused filament fabrication and guidelines for high-throughput system design'

[255]: Singh et al. (2022), 'Sustainable materials alternative to petrochemical plastics pollution'

To close this gap, a large-scale thermoplastic extrusion process based on hollow-core-extrusion 3D printing (HC3DP) is presented (Fig. 4.2). The approach is to print with hollow beads instead of massive ones, to scale-up the 3D printing process through increased layer heights and faster cooling rates while reducing material consumption. Furthermore, HC3DP at large dimensions allows for the internal subdivision of the 3D-printed beads and has the potential to enhance the final components' properties.

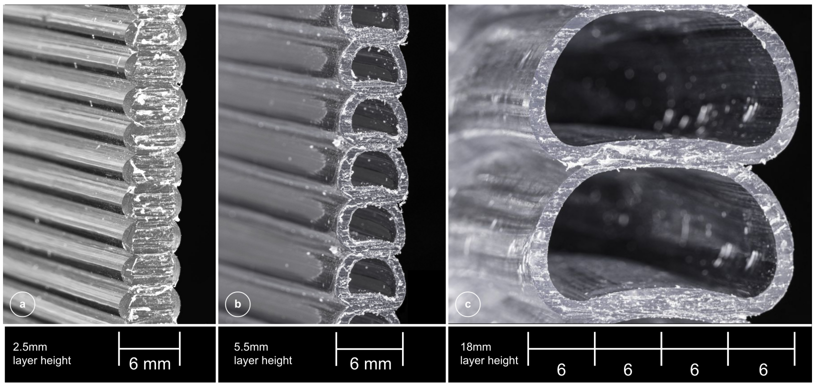

Figure 4.2: Sections of 3D printed single wall samples. (a) regular 3DP using a pellet extruder (b) HC3DP with a 6mm bead width and 5.5mm layer height. (c) HC3DP 24mm bead width and 18mm layer height. Regular ME results in a disco-rectangular shape, HC3DP in sagging beads.

4.2.1 Contribution and Outline

This manuscript contributes to the state of the art by introducing a 3D printing method of large-scale hollow-core plastic beads based on pellet extrusion. The text is structured as follows; first relevant state-of-the-art is presented and current challenges and drawbacks of ME at large dimensions are discussed. Then the concept of HC3DP is introduced and the fabrication setup and process are described. Initial material tests are conducted and the difference in the cool-down rate between HC3DP and regular ME is described. Large-scale HC3DP elements are printed and compared to state-of-the-art 3D printing methods regarding material consumption and print time. Finally, bespoke die geometries are introduced that subdivide the hollow beads into separate air pockets. 3PT bending tests are conducted to compare the different die geometries. The outlook outlines future research trajectories and discusses potential functional integration.

4.2.2 Thermoplastic extrusion

Since its invention in 1989 [8], 3D printing thermoplastics has become one of the most used additive manufacturing (AM) technologies today, especially for prototyping [256, 257]. The latest advancements on thermoplastic 3D printing focus on scaling up the material output (kg/h) by introducing granular feedstock extruders. Those so-called pellet extruders don't rely on pre-manufactured filaments but directly use granular (pellet) feedstock, similar to injection molding machines. By using these extruders, the output of printed material was increased from approx. 0.25 to over 50kg/h [30]. These large tool heads are mounted on either a robotic arm with a high payload and long reach, or on modified gantry systems, as found in large-scale CNC milling. A 3DP setup based on pellet feedstock usually consists of an extruder, a pellet drying/storing, and a material conveying system. Fused granular manufacturing (FGM), large format additive manufacturing (LFAM), or Big Area Additive Manufacturing (BAAM) all describe the process of using a granular (thermoplastic) feedstock to 3D print objects at a large dimension. To address the different extrusion-based 3D printing technologies with plastic, they are here referred to as Material Extrusion (ME).

[8]: Crump (1994), 'Modeling apparatus for three-dimensional objects'

[256]: N. Turner et al. (2014), 'A review of melt extrusion additive manufacturing processes'

[257]: Barnatt (2013), *3D Printing: The Next Industrial Revolution*

[30]: Duty et al. (2017), 'Structure and mechanical behavior of Big Area Additive Manufacturing (BAAM) materials'

4.2.3 Pellet extrusion 3D printing

One of the first times ME using granular feedstock was presented was during the production of the endless chair by the artist Dirk van der Kooji [26]. In parallel, DUS Architects started the development of a thermoplastic extrusion 3D printer for architectural applications of large dimensions [27]. Since 2015 the Oak Ridge National Laboratory has been researching ME with a focus on maximizing material output, increasing the dimension of the printed object [28], overcoming weak layer bonds [29], and characterising different printing materials [30]. ME is, due to its large build volume and material properties, most often used for automotive, naval, aerospace, and architectural applications. A detailed review of large-scale polymer extrusion can be found by [31, 37]. For architectural applications, 3DP polymers are used as molds for concrete [32], 3DP of facades [33, 44], wall elements [34], temporary structures [35], or interior elements such as furniture [36]. The growing interest in polymer 3D printing for diverse applications is reflected in the increasing number of commercially available printing systems (e.g., Thermwood, Ingersoll), pellet extruder providers (e.g., CEAD, Massiv Dimensions, Dyse Design), and companies/startups that focus on providing products or services for large-scale 3D printing (e.g. Nagami, AI build, The New Raw).

[26]: Kooij (2011), *Endless Chair - Kooij*

[27]: DUS Architects (2013), *XL 3D Printer – DUS Architects*

[28]: Love et al. (2015), 'Breaking barriers in polymer additive manufacturing'

[29]: Kishore et al. (2017), 'Infrared preheating to improve interlayer strength of big area additive manufacturing (BAAM) components'

[30]: Duty et al. (2017), 'Structure and mechanical behavior of Big Area Additive Manufacturing (BAAM) materials'

[31]: Pignatelli et al. (2022), 'An application- and market-oriented review on large format additive manufacturing, focusing on polymer pellet-based 3D printing'

[37]: Moreno Nieto et al. (2020), 'Large-format fused deposition additive manufacturing'

[32]: Jipa et al. (2022), '3D Printed Formwork for Concrete'

[33]: Naboni et al. (2022), 'Additive manufacturing in skin systems'

[44]: Leschok et al. (2023), '3D printing facades'

[34]: Branch Technology (2022), *Branch Technology*

[35]: Branch Technology (), *oneCITY Pavilion*

[36]: The New Raw (2015), *Crafting plasitc waste with robots*

4.2.4 Challenges

Although extrusion rate and print bed size have been increased, two major challenges need to be addressed to render the process economically and environmentally viable. One challenge of pellet extrusion methods is the printing process itself [258] due to the slow cool down of thick beads. One can speed up the printing process by increasing the extrusion diameter. However, because the extrusion height and width are coupled (ratio approx. 1:3), this further increases the amount of extruded material. Moreover, the large extruded volume decreases the cool-down rate of the printed material (surface vs. volume) [259] and has been found to be the major limiting factor for large-scale polymer applications [38, 260]. Therefore, unless very large pieces are required, the fabrication time is determined by the minimal layer time (the time the polymer needs to cool down) and results in reduced print speed. One approach to overcome this is to print multiple objects simultaneously. However, this might be challenging as travel moves need to be introduced, the material flow needs to be interrupted, and these starts/stops usually result in visible artefacts in the printed objects. Furthermore, not all commercially available ME systems are equipped with this functionality. Another challenge of current pellet extrusion methods is to improve the properties of the 3D printed parts: a large extrusion diameter leads to material intense parts. Hence, the resulting material properties are suboptimal compared to plastic elements fabricated by standardized fabrication processes such as injection molding or die extrusion. Wall thicknesses are not dictated by, for instance, structural or optical requirements but rather by the thickness of the extruded bead. This can result in walls that are thicker than required, using more material than needed.

[258]: Chesser et al. (2019), 'Extrusion control for high quality printing on Big Area Additive Manufacturing (BAAM) systems'

[259]: Compton et al. (2017), 'Thermal analysis of additive manufacturing of large-scale thermoplastic polymer composites'

[38]: Roschli et al. (2019), 'Designing for Big Area Additive Manufacturing'

[260]: Borish et al. (2020), 'Real-Time Defect Correction in Large-Scale Polymer Additive Manufacturing via Thermal Imaging and Laser Profilometer'

4.2.5 Complex extrusion systems

Over the last few years, complex 3D printing systems have been investigated to create lightweight large-scale elements or improve functional integration. Complex extrusion systems go beyond standard AM technologies as defined in the ISO standard. They allow the fabrication of unseen structures that are hard or impossible to create with traditional manufacturing techniques, even off-the-shelf 3D printing systems. Examples include actuated multi-nozzle tool heads that allow for dynamic co-extrusion [261], spatial 3D printing of thermoplastics to create lightweight cellular-like structures [34], or rotational co-extrusion techniques featuring different mechanical properties [262]. These complex printing systems rely on sophisticated control, measuring, or sensing devices to generate a desired outcome. The 3DP path is not only defined by a series of points in space and speed control of one motor (e.g., RPM/min) but rather through a plethora of different mechanisms that need to be orchestrated.

[261]: Yuan et al. (2016), 'Robotic Multi-dimensional Printing Based on Structural Performance'

[34]: Branch Technology (2022), *Branch Technology*

[262]: Larson et al. (2023), 'Rotational multimaterial printing of filaments with subvoxel control'

For thermoplastics, 3DP of tubular polymer beads was initially envisioned by [263] and first implemented by Hopkins et al. [264]. They showed that it is possible to 3D print tubular beads in a layered fashion, not only as in regular 3D printing but also free in space without being supported from below. However, the experiments are limited to 3D printed samples of approx. 10cm in height for a vase-like object, and larger sculptural elements like a freestanding logo/lettering or a self-supporting spiralling tube with a bead size of approx. 8mm. The extrusion rate of their custom filament 3D printing setup can be calculated based on the die dimension and maximum extrusion rate of the thermoplastic 3D printing tool, 44.73mm3/s (10.4mm3 plastic, 33.39mm3 air). Although the first ones to present tubular extrusion 3D printing, the questions on the feasibility of scaling up the process remain unexplored, while the potential opportunities for large-scale applications are not discussed or investigated. Transferring this method to pellet extrusion systems will allow increased material output, which is crucial for large-scale 3DP, and therefore explored in this paper. Furthermore, the potential benefits of large-scale HC3DP need to be outlined and quantified in regard to material savings and increased volumetric output. No comparison to other polymer extrusion systems or other large-scale 3DP methods exist yet. There is no information about using different feedstock materials or the fabrication of large-scale elements using HC3DP. Finally, until now there has been no precedence of bespoke internal geometries within 3D-printed hollow beads

[263]: Brad Michael Bourgoyne (2015), 'Method and apparatus for additive fabrication of three-dimensional objects utilizing vesiculated extrusions, and objects thereof'

[264]: Hopkins et al. (2020), 'Additive manufacturing via tube extrusion (AMTEx)'

4.3 Method and Materials

4.3.1 Hollow core 3D printing (HC3DP)

3D printing with pellet extruders is a process of creating a three-dimensional object by depositing layers of thermoplastic granular feedstock that is melted and extruded through a nozzle. Pellet extruders are used where large-scale components are required. The process of 3D printing with pellet extruders typically involves the following steps:

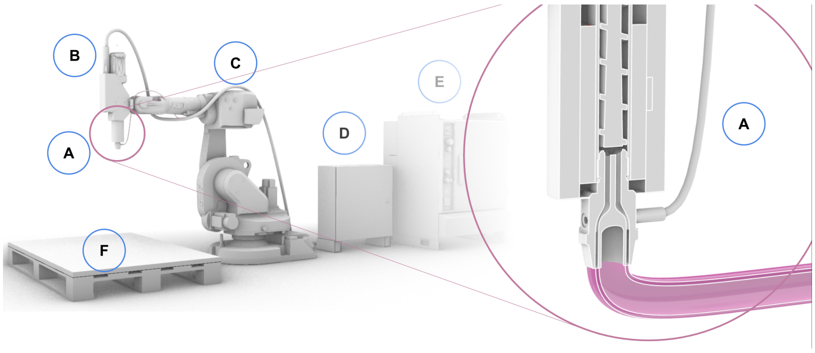

Figure 4.3: Schematic hardware setup for HC3DP. (a), HC3DP nozzle. (b), pellet extruder. (c), Robot, or gantry system. (d), the control unit for printing, including feedback processing. (e) robot controller. Right: Close-up of the closed-loop hollow core extrusion system and air inlet.

- Material Preparation: The first step is to prepare the material for 3D printing which starts by drying the granular feedstock (temperature and drying time are defined by the polymer). Then the thermoplastic pellets, which are typically fed into the extruder hopper through a conveyor system, are heated inside the extruder (heating zone) to a specific temperature to melt the material and prepare it for extrusion.
- Extrusion: Once the material is molten, it is forced through a nozzle using a screw or piston that pushes the molten material through the nozzle at a controlled rate. The nozzle is typically mounted on a movable gantry system or a robotic arm that deposits the material layer by layer to create the desired shape. The size of the nozzle determines the thickness of each layer, as the two are correlated.
- Cooling: After each layer is deposited, the material needs to cool and solidify before the next layer is added. This is typically achieved through a combination of cooling fans and ambient air or by using a heated chamber to control the temperature and humidity. Usually, this cool-down rate defines the layer-cycle time.
- Finishing: Once the printing is complete, the object may need to undergo additional post-processing, such as milling, sanding, painting, or coating, to achieve the desired finish.

[265]: Vlachopoulos et al. (2003), 'Polymer processing'

[263]: Brad Michael Bourgoyne (2015), 'Method and apparatus for additive fabrication of three-dimensional objects utilizing vesiculated extrusions, and objects thereof'

[264]: Hopkins et al. (2020), 'Additive manufacturing via tube extrusion (AMTEx)'

Although the production of tubes/pipes from granular polymer feedstock is well known as die-extrusion [265] and was initially introduced for filament based robotic 3D printing by [263, 264] it remains unexplored for large-scale 3DP. To 3DP hollow-core beads instead of solid ones, adjustments to the aforementioned fabrication setup need to be made. A custom nozzle, compressed air, and a control system must be introduced. This control system manages the printing parameters like temperature, extrusion rate, as well as air pressure for maintaining an inflated bead. The nozzle consists of a hollow mandrel supported by spider vanes to split the molten granular material into a thin wall and an empty core (Fig. 4.3). This hollow mandrel contains a cavity through which air is blown through the hollow core and into the 3DP bead. Providing a certain level of air pressure inside the bead prevents it from collapsing [263, 264]. The HC3DP nozzle replaces the existing nozzle of the pellet extruder and can therefore be easily adopted.

Table 4.1: Comparison of different nozzle geometries and wall thicknesses. Material savings are calculated in comparison to a full bead.

Name	Outer diameter [mm]	Wall thickness [mm]	Area full material [mm2]	Hollow area [mm2]	Plastic area [mm2]	Savings [%]
o6w1	6	1	28.27	12.57	15.71	44.44
o24w2	24	2	452.39	314.16	138.23	69.44
o24w1	24	1	452.39	380.13	72.26	84.03

4.3.2 Printing setup and saving potential

For the experiments, different nozzles are mounted on a commercially available pellet extruder from SAEKI Robotics [266]. The extruder has three different heating zones and is mounted on an ABB IRB 6700 6-axis robotic arm. The robot has a reach of over 3m and a payload of 150kg. For ease of use, a 2×1m wooden plate is used as a print platform which allows for temporarily fixing the large-scale 3D printed objects. The goal of this experimental setup is to allow the creation of elements at large dimensions.

[266]: SAEKI Robotics (), *SAEKI Robotics*

The HC3DP nozzles described in the Table 4.1 low differ in overall size and wall thickness. The most right column shows the material savings compared to an equivalent full cross-section. Depending on the diameter of the printed bead and the wall thickness, material savings can be as high as 84%. However, this initial calculation does not consider the disco-rectangular shape of the extruded bead nor shape deviations of large-scale HC3DP beads.

4.3.3 Thermal imaging and material testing

For large-scale ME, the insufficient cooldown of the printed beads holds the risk of sagging/deforming or even collapsing of the 3D printed object [38, 260]. To illustrate the impact of the cooldown rate of the printed polymer and its correlation to extrusion rate, several single-outline cylinders with a diameter of 40cm, a height of 25cm, and a bead width of 6mm are 3D printed. First, the maximum extrusion rate of a regular 3D-printed cylinder is empirically determined. Over multiple prints, the print speed is increased until the print fails due to overheating, see Fig. 4.9. The printing temperature is kept constant while the material flow is increased to keep the bead width at 6mm. Then HC3DP with identical settings and bead width is used to successfully 3D print the cylinder at the same and even higher extrusion rate. The cooling fan was disabled during these tests to keep the results comparable. The cooling rate of regular and HC3DP beads is documented using a thermal camera (B1L - Hikmicro), taking images at the end of the print, as well as 5 and 20min after the print is finished. The thermal camera is fixed at a distance of 1m from the center of the printed cylinder. The material used for these experiments is Polyethylene terephthalate glycol (PETG).

[38]: Roschli et al. (2019), 'Designing for Big Area Additive Manufacturing'
[260]: Borish et al. (2020), 'Real-Time Defect Correction in Large-Scale Polymer Additive Manufacturing via Thermal Imaging and Laser Profilometer'

The selection of printing material has several implications on the performance of the final product and determines its environmental impact. There is a wide range of thermoplastic materials available for 3D printing. Amongst the most common are PLA, ASA, PETG, and ABS with or without fibers. To prove the viability of the proposed printing method, 40×40×30cm cylinders are 3D printed using different materials. This

Table 4.2: Comparison of different nozzles, showing area of extruded plastic and internal voids [mm2].

Name	Outer diameter [mm]	Wall thickness [mm]	Cores [amount]	Plastic cross section [mm2]	internal void [mm2]	ratio plastic/air [%]
o24w1	24	1	1	73.5	380.13	16.25
o24w2	24	2	1	138	314.39	30.5
o24w1Quad	24	1	4	117.29	334.68	25.93

study should be understood as a first proof of concept and is not an extensive investigation of printing parameters and material behavior. In total, four different materials are tested:

- Polylactic acid (PLA), bio-based and biodegradable
- Cyclic olefin copolymer (COC), translucent amorphous polymer
- Polypropylene (PP), second most produced polymer
- Polyethylene terephthalate Glycol (PETG), nearly transparent polymer

For the large-scale experiments described in chapter 4.4.4, PETG was used due to its high transparency, chemical, and structural resistance [232]. PETG is an established material for manufacturing products for medical and food applications. It is a co-polyester of PET with an extra monomer which suppresses the crystallization process [231] and increases its moldability, making it the preferred option for 3D printing compared to PET.

[232]: Petrov et al. (2021), 'Research into the effect of the 3D-printing mode on changing the properties of PETG transparent plastic'

[231]: Sepahi et al. (2021), 'Mechanical Properties of 3D-Printed Parts Made of Polyethylene Terephthalate Glycol'

4.3.4 Large-scale experiments and comparison

To prove the viability for large-scale applications cylindrical elements of 0.4×2.0m are printed and compared to two conventional ME methods. The proprietary slicing software Blade from the company BigRep is chosen to represent filament-based extrusion systems. Furthermore, values for a standard pellet extruder system with a 6mm nozzle are calculated. Here, the maximum extrusion rate, experimentally determined in Section 4.4.2 is considered. Finally, the print time, material consumption, and weight of the printed objects are compared.

4.3.5 Bespoke die geometries and structural experiments

Large-scale HC3DP allows for the fabrication of large bead sizes, 24mm and above. This provides the opportunity to experiment with different wall thicknesses and introduce internal geometries into the 3D-printed bead. Those internal subdivisions of the bead can be used for reinforcing the large-scale thin-walled beads, or allowing for the individual transportation of fluids or encapsulating other materials. Therefore, three types of HC nozzles are designed and prototyped using 3DP of aluminium (Fig. 4.4). All nozzles have an outer diameter of 24mm, a) is a nozzle with no internal geometry and a wall thickness of 1mm, b) is a nozzle with a 2mm wall thickness, and c) contains a cross to reinforce the bead and separates the bead into four individual areas. A more detailed overview can be found in Table 4.2.

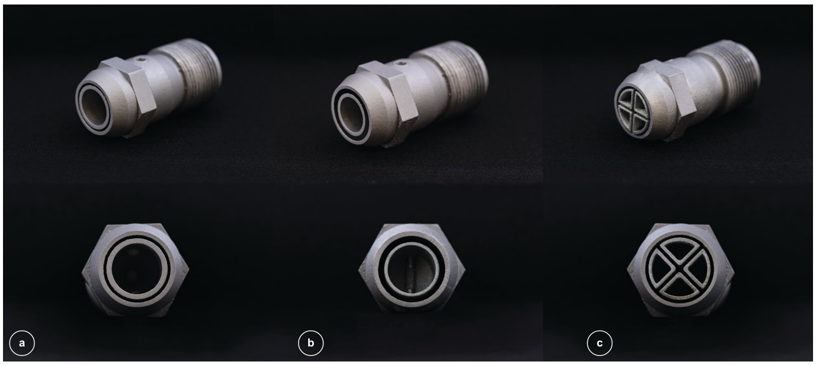

Figure 4.4: Different nozzles types, prototyped using 3DP of aluminum.

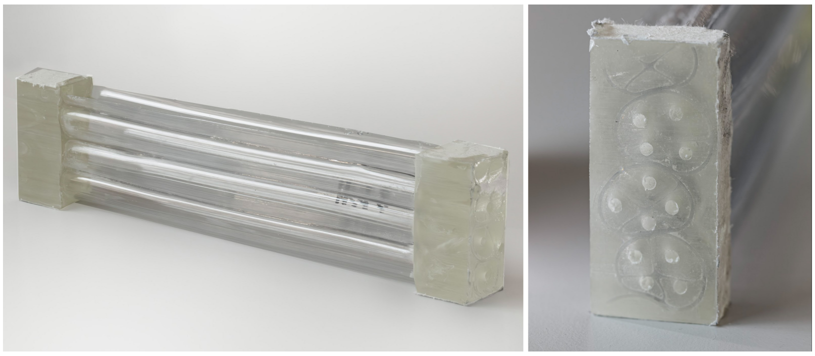

Figure 4.5: Sample preparation for 3PT bending tests.

To conduct 3PT bending tests, comparing the different die geometries to each other, basic rectangular elements with a footprint of 500×50mm and a height of approx. 250mm are 3D printed. The rectangular shape is chosen for the sample to be stable enough to be printed without support, and the distance between the two outlines helps to accommodate for the minimal features size/turning radius of large-scale HC3DP. Due to the large diameter of the HC bead, a minimal radius at corners/ distance between two points is needed, as otherwise, the risk of self-intersection and overinflation increases.

The tested samples have a length of 300mm and consist of three undisturbed layers (Fig. 4.5). The last and first 30mm of the samples are cast into an epoxy resin foot to avoid collapse at the supports during testing. First, one side is cast and once the resin is hardened, holes are drilled into the resin to allow for air circulation. This makes sure that while casting the second side, the resin can enter all internal voids and spread evenly. Finally, the resin blocks are sand to make flat contact with the supports of the universal testing machine (Zwick 1484). The distance between the supports is 270mm and the testing speed is 6mm/s. Before testing, the middle area of the samples are taped with a glass fibre reinforced tape (1 turn with 5mm overlap). The tape should prevent brittle failure and allow for a more equal load distribution into the not perfectly printed elements.

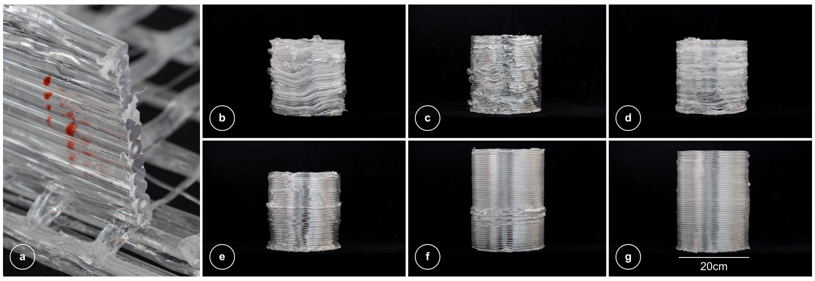

Figure 4.6: (a) Initial experiments of HC3DP without air support, resulting in non-inflated beads. Only two out of 13 beads remain non-solid. (b-g) Series of test prints adjusting printing parameters to increase print quality.

4.4 Results

4.4.1 Process development and geometrical limitations

The following section describes the development of HC3DP for large-scale applications and highlights process-specific constraints. The first design iteration of the hollow-core nozzle had a 6 mm orifice and a solid 4 mm mandrel supported by spider vanes and was fabricated using metal 3D printed (DMLS) titanium. During initial experiments, the pellet extruder was rotated to have an angle of 45 degrees in relation to the print platform. Although successful for some layers/beads, it was impossible to maintain hollow beads throughout the entire object (Fig. 4.6.a). Therefore, the authors decided to introduce air support during the printing process. This approach is similar to the blow extrusion of standardized tubes or pipes. This fabrication technique either operates by pulling a vacuum around the extruded bead or by using positive pressure inside the hollow bead [265]. However, as 3D printing is a fabrication process designed for non-standard production, the latter approach was chosen, confirming the previous findings of [263, 264]. To enable the extrusion of large-scale hollow beads using a pellet extruder and provide a higher degree of control, an electronic pressure regulator is introduced. To facilitate air support, the second iteration of the HC nozzle features an air inlet on the side, allowing air to enter the nozzle and flow into the extruded hollow tube. The introduction of air as support during the print process was successful and led to a series of test prints to iteratively increase the print quality by finding the correct parameters (Fig. 4.6). By introducing the air pressure inside the 3DP bead, the tool head can be positioned perpendicular to the printing platform (Fig. 4.3). Avoiding the constant rotation of a tool reduces tool path planning complexity and therefore makes the process more convenient to use.

[265]: Vlachopoulos et al. (2003), 'Polymer processing'

[263]: Brad Michael Bourgoyne (2015), 'Method and apparatus for additive fabrication of three-dimensional objects utilizing vesiculated extrusions, and objects thereof'
[264]: Hopkins et al. (2020), 'Additive manufacturing via tube extrusion (AM-TEx)'

The five major parameters for a successful hollow-core 3D print are identified as robot speed, extrusion rate, melting temperature, internal air pressure, and external cooling fan. With this, the authors extend the key parameters identified by [264] (speed and flow) in order to gain a higher level of control. When printing with a pellet extruder it is of great importance being able to control all the aforementioned parameters as the process appears to become more sensitive. The external cooling fan works hand in hand with the internal air pressure to maintain the cylindrical shape of the hollow-core extruder bead and prevents the bead from collapsing or overinflating.

[264]: Hopkins et al. (2020), 'Additive manufacturing via tube extrusion (AM-TEx)'

The following recurring errors were observed during the initial test prints (Fig. 4.7):

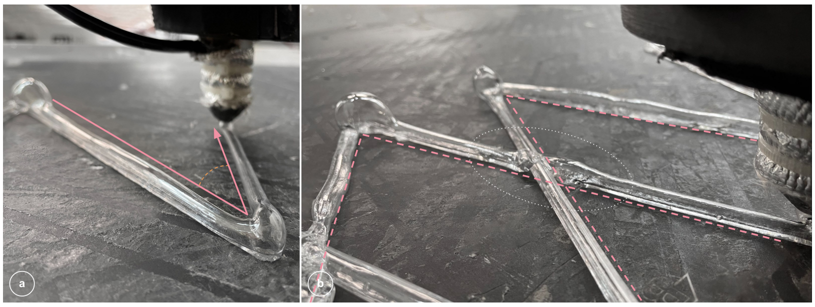

Figure 4.7: Typical printing errors of HC3DP. (a) Sharp corners can result in overinflation of the extruded bead. (b) Crossing of printpaths often results in a collapsed bead.

	HC	Regular	Sheet
wall thickness [mm]	1	n.a.	n.a.
layer width [mm]	6.5	5	6
layer height [mm]	5.2	2.5	2.5
printed width [mm]	200	200	200
printed height [mm]	186	193	200
weight [g]	126.1	219.4	297.6
volume [mm3]	241800	193000	240000
scale factor	0.99	1.24	1
normalised weight [g]	125.16	272.83	297.6
Saving compared 3DP			54.12%

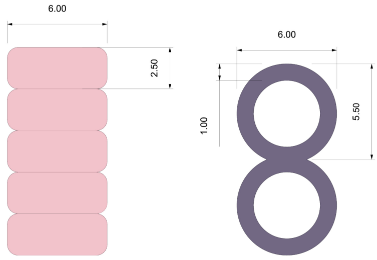

Figure 4.8: Comparison of HC3DP, regular 3DP, and a PETG sheet of similar size. The material savings of HC compared to TE3DP are over 50%. Samples size 200×200×6mm. Measured results and normalized values for a plate of 200×200×6mm.

- Overinflation due to too high pressures, too little extrusion, or material feeding failures
- Sharp corners may result in an internal collapse. The material is forced to twist around itself as the toolhead does not rotate with the change of print direction.
- Self-intersecting toolpaths are challenging and may result in print failures as the freshly extruded hollow-bead collides with the already solidified bead and gets pierced.

4.4.2 Material consumption and cool-down

One of the major implications of HC3DP in comparison to regular ME is the reduction of material usage. Fig. 4.8 compares the material consumption for 200×200×6mm samples printed with HC3DP, regular ME, and a PETG sheet. The printed sample has a wall thickness of 1mm, and the chosen material is PETG. For a 6mm bead width (nozzle o6w1), the material savings of HC3DP are over 50% and can vary depending on the wall thickness of the extruded bead.

Another significant benefit is the increased cool-down rate of HC3DP in comparison to regular ME. The print speed of large-scale ME is often limited by the cooldown of already printed layers [38, 260]. To determine the maximum extrusion rate for traditional ME of the sample geometry (cylinder 40cm diameter), multiple samples were printed at a speed of 20, 30, 40, and 50mm/s. The print with a speed of 50mm/s failed due to overheating (Fig. 4.9. c). However, the failure speed/ minimal layer cycle time is expected to be between 40 and 50mm/s printing speed, equivalent to a layer cycle time between 25 and 31s Table 4.3 shows a more detailed comparison of the printed cylinders and their maximum extrusion rate. The extrusion rate is calculated as follows:

[38]: Roschli et al. (2019), 'Designing for Big Area Additive Manufacturing'
[260]: Borish et al. (2020), 'Real-Time Defect Correction in Large-Scale Polymer Additive Manufacturing via Thermal Imaging and Laser Profilometer'

$$extrusionrate = (section_{polymer}+section_{air})[mm2]*printingspeed[mm/s]$$

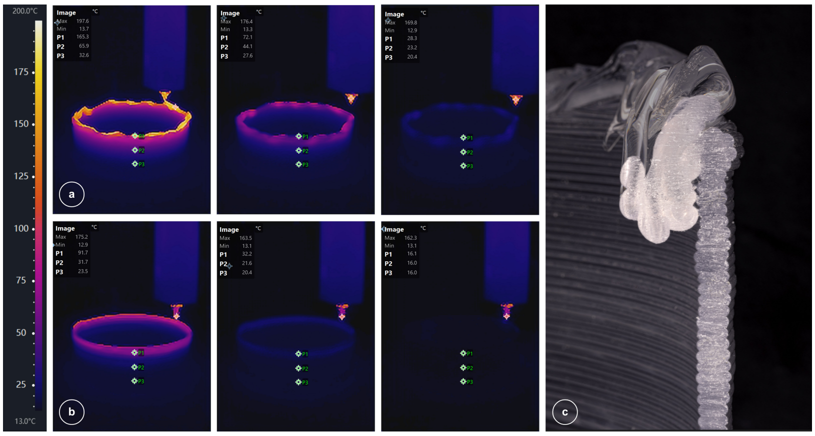

Figure 4.9: Printed samples 40cm diameter, 20cm height. (a) Regular large-scale 3D printing, buildup rate 5.97mm/min, resulting in print failure. (b) HC3DP, buildup-rate 9.19mm/min. Thermal images after 1min, 5min and 20min cooldown time. (c) Cut sample of collapsed regular ME due to overheating.

Table 4.3: Maximum extrusion rate of traditional ME and HC3DP, assuming a symmetric disco rectangular shape. Ambient temperature 10.5°C.

Type	width [mm]	height [mm]	temperature (z1-z2-z3) [C]	diameter [mm]	length / layer [mm]	print speed [mm/s]	extrusion rate [mm3/s]
TE3DP	6	2.5	160 - 200 - 210	400	1256.64	45	614.64
HC3DP	6	5.5	160 - 200 - 210	400	1256.64	35	927.79
improvement							150.95%

Subsequently, the same geometry is 3D printed using HC3DP with an identical bead width of 6 mm. The authors could prove that HC3DP can fabricate the same object at an increased extrusion rate compared to traditional ME. The improvement is over 50%, depending on how the extrusion rate for ME is defined. To calculate a successful ME at a print speed of 45 mm/s is assumed. For both sets of experiments (regular ME and HC3DP) the object fan described in Section 4.3.1 was deactivated. The authors believe that the extrusion rate improvement can be even more significant when active cooling is enabled.

As documented in Fig. 4.9 and Fig. 4.11, the cool-down rate of HC3DP is superior to regular ME. One minute after finishing the print, the measurement point P1 is measured to be at 165.3 °C for regular ME and 91 °C for HC3DP. After 5 min, regular ME holds a temperature of approx. 72.1 °C, whereas the HC3DP sample is already cooled down to 32.2 °C. Twenty minutes after the print has finished ME has a temperature of 28.3 °C and HC3DP 16.1 °C. Although those measurements are not to be understood as absolute accurate, the results are comparable to each other and showcase a dramatic increase in cool-down.

Specifically interesting in the rapid drop down in temperature for the most upper layer (Fig. 4.11). The boundary conditions for large-scale polymer extrusion 3D printing has been described by [259]. However, their thermal model still needs to be adapted for the double-sided cooling of tubular 3D printed beads. Therefore, the authors propose to distinguish between two phases of cooldown. In the most upper layer, the cross-section material to be cooled is proportional to the surface from which radiation can emit heat, which is the sides and the top surface. In this case simply the bead wall thickness is considered. For all layers below, the interfaces of two beads also have to cool down and they will do so by transferring heat to the side walls (Fig. 4.11 right). An equivalent wall thickness is calculated by distributing all extruded material onto the area of the side walls:

[259]: Compton et al. (2017), 'Thermal analysis of additive manufacturing of large-scale thermoplastic polymer composites'

$$bead\,wall\,thickness*(area\,of\,interface+area\,of\,sides)/area\,of\,sides \tag{4.1}$$

In order to build a first order model understanding and in lack of active cooling and for thin sections, thermal radiation, heat conduction and heat convection should be considered. To find the critical phenomena, the Nusselt number Nu is considered [267]. For the most upper layer free convection from a horizontal layer is considered, giving Nu in the range of 60, while for the lower layers a vertical wall and inner geometry are considered, giving Nu of 70 and 56 respectively. This shows that convection dominates over conduction. Furthermore, thermal radiation heat flow from the respective surfaces is compared to thermal convection, giving similar heat rates for both the upper most layer (71 W compared to 75 W) and layers below (161 W compared to 179 W). Given the similarity, thermal radiation is then considered as a simplified surrogate system. Furthermore, the Biot number is considered to distinguish heat conduction in the material and convection at the surface, giving a convection dominated system for the upper most layer and a mixed one for lower layers. This will mean that temperature decrease takes longer in lower layers compared to the simplified model presented here. Since temperature difference is smaller from layer to layer than to air temperature and the distance is longer, the Biot number for lower layers indicates that heat transport from one layer to another is negligible compared to convection. Thus the net radiative heat transfer from the surface to its surrounding is considered, which is the radiation leaving the material, minus the heat arriving from the surrounding. The rate of net heat transfer is calculated with the Stefan-Boltzmann law according to $e\sigma A(T^4 - T_e^4)$ with T the temperature of the surface, T_e the temperature of the environment, A the radiating surface, σ the Boltzmann constant and ε the emissivity and assuming similar values for both surface and environment.

[267]: Churchill et al. (1975), ‘Correlating equations for laminar and turbulent free convection from a vertical plate’

The temperature of the material decreases over time by the rate of the net heat transfer, with the material volume as its heat reservoir. For simplicity α here encapsulates all factors not related to geometry and temperature.

$$-\frac{dT}{dt}V = \alpha\ A(T^4 - T_e^4)$$

This form of differential equation is inconvenient to solve by separation of variables and thus the following approximation is used, where the factor $(T^4 - T_e^4)$ is expanded to $(T - T_e)$c with $c = (T + T_e)(T^2 + T_e^2)$. It can then be assumed that for small changes of temperature the factor is constant and the integration can be done for small temperature changes. The ratio $\frac{A}{V}$ is related to the equivalent wall thickness b as follows $\frac{A}{V} = \frac{1}{b}$. The equation thus writes as:

$$\int_{T_j}^{T_{j+1}} \frac{dT}{T - T_e} = -\int_{t_j}^{t_{j+1}} \frac{ac}{b} dt$$

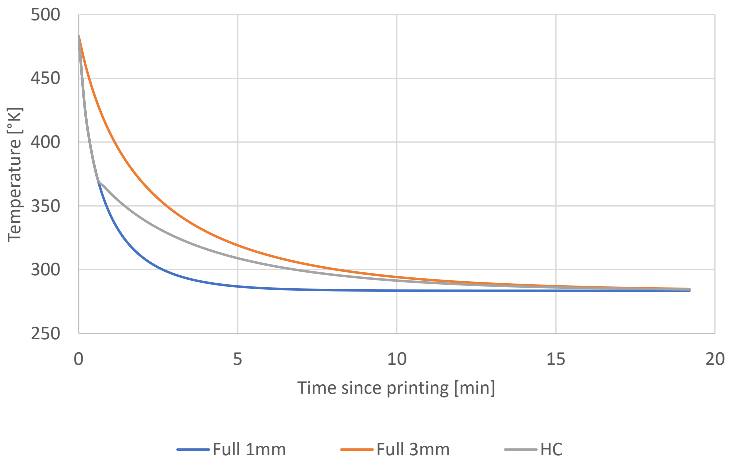

Figure 4.10: Qualitative temperature evolution for full walled filaments and HC (0.6min with 1mm, then 3mm.)

where T_{j+1} is the material temperature at time t_{j+1}. After integration of both sides of the equation, the relationship writes as:

$$\ln\left(\frac{T_{j+1}-T_e}{T_j-T_e}\right) = \frac{ac}{b}(t_j+1-t_j)$$

Separating for the temperature at time the equation writes:

$$T_{j+1} = (T_j - T_e)e^{-\frac{ac\Delta t}{b}} + T_e$$

This relationship shows elegantly that the time to cool a bead by a certain amount is directly proportional to the wall thickness. For a HC filament, the surface available to radiate from is disproportionately higher in the top layer than in consecutive layers, thus while it is fully exposed it can cool much faster than an equivalent full section filament. This in terms means that HC filament can be extruded at a much higher rate. This phenomenon is illustrated in Fig. 4.10.

The model is compared to the experimental results in Fig. 4.11 using a fitting value. The results show that the model captures the rapid temperature drop of HC compared to ME and shows excellent agreement up to 5min after printing. At later stages heat transfer between layers might have a significant effect on the cooling rate, leading to a bigger discrepancy at 10 and 15min.

To summarise, the reasons for the increased extrusion rate are twofold: HC3DP allows the extrusion of more rounded beads compared to traditional ME due to the inflation of the bead. The ratio of extrusion

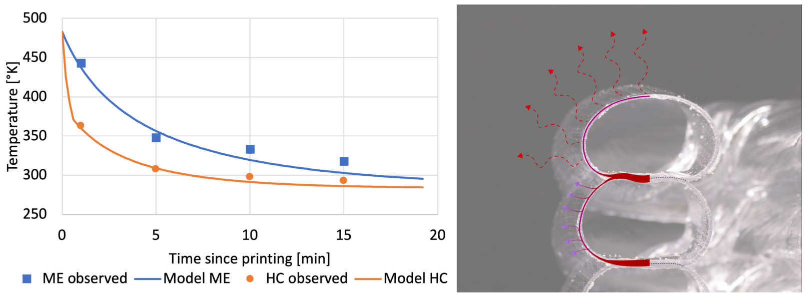

Figure 4.11: Comparison between experimental results. Model ME b=6mm, Model HC b=1mm for 0.6min, then b=3mm. Right: Diagram of equivalent wall thickness.

width to extrusion height is closer to 1:1 instead of the commonly used 3:1, which increases the layer height without increasing the layer width. Furthermore, the increased cooldown rate of the most upper layer allows for a shorter layer cycle time and thus increased extrusion rates.

4.4.3 Large-scale HC3DP and materials

The following section introduces 3D printing of large-scale hollow beads with an orifice of 24mm. Then the results of printing with different materials are described. The focus here lies in showing the potential of HC3DP to fabricate elements at a large dimension and not on the individual printing parameters.

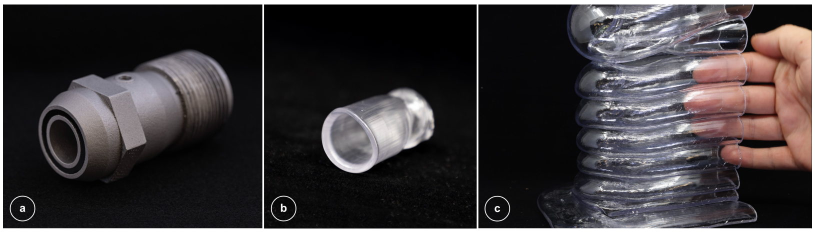

Figure 4.12: HC3DP nozzle with a 24mm orifice and a 2mm wall thickness. (b): Extruded PETG bead. (c): 3D printed sample, cut, with a hand to represent scale and transparency.

Fig. 4.12 shows the first large-scale nozzle for HC3DP with an orifice of 24 and a wall thickness of 2mm. Furthermore, it displays the first extruded bead, as well as a cut sample. The experimental fabrication setup described in section 4.3.1 did not need adjustments to print larger bead sizes. Simply the nozzle was replaced. In regard to the printing parameters, the material flow, as well as the air pressure, needed to be increased to extrude at an increased scale.

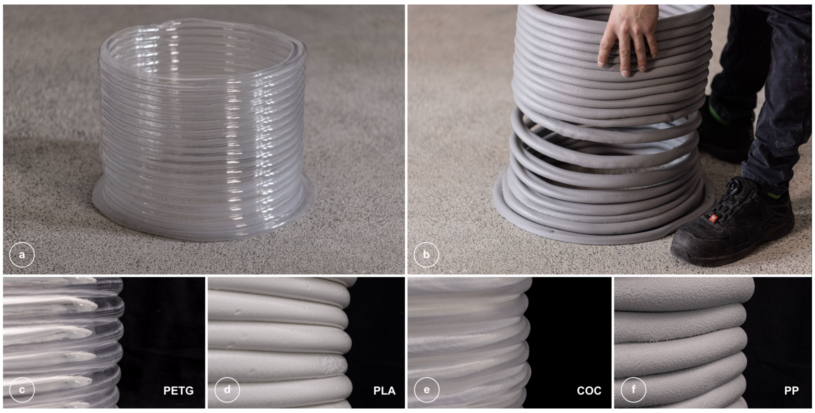

Figure 4.13: HC3DP cylinders. (a) PETG, (b) PP needed an increased printing speed to maintain layer adhesion, the print speed was increased from 6 mm/s to 10 mm/s. Lower row: 40cm diameter samples printed using different materials. (c) PETG, (d) PLA, (e) COC, and (f) PP.

In total, the authors successfully printed large-scale HC samples using four different thermoplastic materials. It was found that all materials can be 3D printed using HC3DP, although the printing parameters like extrusion rate, print speed, and air pressure were adjusted during the experiments. The observations can be summarized as follows: PETG creates elements with high transparency (see Fig. 4.7.c and 4.8.a.): This can be explained by the thin wall thickness of the 3D-printed hollow bead and the reduction of layer interfaces. Those interfaces mainly determine the light transmittance through a 3DP component [197]. It can be printed with consistent quality. COC showed the greatest deviation between the original print path and the final object, which might indicate excessive

[197]: Piccioni et al. (2023), ‘Tuning the Solar Performance of Building Facades through Polymer 3D Printing’

shrinkage. Furthermore, it required the highest pressure values to stay inflated. Only for COC it was necessary to supply air to both air inlets of the nozzle. PLA was easy to print and closely maintained the desired shape. PP needed to be printed at a higher print speed (10 vs. 6mm/s) as the layers did not adhere to each other (Fig. 4.13). The individual printing parameters can be found in Table 4.

Table 4.4: Summary of printing parameters used during the material testing. For all experiments, two 24v 60mm fans with a flow rate of 40m3/h are used for cooling.

Material	Air supply	Air Pressure [bar]	Extrusion rate [RPM]	Print speed [mm/s]	Temperature [°C] [z.1, z.2, z.3]
PETG	single inlet	0.06	66	6	145, 190, 200
COC	both inlets	0.1	84	6	180, 215, 230
PLA	single inlet	0.11	84	6	165, 185,190
PP	single inlet	0.06	108	10	165, 180, 185

4.4.4 Large-scale prototypes

To showcase the unique qualities of HC3DP for large-scale elements, multiple two-meter tall cylinders are 3D printed. Fig. 4.14 documents the printed large-scale elements. To maximise the extrusion rate of the extruder, a new nozzle with a 24mm orifice and a wall thickness of only 1mm (o24w1) is designed and fabricated. This allows to reduce the amount of extruded polymer while at the same time increasing the cooldown rate, as it is mainly determined by the wall thickness. The print speed was 18 mm/s which is equivalent to an extrusion rate of over 7249mm3/s, leading to a total print time of only 1:54 hours. This does not represent the absolute maximum print speed, it was beyond the scope of this manuscript to determine the maximum extrusion rate for this specific nozzle. However, the authors are able to showcase that lightweight elements with large dimensions can be fabricated with dramatically increased printing speed.

Table 4.5 compares two-meter tall cylinders 3D printed using different fabrication techniques. The authors chose to compare the proposed printing method against off-the-shelf polymer 3D printing methods, as well as 3DP methods specifically designed for large-scale applications like concrete 3D printing or Gel Dispensing Printing (GDP). As an off-the-shelf large ME 3D printer the BigRep pro.2 is chosen. The version 3.6.2 of *Blade* is used to generate the toolpath for the bigRep 3D printer. As the printer has a build height of max. 985mm, a cylinder of 400mm diameter and 500mm height is imported. PETG transparent is chosen as a printing material and the standard 0.6mm settings for slicing are used. The infill

Table 4.5: Comparison of extrusion rate [mm3/s] for different printing setups. Regular ME, HC3DP, BigRep pro.2 3D printer. The values represent a single outline print.

Type	l. width [mm]	l. height [mm]	disco rectangle area [mm2]	print speed [mm/s]	extrusion [mm3/s]	2m cylinder [h:m:s]
BigRep	1	0.6	0.52	20	10.45	58:10:40
ME	6	2.5	13.66	45	614.64	06:12:20
HC3DP 6mm	6	5.5	26.51	35	927.79	03:37:36
HC3DP 24mm	24	18	362.47	20	7,249.38	01:56:21

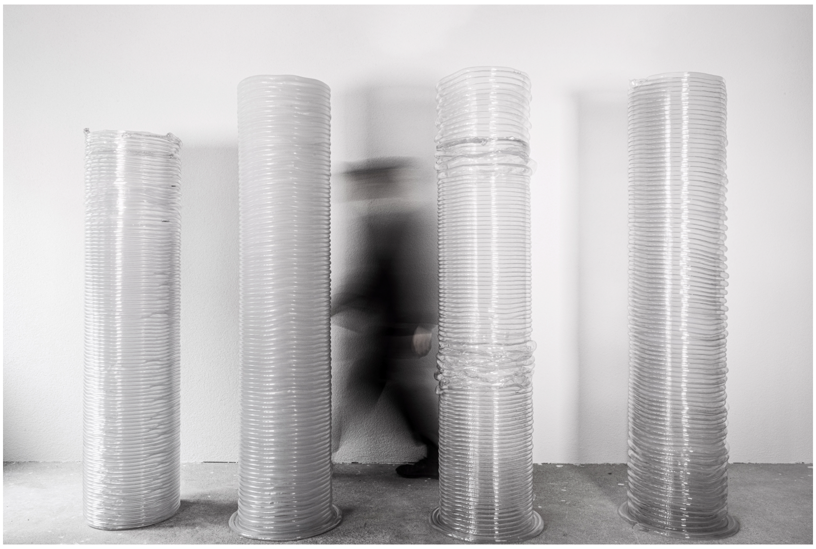

Figure 4.14: Series of 40cm diameter cylinders printed at different layer heights. The final demonstrator (right) is 2 meters tall, and the print time is 1:54 hours, weight 10.3kg.

is reduced to 0%, as well as the top and bottom layers are removed. The estimated print time is 14:40h for a 500mm high element. For a 2-meter tall cylinder, the print time is approx. 58 hours. For ME, a print speed of 45mm/s is assumed, which reflects the experimentally determined maximum extrusion rate for the given geometry. The print time for a 2m tall cylinder printed with a layer height of 2.5 and a width of 6mm is 6:12h. For concrete 3DP, an average fabrication speed of 1h/m in height is assumed as stated in [268]. For GDP, the print time is calculated based on the manufacturer reference of a 100 cm diameter cylinder having a fabrication speed of 0.35m/h in height [269]. For the reference cylinder, this results in a print time of 2:17 hours.

[268]: Anton et al. (2021), 'A 3D concrete printing prefabrication platform for bespoke columns'

[269]: Massivit (2022), *Massivit*

The comparison shows that none of the listed thermoplastic 3DP technologies can compete with the extrusion rate of HC3DP. The extrusion rate of hollow-core is more than 10 times higher than state-of-the-art pellet extrusion systems. Only concrete 3DP and GDP provide a similar printing speed for the given geometry.

4.4.5 Bespoke die geometries and differentiated air pressure values

To successfully 3D print large-scale hollow beads with bespoke die geometries it is necessary to introduce the concept of differentiated air pressures per print point. So far, the internal air pressure is kept constant to keep the beads inflated and can only be turned off/on. However, changes in print direction (sharp corners) are challenging to print if the air pressure inside the bead is kept at a constant value. Typical errors/failure modes are documented in Fig. 4.7 and Fig. 4.16. This becomes especially problematic when the hollow bead is subdivided into several air pockets. During turns and sharp corners, the printed bead twists and so does its internal structure, potentially causing the air pockets to collapse in themselves. Three possible solutions for this problem are identified:

- adapting the object geometry. Adjusting the minimal radius for corners and giving the bead more length to perform the twist

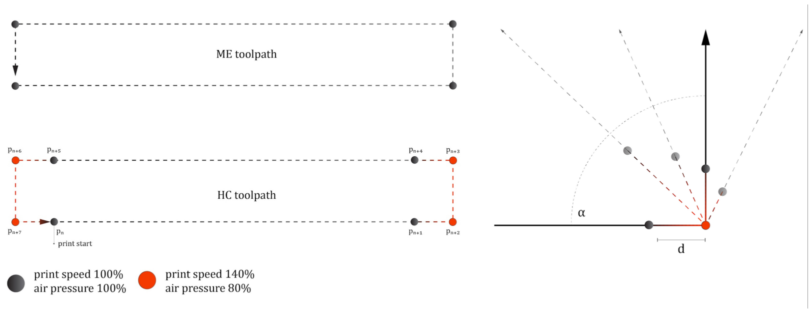

Figure 4.15: Differentiated air pressure per print point. Difference between a ME and HC toolpath. The increase in speed and reduction in air pressure and the distance (d) to the corner is influenced by the angle α.

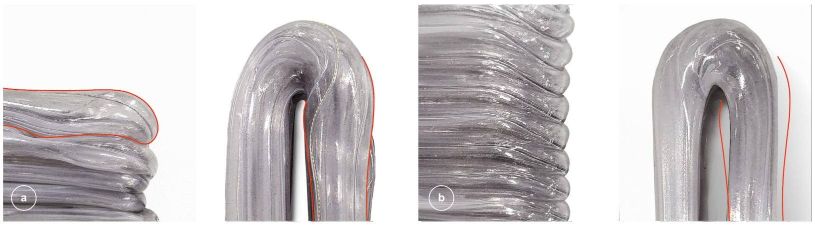

Figure 4.16: (a): overinflation due to constant internal air pressure. (b) successful print due to active control of air pressure. Red indication overinflated bead. Yellow indicates the twisting of the bead due to constant tool orientation.

- introducing a rotational tool head that can control the deposited bead precisely
- changing the speed/extrusion rate and the internal air pressure at certain points during the printing process.

The authors decided to investigate the third approach as it does not introduce new design/slicing constraints which might restrict the design freedom, nor require changes to the hardware setup. We propose to:

- reduce the extrusion rate, either by increasing the print speed and not adjusting the extrusion, or keeping the speed constant and reducing the extrusion
- reducing lowering the internal air pressure during the corner movements.

A standard toolpath for the basic rectangular geometry is defined by the four corner points of the print path. For differentiating the air pressure at the corners, four more points are introduced, at the beginning and the end of the straight print lines. Fig. 4.15 illustrates the toolpath design for ME and HC3DP. The black dashed lines represent 3D printing with normal print settings, p_n, p_{n+1}, p_{n+4}, p_{n+5} are printed with standard settings. The red dashed lines represent an increased print speed and lowered air pressure for the print points p_{n+2}, p_{n+3}, p_{n+6}, p_{n+6}. Although shown here in a basic example, the print speed and pressure can be controlled in a gradient manner, accommodating for various print radii and internal die geometries. The increase in speed and reduction in pressure, as well as the distance d, is mainly defined by the angle α (Fig. 4.15 right).

Fig. 4.16 showcases the difference between constant print settings (a) and differentiated internal air pressure per print point in (b). For the experiments the robot speed was adjusted from 5mm/s for long straight lines, to 7mm/s for the corners. The air pressure was reduced from 0.15 to 0.12 bar, as indicated for the red areas in the toolpath diagram (Fig. 4.15)

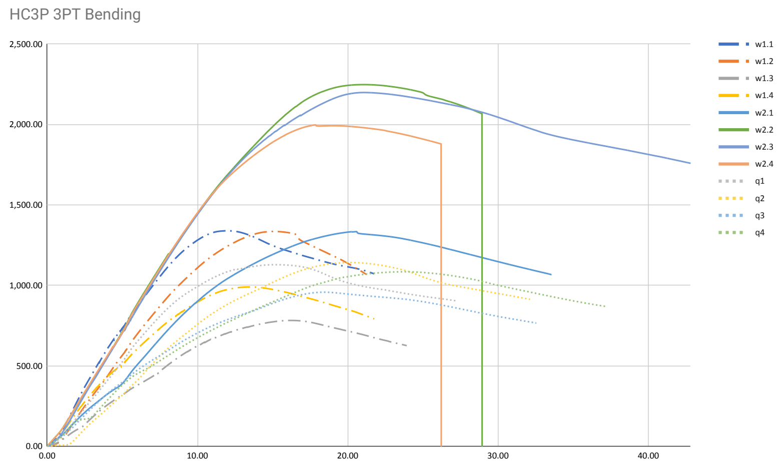

Figure 4.17: Results of the bending tests with different bead cross sections.

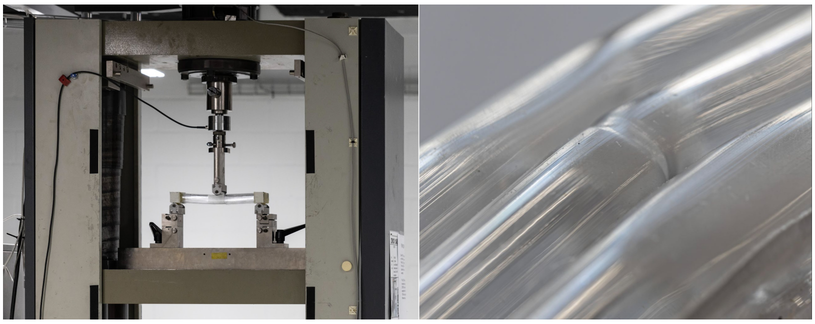

Figure 4.18: Testing setup. Close up of ductile failure behaviour. Thinning out before breaking.

4.4.6 3PT Bending

The 3PT bending tests were carried out using a Zwick 1484 with a 270mm support span (Fig. 4.18 left). The bending tests showed that the elements with the 2mm wall thickness withstand the highest load and that nearly all samples show a ductile behaviour. Besides two samples, all failed due to buckling as the elements are thin walled and slender. Two of the 2mm wall thickness samples (w2.2 and w2.4) failed with brittle behaviour after their maximum load had been reached and the sample continued deforming without taking more load. This can be explained with the plasticization of the material and the resulting constriction of material (Fig. 4.18 right). Nearly all samples exhibit this kind of behaviour and show whitening in the centre area, where the load is applied. Once, the material is thinned out too much, due to the continued deformation, the tension zone fails and the sample shatters. The specimens with the internal subdivision (q.x) display a more ductile behaviour than the hollow tubes with 1 mm wall thickness (w1.x).

Although the different elements showcase different maximum loads, their bending strength ranges from 60-74 MPa, and are calculated based on the actual sample dimension (Appendix 4.6). These values are close to the maximum bending strength of the material (69MPa) provided by the manufacturer [270].

[270]: Extrudr (), *PETG transparent - High Quality Filament*

4.5 Discussion

The main goal, gathering fundamental information and understanding of a 3D printing method for large-scale applications, was successful. HC3DP was tested in different scales and with different materials and validated through the production of several 2m tall cylinders. Furthermore, experimental findings show that different materials can be used for the production of large-scale, lightweight elements. For the first time, internal subdivisions/bespoke cross sections for large-scale HC3DP beads have been presented.

4.5.1 Materials and thermal cooldown

However, further investigations into material characteristics/behaviors are still to be conducted. Although it was shown that higher extrusion rates can be achieved using HC3DP, compared to ME, the challenge that might arise from this is also highlighted. The increase in cooldown can have, depending on the thermoplastic material and print path length per layer, a negative impact on the printed part. If the printed material cools down too much, layer adhesion cannot be guaranteed and the risk of delamination increases. To overcome this, partial remelting using an infrared heat source, as shown by [29], can be introduced. On the contrary, if the layertime is too short, the too hot previous layer will result in a collapse. The limiting range of contour length for a certain extrusion setting needs to be investigated to clearly define the design space for HC3DP.

[29]: Kishore et al. (2017), 'Infrared preheating to improve interlayer strength of big area additive manufacturing (BAAM) components'

Although it was shown that the most upper layer is cooling down significantly faster than the layers below, more research needs to be conducted to understand the trade-offs between the extruded wall thickness, the diameter of the tube, and the number of contours per layer. For now, only single contour/outline objects have been 3D printed. The observations that have been made regarding the increased equivalent wall thickness need to be transferred to multi-contour objects to understand the implications on increased extrusion rates.

4.5.2 Large-scale prototypes

The production time for an HC3DP 2m tall column is under 2 hours. The print speed is limited to 18mm/s, which is equivalent to an extrusion rate of 7,249.38mm3/s. As for higher extrusion rates first signs of overheating became visible. More complex geometries with longer print paths (per layer) could be fabricated at higher extrusion rates, as the chosen print speed is still limited by the cooldown rate and not the maximum volumetric extrusion. For the large-scale cylinders, the extrusion rate of the HC3DP system is higher than other state-of-the-art pellet-based ME systems as calculated based on the layer height and bead thickness. For the columns, an extrusion rate as high as 7249 mm3/s is achieved. Other systems like the BAAM at the Oak Ridge National Laboratory have approx. 4550 mm3/s [271]. Keeping in mind the aforementioned potential for increasing print speed based on the print path length or improved external cooling, the experiments indicate that even higher

[271]: Duty et al. (2015), *Cincinnati Big Area Additive Manufacturing (BAAM)*

extrusion for HC3DP can be achieved without adjustments to the 3D printing setup.

Despite the high extrusion rate, HC3DP only uses a fraction of material compared to other thermoplastic 3D printing methods. These savings can have a significant impact on the component's cost and sustainability. However, depending on the final use case of the element, thin wall elements might be not favourable. In this regard, due to extreme layer heights and minimal wall thickness, the large-scale cylinders are deforming under load. In this manuscript nozzles with different wall thicknesses are used to control the wall thickness of the extruded bead. In blow moulding, on the other hand, adjustable lips are used to define the thickness of the extrudate. HC3DP would benefit from knowledge transfer of the blow moulding industry to improve process stability, as well as capabilities. In addition to that, new design rules for HC3DP at large dimensions need to be investigated and defined, taking into consideration fabrication constraints and thin-wall bead behaviour. For now, too little is known to define those design for additive manufacturing (DFAM) guidelines.

4.5.3 Bespoke die geometry and structural testing

It was shown that single wall elements with a static height of 30mm can resist over 2.2kN. The introduction of internal subdivision does not increase the bending strength but seems to increase the ductility compared to hollow tubes with the same wall thickness. The chosen internal subdivision does not improve the structural integrity of the elements, as the extra material is added in an area where it cannot sufficiently support the load transfer. A non-uniformal die geometry can potentially improve the structural capacity of a printed element while keeping the material consumption low and the extrusion rate high. Having thicker wall thicknesses, e.g. 2mm, in the compression and tension zone, while having the interfaces with a thinner wall thickness, e.g. 1mm, would benefit the structural integrity of the element, while keeping the extrusion rate a maximum. However, a rotational toolhead needs to be implemented for this approach. Furthermore, a non-uniform wall thickness might affect the 3D printing process, as well as the cooling behaviour of the polymer which is for now unknown.

To provide sufficient control over the orientation of the extruded bead, to either allow for non-uniform die geometries, or orient internal substructures, a rotational toolhead needs to be implemented. The extruded bead needs to be actively re-orientable depending on the printing direction. Rotational toolheads have been investigated [262, 272, 273] and further research needs to transfer those findings to large-scale HC3DP.

[262]: Larson et al. (2023), 'Rotational multimaterial printing of filaments with subvoxel control'
[272]: Wüthrich et al. (2021), 'Novel 4-Axis 3D Printing Process to Print Overhangs Without Support Material'
[273]: Raney et al. (2018), 'Rotational 3D printing of damage-tolerant composites with programmable mechanics'

Further research needs to clarify to which extent the testing speed influences the failure behaviour for HC3DP elements. The speed with which the elements are loaded will influence the plasticization of the polymer and therefore might influence the failure behaviour of the elements from ductile to brittle. The problem for elements created by HC is not their stability, but the ductility of the chosen polymer. Depending on the use case, the material selection will influence the structural integrity of the component.

Although it was proven that it is possible to 3D print with internal subdivisions it was necessary to control the pressure inside the bead during printing. This increased control can be implemented irrespective of the chosen die geometry, allows for printing tight turns, and might also facilitate the crossing of 3D-printed beads. For this, new experiments need to be conducted to verify this approach.

The increased scale of the extruded beads opens the opportunity to create either non-circular orifices or introduce other bespoke internal geometries inside the extruded bead. These purpose-made internal structures can serve as reinforcement or allow for functional integration/separation within a printed bead itself. These channels can be filled with liquids, gas, or other granular materials. Furthermore, HC3D potentially allows for the co-extrusion of two or multiple polymers/different materials.

However, during the investigations, it became apparent that the orifice geometry, pattern, and wall thickness have a significant impact on the extrusion rate, material consumption, maximum load, and ductility. The cross-section of the HC3DP bead will furthermore define the performance of the printed object in regard to thermo-optical properties.

4.5.4 Continuous toolpaths and start/stop

For all experiments described in this manuscript continuous tool-paths are used. A lead in is added to the tool path to ensure that the bead is pressurised at the start of the print. This additional print line needs to be manually cut off after the print has finished. Start and stop functionality would allow for the fabrication of more complex geometries, however it's not in the scope of this manuscript. After conducting the aforementioned experiments, the authors identify the following strategy to allow for a controlled start/stop. The start stop procedure builds up on the pressure per print point control, introduced in this manuscript, and the degrees of freedom of the robotic arm and could be implemented as follows:

- reduce the pressure gradually while approaching the last print point of a print line
- turn off the feeding of the extruder and waiting at the last point in order to let the nozzle slightly ooze.
- perform a twist movement using the robotic arm to close the bead
- continue to the next print point

The strategy of pulling vacuum instead of pressurising to close off the extruded bead, as described here [263, 264] has a high risk of clogging the air outlets that pressurise the tubular beads. Similar to 3D concrete printing, at the beginning continuous toolpaths were strictly necessary. Now, with material and process advancements the possibility to start/stop has become state of the art. Therefore, if more research is conducted on HC3DP, the authors believe that similar advancements can be made that will allow for the fabrication of more complex components.

[263]: Brad Michael Bourgoyne (2015), 'Method and apparatus for additive fabrication of three-dimensional objects utilizing vesiculated extrusions, and objects thereof'

[264]: Hopkins et al. (2020), 'Additive manufacturing via tube extrusion (AMTEx)'

4.5.5 Potential applications

The improvements in extrusion rate are pushing HC3DP into a similar performance level as concrete extrusion 3D printing (CE3DP). Anton et al. showcased concrete extrusion 3DP column with a vertical fabrication speed of approx. 1000 mm/h [268]. Especially for the Architecture, Engineering, and Construction (AEC) sector, 3D printing of objects with large dimensions is of relevance. Based on the authors findings, HC3DP of polymers can compete with other large-scale AM methods, achieving relevance for architectural applications. However, large-scale HC3DP produces elements with a lower resolution than common ME methods, comparable to concrete 3D printing. Depending on the final application, the lower resolution and reduced feature size might be critical. Furthermore, post-processing techniques, like milling, HC3DP, as presented here, cannot be used due to the minimized material thickness. For those cases, the process of HC3DP would need to be adapted. Nevertheless, the choice of the printing method, regular ME vs. HC3DP, should always reflect the final usage of the element.

[268]: Anton et al. (2021), 'A 3D concrete printing prefabrication platform for bespoke columns'

To conclude, elements created by HC3DP appear to be superior in their objects' performance in terms of material consumption and printing speed. Due to the good structural characteristics of tubular profiles, this reduction of material does not reduce the strength at the same rate. Similar benefits can be imagined for thermo-optical properties, as this 3D printing technology produces elements with internal air pockets, and the amount of layer interfaces is reduced. For architecture, several applications can be imagined as lightweight formwork/molds, interior elements, furniture, and lights/chandeliers. However, HC3DP is not limited to those specific use cases as material savings, as well as an increase in print speed, are universal and can benefit most applications where large-scale elements need to be produced.

4.6 Conclusion

A thermoplastic 3D printing approach for large-scale, lightweight components has been presented. HC3DP addresses challenges of current thermoplastic extrusion 3D printing systems like scalability, material consumption, and extrusion rate. It is shown that it is possible to print with very large hollow profiles (24mm) in large dimensions using a pellet extruder. The authors have proven that different polymer types can be 3D printed using the proposed method and give indications of material savings. Two case studies showcase that HC3DP can increase the extrusion rate rate in comparison to state-of-the-art ME processes. Furthermore, purpose-made internal geometries open up new avenues for upcoming research trajectories and would allow functional integration by filling voids with gases, fluids, powders, or pulling vacuum. 3D printing with HC3DP can provide value in producing custom elements in a shorter timeframe as the layer heights and cooling rate can be increased while using only a fraction of the material. HC3DP offers a new dimension to large-scale 3DP as it positively influences both the printing process and also properties of resulting parts.

Acknowledgments

This research is financially supported by the National Centre for Competence in Research in Digital Fabrication, funded by the Swiss National Science Foundation (NCCR Digital Fabrication Agreement number 51-NF40141853). The authors would like to thank Marirena Kladeftira, Lex Reiter, Thomas Wuest, and Heinz Richner for their valuable input to the manuscript and Yen-Fen Chan for his support during this research.

Appendix

The bending stress is calculated using two models:

- rectangular hollow beams
- elliptical hollow beams

The cross-sectional area of the samples can be described as stacked discorectangular shapes, and are therefore in between the rectangular and the elliptical shape (Fig. 4.19 right). For the 3PT bending tests, the assumptions using the rectangular shape results in a rather low bending stress, as the compression and tension area are in reality smaller than assumed. The results using the elliptical calculation results in an overestimation of the bending stress, as the areas crucial for the force transmittance are actually larger then calculated.

Therefore both, I_E and I_R are averaged before calculating the final bending stress. The results are close to the maximum tensile strength of the used PETG material (68 MPA)[270].

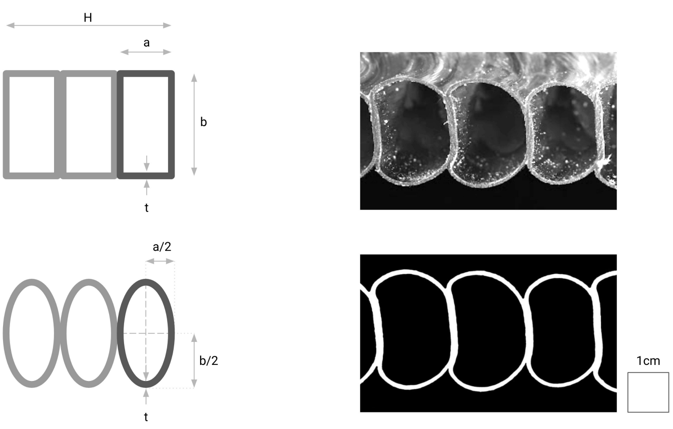

Figure 4.19: Rectangular and elliptical cross section assumption. Actual section of 3DP specimen, and high- resolution 2D scan. The shape of the cross section can be described as non-symmetrical disco rectangular, with a sagging behaviour in the layer build up direction.

$$I_R = \frac{H}{a}\left(\frac{a \times b^3}{12}\right) - \left(\frac{(a\ -\ 2t) \times (b\ -\ 2t)^3}{12}\right))$$

$$I_E = \pi\left(\frac{(a/2) \times (b/2)^3}{4}\right) - \left(\frac{((a/2) - t) \times ((b/2) - t^3)}{4}\right)$$

$$I_{MIX} = \left(\frac{(I_E + I_R)}{2}\right)$$

$$\sigma_{MIX} = \frac{(F \times l \times d)}{8 \times (I_{MIX})}$$

Large-scale Hollow-Core 3D-Printing (HC3DP): Variable Cross Section and Printing Features for Lightweight Plastic Elements

5

5.1 Overview of Paper A . . . 101
5.2 Introduction 103
5.3 Materials and methods . 105
5.4 Results 111
5.5 Discussion 115
5.6 Conclusions 116

5.1 Overview of Paper A

5.1.1 Content

Paper D examines the printing behavior in low-resolution, large-scale HC3DP. It delves into varying extrusion profiles and die shapes, focusing on wall thicknesses and internal substructures. The paper includes a detailed analysis of printed HC3DP specimens, particularly the properties of thin-wall strands. Additionally, it covers the technical aspects of fabrication, including data management, the robotic HC3DP setup, and the development of specific toolpaths for HC3DP. The study also explores printing features like overhangs, bridges, and non-planar 3D printing. Lastly, it discusses the potential of HC3DP across various industries and its broader impact on the field of large-scale 3D printing.

5.1.2 Method

To investigate variable cross-sections for HC3DP, a series of single outline specimens is printed. For each experiment, all printing parameters are constant, except for the layer height and the internal air pressure. Then, the samples are cut by hand using a metal blade and a double-sided guide. The sections are 2D-scanned and analyzed using ImageJ. The wall thicknesses and bead dimensions are measured, and trends highlighted. For the non-tubular dies, the sections are analyzed by visualizing the minimal distance of a pixel to its closest border. In addition, 3D printing experiments are conducted to investigate the behavior of specific printing features. The features investigated are bridging, overhang, and non-planar 3D printing. Bespoke tool-path planning is used and enables a high level of control over these features in regards to printing sequence, speed, and air pressure values.

5.1.3 Results

The results of Paper D can be summarized as follows. The ability to change the bead cross-section by increasing/adapting the air pressure inside the bead is successfully shown in a range from 16 to 32mm. This enables multi-resolution 3D printing without the need for a second extruder, nozzle, or additional hardware. The introduction of bespoke dies with purpose-made cross sections creates a new research trajectory for large-scale HC3DP and is expanding the range of its possible applications. However, the initial experiments with non-tubular cross-sections also show deviations from the initial geometry, demonstrating the need for further investigations to improve quality through tuning printing parameters or differentiated pressure control for each individual air pocket. Printing features such as bridging or overhangs benefit from the increased cooling rate of HC3DP. Non-planar HC3DP, however, is demonstrated to be challenging due to a post-inflation of the extruded bead.

5.1.4 Authors contribution to the paper

Matthias Leschok Conceptualization, Data curation, Formal Analysis, Investigation, Methodology, Project administration, Validation, Visualization, Writing – original draft, Writing – review & editing
Benjamin Dillenburger Conceptualization, Project administration, Supervision, Writing – review & editing
Marirena Kladeftira Investigation, Validation, Writing – original draft, Writing – review & editing
Yen Fen Chan Formal Analysis, Software, Validation, Visualization

Abstract Hollow Core 3D printing proposes a new method for the production of lightweight, material-efficient thermoplastic 3D printed elements. This new fabrication approach promises material savings of 50-80% while increasing the extrusion rate significantly (factor 10). This development pushes Hollow Core 3D printing to a similar fabrication speed as high-resolution concrete 3D printing. However, fundamental research on printing features enabled by this novel 3D printing approach are missing.

Therefore, this paper investigates printing with user-controlled bead dimensions (same nozzle, different size). It is showcased that the size of the extruded cross-section is determined by the positive air pressure used to inflate the beads. Multiple samples are printed changing the layer height and width significantly without making changes to the hardware setup. Sections of the 3DP samples are analyzed and the parameters of 3DP beads are determined. Furthermore, a set of bespoke 3D-printed nozzles is introduced to subdivide the HC3DP beads into distinct areas. So far only regular beads, such as hollow tubes, have been used for 3D printing. Samples of those bespoke sections are analyzed to investigate their behavior when used for 3D printing. Finally, large-scale 3D printing experiments are conducted to investigate how printing features like bridging, cantilevering, or non-planar 3D printing can be manufactured with hollow extrusion beads. In summary, this manuscript provides insights into the fundamental 3D printing behaviors of HC3DP, showcases new design possibilities with bespoke and variable cross sections; and finally proposes new research trajectories based on the findings presented.

5.2 Introduction

Large-scale material extrusion (ME) is one of the most popular AM methods across all industries due to its affordability and large variety of available material [37, 274]. However, the existing large-scale 3D printing systems typically produce material-intense components because of the large size of nozzles and the necessity of thick extrusion widths for fabrication stability and warping prevention. Furthermore, the printing speed of large-scale ME is limited by the cooling rate of the extrudate more than the capacity of the extruder [38].

[37]: Moreno Nieto et al. (2020), 'Large-format fused deposition additive manufacturing'

[274]: Vicente et al. (2023), 'Large-format additive manufacturing of polymer extrusion-based deposition systems'

[38]: Roschli et al. (2019), 'Designing for Big Area Additive Manufacturing'

Large-scale Hollow-Core 3D printing (HC3DP) overcomes these major limitations and enables the production of large-scale, lightweight elements, while using only a fraction of the material by extruding hollow beads [46], see Figure 5.1. HC3DP with its tubular bead structure, holds the potential for great variation in layer height and printing resolution. By injecting air with a user-controlled pressure into the bead's core the printed section can be controlled. Furthermore, due to the size of the extruded hollow bead, it is possible to introduce internal structures, which has not been investigated before. Furthermore, to this date there are no investigations that explore the printing features of those low resolution, large-scale polymer prints.

[46]: Leschok et al. (2023), 'Large-scale hollow-core 3D printing (HC3DP)'

This manuscript contributes to the state of the art by introducing variable extrusion sections in the range of 16-32 mm for HC3DP without

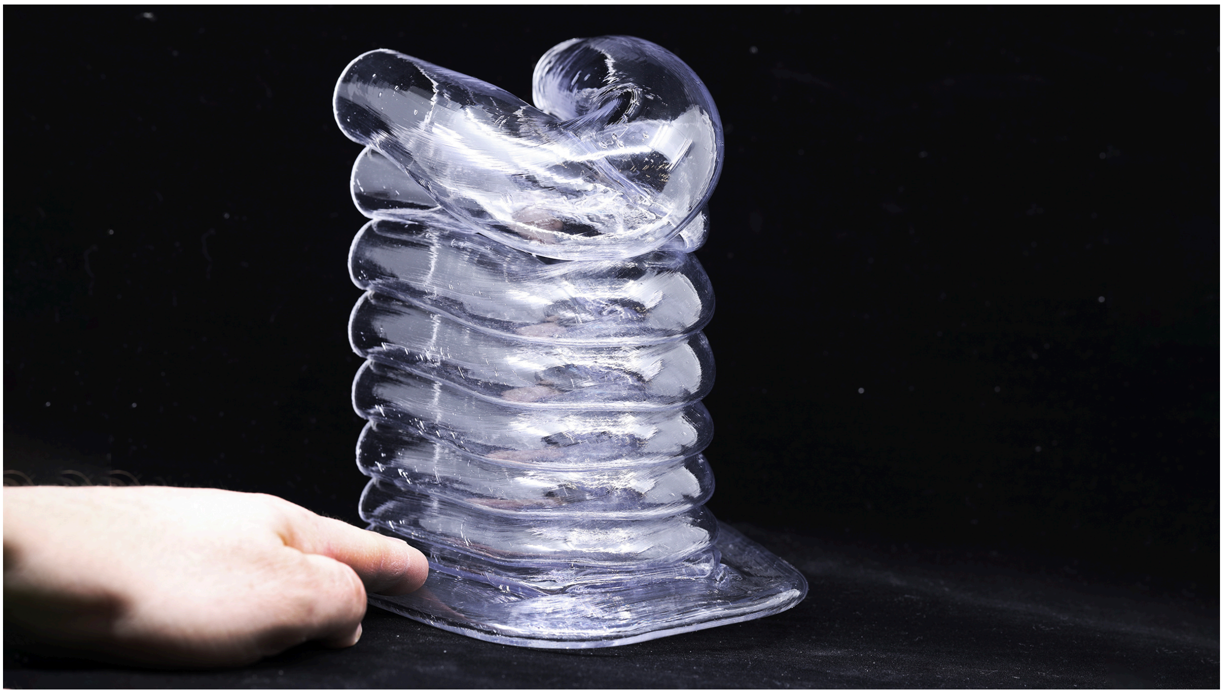

Figure 5.1: Large-scale HC3DP samples. Layer height 18mm, layer width 24mm.

introducing changes to the hardware. Additionally, three different die geometries with internal substructures are introduced. To provide first insights on the printing behavior of these two parameters (layer height, die type), the sections of HC3DP beads have been analyzed for a series of experiments. Finally, investigation on bespoke toolpaths explore printing features, such as the bridging and cantilevering behavior of HC3DP elements.

5.2.1 State of the art

Material Extrusion (ME), has since its invention in 1989 [8], become one of the most used 3D printing methods worldwide [256, 257]. One of the latest trends in ME is the incremental advancements in increasing extrusion rate to reduce fabrication time. The extrusion rate of filament-based extruders was improved by either extending their heating zone, increasing heating power, or combining multiple extruder units to feed into one nozzle [275–277]. However, the extrusion rate of filament-based systems (approx. 0.5 kg/h) is not sufficient for manufacturing large parts (> 1m3) economically. Therefore, pellet extruders have been introduced which rely on pellet/granular feedstock, similar to injection molding machines. Those pellet extruders are specifically designed for extruding thick beads at high extrusion rates that reach as much as 50 kg/h [30]. Pellet extruders are often mounted on 6-axis robotic arms that provide a large-build volume (>1m3). Scaling up ME using pellet extrusion systems dates back to 2011 [26]. A large body of research focuses on technical advancements like material behavior, layer bonding, design guidelines, and bridging behavior [29, 30, 234, 258, 278]. ME has been used for various projects and prototypes like formwork, temporary pavilions, or facades [40, 86, 111, 116, 224, 279].

[8]: Crump (1994), ‘Modeling apparatus for three-dimensional objects’

[256]: N. Turner et al. (2014), ‘A review of melt extrusion additive manufacturing processes’

[257]: Barnatt (2013), *3D Printing: The Next Industrial Revolution*

[275]: Leapfrog (), *Leapfrog XceL | Large Scale Industrial 3D Printer*

[276]: Prusa (2021), *Max volumetric speed | Prusa Knowledge Base*

[277]: E3D (2018), *Product Specifications SuperVolcano*

[30]: Duty et al. (2017), ‘Structure and mechanical behavior of Big Area Additive Manufacturing (BAAM) materials’

[26]: Kooij (2011), *Endless Chair - Kooij*

[29]: Kishore et al. (2017), ‘Infrared preheating to improve interlayer strength of big area additive manufacturing (BAAM) components’

[30]: Duty et al. (2017), ‘Structure and mechanical behavior of Big Area Additive Manufacturing (BAAM) materials’

[234]: Eyercioglu et al. (2019), ‘Determination of the Maximum Bridging Distance in Large Scale Additive Manufacturing’

[258]: Chesser et al. (2019), ‘Extrusion control for high quality printing on Big Area Additive Manufacturing (BAAM) systems’

[278]: Wu et al. (2023), ‘Study on Support-Free Printing of Large-Flow Material Extrusion Process’

Minimizing the fabrication time of large-scale ME has also been addressed from a computational design perspective. In order to create elements as time-efficient as possible, different layer heights/ resolution can be used. One can distinguish between areas to print in low resolution to build up volume fast, and high resolution where details are needed. Changing printing resolution significantly (50% or more) during the printing process requires a multi-toolhead 3D printing setup [280], multi-robot setup [281], an automatic tool changer, or manual swapping of nozzles. For pellet based ME, Chesser et al. have introduced an actuated nozzle design that can switch between two different die extrusions diameters [258].

Finally, for complex elements, overhangs etc. typically support structures are needed. Those, depending on the printing geometry, can take up a significant amount of printing time and material. Especially, for large-scale ME this is to be avoided. One way to reduce the amount of support structures, or to get rid of it entirely is to use non-planar 3D printing. In non-planar 3D printing the layers are not structured in a simple 2.5-dimensional manner, but layers can be defined freely in XYZ space and allow for greater overhangs to be printed [101].

However, even with all those developments, the maximum print speed for large-scale ME (extrusion rate) is not limited by the performance of the extruder (hardware) or the optimal tool path planning (software) but by the cooldown of the prior extruded layer. This is increasingly relevant the larger the bead size (extruded plastic strand), as large beads need a long time to solidify due to their surface to volume ratio [38].

The extrusion of thermoplastics to form tubular structures like pipes, tubes, or window-frame profiles is known in the industry as die extrusion [265, 282]. This manufacturing approach has recently been adapted for 3D printing and enables the fabrication of 3D objects based on hollow beads. To the best of the authors knowledge only two precedents exist; for small scale filament-based extrusion [263, 264] and Leschok et al. for the extrusion of bead sizes of over 20mm using a pellet extruder [46]. Hollow Core 3D Printing (HC3DP), at large-dimensions scales up ME while addressing the most pressing limitations: material cooldown, material efficiency, and fabrication speed by 3D printing tubular beads/roads instead of solid ones. In this manuscript variable sections, cross sections with internal reinforcements, as well as printing features like bridging and non-planar printing are investigated.

[40]: Moritz Basil Mungenast (2019), '3D-Printed Future Facade'

[86]: Naboni et al. (2019), 'Multi-scale design and fabrication of the Trabeculae Pavilion'

[111]: Taseva et al. (2020), 'Large-Scale 3D Printing for Functionally-Graded Facade'

[116]: Snooks et al. (2020), 'Fabricate 2020'

[224]: Jipa et al. (2019), '3D-Printed Formwork for Integrated Funicular Concrete Slabs'

[279]: Leschok et al. (2020), 'Sustainable Thin-Shell 3D Printed Formwork for Concrete'

[280]: Yoon et al. (2019), 'Development of Three-Nozzle Extrusion System for Conformal Multi-Resolution 3D Printing With a Robotic Manipulator'

[281]: Bhatt et al. (2019), 'A Robotic Cell for Multi-Resolution Additive Manufacturing'

[258]: Chesser et al. (2019), 'Extrusion control for high quality printing on Big Area Additive Manufacturing (BAAM) systems'

[101]: Mitropoulou et al. (2020), 'Print Paths Key-framing'

[38]: Roschli et al. (2019), 'Designing for Big Area Additive Manufacturing'

[265]: Vlachopoulos et al. (2003), 'Polymer processing'

[282]: Baird (2003), 'Polymer Processing'

[263]: Brad Michael Bourgoyne (2015), 'Method and apparatus for additive fabrication of three-dimensional objects utilizing vesiculated extrusions, and objects thereof'

[264]: Hopkins et al. (2020), 'Additive manufacturing via tube extrusion (AMTEx)'

[46]: Leschok et al. (2023), 'Large-scale hollow-core 3D printing (HC3DP)'

5.3 Materials and methods

5.3.1 Large-Scale ME and HC3DP

A robotic setup for large-scale material extrusion (ME) using granular feedstock involves several components and steps [271]. The extruder, mounted on the robotic arm, is responsible for melting and depositing granular material into the desired 3D object. The extruder generally consists of a motor with a gearbox, a heated barrel with different heating zones, a screw mechanism to move the material forward, and multiple heating elements to melt the polymer granules. The nozzle, at the end of

[271]: Duty et al. (2015), *Cincinnati Big Area Additive Manufacturing (BAAM)*

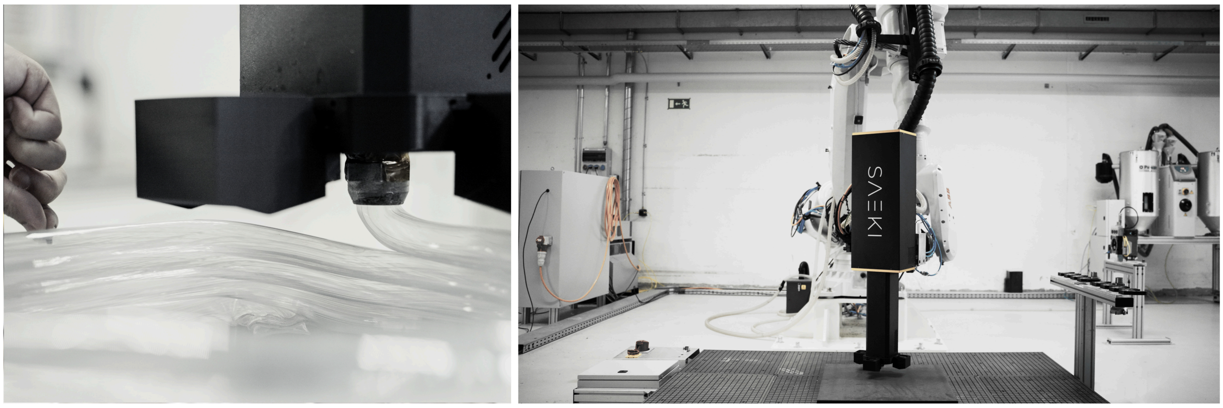

Figure 5.2: The 3D printing setup includes ABB IRB6700, a pellet extruder, a control cabinet, and a material handling system. Right: Close-up of the printing process.

the extruder, defines the size and shape of the extruded polymer bead. The nozzle size and design can vary depending on the desired printing resolution and the specific requirements of the printing process. A control system regulates various parameters such as temperature, material flow rate, and printhead movement.

The robotic arm provides precise control over the movement of the extruder, enabling intricate and complex printing patterns. With its six degrees of freedom, the robotic arm can manipulate the extruder in various directions, allowing for the creation of bespoke geometries and curved surfaces. Finally, a granular feedstock is required, which must be dried before 3D printing. A material handling system is necessary to handle and deliver the granular feedstock to the printing system. This handling system typically includes storage containers, dryers and mechanisms like hoppers, or conveyors to transport the material to the printing unit.

HC3DP

To 3D print hollow-core beads instead of regular ones, adjustments to the aforementioned fabrication setup need to be made and have been described by the authors in detail in a previous publication [46]. The two major adjustments are, changing the nozzle to a hollow mandrel supported by spider legs, that splits the molten plastic into a thin wall and empty core, as well as positive air pressure to keep the hollow-core bead inflated. For the experiments described in this manuscript an ABB IRB 6700 industrial robotic arm with a pellet extruder system from SAEKI Robotics is used, see 5.2. A 2x1m wooden plate serves as a print platform and allows for easily fixing the printed object during printing experiments.

[46]: Leschok et al. (2023), 'Large-scale hollow-core 3D printing (HC3DP)'

For the experiments in this manuscript several die geometries are presented. They have an outer diameter of 24mm and display a varying wall thickness and internal subdivisions/ reinforcements. Table 5.1 provides detailed information regarding the different nozzle types, material cross section and ratio of air to plastic. Those nozzle prototypes are manufactured with an Aluminum Alloy (AlSi10Mg) using Direct Metal Laser

Sintering (DMLS) technology. The resolution of the printing process allows for the fabrication of intricate and complex geometry at reasonable cost. The aluminium is sufficiently though to be used the prototypical 3D printing setup, while having good heat transfer for the molten pellets to maintain the necessary temperature for extrusion.

Fabrication data and communication

Commercial software packages like AI built, Adaxis, or open-source developments like Compas Slicer, allow the creation of robotic toolpaths for large-scale ME based on the 3D representation of a 3D model. However, these software packages do not create individual air-pressure values for the HC3DP process, nor do they allow adjusting the toolpath for each individual layer, such as increasing overhangs or cantilevers used in this manuscript. Therefore, to have full control of the robot movements and to integrate different air pressure values, the toolpaths are generated with a custom script that produces a custom array of points. Each experiment will later describe the rules of the toolpath creation in more detail. The fabrication data is generated using a custom python script. The input is a list of points, velocities, tool orientation, speeds, and air pressure values and each individual set of information per print point is exported into a JSON dictionary. The communication between 3D printing setup and user is established by compasRRC, an online communication library for ABB Robots [283]. CompasRRC is able to read JSON dictionaries and send this data as robot code (RAPID) to the ABB robot. The information is sent to the robot includes:

[283]: Fleischmann Philippe (), *compas_-rrc - COMPAS RRC*

- position
- tool orientation
- speed
- zone, and
- a pressure value for each specific point.

This allows for a high level of control over the toolpath and its materiality and increases the stability of the HC3DP process.

Printing material and parameters

For the experiments presented in this manuscript Polyethylene Terephthalate Glycol-Modified (PETG) is used. PETG is a popular material for 3D printing due to several key advantages it offers, like good chemical, structural resistance, and high transparency [232]. Before printing, the PETG was dried for 4 hours at 60°C. While printing, the three heating zones of the extruder were set to 145, 175, and 205°C and the ambient temperature was 14.2°C. The most crucial printing parameters are robot speed, RPM of the extruder, air pressure values to inflate the bead, and the temperatures of the extruder. For each experiment the values of those are provided. For all experiments the authors print the first layer at a reduced speed (50%) to ensure good adhesion between the print platform and the printed object.

[232]: Petrov et al. (2021), 'Research into the effect of the 3D-printing mode on changing the properties of PETG transparent plastic'

5.3.2 Sample design and fabrication

Two specimen types have been designed and printed for the presented research. First, a single-outline rectangular box with a footprint of 500x75 mm, and second, bespoke cylinders with a radius of 400mm with varying height. The simple rectangular boxes are cut by hand using a fine metal blade and double-sided custom guide, and the sections are analyzed. The complex cylindrical geometries are designed to investigate the behavior of printing features at large dimensions. The focus here lies in creating cantilevering structures, observing bridging behavior, and testing non-planar 3D printing.

For all specimens, the following design principles are considered:

- Continuous toolpath, no start and stop, no individual printing islands
- Blend between individual layers, no straight z movement upwards
- No self-intersecting toolpaths
- Blend radius for corners / minimal feature size

Variable cross-section

The footprint of the printed samples is 500 x 75mm and the height of the elements vary, at least seven layers are printed. The single outline toolpath is chosen, as it allows for a stable printing process and a fast cool down (fast fabrication time). Furthermore, the single outline print eliminates interface interactions between different beads within the same layer.

The distance between the layers (resolution in Z direction) varies for every print. The experiments start with a layer height of 16mm and increase in 2mm steps until a layer height of 32mm is reached. Although the layer height is not limited to 32mm, it is beyond the scope of the manuscript to define the maximum printable layer height for the given fabrication setup.

All samples are fabricated with identical printing parameters, only the layer height and internal air pressure are changing. For each experiment, the internal air pressure is gradually increased to adjust the size of the extruded bead.

Static printing parameters:

- temperature: 145, 175, 205°C
- robot speed: 12mm/s
- extrusion rate: 90 RPM

Sample preparation and measurements

After printing, the samples are cut by hand using a fine metal blade and a custom double-sided guide. Cutting with electric devices holds the risk of damaging the part, as the polymer is heated beyond its melting temperature and debris might stick to the sample.

The sections are 2D scanned using an EPSON Perfection v39 with a resolution of 600 DPI. ImageJ [284] was used to analyze the sections and

[284]: Schneider et al. (2012), 'NIH Image to ImageJ'

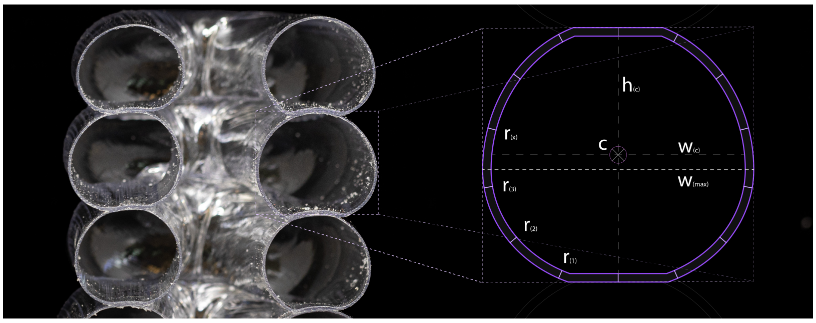

Figure 5.3: Closeup of a section, layer height 24 and diagram of measurement points. C: Center point, determined by ImageJ. H(c): height at point C. W(c): width at point C. W(max): maximum width, determined by ImageJ bounding box. R(x): wall thickness at point X.

determine the center point (c) of each bead. Then for each individual bead the vertical distance between layer interfaces (hc), the width at the center of the bead wc, as well as the maximum width of the bead wmax is measured. Furthermore, the wall thickness at several points (rx), see Figure 5.3. Finally, the widths, heights, and wall thicknesses for each specimen is averaged to understand the trends in wall thickness, layer width, and the width to height ratio. The first printed layer is not included in the measurements, as it is connected to a second outline printed (brim) to increase the adhesion to the print bed, see Figure 5.7.

5.3.3 Different nozzles - internal geometry

The increased dimension of the 3D printable bead offers the opportunity to create subdivided die geometries. Those internal substructures can potentially improve the properties of the printed component in regard to structural, optical, or thermal performance.

As a first attempt four different die typologies are designed and fabricated. All nozzles have an outer diameter of 24mm, a) is a nozzle with no internal geometry, b) contains a cross to reinforce the bead, c) contains a crosshair pattern and d) consists of five individual tubes. Table 5.1 provides a detailed overview of the shape, pocket size, and plastic cross section for each design. Similar to the experiments described in section 5.3.2, basic rectangular elements are 3D printed and sections of the printed object are analyzed. This time, the wall thickness of the scanned sections (4800 DPI) is visualized using a color gradient, representing the minimal distance of a pixel to its closest border using the Rhino & Grasshopper environment.

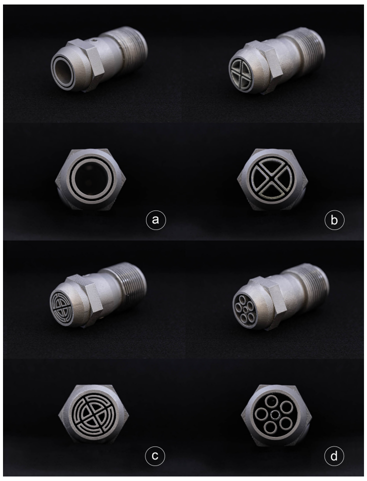

Figure 5.4: Different nozzles types, prototyped using 3DP of aluminum.

5.3.4 3D printing features

To provide initial explorations on printing features several undulating cylindrical geometries with an average diameter of 400mm are designed

Table 5.1: Comparison of different nozzles, showing area of extruded plastic and internal voids [mm2]. The nozzles are sorted by increasing the extrusion footprint.

Name	wall thickness [mm]	Hollow cores [amount	Plastic cross section [mm2]	internal void [mm2]	ratio plastic/air [%]
o24w1 (a)	1	1	73.50	380.13	16.25
o24w1Quad	1	4	117.29	334.68	25.93
o24w1Crosshair	8	1	158.36	294.03	35.01
o24tubeInTube	0.8-3.3	6	220.54	231.85	48.75

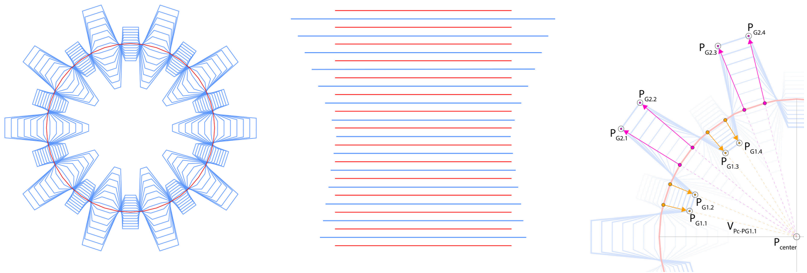

Figure 5.5: Bespoke toolpath with strong undulations in XY direction. Red represents bridges with a distance of 60mm, blue indicates cantilevering areas.

and fabricated. Those geometries are designed with the manipulation of points in either XY or Z direction of the base cylinder using the parametric design environment of Grasshopper. Three aspects of 3D printing are investigated, cantilevering, bridging, and non-planar 3D printing.

Bridging and cantilevering

Bridging describes segments of a print path that are only supported on their start and end point and not constantly supported from below. Researchers have investigated the bridging behavior for large-scale ME [234, 278]. Hopkins et al showcased unsupported 3DP using small scale tubular extrusion, however, their printing speed was limited to 0.8mm/s [264]. The bridging behavior of HC3DP at large-dimensions and regular printing speed remains unexplored.

[234]: Eyercioglu et al. (2019), 'Determination of the Maximum Bridging Distance in Large Scale Additive Manufacturing'
[278]: Wu et al. (2023), 'Study on Support-Free Printing of Large-Flow Material Extrusion Process'
[264]: Hopkins et al. (2020), 'Additive manufacturing via tube extrusion (AMTEx)'

Figure 5.5 shows the alternating print pattern that moves printing points in the XY plane away from the center of the cylinder, based on the points Z value/ layer (from 3 to 8.8 cm). Two cantilever types are tested with this design, (red) straight bridging between two single supports and (blue) the unsupported print of a polyline.

The base circle is subdivided in 40 equally long segments, defining 40 points on the polyline. Each layer N is defined by this geometry, see red lines Fig. 5.5. Then for every second layer the list of points is divided into pairs, creating two lists of points (Group 1 orange and group 2 pink). The translation is defined by the vector V starting from the center point the layer P-center and each individual Point PG.X . The distance for each translation is defined by two ranges, -100 to 100 for group 1 and 40 to -40 for group 2. Depending on which group a point is associated to, it moves either inwards or outwards depending on the current layer.

Non-planar 3DP

Another set of experiments investigates the behavior of non-planar 3D printing with HC beads. Figure 5.6 shows the toolpath, created similarly to the aforementioned method. Print points of the base cylinder are moved, this time in vertical direction. The tool was kept at a constant frame/position during these initial experiments for easy programming.

The toolpath is based on the identical subdivided circle, described in section 5.3.4. This time each individual point is moved in Z direction, perpendicular to the construction plane. The translation vector is defined by a sine function, whereas the frequency of this specific design is defined by a range from -1 to 9. The amplitude for each individual layer is

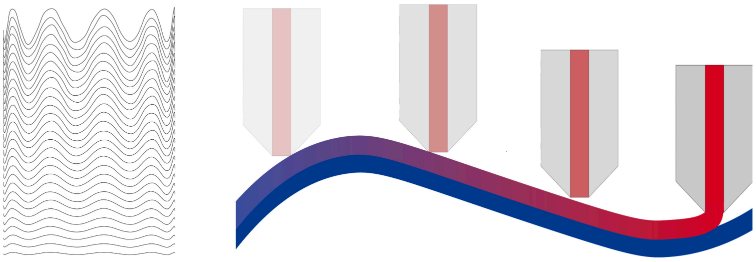

Figure 5.6: A) bespoke toolpath design for large-scale elements, non-planar 3D printing with increasing amplitude in Z direction. B) Diagram for non-planar printing with fixed tool head orientation.

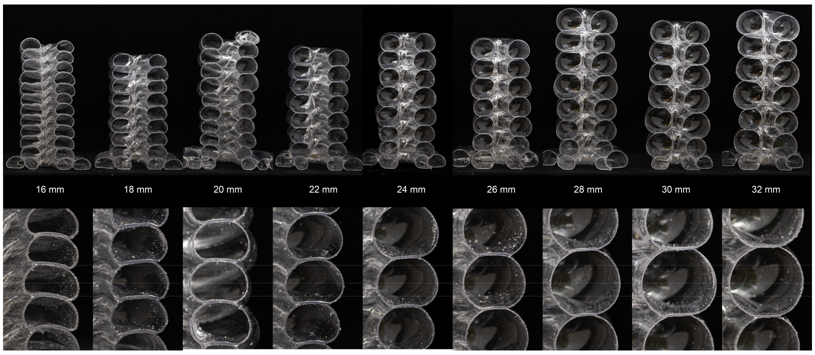

Figure 5.7: Sections of specimen printed with the same nozzle, but increased layer height.

remapped using a series of domains, with increasing range for increasing layer heights, starting from -3 to 3 for the first layer, to -47 to 46 for the last layer.

5.4 Results

5.4.1 Variable cross-section

The results show that it is possible to change printing resolution using HC3DP. The layer height was successfully changed from 16 to 32mm without requiring changes to the hardware setup, see Figure 5.7.

The observations can be summarized as follows:

- As the extrusion rate was kept constant the wall thickness, as expected, becomes thinner with larger inflated beads.
- The shape of the HC3DP bead changes from a rectangle with half circular ends (low layer heights) to a nearly round shape for large layer heights.
- The bead dimensions are not constant and become less consistent the higher the layer height. Partially, this can be explained by the adjustment of air pressure during the experiments.
- The increase in height always goes in hand with an increase in width, because of the uniform inflation of the core

Table 5.2 summarizes the measurements and provides the average dimensions for each layer height. There are clear trends in increasing layer width, reducing wall thickness, and reduced ratio of width to height.

5.4.2 Different nozzles - internal geometry

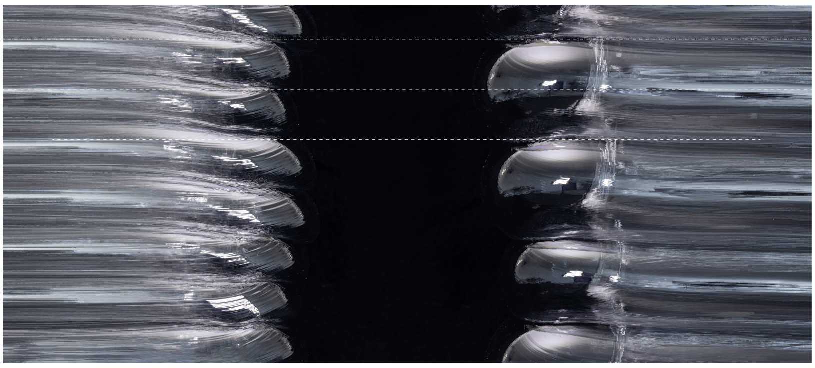

Figure 5.8: Left 16mm layer height, right 32mm layer height.

Table 5.2: Summary of changing printing resolution. All parameters are kept constant, only the layer height and pressure increase.

layer heights	pressure	avg. width	avg. width/height	avg. wall thickness
[mm]	[bar]	[mm]	[%]	[mm]
16	0.14	28.13	1.76	1.01
18	0.17	28.78	1.6	0.99
20	0.2	28.38	1.42	0.90
22	0.23	29.91	1.36	0.87
24	0.27	29.73	1.24	0.85
26	0.29	31.28	1.20	0.82
28	0.32	35.06	1.25	0.74
30	0.34	36.00	1.20	0.73
32	0.36	36.34	1.14	0.79

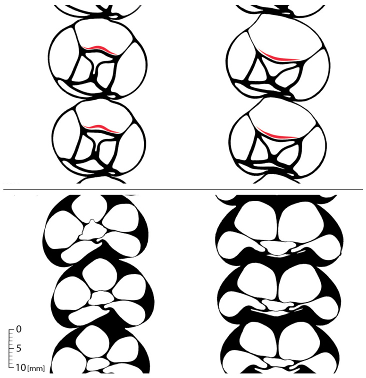

Figure 5.9: 2D scan of the bead cross sections, printed with static tool orientation. Left and right wall printed with die at 0 respectively 180 degree. (a) Crosshair die, different deformations inside the bead, probably caused by unequal air pressure distribution inside the individual air pockets. (b) Tube in tube die, non-symmetrical nozzle geometry causes different sections.

The authors successfully 3D printed specimens using all nozzles with bespoke internal substructures. For doing so, a new concept of differentiated air pressure per print point needed to be introduced 4. Figure 5.10, and Figure 5.11 documents the sections of the different nozzles; the scans generally show:

- all die geometries can be used for 3D printing
- there are deviations in the bead geometry, between individual layers and from one wall to the other
- the deviations are more significant for cross-sections with more material/ unequal wall thicknesses
- The lower air pockets, interfacing with the previous layer, are less inflated than the corresponding upper air pocket
- asymmetric die geometries create, depending on the tool rotation, different 3DP cross sections.

The section of the crosshair nozzle is specifically interesting as it shows different internal deformation depending on the printing direction. As shown in the Figure 5.9.a, the internal ring shows either a convex, or concave deformation (red stroke). This indicates that the pressure inside the single air pockets is not equally distributed. The design of the air

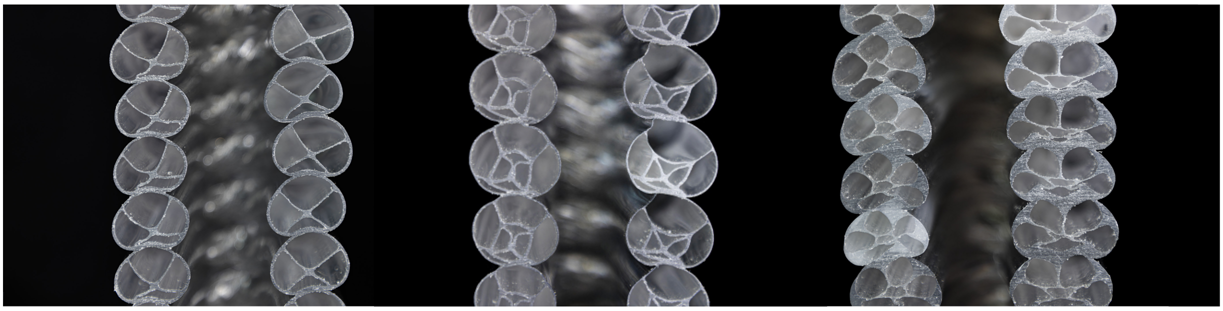

Figure 5.10: Section of 3D printed samples. A) Quad. B) Crosshair. C) Tube in tube.

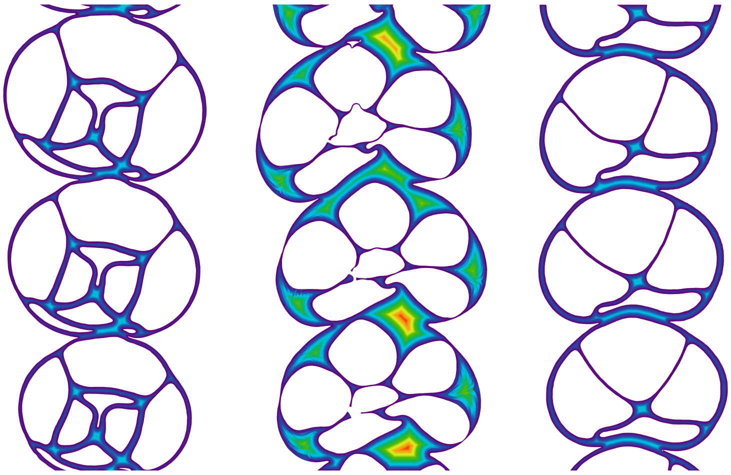

Figure 5.11: Visualization of the material distribution in the HC3DP beads, the color gradient displays the distance from a pixel to the closest border.

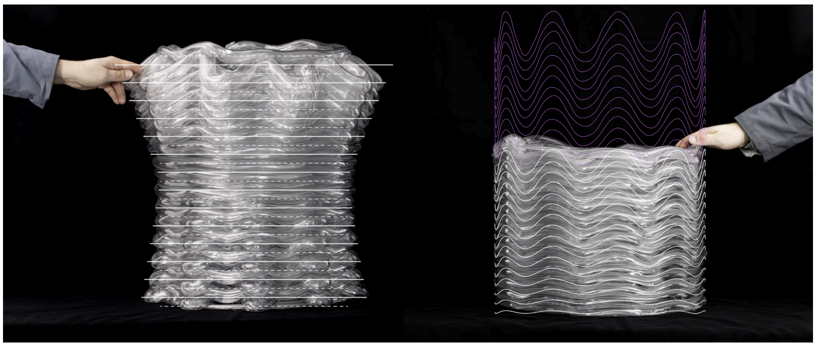

Figure 5.12: 3D printed specimen overlaid with actual toolpath.

inlets, or the manufacturing process of metal 3D printing, might be the reason for this phenomenon. For asymmetric die geometries (tube in tube), the cross section of the printed bead changes for different printing directions if the tool orientation is static (Fig. 5.9.b).

5.4.3 3D printed features

Bridging and cantilevering

The results show that HC3DP bridges distances of 60mm successfully at print speed of 12mm/s, Figure 5.12.a. However, the sagging behavior is observed to be different from common ME. As shown in Figure 5.15, the upper and lower sag is significantly different. The upper side of the bead sags approx. 2.8 mm, the lower portion of the bead is sagging up to four times more, approx. 12.2mm. This difference can be explained with the active cooling that is reaching the upper side of the bead, but not the lower. The material exposed to forced airflow solidifies faster than the bottom area, which then stretches due to gravitational forces. For a more equal cooling, the current set of fans need to be redirected to also hit the sides of the extruded bead, or external fans need to be set up.

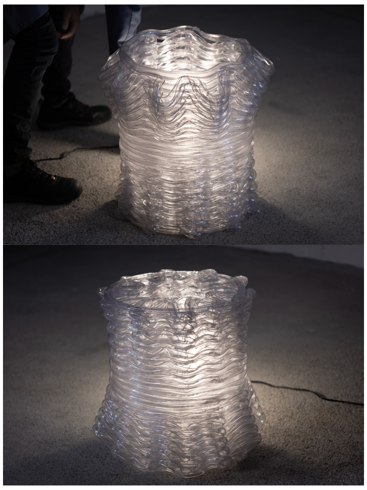

Figure 5.13: Large-scale specimen with light source in background.

Printing in air cannot be reproduced with large beads at fast printing speeds, as shown in small scale tubular printing of Hopkins et. al [264, p. 2cm]. However, the print does not fail, only strong deviations occur, Figure 5.14 and 5.13. Although only every second layer is printing the cantilevering structure, the cantilever is still building up, with a maximum deviation of 3 layers missing. This can be partially explained as the beads

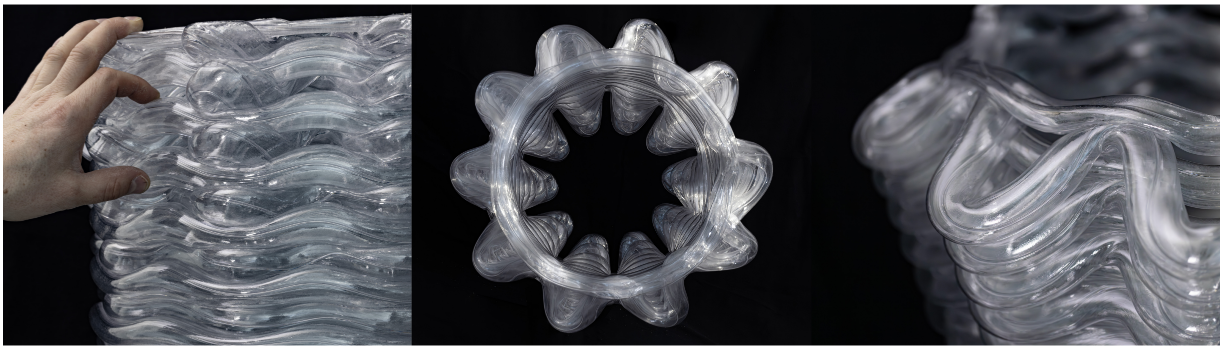

Figure 5.14: Bespoke toolpath design for large-scale elements.

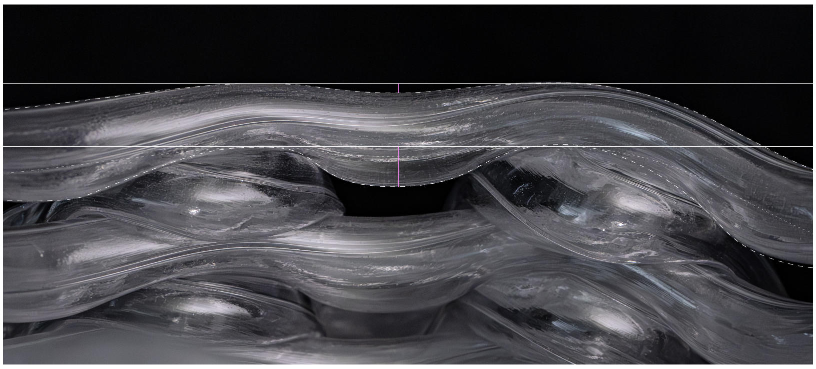

Figure 5.15: Sagging behavior of HC3DP during bridging.

that are not supported from below, and therefore not squeezed between the previous layer and the extruding nozzle. Those beads have a round and not a rectangular shape with half circular ends, similar to the experiments in chapter 5.3.2, and showcase a larger layer height than designed for.

Non-planar 3DP

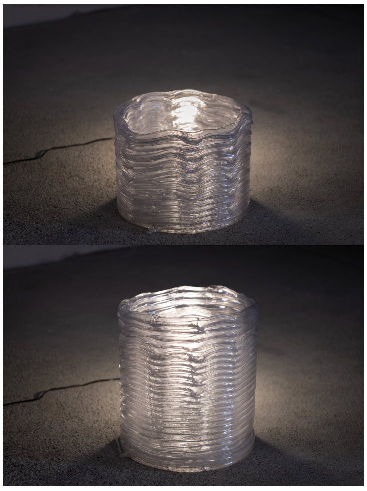

Figure 5.16: Non-planar HC3DP, the print failed after a height of 250mm. B) Non-planar HC3DP, printed to the end, as the undulations in Z directions are less strong.

Figures 5.12.a and 5.16 show successful non-planar HC3DP. However, as the tool was not reoriented during printing, collisions with previous layers caused the print to fail. It was observed that when moving the toolhead downwards, towards an already printed bead, the distance between nozzle and printed objects becomes too little for the tubular bead to be inflated. Instead, the hollow bead gets squeezed together and becomes solid. Then, when the toolhead rises to follow the trajectory of the toolpath, the distance between printed object and nozzle increases and the hollow-core bead is over inflating. This causes the consecutive layer to collide with the object and the experiment needed to stop after layer 15.

The observations are showcasing a different behavior than ME. Although the HC3DP layers can be squeezed down, the inflation of the bead continues once the extruder moves along the printing path, see Figure 5.1. This post inflation of beads results in strong deviation to the desired toolpath and remains a challenge for non-planar 3D printing. More research is needed to fully understand the post-print inflation and achieve controlled results.

5.5 Discussion

5.5.1 Variable cross-section

Changing the extruded cross section without changing extrusion rate has been successfully demonstrated. If the same result can be achieved while maintaining a constant wall thickness is still to be investigated. The difference in wall thickness measured in table 5.2, can be potentially used to determine an extrusion multiplication factor. Controlling the layer height, and the wall thickness precisely would increase the versatility of HC3DP and allow for the fabrication of even more material efficient components. To which extent these findings can be transferred to a multi-outline (contour) print is still to be investigated. How to dynamically change the cross section during printing remains unexplored. Although the hardware setup allows for it, the software will need to map pressure values to certain layer heights, similar as for tight geometrical features [46].

[46]: Leschok et al. (2023), 'Large-scale hollow-core 3D printing (HC3DP)'

Main benefits of dynamically controlling the cross sections are, but not limited to:

- increased print speed for fast vertical build-up in low resolution HC3DP
- more detailed areas can be printed in high resolution
- Stronger overhangs can be printed at low layer heights, as the stepover per layer reduces

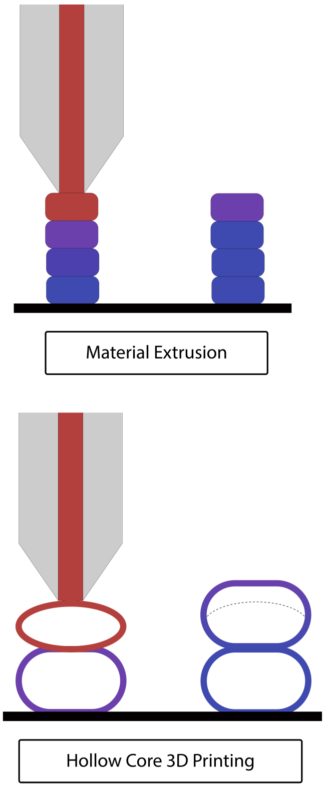

Figure 5.17: Post inflation diagram. A) In ME the bead is squeezed down during the printing process and receives its typical rectangular shape with half circular ends. The extruded beads stay in place during the cool down process. B) In HC3DP the bead can be squeezed down during the printing process, but due to the positive air pressure within the bead, might inflate and stretch the bead after the extruder continues to print.

5.5.2 Different nozzles - internal geometry

The initial experiments with bespoke cross-section, although inflated, show deviations from the initial geometry. Further investigations need to clarify if the quality can be improved by tuning printing parameters, or if it is necessary to have differentiated pressure control for each individual air pocket. If individual pressure zones are implemented, these differences can be potentially counteracted. However, hardware/software requirements change, and the HC3DP nozzle and control system will increase in complexity.

Furthermore, there is a tradeoff between maximum print speed and the number of subdivisions, as internal geometries will increase material consumption. The maximum print speed will be determined either by the maximum extrusion of plastic, or the cooldown rate of the extruded bead.

The benefits of subdividing the internal core, although a unique feature, must be investigated further for specific applications. Structural experiments are still to be conducted, as well as the potentially improved thermal resistance. Finally, it would be interesting to see to which extent adapting the extrusion section is possible with those bespoke die geometries.

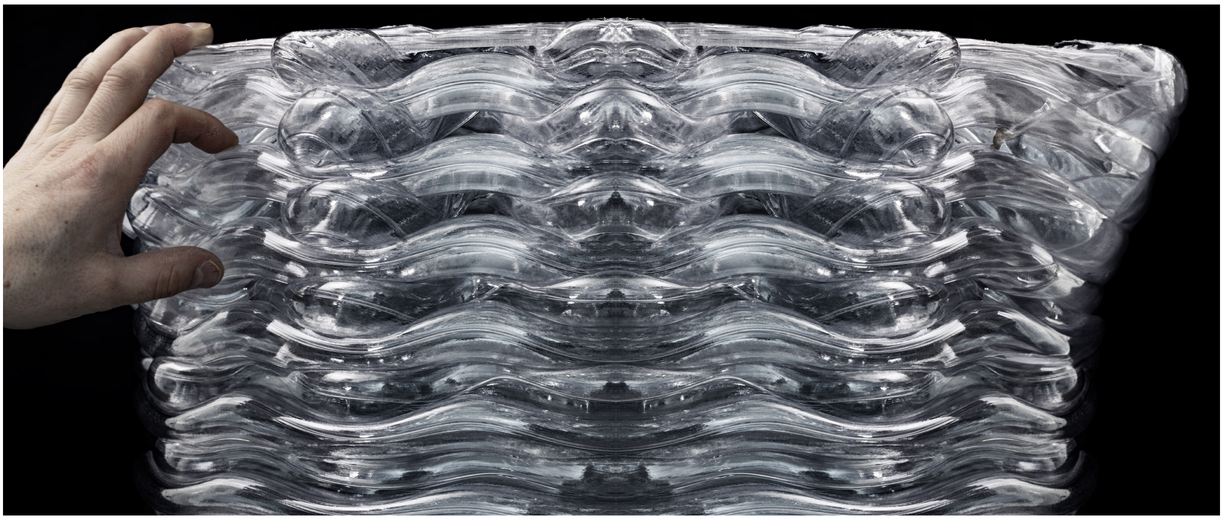

Figure 5.18: Close up of the bridging sample. Sample flipped.

5.5.3 3DP features

The fundamental behavior of HC3DP features has been presented in this manuscript. With this understanding, a fabrication aware design tool can be created to eliminate printing errors, and increase the ease of use of this novel printing technology.

Initial observations show an improved bridging behavior for HC3DP compared to state-of-the-art large-scale ME, see Figure 5.18. mainly due to the increased cooling rate of the thin-walled beads. However, future investigations must quantify this trend to understand the dependency of print speed, bridging distance, and material.

5.6 Conclusions

The authors have proven that it is possible to change the extruded section by increasing/adapting the air pressure inside the bead. Multi resolution 3DP can now be achieved without the need for a second extruder or additional hardware. Research on dynamically changing the extruded section is still to be conducted.

The introduction of dies with purpose made cross section creates a new research trajectory for large scale HC3DP. Now, not only the design/-toolpath defines the functionality of a 3D printed component, but also the 3D printed bead geometry. HC3DP at large dimensions provides the opportunity to create bespoke, non-circular etc. cross sections that increases the range of possible applications.

Adaptive extrusion section control allows for the creation of unseen designs, material efficient structures, and significant improvements on fabrication speed. With this manuscript the authors hope to provide fundamental understanding of this novel printing technology to foster more in-depth research, new design strategies, and production of material efficient 3D printed elements.

Acknowledgements

This research is financially supported by the National Centre for Competence in Research in Digital Fabrication and funded by the Swiss National Science Foundation (NCCR Digital Fabrication Agreement number 51NF40141853). The authors would like to acknowledge Philippe Fleischmann for his technical support on the compass RRC communication and SAEKI Robotics AG for their time, dedication, and providing 3D printing capacities.

Prōtóplasto: A discrete roof-column system with hollow-core 3D printing and bespoke space frames

6

6.1 Overview of Paper E . . . 119
6.2 Plastic Architecture in the Digital Age 121
6.3 Towards Discrete Prefabricated Architecture 122
6.4 Constructive System and Digital Workflow 123
6.5 A Plastic Future? 128

6.1 Overview of Paper E

6.1.1 Content

Paper E describes the design and fabrication an ultra-lightweight pavilion made from tubular plastic elements. HC3DP columns are combined with a large-spanning space frame roof to form modular mushroom columns. The pavilion consists of three column-roof elements and covers a footprint of 65 m2 with a weight of only 3.8 kg/m2. The paper discusses the role of plastic in architecture and discrete prefabricated systems, where differentiated articulation of building elements are designed according to their role and position in the constructive system. Then, the constructive system is introduced as well as the fabrication setup, consisting of the robotic HC3DP setup, a collaborative robotic cutting station for the members of the space-frame, and the MultiJet Fusion (MJF) 3D printer used for the nodes of the space-frame (SF). The space frame is designed for an support-free assembly scheme, minimizing the manual labor on site, and allowing the pavilion to be assembled by a single person.

6.1.2 Method

The pavilion is composed of three long-spanning mushroom columns and a radial SF roof. The columns are manufactured using the HC3DP process, which involves the extrusion of thin-walled hollow-tubular polymer beads. The columns are printed as single outline tool-path, making them extremely lightweight, material efficient, and fast to fabricate. Therefore, the cores of the columns are hollow and accommodate post-tensioning cables and light sources that produce the final illuminating effect. The space-frame roof features a unique topology enabled by novel typologies of 3DP interlocking connections. The roof interlocks with the hollow columns through an intermediate component. A post-tensioning cable runs through the central joint of this intermediate module, traverses the column, and is anchored to the concrete footings upon which the columns are positioned. The footings are shaped in continuity of the column geometry, and HC3DP formwork was used to cast concrete matching the scale and resolution of the layered-based materiality of the column shaft. The pavilion is designed and fabricated through a computational parametric workflow, which allows for direct export of fabrication data.

6.1.3 Results

By utilizing HC3DP and support-free assembly of bespoke space frames, the project demonstrates the potential for creating lightweight, modular structures with minimal material usage. The use of hollow plastic elements and smart geometric articulation not only contributes to the design and fabrication of the pavilion but also opens up new possibilities for playful and ephemeral architecture. For the first time, large-scale HC3DP elements are produced for an architectural application and result in quasi load-bearing structural elements. The fabrication time of these bespoke elements range between four and six hours, proving the production viability of HC3DP. Furthermore it was shown that HC3DP is sufficiently precise to be combined with other construction methods such as concrete cast supports (butt joint), or space-frame elements (insertion). Finally, it was proven that HC3DP can also be used as formwork for concrete casting despite its minimal wall-thickness of the extruded bead (1mm). Appendix B, documents the casting of a 2.1m tall column into one of the prototype columns of the protoplasto pavilion.

6.1.4 Authors contribution to the paper

Matthias Leschok Conceptualization, Investigation, Project administration, Software, Visualization, Writing – original draft, Writing – review & editing.
Marirena Kladeftira Conceptualization, Investigation, Software, Writing – original draft, Writing – review & editing.
Nik Eftekhar Investigation, Visualization, Writing – review & editing.
Benjamin Dillenburger Supervision, Writing – review & editing.

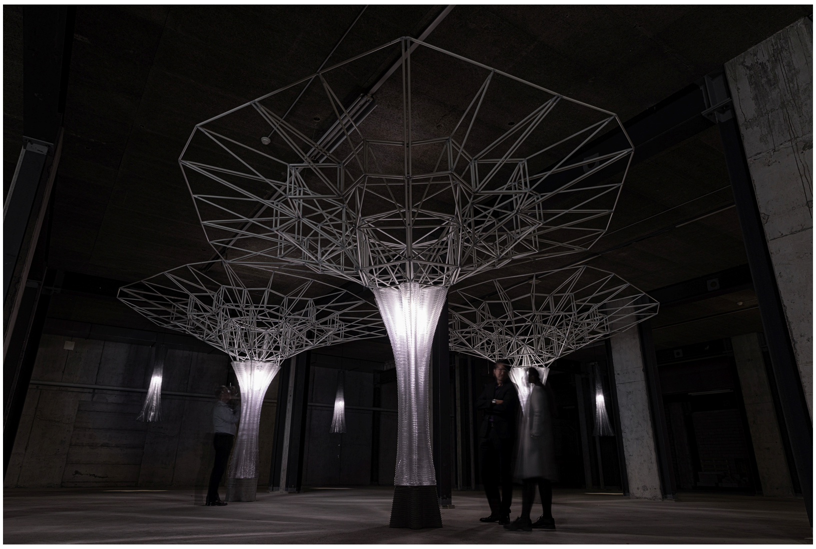

Figure 6.1: Protoplasto exhibition. Credit: Andrei Jipa, DBT.

Abstract Prōtóplasto, an ultra-lightweight plastic media installation, introduces the novel process of Hollow Core 3D Printing (HC3DP) to upscale polymer 3D printing (3DP) for architecture, and the novel method of support-free assembly of bespoke space frames (SF) through the geometric articulation of 3DP joints. The pavilion is a light installation in an upcoming innovation hub in Switzerland and consists entirely of hollow plastic elements produced through 3DP and off-the-shelf parts Figure 6.1. Learning by nature, creating hollow structures paired with smart geometric articulation, one can achieve architectural height and volume with minimum material and weight. The design and fabrication of the pavilion was formulated as a studio brief for the MAS in Architecture and Digital Fabrication (MAS DFAB) at ETH Zurich. Contextualising the research on 3DP plastics in architecture to discrete, deconstructable, and reconfigurable systems with different properties provides new ground for exploration in 3DP architecture which until recently was envisioned as mainly monomaterial and monolithic. The mixed use of processes and systems in this project finds unity in its expression through plastic materials and allows for the exploration of a more playful architecture towards an ephemeral definition of space freed of constraints of more massive, permanent materials used in construction.

6.2 Plastic Architecture in the Digital Age

The introduction of plastics in architecture dates to the beginning of the 20th century, when the fascination of architects with this synthetic material sparked the imagination of "featherweight" houses, in the words of B. Fuller [13]. The lightweight quality of the material and high strength-to-weight ratio provided by products like fibreglass embodied the utopian image of cheap, transportable, bespoke, and organic buildings that could be accessible to all. The acceptance of synthetic materials as the future of architecture in the '60s provided further ground for modular buildings that would replace concrete and steel. While the fascination of the material soon transcended to light membranes and tensile structures used still today, the production of entire building components out of plastics was put to rest until recent years, when 3DP and especially

[13]: Simone Jeska (2008), 'A Brief History of Plastic Buildings'

Material Extrusion (ME) provided a cost-effective method accessible to all for creating customizable plastic parts of large dimension using thermoplastic feedstock without moulds or falsework [274].

[274]: Vicente et al. (2023), 'Large-format additive manufacturing of polymer extrusion-based deposition systems'

Technological advancements today have not only eased and democratised the use of plastics through 3DP but present new opportunities to imagine the "new" plastic architecture in the digital era. Furthermore, the use of synthetic plastics presents an additional material resource that relies on chemical by-products of refinement processes of fossil fuels [285], thus maximising the use and value of the resources that are already extracted. Their recyclability can be achieved with lower consumed energy than other construction materials like metals or concrete due to their low melting point, especially when not formed into composites. Their reuse is also achievable due to the durability of many synthetic polymers. In the future, the increased use of bioplastics can be seen as an alternative to synthetic ones as the extraction of fossil fuels is slowly eliminated.

[285]: Center of International Environmental Law (2017), *Fossils, Plastics, & Petrochemical Feedstocks*

With this project the authors examine anew principles of lightness, modularity, and temporality of architecture with a mixed use of manufacturing methods and plastics with the goal to explore new architectural aesthetics, novel production methods promoting material savings, methods for (dis)assembly, geometric articulation for modular components, as well as pushing the limits of light construction to Fuller's notion of "featherweight".

6.3 Towards Discrete Prefabricated Architecture

Digital prefabrication of discrete elements is a core principle of *Prōtóplasto* that the authors believe is relevant for the adoption of digital fabrication techniques in construction. In this spirit, the most appropriate techniques, materials, and methods are identified and employed for the different parts of the constructive system. Macroscopically, the structure is a slab-column pair for which two systems are combined to deliver the different properties required for those two elements in the most efficient manner: large-scale ME and 3DP-enabled SFs. Although technical advancements in 3DP have achieved significant increase in build volume, contemporary approaches result in heavy, material-intense elements. The increasing size of 3DP machines has alluded to the continuous in situ fabrication of entire buildings, nevertheless the fabrication of vertical and horizontal elements in a continuous process at an architectural scale in reality is challenging. Therefore, a radical position is presented where the necessity for discrete fabrication is celebrated through differentiated articulation of building elements according to their role and position in the constructive system (Figure 6.2).

Large-scale ME offers the opportunity for geometric freedom and high articulation, however, it is better employed for the production of vertical elements due to the anisotropic behaviour of the layer-based material deposition. The process of ME is scaled up with larger tool-heads and extruding thicker and heavier beads [30]. Investigating methods to upscale ME with lower material intensity and higher volume output is necessary. Elements of architectural size need to be fabricated within hours, not days or weeks. HC3DP at large-dimensions, introduced by

[30]: Duty et al. (2017), 'Structure and mechanical behavior of Big Area Additive Manufacturing (BAAM) materials'

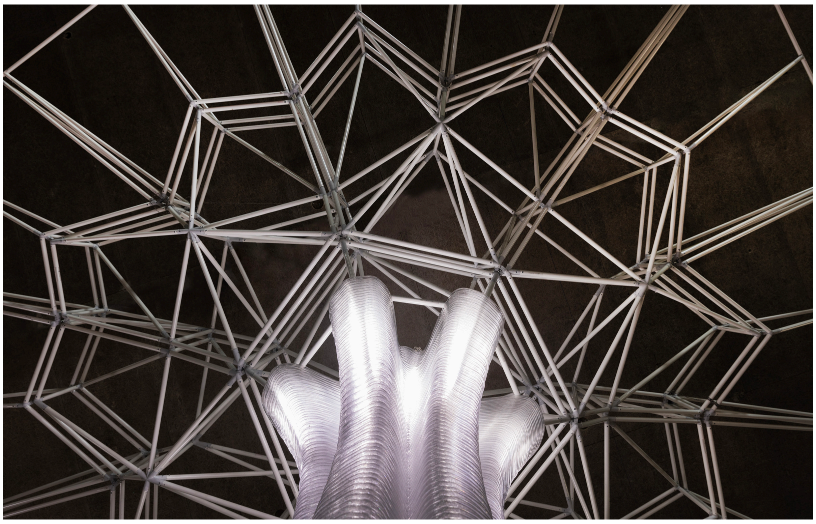

Figure 6.2: Transition between column and roof structure. Photo: Andrei Jipa, DBT.

[46] overcomes those problems by fundamentally changing the way large elements are 3D printed. With the introduction of HC3DP, the extrusion rate of thin-walled hollow-tubular polymer beads can compete with those of concrete 3D printing, while only using a fraction of material.

[46]: Leschok et al. (2023), 'Large-scale hollow-core 3D printing (HC3DP)'

On the other hand, for horizontal elements such as slabs and roofs, SFs present a more efficient system due to their three-dimensional action. Previous research has shown the benefits of 3DP joints for non-standard SFs minimising production waste and employing lower-energy-consuming materials [286]. However, the fabrication of non-standard structures in situ requires the assembly of individual elements at great heights and heavy machinery. Often, support structures are as dense as the structure itself. In this project the elimination of support structures was studied in combination with a customised modularization strategy enabled by 3DP joints allowing for efficient assembly with safe conditions by humans at a fast pace without heavy or special equipment. Extensive research on connection principles and detailing between modules was performed as well as patterning and sequencing strategies that allow for gradual loading of the structure throughout the assembly process.

[286]: Kladeftira et al. (2022), 'A Study on Bamboo, 3D Printed Joints, and Digitally Fabricated Building Components for Ultralight Architectures'

6.4 Constructive System and Digital Workflow

The pavilion is conceived as a modular aggregation of three long-spanning mushroom columns. It is composed of a 3D-printed column and a radial SF (Figure 6.3). The columns are manufactured with HC3DP with a single outline, while the core of the column is hollow to accommodate post-tensioning cables and light sources that produce the final illuminating effect. The SF roof features a unique topology enabled by novel typologies of 3DP interlocking connections. The roof interlocks with the hollow columns with an intermediate component. The geometry of this SF module is adapted for each bespoke column such that it interlocks with the column's undulating geometry in the upper 25 layers. A post-tensioning cable runs through the central joint of the intermediate module, traverses the column and is anchored to the concrete footings on which the columns are placed. The footings are shaped in continuity of the column geometry and HC3DP formwork is used to match the scale

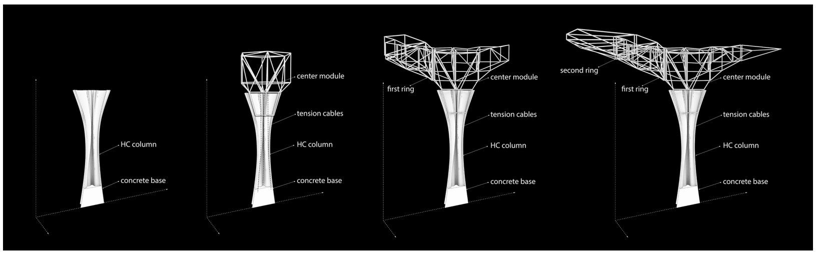
HC column
concrete base
center module
tension cables
HC column
concrete base
first ring
center module
tension cables
HC column
concrete base
second ring
first ring
center module
tension cables
HC column
concrete base

Figure 6.3: Assembly scheme. Photo: Matthias Leschok.

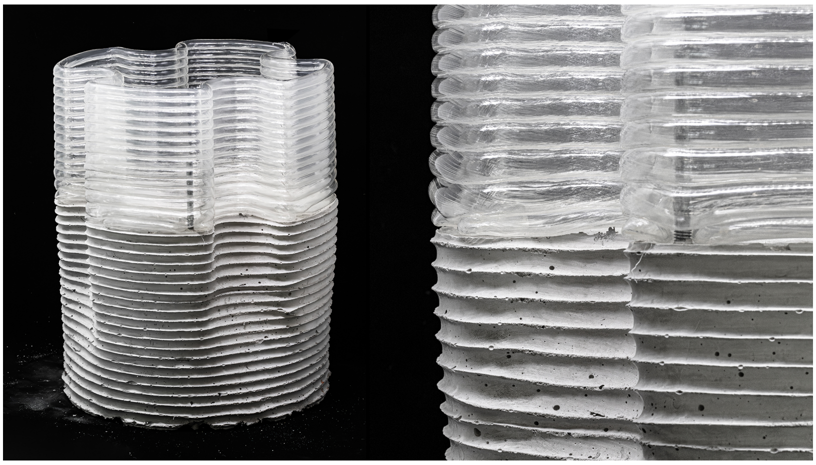

Figure 6.4: Prototype of concrete feet, SCC cast into HC3DP formwork. Photo: Matthias Leschok, DBT.

and resolution of the layered-base materiality of the column shaft (Figure 6.4).

Each column-roof pair is designed and fabricated through a computational parametric workflow. Each "mushroom" reacts to its relative position in the structure and the desired pavilion outline. The parameters for column design include fabrication constraints, such as continuous toolpaths, maximum overhangs, and minimum feature size. The designed undulations increase the stiffness of the 3DP elements in addition to the insertion interface for the SF. The design tool for the joints calculates the minimum joint volume needed to connect the tubes and orients the necessary connection details in order to create unique hybrid-detail connections tailored for their specific position in the structure.

6.4.1 Fabrication Setup

To fabricate the pavilion multiple complementary digital fabrication techniques are used. The columns and concrete formwork are HC3DP using a pellet extruder, mounted on a 6-axis ABB 6700. The nodes are 3DP in PA12, with a 48 MPa characteristic tensile strength, using the MultiJetFusion technology, a powder-bed process ensuring isotropic behaviour and high accuracy. The linear members employed for the SF are industrial 20mm glassfibre polymer rods. The bespoke-length tubes are cut in a human-robot collaborative setup, in which the human loads the feedstock and the robot slides the tube into the corresponding position for the cut to be executed with a stationary bandsaw. Pneumatic grippers are employed to temporarily lock the tubes' position during this process.

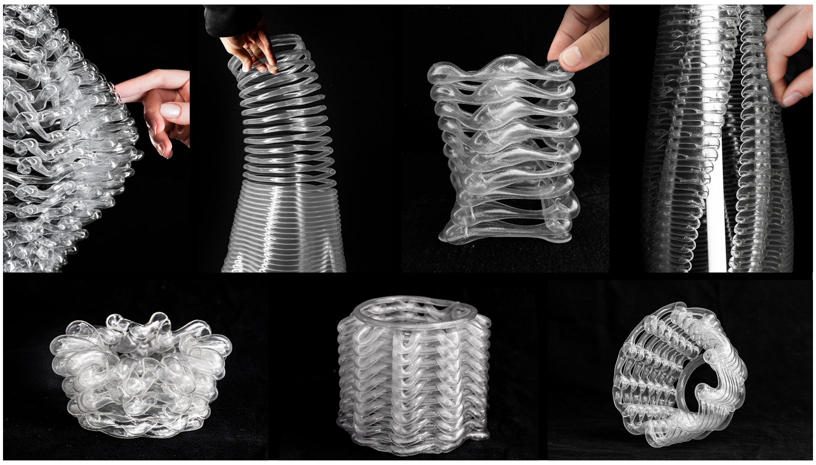

Figure 6.5: A series of design explorations conducted by the MAS DFAB students 2023. Filament based HC extrusion with a diameter of 10mm. Photo: Fen Chan, DBT.

6.4.2 HC3DP - Creating Lightweight Architecture

In HC3DP polymer feedstock is used to 3DP large-scale hollow tubular beads (strands) instead of full cross sections. This novel approach has multiple advantages compared to off-the-shelf large-scale 3DP methods such as high printing speed due to increased cooling rate, reduced material consumption, as well as increased transparency. HC3DP pushes polymer 3D printing into an architectural-relevant scale, as the printing layer ranges from 10-24mm while the build-up rate is comparable to concrete 3D printing [287]. High-performance parts can be printed with a wall thickness of 1.0-2.0mm because of the higher strength- to-weight ratio tubular sections display, saving over 85% of material, compared to conventional ME.

[287]: Anton, Ana et al. (2020), 'Fabricate 2020'

PETG was used for the HC3DP of the columns, a co-polyester derived from the commoditized PET polymer, modified to improve its printability and features high transparency. Design explorations with robotic filament-based HC3DP were performed to investigate material and process limitations. An off-the-shelf extrusion system was adapted to use the HC3DP technology with a resolution of 10mm. The new aesthetics enabled through low resolution highly transparent polymer 3DP were explored in small scale prototypes. This new printing technology allows for the creation of elements with extreme overhangs, woven structures and non-planar 3DP. Elements of medium size were printed to understand manufacturing constraints and design possibilities, as shown in Figure 6.5.

Over the last two years a robotic end-effector was developed specifically for HC3DP enabling the 3DP of large-scale tubular beads increasing the extrusion rate dramatically. The process was then adapted for the commercial pellet-extrusion system of SAEKI Robotics (Figure 6.7). The tubular geometry of the beads is materialised with a bespoke nozzle and positive air pressure. The nozzle splits the molten pellet feedstock into a thin-walled bead and an empty core. Compressed air is injected into the hollow bead to create positive air pressure and prevents the bead from collapsing. For the final design of the columns a nozzle design with internal bracing was used. The core is reinforced with a "X" cross instead of an "O" section. This was necessary to increase the stiffness of the elements and achieve higher loading capacity.

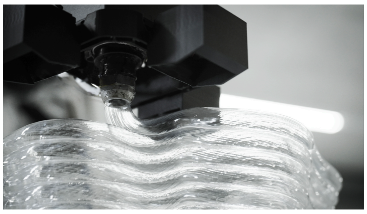

Figure 6.6: Close-up of HC3DP process. Diameter of extrusion 24mm. Right: Section of HC3DP element. Photo: Girts Apskalns, girtsapskalns.com. Matthias Leschok, DBT.

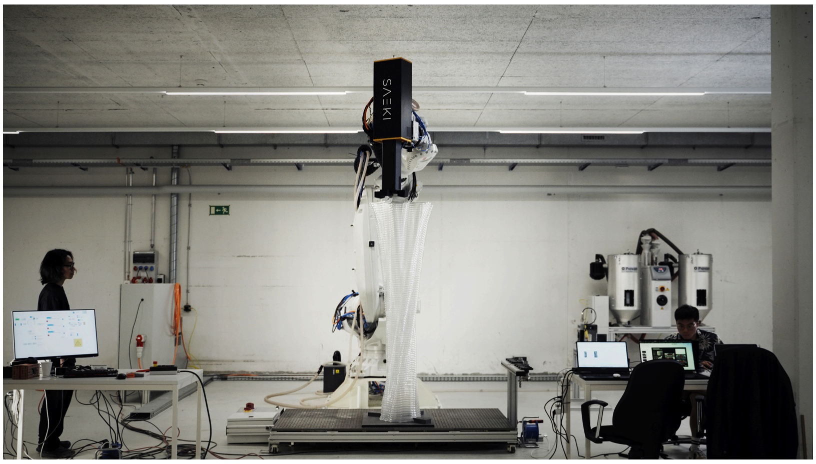

Figure 6.7: All columns were 3D printed at the fabrication hall of SAEKI Robotics, using one ABB IRB 6700 industrial robot. Photo: Girts Apskalns, girtsapskalns.com.

A diameter of 24mm and a layer height of 19mm was used in the project (Figure 6.6). The extrusion rate is 7250 mm3/s (1308 material, 5942 air) rendering the 3DP of the 2.2m tall columns in only 4-6 hours and with a weight of 10Kgs each for the "O" section and 18-20 Kgs for the "X" section. A column with a comparable volume, printed with regular ME (6mm width, 3mm layer height, two outlines, one of them zigzagging), results in a 10-fold longer print time and 4-5x higher material consumption.

6.4.3 3DP Enabled Support-free Assembly of Modular SFs

The design of the roof is governed by three principles: modularity, support-free assembly, and disassembly through dry self-interlocking connections. The unique constellation of the structure and its non-standard layout require a custom SF enabled by 3DP joints light enough to be supported by the columns and stiff enough to span the 5.5m distance between them, as well as the 3m horizontal overhang (Figure 6.12).

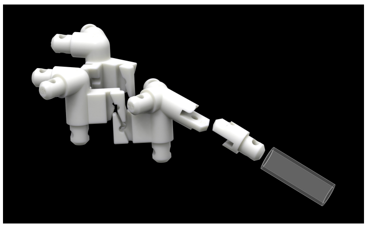

Figure 6.8: Module-module connection details for support free assembly. Photo: Marirena Kladeftira, DBT.

The roof is first discretized into three segments designating the portion of the roof that is supported by each column. Subsequently, each segment is discretized further into modules according to the following principles: a radial array of primary beams ("meridians") is formed stemming from each column outward to the exterior ring of the SF. Perpendicular to the radial lines, parallel concentric polygons are formed through a subdivision schema ("parallels"). This 2-way hierarchical grid and its density defines the amount and number of modules and signifies the axes along which doubling of members will occur. Each module is further subdivided in 3-dimensional space adding diagonals for rigidity and stability during assembly (Figure 6.9).

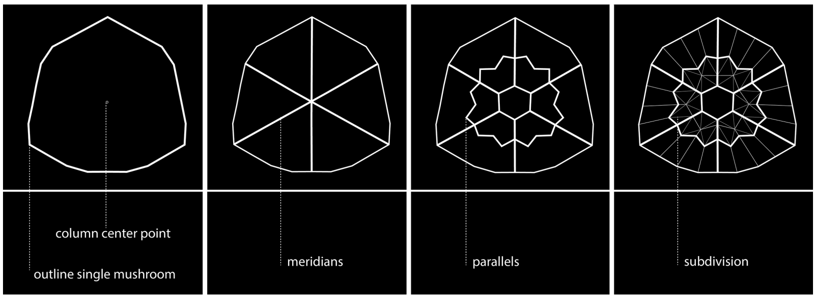

Figure 6.9: Computational design framework. Photo: Matthias Leschok.

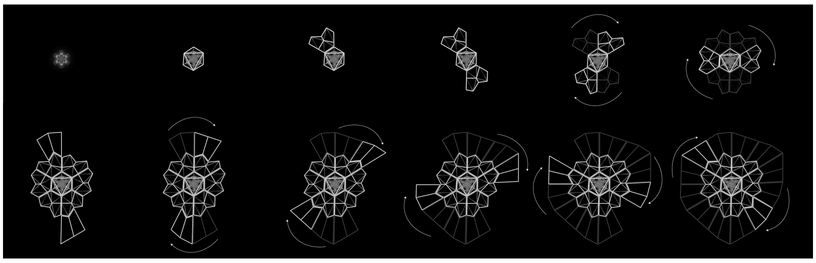

Figure 6.10: Assembly sequence. Photo: Nik Eftekhar.

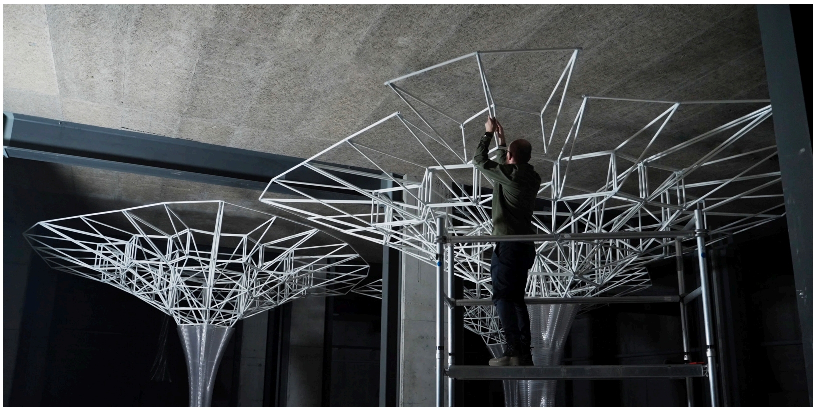

Figure 6.11: Supportfree assembly, last element being placed. Photo: Girts Apskalns, girtsapskalns.com.

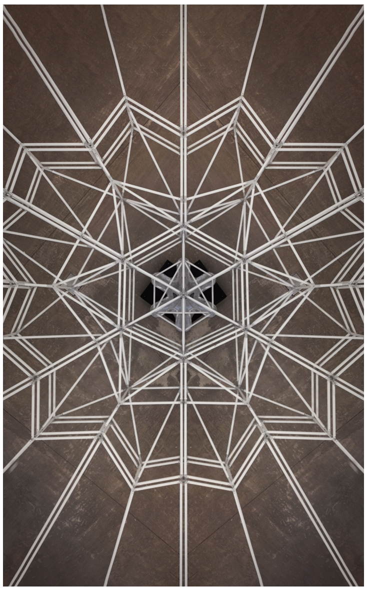

Figure 6.12: Top view of one mushroom column. Photo: Marirena Kladeftira, DBT.

Three typologies of joints were developed. Their geometry is a hollow shell with a seamless connection to the tubes and a 3mm wall thickness, which after mechanical testing was fine-tuned to match the ultimate tensile strength of the plastic tubes. Two types of intra-module joints feature a) a socket pin connection for the members of the boundary frame that are assembled first, and b) an intermediate piece for stiffening diagonals first attached via a socket connection to the tube and later fastened on the joint with a self-guiding slit and an interlocking pin. Finally, the module-module connections are formed via added self-interlocking details on the shell of the joints positioned at the interfaces of adjacent modules. They consist of a male-female self-guiding interlocking fork that allows for vertical insertion of the introduced module (Figure 6.8). The assembly follows a semi-circular sequence dictating the position of male/female details (Figure 6.10, Figure 6.11). First the intermediate module is inserted for connection to the column, and subsequently two cross-facing modules of the first parallel are placed to balance the weight. The size and weight of the modules are tailored such that they can be handled by one human, featuring an average weight of 3.7 Kgs. Two people start adding modules radially until the full circle is assembled. Due to the segmentation scheme all column-roof pairs can be fabricated in parallel with no expertise by crowdsourcing the assembly.

6.4.4 Exhibition

The pavilion is exhibited in an industrial underground setting of Halter AG in Switzerland. The exhibition consists of the pavilion and suspended HC3DP chandeliers, surrounding the pavilion (Figure 6.15,Figure 6.13). No other light sources exist in the room except for the ones installed inside the HC3DP elements contributing to a more dramatic effect of the installation.

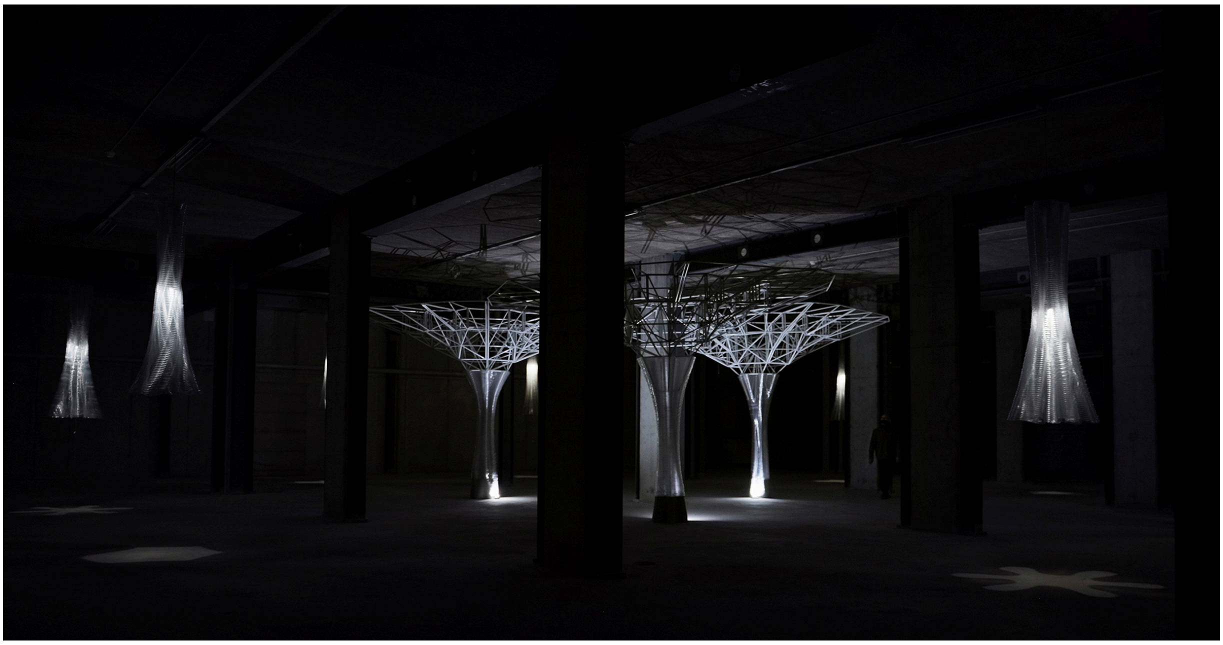

Figure 6.13: Installation view showing the 2.2m tall HC3DP chandeliers surrounding the pavilion display.

6.5 A Plastic Future?

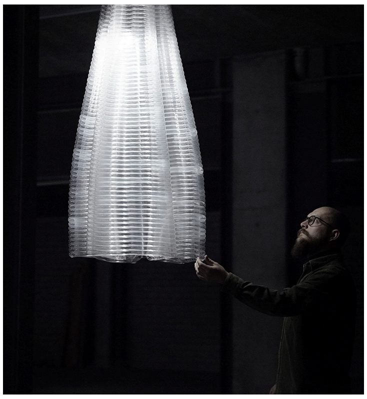

Figure 6.14: 2.2m tall HC3DP chandeliers suspended from the ceiling are framing the exhibition. Photo: Girts Apskalns, girtsapskalns.com.

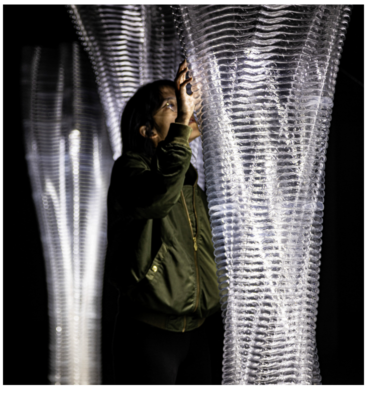

Figure 6.15: A series of 2.2m tall HC3DP elements aligned and alight. Photo: Nijat Mahamaliyev .

Prōtóplasto opens up a dialogue about the controversial use of plastics in architecture in-hand with design-for-disassembly methodologies. It revisits the ideals for lightweight plastic architecture and proposes a new perspective on how to use circularly synthetic materials that can be reused or recycled multiple times during their lifecycle. The combination of techniques and materials is an experimental search for more efficient use of materials and systems that leverage digital fabrication technologies and innovate equally in the microscale (material system) and the macroscale (construction system), evident by the extremely low weight of the structure at 3.8 Kgs/m2.

HC3DP provides further ground for experimentation at the architectural scale in building envelopes, formwork creation, ephemeral architectures, and product design such as bespoke lights. Furthermore, the validation of modular support-free assembly with tailored connection details can provide a basis for future research founded on the same principles for aerial automated assembly by flying machines and collaborative human-drone construction thanks to the ultralight character of the modules and self-interlocking details.

Acknowledgments

This research was supported by the NCCR Digital Fabrication, funded by the Swiss National Science Foundation (NCCR Digital Fabrication Agreement #51NF40-141853). We recognise the commitment of our students from the MAS DFAB 22-23, ETHZ as well as the support from the Halter Group, SAEKI Robotics, Castioni Kunststoffe, and K. Studer AG. Our sincere gratitude goes to Michael Lyrenmann, Tobias Hartmann, Luca Petrus, and Jonathan Leu for their engagement.

MANUSCRIPTS RELATED TO HC3DP FACADES

Hollow-Core 3D Printing for highly insulated, lightweight and translucent facades

7

7.1 Overview of Paper F . . . 131
7.2 Introduction 134
7.3 Methods and materials . 138
7.4 Results 149
7.5 Discussion 153
7.6 Outlook 154
7.7 Conclusion 155
7.8 Appendix A - Print time calculations 157
7.9 Appendix B 159

7.1 Overview of Paper F

7.1.1 Content

Paper F investigates the use of Hollow-Core 3D Printing (HC3DP) for creating highly insulated, lightweight, and translucent facades. It covers various aspects related to the thermal performance of large-scale 3D printed elements, including the influence of infill structures, printing methods, and materials. The research compares the thermal resistance of 3D printed specimens to off-the-shelf ME and established construction methods for opaque and transparent facades. It discusses the potential of HC3DP in improving thermal resistance, reducing material consumption, and increasing fabrication speed. Additionally, the manuscript explores the combination of HC3DP with aerogel to create ultra-lightweight and highly insulating 3D-printed facade elements. Furthermore, it provides insights into the thermal performance of 3DP facades at different printing resolutions and emphasizes the importance of printing time and material consumption in determining the best 3D printing approach for lightweight and highly insulating 3DP facades.

7.1.2 Method

The manuscript uses a combination of design, fabrication, and experimental testing methods to investigate and compare the thermal performance of 3DP facades. The printing methods used include off-the-shelf "desktop" 3D printers and large-scale HC3DP. The infill structures and densities of the specimens are varied to understand their impact on the thermal performance. For the large HC3DP specimen the cross-section (size and shape), and the geometry of the specimen are varied, investigating the influence on the thermal performance. The thermal characterization of the specimens is performed using the transient hot-wire method for the desktop 3DP specimens, and the steady-state hot box heat flux meter approach for the large-scale elements. The resulting data is then analyzed and compared to off-the-shelf material extrusion methods and established construction methods for opaque and transparent facades. Finally, the production time per square meter is calculated for the printing methods investigated. For desktop 3DP, the proprietary slicing software is used to estimate the printing time for different infill densities. To calculate the printing time for robotic ME and HC3DP, a theoretical model is established taking into consideration the maximum extrusion rate of the pellet extruder, as well as the minimal cool down time per layer for the given 3DP methods. Finally, the results are compared to the findings of Paper B, comparing off the shelf robotic ME to HC3DP.

7.1.3 Results

The manuscript presents several key results related to the thermal performance of 3D printed facades using HC3DP and off-the-shelf ME. More specifically, for desktop ME it is shown that at this high resolution, the effect of cell configuration, closed or open, and geometry is negligible. Therefore it can be concluded that the infill geometry can be based on other performance related aspects, like structural, optical, or by design intention. However, the print time at this resolution is significantly higher than for other ME methods, which put into question the production viability of desktop 3DP for facades. For HC3DP the results can be summarized as follows, compared to the ME samples (Paper B), HC3DP exhibits lower thermal conductivity regardless of the chosen die geometry. Similar to the findings of high-resolution ME, the thermal conductivity is not influenced by the orientations created by the orientation of the infill orientation. Based on the print-time model established in this paper, it is shown that HC3DP facades can be fabricated at a print speed of as low as 1.5 h/m2. This is a significant impovement over 780 % compared to off-the-shelf ME. The combination of HC3DP with aerogel is demonstrated to be fast to fabricate and highly insulating composit, designed to be dissassembled at the end of life. In summary, this manuscript highlights the potential of HC3DP in improving thermal resistance, reducing material consumption, and increasing fabrication speed of 3DP facades significantly.

7.1.4 Authors contribution to the paper

Matthias Leschok* - Conceptualization, Methodology, Investigation, Writing – Original Draft Preparation, Visualization.
Valeria Piccioni* - Conceptualization, Methodology, Formal Analysis, Writing – Original Draft Preparation, Visualization.
Gearoid Lydon - Methodology, Writing – Review & Editing
Matthias Kohler - Supervision, Writing – Review & Editing.
Fabio Gramazio - Supervision, Writing – Review & Editing.
Arno Schlueter - Supervision, Writing – Review & Editing.
Benjamin Dillenburger - Supervision, Writing – Review & Editing
* M Leschok and V Piccioni contributed equally to this work.

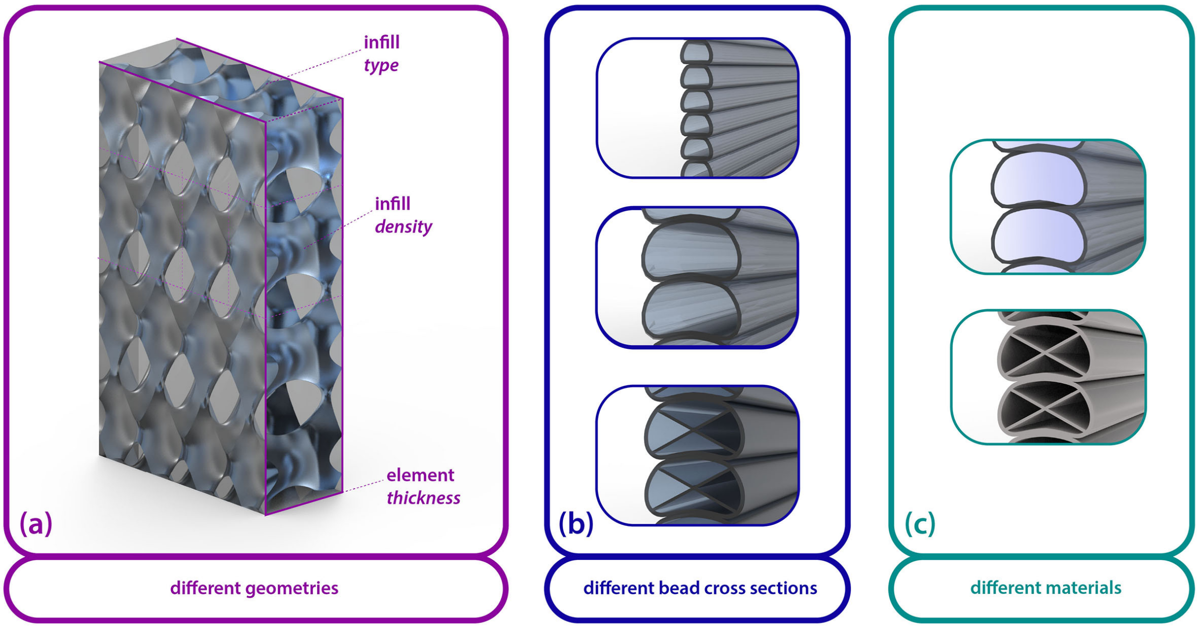

Figure 7.1: Overview of different aspects investigated, part geomerty, bead cross sectiond, and materials.

Abstract High-performance facades play an important role in achieving Net-Zero goals by 2050. As a facade manufacturing technology, 3D printing offers the opportunity to create site-specific and high-performance building envelopes. In this manuscript, the thermal performance of components fabricated with different Material Extrusion methods is studied experimentally, and the fabrication time is calculated, thereby examining both performance and fabrication viability. More specifically, this manuscript investigates the thermal performance of 3D-printed facades using Hollow-Core 3D Printing (HC3DP) and explores the potential of this novel approach in creating highly insulated, lightweight, and translucent building envelopes. The research compares the thermal resistance of 3D printed specimens to off-the-shelf material extrusion methods, such as desktop 3D printers, and granular-based, large-scale pellet extrusion. Different methods are used to determine the thermal resistance of specimens, including the transient hot-wire method for the desktop 3DP specimens, and the steady-state hot box heat flux meter approach for HC3DP. The results demonstrate that HC3DP enables lower U-values at lighter weight and faster printing speed, making it a promising avenue for further research. Additionally, the combination of HC3DP with aerogel is shown to create ultra-lightweight and highly insulating 3D-printed facade elements. The potential of this new facade technology is also highlighted in comparison with established facade systems. All in all, the manuscript provides insights into the thermal performance of 3D-printed facades at different printing resolutions and emphasizes the importance of printing time and material consumption in determining the most promising 3D printing approach for lightweight and highly insulating facades.

7.2 Introduction

Building envelopes play a significant role in the energy performance of buildings. They define the boundary between the in- and outside and impact the comfort of users and the environmental conditions inside the building [50]. With stringent regulations for the building sector's decarbonization, the thermal insulation of building envelopes is of great importance to minimize operational energy such as heating or cooling. The construction and improvement of high-performance building envelopes is a critical factor in reaching the Net Zero Emission goal by 2050 [3].

To tackle these strict requirements, high-performance facades need to be tailored to the building's use, services, location, and orientation [39]. Today, those are commonly constructed in a multimaterial system made from mass-produced components, which hinders their adaptability to a specific location. With the introduction of site-specific facade designs, novel opportunities for enhanced performance arise, like improving air quality, air tempering, or even electrical energy production [51, 288]. Although these facades seem to be a promising avenue toward operational efficiency, they come with limitations relative to their high complexity. The use of multiple parts and components limits their service life due to different durability properties and interdependencies between the parts and increases recurring replacement emissions [4]. These multicomponent facades also have limited reusability and recyclability potential due to the wide use of permanent adhesive connections, for example, in structural and weather-proofing seals using silicon and epoxy and laminated glass, which limit disassembly [42]. Moreover, these systems are usually made of energy-intensive materials and require high investment costs, which hinders their wide spread use [289].

Since the 1980s, architects have envisioned multifunctional, multi-purpose building envelopes, such as the polyvalent wall by M. Davies [5]. However, the highly industrialized production methods developed for standardized elements were struggling to manufacture those efficiently. Now, with the advent of Additive Manufacturing (AM) technologies, 3D printing of thermoplastics offers, specifically for translucent facades, the possibility to create multifunctional components using a single material, allowing the vision of the polyvalent wall to be materialized [44, 45, 197]. A monomaterial facade, enabled through 3D printing (3DP), allows for a circular construction scheme, where each individual element can be tailored to specific needs or environmental conditions and be easily recycled at the end of life [40, 106]. The use of transparent polymers for this purpose is particularly interesting thanks to the possibility of controlling the most critical environmental factors for facade design, namely solar radiation and temperature [39] while creating aesthetically appealing translucent facade elements.

Material Extrusion (ME) is a 3D printing technology using thermoplastic materials as a feedstock [7]. ME was invented in 1988 and quickly became one of the most prominent printing techniques for rapid prototyping. Due to the widespread availability of desktop 3D printers, a significant amount of research has been conducted using them to investigate facade-related performance. However, due to their limited build volume and extrusion rates, there has been a trend over the last years, towards scaling

[50]: GhaffarianHoseini et al. (2013), 'Intelligent Facades in Low-Energy Buildings'

[3]: Delmastro et al. (2022), *Building Envelopes – Technology deep dive*

[39]: Aelenei et al. (2016), 'Adaptive Façade'

[51]: Juaristi et al. (2018), 'Qualitative analysis of promising materials and technologies for the design and evaluation of Climate Adaptive Opaque Façades'

[288]: Svetozarevic et al. (2019), 'Dynamic photovoltaic building envelopes for adaptive energy and comfort management'

[4]: Hartwell et al. (2021), 'Circular economy of façades'

[42]: Hartwell et al. (2019), 'Unlocking the Re-use Potential of Glass Façade Systems'

[289]: Pelletier et al. (2023), 'The viability of double-skin façade systems in the 21st century'

[5]: Davies et al. (1981), 'A wall for all seasons'

[44]: Leschok et al. (2023), '3D printing facades'

[45]: Piccioni et al. (2023), 'Printing thermal performance'

[197]: Piccioni et al. (2023), 'Tuning the Solar Performance of Building Facades through Polymer 3D Printing'

[40]: Moritz Basil Mungenast (2019), '3D-Printed Future Facade'

[106]: Sarakinioti et al. (2018), 'Developing an integrated 3D-printed façade with complex geometries for active temperature control'

[39]: Aelenei et al. (2016), 'Adaptive Façade'

[7]: ISO/ASTM (2020), *ISO/ASTM 52903-1:2020 - Additive manufacturing. Material extrusion-based additive manufacturing of plastic materials*

up ME to accommodate large-scale applications. The material output (extrusion rate), as well as the build volume, has increased dramatically. Today, large-scale robotic ME is capable of extruding over 50 kg/h in a build volume of multiple cubic meters, enabling the production of architectural components [30, 104]. However, the print speed is limited by the cooling rate of the extruded plastic [38], and the parts fabricated are material-intensive due to the thick extruded plastic beads. First prototypes and projects utilizing ME have explored the feasibility of fabricating large-scale building envelopes [40, 112, 114].

Therefore, we introduce and investigate a novel concept of ME that creates lightweight and high-insulating 3D-printed facade (3DPF) elements at a fast speed. The process of Hollow Core 3D Printing (HC3DP) scales ME significantly and pushes its extrusion rate to similar rates as 3D concrete printing [46], which is of special relevance when it comes to 3DP of large elements, like building envelopes. This increase is made possible by extruding hollow, tubular beads at large dimensions (≥ 20 mm) instead of solid ones. Additionally, these hollow beads have the potential to reduce the thermal transmittance of 3DP facade elements without increasing the depth of elements. Due to the flexibility of the manufacturing process of 3D printing, the integration of passive design features like box cavities for natural ventilation [290] can be directly embedded in the design and do not require additional manufacturing steps.

A systematic approach and comparison of the thermal properties of ME for 3DPF across different fabrication scales (desktop 3DP, robotic ME, and HC3DP) are missing, especially linking the thermal performance to the resulting printing time and material consumption. Therefore, in this manuscript, we provide a broad range of experiments on the thermal performance of elements fabricated with different ME methods and their production viability. Moreover, we show how a novel ME method can improve the thermal performance of 3DPF while keeping material consumption and print time at a minimum.

7.2.1 State of the art

ME for Facades

3DP or Additive Manufacturing (AM) are collective terms for different processes using different feedstock materials to fabricate elements in a layer-based manner. There are several opportunities and benefits of using AM for the fabrication of facade components [60]. For a detailed review of 3D printing for facades applications, please refer to [33, 44].

Over the last few years, researchers have been using ME for their investigations on 3D-printed facades (3DPF), or aspects related to facade construction. With its broad material portfolio, ME is one of the few 3DP methods that allow for the fabrication of translucent, nearly transparent, large-scale structures. Recent developments focusing on increasing material output (extrusion rate) and maximum build volume make ME one of the promising 3D printing technologies for large-scale applications, such as facades.

[30]: Duty et al. (2017), 'Structure and mechanical behavior of Big Area Additive Manufacturing (BAAM) materials'

[104]: Thermwood (2023), *Thermwood LSAM - Large Scale Additive Manufacturing*

[38]: Roschli et al. (2019), 'Designing for Big Area Additive Manufacturing'

[40]: Moritz Basil Mungenast (2019), '3D-Printed Future Facade'

[112]: Mohamed et al. (2021), 'Super Composite'

[114]: DUS Architects (2015), *Urban Cabin*

[46]: Leschok et al. (2023), 'Large-scale hollow-core 3D printing (HC3DP)'

[290]: Catto Lucchino et al. (2022), 'Modelling and validation of a single-storey flexible double-skin façade system with a building energy simulation tool'

[60]: Strauß (2013), 'AM Envelope: The potential of Additive Manufacturing for façade construction'

[33]: Naboni et al. (2022), 'Additive manufacturing in skin systems'

[44]: Leschok et al. (2023), '3D printing facades'

ME at different scales has been used to 3D print facade prototypes using thermoplastics like PETG, Polycarbonate, or ABS. DUS architects, in collaboration with Actual, have 3D-printed the facades of the temporary pavilion for the European Union [113] and the Urban Cabin [114]. For both projects, the 3D-printed elements were used as lost formwork, where concrete is cast into the printed components. SOM and the US Department of Energy constructed a prototype for the Additively Manufactured Integrated Energy (AMIE) project, a 10.9 m x 3.6m x 4.2m movable home [115]. Multiple structural large-scale 3D-printed elements were used, which were post-tensioned and insulated using low-cost vacuum insulation pads. At TU Munich, researchers investigated a large-scale 3D-printed, mono-material facade prototype and its response to structural loading and fire propagation [40].

[113]: DUS (2015), *Europe Building – DUS Architects*

[114]: DUS Architects (2015), *Urban Cabin*

[115]: Biswas et al. (2017), 'Additive Manufacturing Integrated Energy - Enabling Innovative Solutions for Buildings of the Future'

[40]: Moritz Basil Mungenast (2019), '3D-Printed Future Facade'

However, those projects and research prototypes focus mainly on the validation of the fabrication method and showcasing the design freedom of 3DP technologies [43, 111]. There are research gaps in relation to the thermal performance, fabrication time, and production viability of those 3DP elements.

[43]: Cheibas et al. (2023), 'Thermoplastic large-scale 3D printing of a light-distribution and fabrication-informed facade panel'

[111]: Taseva et al. (2020), 'Large-Scale 3D Printing for Functionally-Graded Facade'

HC3DP

Hollow-Core 3D Printing (HC3DP) describes a large-scale 3D printing process using thermoplastic feedstock. HC3DP falls into the category of ME but differentiates itself because of the tubular bead structure of the extruded plastic. The approach to creating hollow plastic elements like bottles, tubes, or window frames is known in the industry as die-extrusion, or blow-molding [265, 282]. The thermoplastic is split into a tubular plastic shell and an empty inner core. This approach has been recently adapted to 3D printing with significant benefits on printing speed and extrusion rates, reduced material consumption, and strength-to-weight ratio [46, 264]. Furthermore, the increased printing diameter (20mm) allows to further subdivide the large-scale empty core into smaller-scale cavities [47].

[265]: Vlachopoulos et al. (2003), 'Polymer processing'

[282]: Baird (2003), 'Polymer Processing'

[46]: Leschok et al. (2023), 'Large-scale hollow-core 3D printing (HC3DP)'

[264]: Hopkins et al. (2020), 'Additive manufacturing via tube extrusion (AM-TEx)'

[47]: Leschok et al. (), 'Large-Scale Hollow-Core 3D Printing'

Therefore, we introduce HC3DP to facade applications to increase the thermal performance of the printed element. However, so far, there is no research on the thermal performance of HC3DP elements in comparison to off-the-shelf ME methods.

The increased bead dimension opens up new research possibilities, notably the potential of infusing the tubular beads with liquids or granular substances. This approach has, for instance, potential applications in enhancing the thermal efficiency of 3D-printed structures. A similar application, explored by Tenpierik et al., involves incorporating phase-changing materials (PCM) into 3D-printed facade elements [107]. However, this technique faces challenges due to the heat produced during the phase change, which can elevate temperatures beyond the polymer's glass transition point.

[107]: Tenpierik et al. (2018), 'Double Face 2.0'

Additionally, there have been explorations into managing heat transfer in 3D-printed facade elements using air pockets and a movable water-based fluid. While promising in theory, achieving water-tight channels and tubular structures with ME is extremely challenging [106]. Conversely, HC3DP shows promise in overcoming these limitations, thanks to the

[106]: Sarakinioti et al. (2018), 'Developing an integrated 3D-printed façade with complex geometries for active temperature control'

direct extrusion of tubular beads, comparable to pipe extrusion. The extruded beads themselves must be airtight for a successful print and, therefore, can be potentially used for fluid transport. The possibility of directly 3D printing water and air-tight hollow beads has not been investigated yet.

7.2.2 Thermal performance

Research on the thermal performance of 3D-printed elements at an architectural scale has primarily focused on concrete robotic printing, often resulting in large cavities and opaque structures [154, 158], with no ability to harness solar gains. In contrast, studies on translucent components have been enabled by off-the-shelf desktop printers with thermoplastics. Piccioni et al. investigated the optimization of cellular infill structures to improve thermal insulation of a 3DPF [110]. In parallel, Sarakinioti et al. have investigated the thermal insulation of closed cellular structures and validated the research using an experimental calorimetric setup [106]. For robotic large-scale ME, the influence of air pocket size and air pocket orientation has been investigated by Piccioni et al. [45] using calorimetric measurements and simulations. The novel HC3DP method can modify heat transfer rates due to the tubular bead structures that encapsulate air. These effects are examined and quantified for the first time in this study.

[154]: Dielemans et al. (2021), 'Additive Manufacturing of Thermally Enhanced Lightweight Concrete Wall Elements with Closed Cellular Structures'

[158]: Pessoa et al. (2021), '3D printing in the construction industry - A systematic review of the thermal performance in buildings'

[110]: Piccioni et al. (2020), 'A Performance-Driven Approach for the Design of Cellular Geometries with Low Thermal Conductivity for Application in 3D-Printed Façade Components'

[106]: Sarakinioti et al. (2018), 'Developing an integrated 3D-printed façade with complex geometries for active temperature control'

[45]: Piccioni et al. (2023), 'Printing thermal performance'

7.2.3 Outline and Contributions

This manuscript explores the thermal performance and fabrication viability of facade components fabricated with ME. Different 3D printing technologies, including desktop 3D printing, large-scale robotic extrusion, and the innovative HC3DP are examined. While research by the authors has moved towards large-scale robotic extrusion systems, the comparison with desktop 3D printers remains significant, as the majority of research precedents on 3D-printed facades utilize this technology. For each manufacturing technique, we explore the relevant factors that influence thermal insulation, such as infill design, printing method, and material selection. Our objective is to identify the most effective approach for efficiently fabricating lightweight, insulating elements using these diverse 3D printing methods.

The manuscript is structured as follows. First, we introduce the printing methods and printing materials. We then highlight the importance of infill structures of 3D-printed elements. Those infill structures can be varied in their density, as well as their pattern/typology. As a first set of experiments, we use desktop 3D printers to investigate the influence of infill pattern and density on the thermal behavior on a sample size of 100x100x50 mm. As those desktop 3D printers only have a limited build volume and extrusion rate, we continue our facade-related research using large-scale ME, using a novel 3D printing method based on hollow tubes, HC3DP. We print large prototypes of 500 x 500mm with varying depth and infill structures and measure the thermal resistance of those. We describe the testing equipment and procedure, as well as the sample preparation. To conclude our experiments, we introduce a highly insulating and lightweight 3D-printed facade prototype by combining HC3DP together with aerogel.

This manuscript contributes to the state of the art by providing investigations on the thermal performance of ME at different scales, from desktop 3D printing to the novel concept of HC3DP. With this study, we provide insights into the thermal performance of 3DPF at three different printing resolutions, from 0.2mm to 5.0mm to 20mm. We build on previous research and extend and compare the existing data on "off-the-shelf large-scale material extrusion" [45] to a new set of samples fabricated using HC3DP. Finally, we showcase how HC3DP can be paired with loose granular insulation material like aerogel to create ultra-lightweight and highly insulating 3DP facade elements. Notably, in this manuscript, we relate thermal performance to scale-up potential, highlighting the importance of printing time and material consumption, to determine the best 3DP approach for lightweight and highly insulating 3DPF.

[45]: Piccioni et al. (2023), 'Printing thermal performance'

7.3 Methods and materials

Our methodology encompasses design, fabrication, experimental testing, and data visualization/ comparison. Figure 7.2 illustrates the different resolutions the research presented here covers. Starting with the macro level, from (a) the design of the printed element to (b) the printing resolution and bead structure, up to (c) the materials used for printing and filling. Printing methods, materials, and design principles are presented before describing the relevant experimental approaches for each resolution.

7.3.1 Printing Methods and Resolution

All specimens are fabricated using additive manufacturing of thermoplastics, more specifically, material extrusion (ME). We use two different types of ME, namely off-the-shelf "desktop" 3D printers and ME at large dimensions using pellet extruders. 3D printing, or additive manufacturing, describes the process of fabricating an object using a layer-based

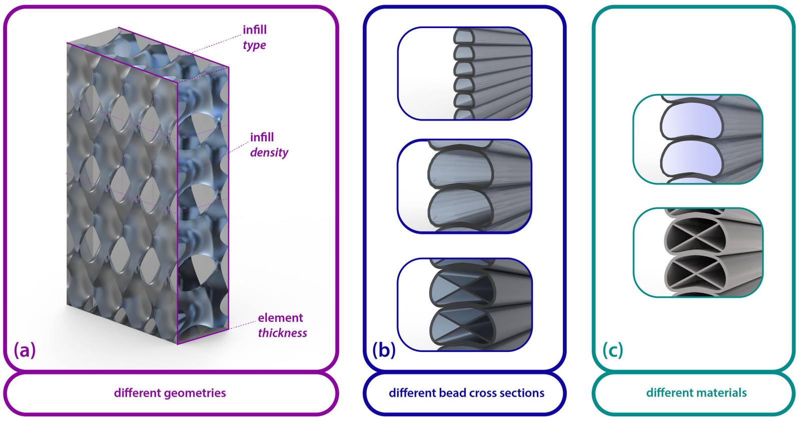

Figure 7.2: Approaches to improve thermal insulation: (a) geometry (b) bead cross-section and (c) material. For desktop 3DP only approach can be used; for HC3DP option a) b) and c) are possible.

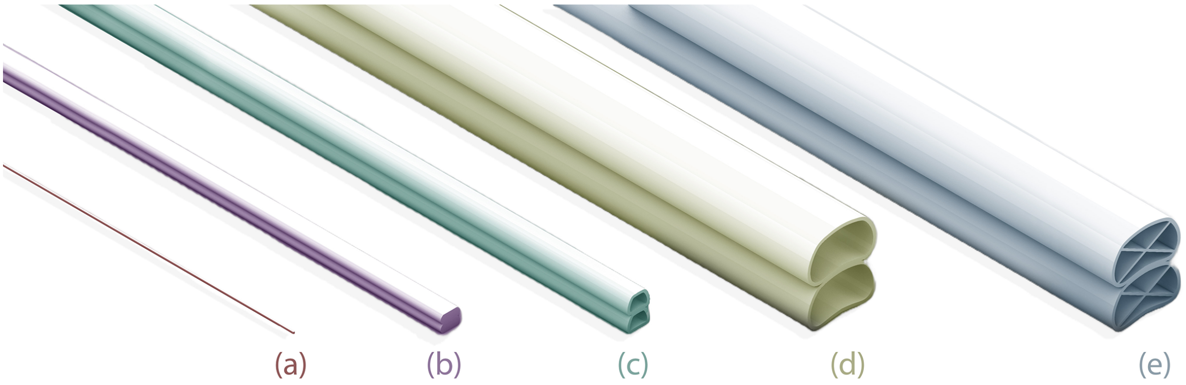

Figure 7.3: Fig. 2. Different types of ME, scale relative to each other. (a) desktop 3DP. (b) Pellet Extrusion, width 6mm height 2.5. (c) HC3DP width 6mm, 5.5mm height, (d) HC3DP, 24mm width, 19mm height. (e) HC3DP with internal subdivision, 24mm width, 19mm height.

approach. ME is a type of 3D printing that uses thermoplastic feedstock to create 3D objects in a layered manner [242]. In ME, the thermoplastic material is melted and extruded through a nozzle; the extruded polymer is often referred to as strand, bead, or road. The size of the orifice, the tip of the nozzle, defines the size of the bead and, therefore, the printing resolution. Today, a large variety of ME systems exist with material output ranging from 0.25 kg/h to 50 kg/h [30, 276]. This increased extrusion rate is facilitated by using larger tool heads, capable of printing thicker bead sizes. Figure 2 demonstrates the relative relationship between the different printing resolutions and techniques considered in this manuscript. In this study, we do not directly address off-the-shelf large-scale ME but refer to our previous article where this topic was explored. Our current results will be compared with those findings.

[242]: Secretary (2014), *ISO 9869-1:2014(en), Thermal insulation — Building elements — In-situ measurement of thermal resistance and thermal transmittance — Part 1: Heat flow meter method*

[30]: Duty et al. (2017), 'Structure and mechanical behavior of Big Area Additive Manufacturing (BAAM) materials'

[276]: Prusa (2021), *Max volumetric speed | Prusa Knowledge Base*

For the experiments described in this manuscript, we use two different types of ME to 3D print objects at different scales. We start with desktop 3D printers to 3DP small-scale elements at a resolution of 0.6mm. Then, we move on to a large-scale robotic 3D printing setup that uses granular feedstock and is able to print with the novel ME approach described in Section 1.1.2, HC3DP.

In HC3DP, the extruded bead is inflated using pressurized air to maintain its shape during the printing process. A hollow mandrel supported by spider vanes is needed to split the molten thermoplastic into a thin wall and an empty core. For a more detailed description of the fabrication setup please refer to [46]. The specimens, geometry, size, as well as slicing parameters investigated in this manuscript are explained in detail in the following sections.

[46]: Leschok et al. (2023), 'Large-scale hollow-core 3D printing (HC3DP)'

The print speed for large-scale elements is potentially limited by two factors a) the maximum extrusion rate of the extruder (cross section of the extruded bead * print speed) or b) the material cool-down. Both factors can be greatly improved by using HC3DP.

7.3.2 Infill

In 3D printing, the internal geometry of the part, often referred to as 'infill', can be differentiated as opposed to traditional fabrication methods such as CNC-milling, casting, or injection molding and is often referred to as ’infill’. The infill, characterized by its density and pattern, can be varied to suit the specific functional requirements of the 3D-printed parts [291]. The configuration of this internal structure can be determined either by the slicing software used in the printing or can be explicitly modeled during design.

[291]: Dave et al. (2021), *Fused Deposition Modeling Based 3D Printing*

Slicing describes the process of creating the toolpath for a 3D printer based on a 3D representation of the object. Usually, off-the-shelf 3D printing systems use proprietary slicing software that is specifically designed for creating tool paths for a certain brand and model of a 3D printer. Slicing software has multiple built-in infill patterns to choose from, with their density as a user parameter. Alternatively, to directly design infill structures, different modeling techniques, such as volumetric modeling (VM), are used. VM is a method that describes geometry using function representation (FRep) instead of boundary representation (Brep) [80]. Commercial software solutions for VM include Ntopology [81], and open-source packages, like Axolotl [83], also exist.

[80]: Kladeftira et al. (2020), ‘Redefining Polyhedral Space Through 3D Printing’

[81]: ntopology (2021), *nTopology. Next-Generation Engineering Design Software*

[83]: DBT (2021), *Axolotl*

Especially for large-scale applications, like facades, the design of infill structures has major implications on performance, fabrication time, material consumption, and, consequently, the environmental impact of the elements. This correlation is not true for all 3DP methods; however, for ME, the toolpath length (density of the infill) is directly correlated to the print time. For each specimen resolution, the infill structure and the density chosen will be described in more detail.

In this study, we use two terminologies to define the density of infill structures. Commonly in 3D printing, the infill density is defined as a percentage of the filled geometry. A 30% infill, therefore, describes an element with 30% plastic and 70% air content. Later in the manuscript, we will discuss and compare the different specimens based on their porosity, a more common way to address the density of porous structures in material science. A 70% porosity part means a part is defined by 30% material and 70% air content.

7.3.3 Materials

In selecting a material for our desktop 3D-printed specimens, we opted for PLA, renowned for its reliability in 3D printing and its status as the second most commonly used polymer in ME [256]. PLA’s particularly low shrinkage rate makes it an ideal choice for 3D printing applications [292]. This decision was further influenced by our need to minimize the risk of print failures, given that our experiments involved designing and printing a total of 27 samples, accumulating over 100 hours of print time. PLA is the most used bioplastic in the current market [293] and it is synthesized using bio-based carbohydrate sources like corn, sugarcane, or tapioca [294]. PLA is commonly used for commodities like compost bags, food packaging, and loose-fill packaging material. Furthermore, PLA finds diverse applications in the medical sector, like screws, anchors, or plates [294].

[256]: N. Turner et al. (2014), ‘A review of melt extrusion additive manufacturing processes’

[292]: Van den Eynde et al. (2018), ‘3D Printing of Poly(lactic acid)’

[293]: Ceresans (2023), *Bioplastics Market Report*

[294]: Auras et al. (2010), *Poly(Lactic Acid)*

[294]: Auras et al. (2010), *Poly(Lactic Acid)*

For the large-scale experiments, we choose to print with PETG, a copolymer of PET. PET is the 4th most-produced polymer on the market, with its main application in fibers (fabrics) and containers for liquids and

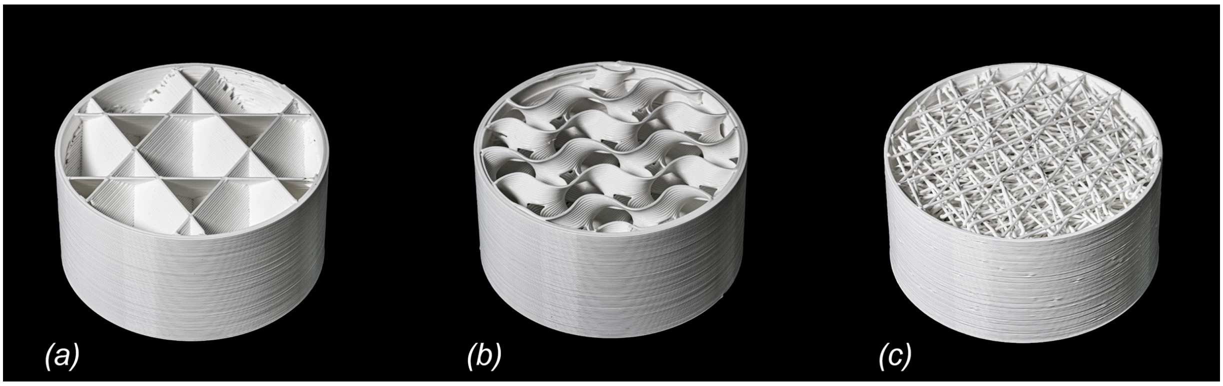

Figure 7.4: Different types of infill typology. A) Cubic. B) Gyroid. C) Random.

food [295]. It is commonly used due to its high transparency, and its chemical and structural properties [232]. PETG has been developed as a glycol-modified PET to suppress the crystallization process, leading to increased transparency, and to improve moldability, especially needed for 3D printing [231]. We use PETG from the provider Extrudr [270] and condition the granular feedstock to a dry state at 60°C for four hours before printing.

For our final experiment, we use aerogel as a granular insulating material within the 3D-printed hollow beads. Aerogel was first discovered in the 1930s [296] and has since been investigated for its application in building insulation [297, 298]. Thanks to high porosity and small-scale pore size, aerogel in granular form ensures thermal and acoustic insulation, while being translucent [299]. Its extremely high porosity is reflected in the remarkably low density of as low as 3 kg/m3. The granular aerogel used in this research, provided by AGITEC, has a density of approximately 90 kg/m3 and a thermal conductivity of 0.01 W/mK. Silica-based aerogel is non-flammable and non-toxic, which makes it a good fit for the application of facades [300].

[295]: Ji (2013), 'Study on Preparation Process and Properties of Polyethylene Terephthalate (PET)'

[232]: Petrov et al. (2021), 'Research into the effect of the 3D-printing mode on changing the properties of PETG transparent plastic'

[231]: Sepahi et al. (2021), 'Mechanical Properties of 3D-Printed Parts Made of Polyethylene Terephthalate Glycol'

[270]: Extrudr (), *PETG transparent - High Quality Filament*

[296]: Kistler (1931), 'Coherent Expanded Aerogels and Jellies'

[297]: Hüsing et al. (1998), 'Aerogels—Airy Materials'

[298]: Ganobjak et al. (2023), 'Get the light & keep the warmth - A highly insulating, translucent aerogel glass brick for building envelopes'

[299]: Baetens et al. (2011), 'Aerogel insulation for building applications'

[300]: AGITEC (2013), *Granular Aerogel Datasheet*

7.3.4 Small scale, typology experiments

As a first set of experiments, we designed and fabricated cylindrical specimens with a diameter of 100mm and a height of 50mm. We use an off-the-shelf desktop 3D printer, "Pro2 Plus" from the company Raise3D, to print the specimen. Three different infill patterns are investigated, of which two are open and one is a closed cell typology:

- Cubic, closed cell
- Gyroid, open cell
- Random Lines, open cell

For each pattern typology, we 3D print samples with densities of 10% to 90%, in increments of 10%. This creates cavities with sizes ranging from 36 to 1.5 mm, depending on the pattern and density. We choose open and closed cell typologies to investigate different heat transfer modes and the role air inclusions play within the printed elements. For the cubic and gyroid infill typology, we use the proprietary slicing software IdeaMaker of Raise3D. We slice a single outline (contour) object with no top and

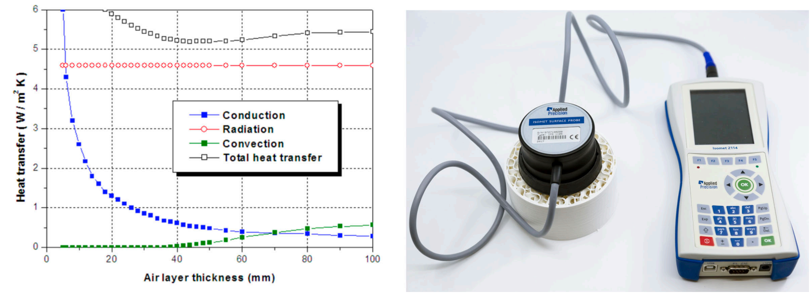

Figure 7.5: Left: Estimated heat transfer in closed air cavity bounded by ordinary material. Graphic from Bekkouche et al., 2013 [304]. Right: Transient Hot Wire Method, testing setup.

bottom solid infill so the measurement device is in direct contact with the infill pattern.

The 27 elements are sliced with a layer height of 0.6mm and a layer width of 1.2mm. The print time ranges from 0:57 h for the 10%, up to 04:05 h for the 90% filled specimen. In total, 27 elements are printed with a print time over 105h. The weight of the elements ranges from 90 g for the 10% filled, to 446 g for the 90% filled samples.

Small-scale, topology experiment methodology

Thermal characterization of the specimens in Figure 3 was performed according to the transient hot-wire method [301]. The transient measuring technique was chosen for its speed, compared to steady-state measurements, and its suitability for measuring the thermal properties of cellular insulation materials [302]. The measurement involves placing a heated wire, which serves as an electrical heating element, within the sample. Once activated, heat radiates outward from the wire into the surrounding material, and the temperature of the wire itself is monitored (Fig.7.5.b). A graph plotting the wire's temperature against the logarithm of time is used to deduce the material's thermal conductivity, assuming that its density and heat capacity are known [303].

[301]: International (2019), *ASTM C1113/C1113M-09(2019) - Standard Test Method for Thermal Conductivity of Refractories by Hot Wire*

[302]: Hu et al. (2018), 'Transient hot wire measures thermophysical properties of organic foam thermal insulation materials'

[303]: Mathis (2000), 'Transient thermal conductivity measurements'

This characterization method features a brief measurement duration, typically just a few seconds, which precludes the possibility of assessing the impact of convective transfer. However, in structures with such small cavities, the influence of convective transfer should be minimal and can be neglected [304](Fig.7.5.a). The data acquisition was facilitated by a calibrated portable instrument (ISOMET 2114 by Applied Precision), which measures, stores data, and automatically calculates the thermal conductivity and diffusivity of the sample. The measurements were performed using a probe with a constant power supply. For the measurements, a suitable surface probe for low-conductivity foams (IPS 1100) was placed on top of the sample. Measurements were repeated three times to ensure the reliability of the results.

[304]: Bekkouche et al. (2013), 'Thermal resistances of air in cavity walls and their effect upon the thermal insulation performance'

The specimens featuring different cell typologies and infill densities were measured with the objective of understanding the relationship between thermal properties, infill density, and topology. We used the property porosity, to characterize the ratio between the plastic (solid) and air (fluid) volumes in the sample, measured as follows:

$$\varphi = \frac{Vf}{(Vs + VF)}$$

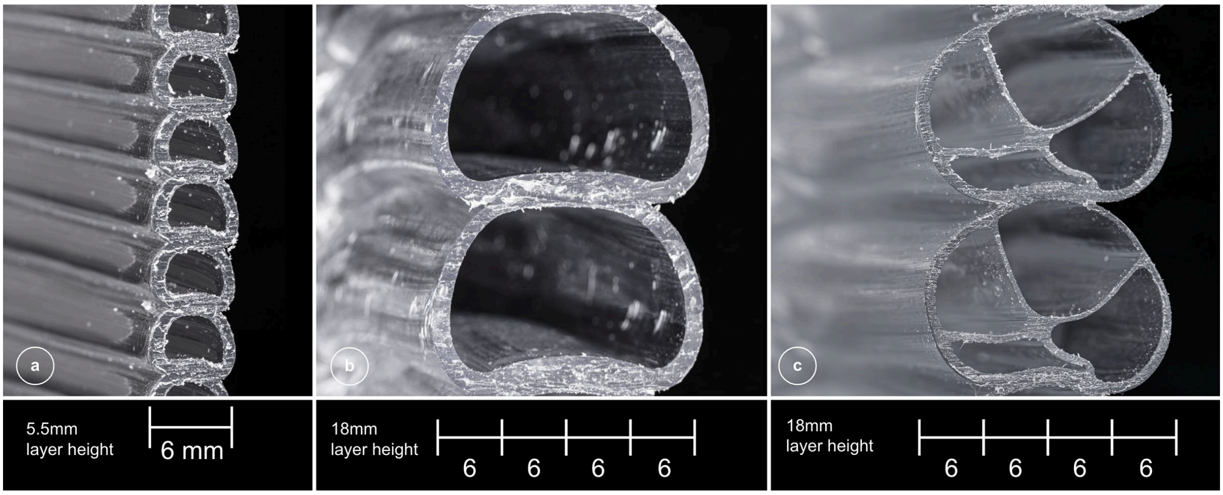

Figure 7.6: Different cross-sections tested. a) HC3DP with the nozzle o6w1, resulting in a 6mm layer width and a 5.8mm layer height. Wall thickness 1mm. b) HC3DP with the nozzle o24w1, resulting in a 24mm layer width and a 19mm layer height, at a 1mm wall thickness. c) HC3DP with the o24w1Quad nozzles, resulting in a 24mm layer width and a 19mm layer height, at a 1mm wall thickness.

The results of the measurements were compared to analytical models for validation in Seshadri et al. [305]. Analytical models for the calculation of effective thermal conductivity in porous structures, such as the arithmetic mean, harmonic mean, and geometric mean, were examined and compared.

[305]: Seshadri et al. (2024), 'Three-dimensionally printed hierarchical sand structures for space heating applications'

7.3.5 Hot Box experiments for low-resolution HC3DP

In this manuscript, different sizes of HC beads are investigated, starting from a cross-section similar to "off-the-shelf" pellet extrusion (6x5mm), to tubes with a significantly bigger section (24x19mm) to finally, extrusions featuring an internal subdivision. This internal subdivision separates the hollow interior into four distinct areas and potentially improves the performance of the 3DP element.

Different nozzles can be used to 3D print with the novel HC3DP technology at different resolutions. Those nozzles are interchangeable, similar to off-the-shelf pellet extrusion systems, and allow choosing the bead cross-section depending on the final use case of the printed element. The cross sections presented here are to be understood as a first set of experiments, showing the broad spectrum of possibilities enabled by HC3DP. None of the presented cross-sections is optimized to increase the thermal resistance of a 3DP facade yet. With no prior knowledge of the performance of HC3DP elements it is important to understand the implications of resolution, bead thickness, as well as internal substructures. The design of the nozzle and, therefore, the 3D-printed bead has direct implications on the performance of the 3D-printed element in regards to printing parameters (material consumption, weight, and print speed) and performance parameters (thermal resistance, strength, transparency). Therefore, in this manuscript, we test three different types of HC3DP beads in regard to their thermal performance and compare their print time and weight/m^2. Figure 5 shows the different HC cross-sections used in this research, and Table 1 documents the specifications of the HC3DP in regards to dimensions, wall thickness, and material usage.

Table 7.1: Die geometries and their specifications.

Name	Outer diameter [mm]	Wall thickness [mm]	Hollow cores [amount]	Plastic cross-section [mm2]	internal void [mm2]	ratio plastic/air [%]
o6w1	6	1	1	15.71	12.57	55.56
o24w1	24	1	1	73.5	315.2	16.25
o24w1Quad	24	1	4	117.29	334.68	25.93

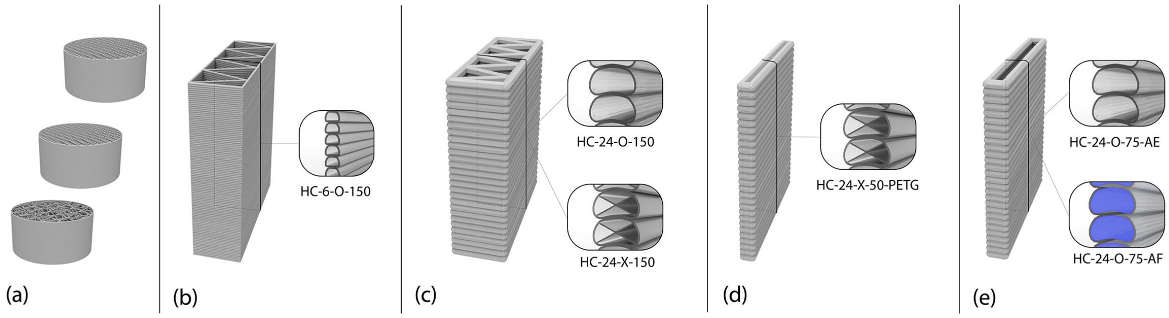

Figure 7.7: Fig. 6. Different types of samples presented and discussed. (a) desktop 3DP cylinders. 100x100x50mm (b) High resolution HC3DP, 6mm layer width, 5.5mm layer height. (c) Low resolution HC3DP, sample size 500x500x150mm. Layer width 24mm, 19mm layer height, two different cross sections, empty and cross. (d) Low resolution HC3DP, sample size 500x500x50mm no infill. 24mm layer width, 19mm layer height, printed in PETG and PP. (e) Low resolution HC3DP with one continuous air pocket, 24mm layer width, 19mm layer height, tested empty and filled with aerogel.

Sample Size and infill density

The sample size for the low-resolution elements is 500x500 mm and the depth ranges from 150 to 75mm. This range is informed by preliminary studies regarding the structural performance of the HC3DP elements for the use case as a facade. The depth of the cavities therefore varies between the different samples and can be calculated by subtracting the bead width from the thickness of the panel; the geometry in Figure 7.7.d does not feature an air cavity. We selected a sample size that matches that used in previous thermal experiments [45], employing the same experimental setup to reduce thermal edge effects at the connection between the specimens and the testing apparatus. Additionally, larger samples enable more precise estimates of printing times for low-resolution 3D-printed elements since for low-resolution AM, fabrication time is not constrained by the extrusion speed but is primarily limited by the rate at which the polymer cools [38].

[45]: Piccioni et al. (2023), 'Printing thermal performance'

[38]: Roschli et al. (2019), 'Designing for Big Area Additive Manufacturing'

To investigate thermal performance in correlation with fabrication speed and material consumption, we designed and fabricated three different types of HC3DP specimens. The first samples feature the identical print path as tested in the previous experiments [45], see 7.9, and are printed in two different cross sections. The specimen is printed with high-resolution HC3DP to mimic an identical bead width compared to off-the-shelf pellet extrusion, 6mm (HC-6-O-150). Then we print the same print path in low resolution using the hollow, and subdivided bead structure, as shown in Figure 7.7.c.

[45]: Piccioni et al. (2023), 'Printing thermal performance'

We then take the absolute minimum thickness, printing only a double outline with no infill in between. For the double outline print, we use the nozzle with a large bead width (24mm) to maintain good structural performance of the element at minimal thickness, Figure 7.7.d. The third and last type of specimen also has no infill to keep printing time, material consumption, and weight at a minimum. The thickness of the

Table 7.2: Summary of all samples. See figure 6 7.7 for visual reference.

Name	Layer Height [mm]	Layer Width [mm]	Nozzle [type]	Thickness [mm]	Material [type]	Infill [type]
HC-6-O-150	5.5	6	o6w1	150	PETG	zig zag
HC-24-O-150	19	24	o24w2	150	PETG	zig zag
HC-24-X-150	19	24	o24w1Quad	150	PETG	zig zag
HC-24-X-50-PETG	19	24	o24w1Quad	50	PETG	none
HC-24-O-75-AF	19	24	o24w2	75	PETG & Aerogel	air gap
HC-24-O-75-AE	19	24	o24w2	75	PETG	air gap

element is increased from 50 to 75mm to create an air gap between the single outlines. This gap improves the material cool-down during the printing process and potentially increases the thermal resistance of the final component. A summary of all specimens can be found in Table 7.2 and Figure 7.7.

The infill structures in our specimens are designed with a simple, non-overlapping zigzag pattern to maintain high-quality printing. While a wide variety of infill patterns is available for current 3D printing systems, HC3DP faces limitations in printing overlapping or self-intersecting lines, as these can lead to bead deflation. We have standardized the spacing between the base triangles of the zigzag pattern at 125mm, based on the results of preliminary structural tests. The zigzag pattern creates unidirectional open cell infill structures and allows testing the specimen in two orientations. In one orientation, a continuous air gap from top to bottom facilitates convection. When the sample is rotated, closed air pockets prevent the air from traveling throughout the entire height of the object.

Granular Insulation for HC3DP Elements

To create highly insulating and fast-to-fabricate 3D-printed facade elements with minimal thickness, we propose to combine HC3DP with granular aerogel. The materials are not permanently connected but are designed to be separated at the end of life (Figure 7.8.d). This way, the expensive aerogel can be reused while the polymer can be recycled [25].

[25]: Vidakis et al. (2021), 'Sustainable Additive Manufacturing'

In order to fabricate such a composite, we design and fabricate a sample with a continuous internal cavity and fill granular aerogel into the 3D-printed bead. The sample size is 500 x 500 x 75mm with a double contour. A two-centimeter air gap is created between the exterior and interior printed lines to facilitate the connection between the two through a turn of suitable radius (Figure 7.8.a). If changes in printing direction are too sharp, there is a risk of the hollow bead collapsing. If a narrow-radius turn was created with a sharp change in the printing direction, there would be a risk of the hollow bead collapsing during twisting. In fact, the bead is forced to twist around itself if the printing direction changes while the tool orientation remains static [46]. By keeping a minimal radius at the turn and separating the two contours, the entire element forms a single connected air cavity. We use this continuity to insert aerogel into the printed bead using an off-the-shelf plaster spraying gun, as seen in Figure 7.8.b. To quantify the benefits of aerogel-filled 3D-printed beads, we measure the U-value of the specimen once filled and empty.

[46]: Leschok et al. (2023), 'Large-scale hollow-core 3D printing (HC3DP)'

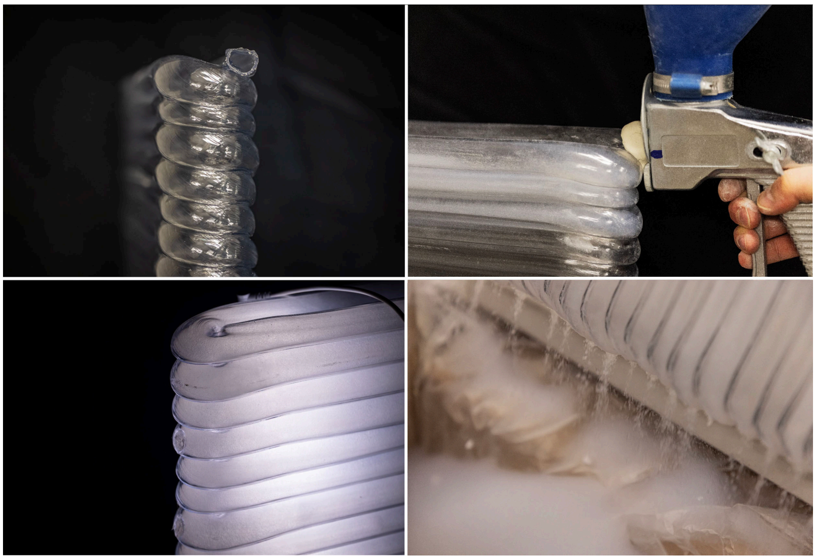

Figure 7.8: Production steps and design of the HC3DP element filled with aerogel. A) Close-up of the specimen, focus on non-collapsed tight corners and opening to insert aerogel.

Sample Preparation and Testing Orientation

To achieve comparable results among different resolution specimens, all 3D-printed large-scale specimens are prepared following the same procedure. For large-scale HC3DP, the increased layer height results in an undulated surface texture, see Figure 7.8.c. We use thermally conductive glue to create flat contact surfaces and glue a thin Vivak (PETG) sheet to it to provide an even surface for the sensor to attach to. Furthermore, to ensure air tightness, the top and bottom of each sample are sealed by gluing a thin sheet of Vivak onto it. This straightforward method avoids the challenge of printing unsupported horizontal surfaces, often referred to as bridging [234]. These preparations ensure repeatable and reproducible measurement results, as the sensors are in full contact with the specimens' surfaces, and air tightness of the part. Irrespective of the print resolution, each sample that features infill geometry is tested in two different cavity orientations: once with the cavities spanning from bottom to top, and once from left to right. This way, the effect of convective heat transfer due to buoyancy could be observed.

[234]: Eyercioglu et al. (2019), 'Determination of the Maximum Bridging Distance in Large Scale Additive Manufacturing'

Hot box experiment methodology

Thermal experiments were performed according to the steady-state hot box heat flux meter approach [236]. The hot box (Figure 7.9.a) is located at an underground level in a test room, measuring 8 m × 5 m × 2.2 m. This location minimizes notable thermal disturbances, such as solar loads, ensuring consistent and stable thermal conditions throughout the experiments. A detailed description of the experimental set-up is provided in [306], along with a schematic of the sensor groups. A total of 35 sensors were deployed to monitor the state of the metering chamber in terms of surface and air temperature. Moreover, an array of PT100 resistance temperature detectors (Omega Engineering) were installed on each side of the 3D-printed samples to measure surface temperatures. A heat flux plate (Hukseflux HFP01) was centrally placed on the specimen's outer surface to measure the normal one-dimensional heat flux (Figure 7.9.b). The entire data acquisition process was conducted using a NI

[236]: Meng et al. (2015), 'Feasibility experiment on the simple hot box-heat flow meter method and the optimization based on simulation reproduction'

[306]: Lydon et al. (2023), 'Small-scale experiments on the operational performance of a lightweight thermally active building system'

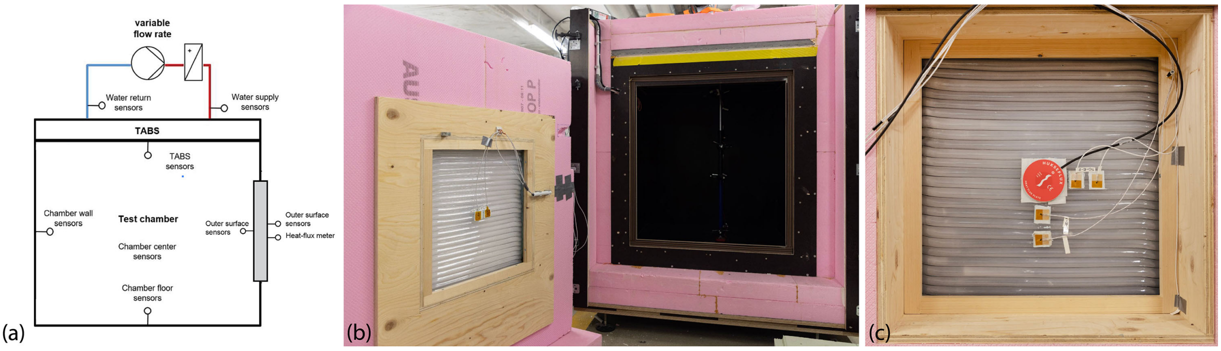

Figure 7.9: Hotbox testing setup. A) Schematics of the hot-box setup. B) installation of HC3DP sample, filled with aerogel. C) Door installed with sensors in place.

cDAQ-9133 system and LabView software was used to collect and store the data at a high-resolution rate of one second.

A heat source inside the hot box creates a temperature difference (minimum 10 C) between the interior and exterior surfaces of the HC3DP sample. The effective thermal conductivities and U-values of each sample were calculated based on the heat flux and surface temperature measurements in these conditions. The measurements were conducted replicating the procedure described in [45] where pellet-based ME samples were tested. In particular, to ensure steady-state condition, measurements were performed for a minimum of 72h, and test termination was verified according to the standard procedure described in [242]. Additionally, the experimental procedure was calibrated by measuring the thermal properties of an XPS sample of known thermal conductivity and only a small deviation (less than 3%) was found. The adoption of the same experimental procedure used in the previous study facilitates the comparison of the new results with earlier collected data and reduces possible experimental discrepancies.

[45]: Piccioni et al. (2023), 'Printing thermal performance'

[242]: Secretary (2014), *ISO 9869-1:2014(en), Thermal insulation — Building elements — In-situ measurement of thermal resistance and thermal transmittance — Part 1: Heat flow meter method*

7.3.6 Print time calculations

To facilitate comparison among different fabrication techniques, we study not only the thermal properties but also the fabrication viability of different ME approaches. In particular, we use two methods to provide comparable calculations for the print time per square meter of facade using the different ME methods. Both are based on the geometries investigated in this manuscript in regard to sample thickness, infill pattern, and density. For the desktop 3D-printed samples, we use the proprietary slicing software IdeaMaker, as introduced in Section 2.4. For the calculation, we assume a print path with a double contour/outline and a 20% cubic infill ratio, identical to the investigations conducted at TU Munich [40]. We consider a 1x1m panel with a thickness of 5cm, identical to the thickness of our specimen. To slice large objects in IdeaMaker, it was necessary to set up a custom 3D printer configuration. We defined it based on the initial settings, with the primary modification being an expansion of the print volume.

[40]: Moritz Basil Mungenast (2019), '3D-Printed Future Facade'

As no standard/proprietary slicing software exists for large-scale robotic pellet-based ME, we take the following assumptions to calculate the print time for a $1m^2$ 3DPF element. With the introduction of pellet extruders,

Table 7.3: Maximum print speed and minimal layer time on the cross sections printed during this research and a maximum extrusion rate of 1500 mm3/s.

nozzle	layer width [mm]	layer height [mm]	cross section plastic [mm2]	Max. print speed [mm/s]	Min. layer time [s]
o6w1	6	5.5	15.71	95.48	24
024w1	24	19	72.26	20.76	24
o24w1quad	24	19	117.29	12.79	24
ME	6	2.5	13.66	109.81	112

the maximum print speed is most often not limited by the maximum extrusion rate of the extruder anymore. The maximum printing speed must be defined using two boundaries: a minimum layer time and a maximum layer time. We provide calculations for regular ME and HC3DP as we compare the findings of this manuscript to previously conducted research on 3DPF fabricated using regular ME [45].

[45]: Piccioni et al. (2023), 'Printing thermal performance'

The minimum layer time, or the maximum speed, is governed by the maximum feasible extrusion rate. The extrusion rate is the amount of material that can be extruded in the unit of time and can be represented as:

$$ExtrusionRate\ (mm^3/s) = VolumePerUnitLength \times PrintSpeed \tag{7.1}$$

Where for HC3DP:

$$\begin{aligned} VolumePerUnitLength(mm^3) = \\ PolymerCrossSection + AirInflatedSection \end{aligned} \tag{7.2}$$

7.8 describes the maximum extrusion rate for the fabrication setup used and the resulting maximum extrusion rate, which is used to calculate the minimum printing time per layer, see Table 7.3.

The lower boundary for printing speed is correlated with the cool-down rate of the extrudate, as a minimum cooling time needs to be allowed before successive layers are printed. A simplified model to calculate the cooling rate has been developed by [46] according to the bead cross-section. The model is valid for both regular ME and HC3DP and is based on the net radiative heat transfer, considered as the dominating heat transfer mode. Therefore:

[46]: Leschok et al. (2023), 'Large-scale hollow-core 3D printing (HC3DP)'

$$-\frac{dT}{dt}V = \alpha A(T^4 - T_e^4) \tag{7.3}$$

Where:

- $\frac{dT}{dt}$ is the rate of temperature change over time
- V is the volume of the extruded material
- α encapsulates all factors not related to geometry and temperature, such as emissivity and Stefan-Boltzmann constant
- A is the area of the radiating surface
- T is the temperature of the surface
- T_e is the temperature of the environment

The equation shows that the material's temperature reduces progressively in accordance with the rate of overall heat transfer, utilizing the material's volume as a thermal storage. The cooling rate assumptions are based on a double-sided cooldown scenario. For thin wall elements (large-scale infill and aerogel samples), the double wall print with no air separation will suffer from slower cool down [38]. 7.8 provides assumptions and calculations for the cool-down model.

[38]: Roschli et al. (2019), 'Designing for Big Area Additive Manufacturing'

Finally, considering the two boundaries, the suitable time to print a layer can be calculated as the maximum between the threshold derived from the maximum extrusion rate and that derived from the minimum cooling time. Therefore:

$$t_{layer} = max(t\ cooldown_{layer},\ t\ extrusion_{layer}) \tag{7.4}$$

Then, the total time to print the entire part is the sum of the time required for each of the N layers:

$$t_{print} = \sum_{n=1}^{N} max(t\ cooldown_{layer},\ t\ extrusion_{layer}) \tag{7.5}$$

7.4 Results

7.4.1 Small scale, typological experiment results

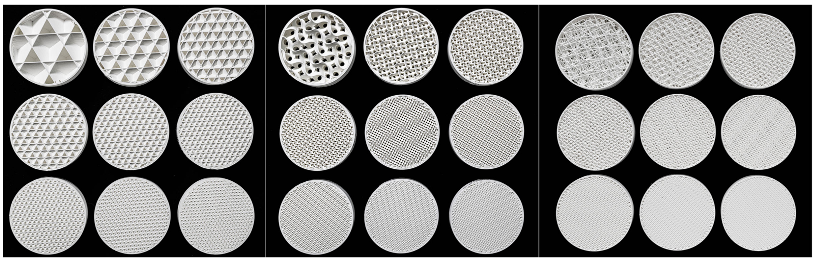

Figure 7.10: All 3D printed samples. Upper left, 10% infill to lower right 90%. Left cubic, middle gyroid, and right random infill.

The results of the measurements were compared to analytical models for validation in [305]. Analytical models for the calculation of effective thermal conductivity in porous structures, such as arithmetic mean, harmonic mean, and geometric mean, were examined [307]. It was found that for all the examined geometries, the measurement results are in close agreement with the predictions of the geometric mean model. According to the model, the thermal conductivity of the samples can be derived from the thermal conductivity of the PLA (λ_{solid}) and air (λ_{fluid}) considering porosity (ϕ) as:

[305]: Seshadri et al. (2024), 'Three-dimensionally printed hierarchical sand structures for space heating applications'

[307]: Preux et al. (2021), 'Thermal conductivity model function of porosity'

$$\lambda_{GM} = \lambda_{solid}^{1-\Phi} \times \lambda_{fluid}^{\Phi} \tag{7.6}$$

Therefore, thermal conductivity depends on porosity, as it can be solid-dominated or fluid-dominated depending on the balance between the solid and fluid phases. The results furthermore show that, at this printing resolution, the effect of cell configuration, closed or open, and geometry is negligible. The differences observed in the thermal conductivity for the sample measurements are often within the precision range of the measuring instrument. It can be concluded that the infill geometry for high resolution 3DP can be chosen based on other performative aspects, like structural, optical, or design intention.

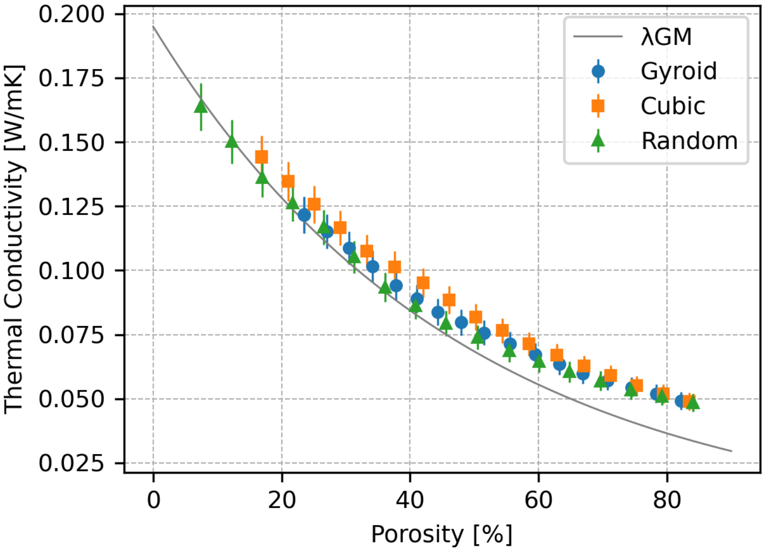

Figure 7.11: reports the measured effective thermal conductivities for the 3DP samples.

7.4.2 Hot box experiment results

Measurement results for the large-scale HC3DP are reported in Figure 7.13 and an overview of the samples can be found in Figure 7.12. The experimental results of [45] are reported for the identical geometry (150mm thickness) including infill to compare between ME and HC3DP. The effective thermal conductivity of the 150cm HC samples ranges from approximately 0.3 to 0.15 W/mK, depending on the chosen cross-section. Lower thermal conductivity values are found for the elements printed with the 24mm layer width compared to the thinner cross-section (6mm-width) as a result of the larger volume of encapsulated air in the tubes. A three-fold increase in the cross-section dimensions, from 6mm to 24mm width, results in approximately a 50% decrease in thermal conductivity. Compared to the ME samples, the HC3DP exhibits lower thermal conductivity for any cross-section, with up to a 52% decrease. The difference in measured thermal conductivity for the horizontal and vertical cavity orientation is not significant and falls within the range of the experimental error.

[45]: Piccioni et al. (2023), 'Printing thermal performance'

Finally, samples HC-24-O-150 and HC-24-X-150 with identical geometry, but different bead cross-sections, show similar behavior, with the latter exhibiting a slightly higher thermal conductivity. This shows that the subdivision of the cross-section into four air chambers does not bring benefits in terms of thermal insulation. This may be attributed to the fact that there is currently no control over the orientation of those internal subdivisions. Moreover, the tubular cavity is already small enough ($\leq$ 30mm) to prevent large convective air movements [304] so further subdivisions can hinder convective movements but this effect does not compensate for

[304]: Bekkouche et al. (2013), 'Thermal resistances of air in cavity walls and their effect upon the thermal insulation performance'

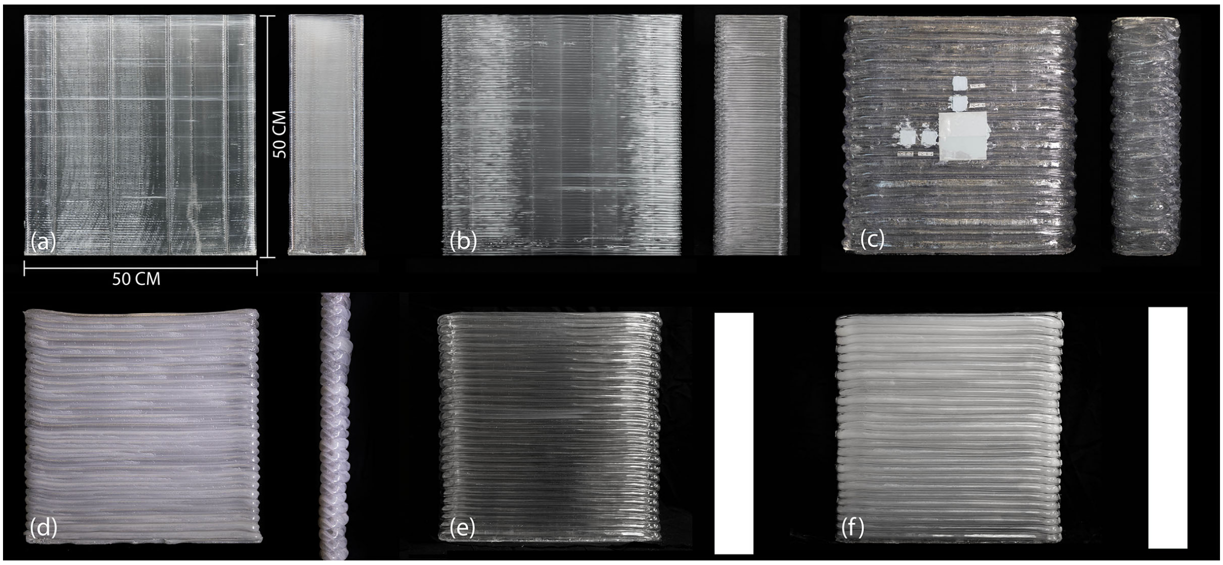

Figure 7.12: Printed specimen. (a) ME-6-150 (b) HC-6-O-150 (c) HC-24-O-150. (d) HC-24-X-50-PETG (e) HC-24-O-75-AE (f) HC-24-O-75-AF.

the additional material required by the internal reinforcement. However, other aspects relevant to facade construction, like structural or acoustic aspects, might benefit from the internal subdivision and need to be investigated. Furthermore, the internal subdivision does increase material consumption (+60% for an equivalent bead with identical wall thickness) and, therefore, might affect the production time.

The thin sample printed without infill in PETG, HC-24-X-50-PETG, has a low effective thermal conductivity of 0.09 W/mK, corresponding to a U-value of 1.5 W/m^{2}K for a 4.5cm thick components. Finally, sample HC-24-O-75-AE, printed with a double line and internal air cavity, has a higher effective thermal conductivity than the previous samples, showing that the air cavity does not contribute to an increase in insulation. The aerogel-filled sample, HC-24-O-75-AE, instead shows the lowest effective thermal conductivity (0.07 W/mK), demonstrating how the addition of as little as 600g of aerogel - equivalent to 2.4kg for a 1m^2 facade component - can determine an improvement of 40% in thermal insulation. The aerogel-filled element, with a thickness of only 7.5cm, has a U-value of 0.85 W/m^{2}K, corresponding to high-performance triple glazing.

7.4.3 Print time experiment results

Table 7.4 and Figure 7.14 summarize the comparison of u-values, estimated print time, and costs for the different ME approaches for facade application per m^2. Depending on the assumptions of price/kg of aerogel and charge of 3D printing hour, the best performing 3D-printed facade with a u-value below 1.0 W/m^{2}K is either a mono-material HC3DP facade with a thickness of 150mm, or an HC3DP element with a thickness of 75mm and aerogel filling.

Small-scale, desktop 3D printing, exhibits the highest cost of production due to the highest printing time per square meter and the fact that filament feedstock is, in the case of PETG, approximately 3.5 times more expensive than its granular equivalent. The print time for a 10% infill is

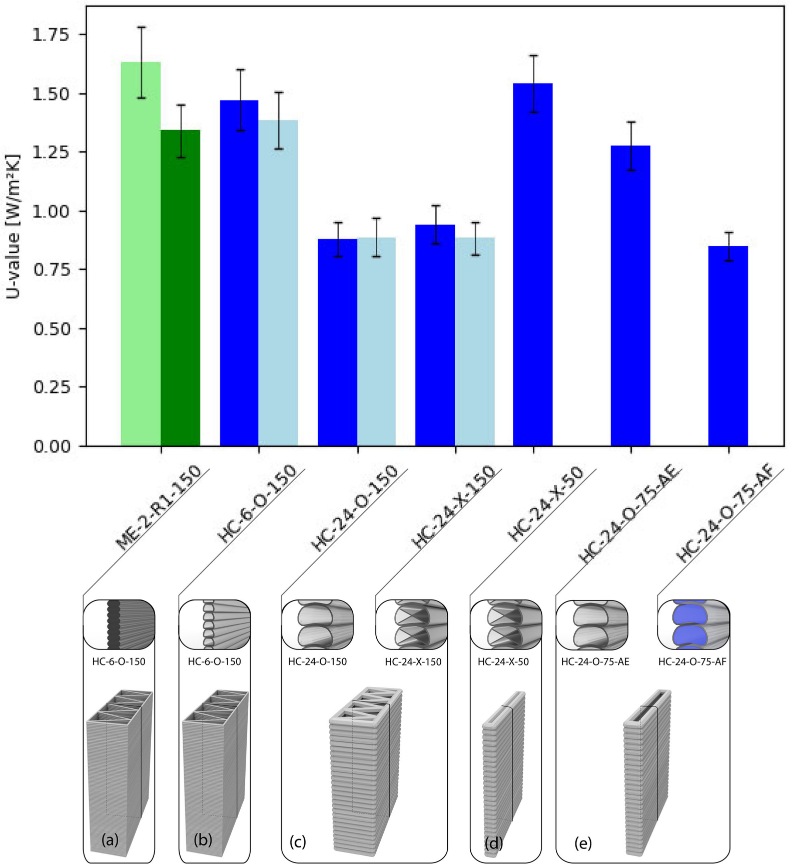

Figure 7.13: Comparison matrix for investigated methods against off-the-shelf facade solutions.

approx. 110h and increases to 500h for the 90% filled element. Notably, in this case, high thermal insulation would correspond to limited structural performance due to the thin-shell mechanical capabilities. Researchers from TU Munich, using a similar printing resolution and printing material to build 3D facade components, suggest using at least two outlines and 20% infill, which results in a print time of approx 180h/m^2. This brings into question the feasibility of "off-the-shelf" desktop 3D printers for the fabrication of bespoke facade elements.

For the calculations, we assume a price of 35 CHF/kg for PETG filament and 5 CHF/kg for granular PETG feedstock. The printing time, or robot time including utilities, we count at 50 CHF/h, and the aerogel at a price of 58 CHF/kg. Those prices are to be understood as estimations and reflect prices that can be found directly on the homepages of material providers. Reduction of prices due to bulk orders etc. are not taken into account, as well as benefits from recycling the PETG, or reusing the aerogel.

Table 7.4: Comparison of different ME methods for facade applications.

type	thickness [mm]	weight [kg/m2]	print time [h/m2]	cost [CHF/m2]	U-value [W/m²K]
Desktop3DP	50	18	181	9,688.18	0.93
ME-6-150	150	34.12	11.95	938.94	1.65
HC-6-150	150	17.84	2.57	307.08	1.43
HC-24-150	150	23.75	3.54	414.47	0.88
HC-24-75-AF	75	12.67	1.53	306.47	0.86

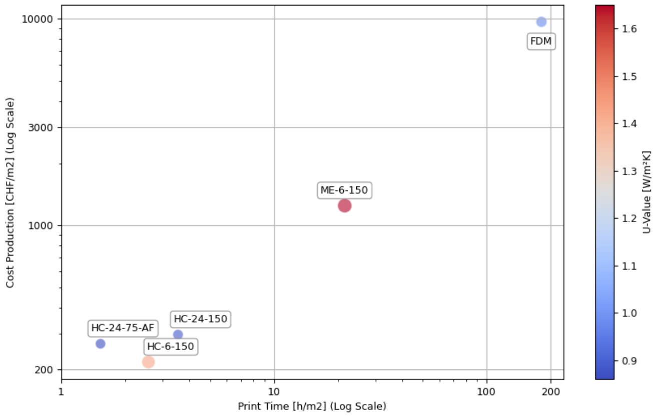

Figure 7.14: Comparison of print time, production costs, and achieved u-value for 1m2 of 3DPF.

7.5 Discussion

Although FDM samples show good u-values we have shown that their production viability is limited. Printing times per square meter from 180 - 500h render this process economically not viable. Furthermore, the filaments (feedstock) needed for small-scale ME is 6-7 times more expensive per kg than their granular equivalent, which is critical for large-scale applications. For large-scale applications printed in high resolution (smaller than 1mm), the effect of cavity convection could become significant and would need to be investigated.

The two most promising methods, with the best U-value to print time ratio, for bespoke 3DP facades are mono-material HC3DP with a large bead size and HC3DP with no infill but supplemented with an aerogel filling (HC-24-75-AF and HC-24-150). These approaches offer the best balance of thermal performance, print time, and material consumption. In comparison to standard Material Extrusion (ME), HC3DP is advantageous for fabricating insulating elements as it reduces both material consumption and printing time. Additionally, the entrapped air within the extruded beads significantly enhances thermal insulation. In terms of large-scale samples, it was observed that the orientation of cavities has minimal impact on the thermal performance of the 3DP element. Yet, for elements with larger vertical dimensions, the influence of cavity orientation is presumed to be more significant.

The benefits of HC3DP have been highlighted in terms of reduced fabrication time, lower material consumption, and enhanced thermal resistance. In comparison, other fabrication methods are found to be less suitable than HC3DP for facade construction. However, to provide a comprehensive overview of HC3DP's applicability in facade construction, other facade-related requirements need thorough investigation. These include but are not limited to, structural and acoustic performance, as well as the optical properties or G-value of HC3DP elements.

One of the major benefits of 3DP facades, the freedom to design bespoke shapes tailored to the project, and specific local/environmental needs, has not been explored yet for HC3DP. Specifically, the lower resolution of HC3DP on the one hand, improves performance and material efficiency, but also limits the level of detail and differentiations possible. However,

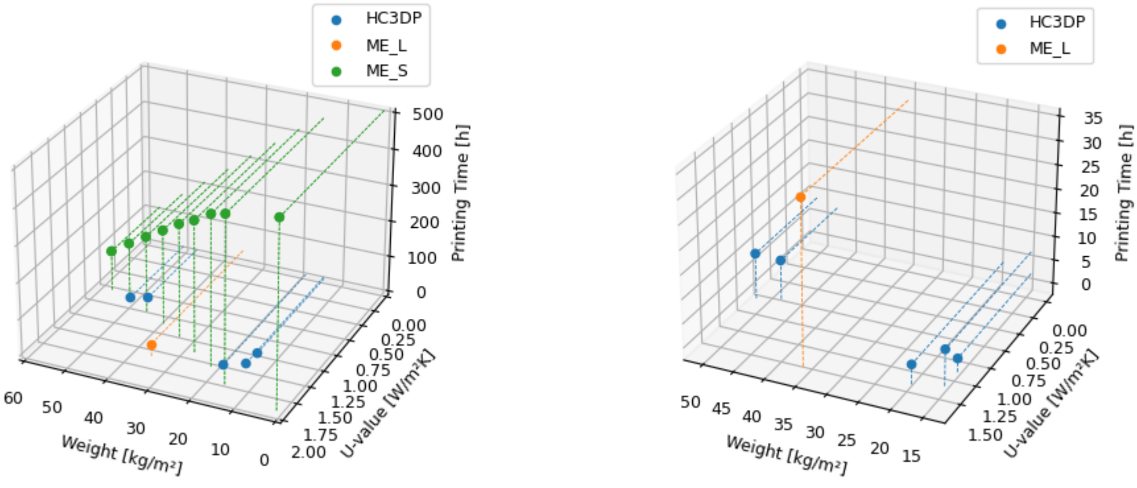

Figure 7.15: Comparison matrix for all tested samples, calculated for 1m2 of 3DPF. Weight, u-value and printing time provide insights about the production viability of a 3DF.

with the fundamental investigations conducted here, the authors hope to provide a better understanding of the design space given to fabricate not only bespoke but also performative designs. Although the experiments have been conducted on simple rectangular shapes, and the cost and fabrication time have been calculated for those, 3D printing offers increased complexity without increasing costs.

In addition to exhibiting good thermal performance, reducing the thickness of facade elements through technologies like the proposed HC3DP-Aerogel composite might offer added benefits due to their compactness compared to the other specimens presented in this manuscript. This reduction is particularly relevant in the context of increasing floor demand and prices, as well as the ongoing challenge of insufficient housing availability.

Figure 16 compares the results of this research to off-the-shelf ME methods, as well as other established construction methods for opaque and transparent facades. The graph shows a lower thermal performance of 3D-printed specimens compared to opaque wall constructions. However, it is noteworthy that the 3D-printed components have a 2-3 times lower thickness compared to opaque ones. 3D-printed components rather compete with transparent components in terms of thermal resistance and weight. Compared to off-the-shelf ME, HC3DP enables lower u-values at a lighter weight and faster printing speed. Although HC3DP provides similar U-values at lighter weight/m^2 compared to glazing, the transparency of windows cannot be matched.

7.6 Outlook

To improve the thermal performance of HC3DP elements, new nozzles with minimized wall thicknesses could be designed and fabricated.

Reduced thickness would result in an increased air-to-solid ratio and, therefore, higher insulating properties, and less material consumption. The nozzles presented in this research are fabricated using DMLS of aluminum, which is restricted to minimal wall thicknesses and feature sizes of approximately 1mm. With more complex, or multipart nozzle designs, fabricated using CNC machining, the orifice can feature wall thicknesses smaller than 1 mm. This will ensure better thermal resistance, faster printing times, and even higher material savings, as observed for translucent building elements made of polycarbonate [13]. To which extent the reduction in wall thickness is reasonable from a structural perspective is still to be investigated.

[13]: Simone Jeska (2008), 'A Brief History of Plastic Buildings'

To fully understand the environmental impact of 3DPF future research must evaluate the embodied energy and the impact of the fabrication process. This assessment should be balanced against the potential for reusability over multiple life cycles (thermoplastic and potentially aerogel) and the possibility of recycling (thermoplastic). For aerogel-filled 3D-printed facades future research must investigate if, after separating the filling from the component, residual aerogel hinders recycling and if so, to which extent. Such analysis is crucial in determining the long-term sustainability and cost-effectiveness of these materials. Moreover, the structural performance of these slender elements requires verification. It is important to ensure that these thinner, more compact facade elements can maintain their structural integrity and safety standards.

7.7 Conclusion

In this manuscript, different ME methods are used to fabricate, test, and compare thermal performance and production viability. We highlight the most promising ME approach for lightweight, insulating, and fast-to-fabricate 3DPF. We provide data for all samples like U-Value, print time and material consumption. Finally, we compare the results against state-of-the-art solutions for facade applications. During this research, it was shown that different strategies can be addressed to influence the thermal performance of a 3DPF at the distinct scales of geometry, fabrication, and material. First, the geometrical manipulation of the element, like thickness, infill geometry, and density. In addition, when using HC3D, the hollow printed bead positively impacts the insulation performance and can be changed according to project-specific requirements. Third, the material used to either print the facade or fill the resulting gaps can increase the components' performance. Lastly, another benefit of HC3DP lies in its bespoke application and tunability compared to standardized products.

Building upon these insights, it was found that HC3DP is a promising ME approach for the fabrication of 3DPF facade systems. This novel 3D printing approach improves the thermal resistance of a 3DPF while reducing material consumption and increasing fabrication speed significantly, making it a promising avenue for further research. When aspects like durability and weather resistance are solved, HC3DP can become a

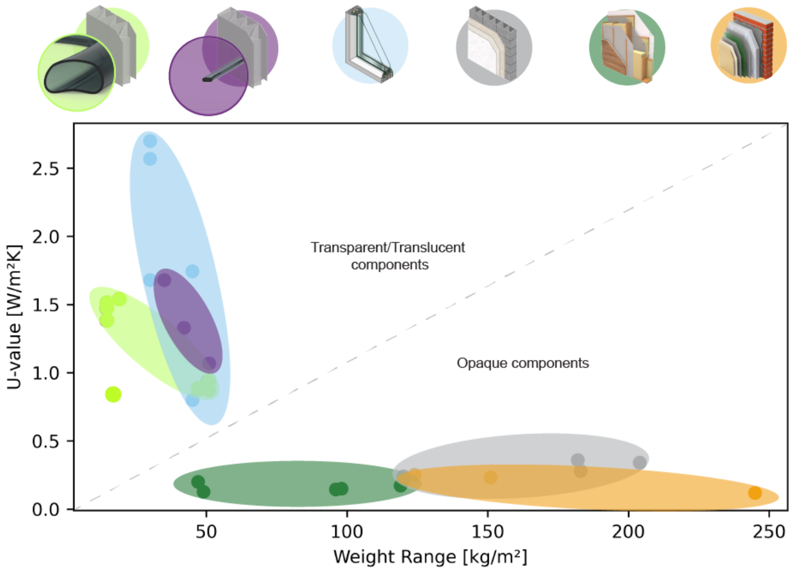

Figure 7.16: Comparison matrix for investigated methods against off-the-shelf facade solutions.

viable alternative to conventional facade systems, also offering potential for customization of performance and geometry, resulting in functional integrated and site-specific facades in a mono-material construction scheme.

7.8 Appendix A - Print time calculations

A.1 Determination of the upper boundary for print time

To calculate the maximum extrusion rate for our fabrication setup, printing material, and nozzle diameter, we assume the extruder runs at maximum capacity and record the weight of the extrudate. The extruder used for the regular ME experiments is rated for a maximum extrusion of 12kg/h (PLA at 20mm nozzle). However, for the material and nozzle diameter used (PETG and 4mm), the maximum extrusion value was found to be approx. 7kg/h. Considering PETG's density of 1.29 g/cm3, this is equivalent to 1500 mm3/s. The maximum extrusion rate determines different maximum print speeds depending on the cross-sectional area of the bead:

$$max.speed\ [mm/s] = \frac{max.extrusion\ rate\ [mm^3/s]}{cross - section\ bead\ [mm^2]} \tag{A.1}$$

Table 7.3 reports the calculated maximum speed considering the different cross-sections investigated. For HC3DP, the cross-section surface area is 15.71 mm^2 for o6w1, which results in a maximum print speed of 95.5 mm/s. The HC nozzles for larger cross sections extrude 72.26 mm^2 (o24w1), and 117.29 mm^2 (o24w1Quad), which is equivalent to a maximum print speed of 20 and 12 mms. The maximum speed for regular ME is 109.8 mm/s, for the given layer width and height (6 x 2.5) with a disco rectangular cross-section of 13.6mm^2.

From the equations above, we can calculate the minimum printing time per layer as:

$$t\ extrusion_{layer}\ [s] = \frac{length_{layer}[mm]}{max.speed\ [mm/s]} \tag{A.2}$$

A.2 Determination of the upper boundary for print time

For HC3DP, we assume a 1 mm wall thickness for a 6 mm round bead. According to the thermal model (Figure A.1), the cooling rate for HC3DP is high for the first minute after deposition; after that, it is similar to a full bead of equivalent thickness. For ME, we assume a round bead with a diameter of 4.3 mm, which is equivalent to an area of a 6 x 2.5 mm bead cross-section.

To derive an optimal printing speed from the model, we need to define a minimal layer and a maximum layer time which is directly related to the cool-down of the previous layer. This threshold is defined by the time the material maintains a workable temperature. A minimal layer time is critical for providing sufficient cooldown of the extruded layer before the consecutive can be printed on top. Printing faster than the minimum layer time will result in sagging, or collapsed walls, as the previously extruded layers are still too hot and therefore soft. Although this phenomenon is described by multiple researchers, temperature ranges or guidelines are not explicitly mentioned [38, 308].

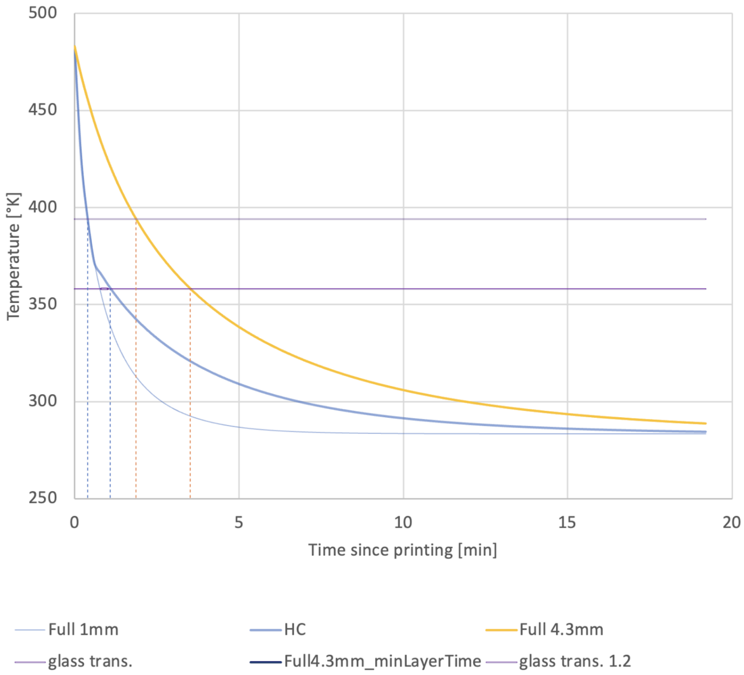

Figure A.1: Thermal cool down behavior of regular ME (6x2.5mm) orange, and HC3D (6 diameter, 1mm wall thickness) blue. The violet horizontal lines describe the optimal printing time window. Lower boundary represents the glass transition temperature for the polymer, and the upper is estimated to be 391K

To define the maximum layer time we consider the glass transition temperature, which in the case of PETG equals 76°C (349 K). The glass transition temperature has been found to be a critical factor, especially for large-scale, thin-walled 3DP elements [259], such as the facade elements proposed in this research. If the temperature of the uppermost printed layer drops below the glass transition temperature, the risk of delamination or cracking increases. We, therefore, make assumptions according to the findings of [46], which showcased that a 3D print with an upper layer temperature of 95C results in good printing quality while 160 results in print failure. We assume the average of 160°C - 76°C, 118°C (391.15 K) for the upper temperature boundary.

Above 118 degrees (391.15 K), there is a high risk of print failure; below 76 degrees (349 K), the risk of delamination and cracking increases. To provide a more accurate upper boundary, more research needs to be conducted. However, the chosen values result in realistic minimal layer times ranging from 105 - 180 seconds, which are validated by our own experience and in discussion with large-scale 3D printing experts.

By implementing appropriate simplifications to the model (Equation 7.3), Leschok et al. [46] derived the following equation to describe temperature change over time:

$$T_{j+1} = (T_j - T_e)e^{-\frac{\alpha c \Delta t}{b}} + T_e \tag{A.3}$$

Where:

- T_{j+1} is the material temperature at time t_{j+1}
- T_j is the material temperature at time t_j
- $T_e$is the temperature of the environment
- t is the change in time between the two time steps
- b is the equivalent wall thickness of the bead
- α encapsulates emissivity and Stefan-Boltzmann constant

- c is the linearization parameter to simplify the fourth power temperature dependency

The temperature change exhibits an exponential decay behavior, influenced by the time and material properties. Over time, it tends to approach the temperature of the environment. Equating T_{j+1} to the chosen layer cooling temperature, $T_{cool}()$, and solving for Δt we obtain:

$$T_{cool} = (T_j - T_e)e^{-\frac{\alpha c \Delta t}{b}} + T_e$$

$$\Delta t = -\frac{b}{\alpha c} \ln\left(\frac{400K - T_e}{T_j - T_e}\right) \tag{A.4}$$

Δt can also be derived from Figure A.1 intersecting the cooldown curve with the temperature threshold.

7.9 Appendix B

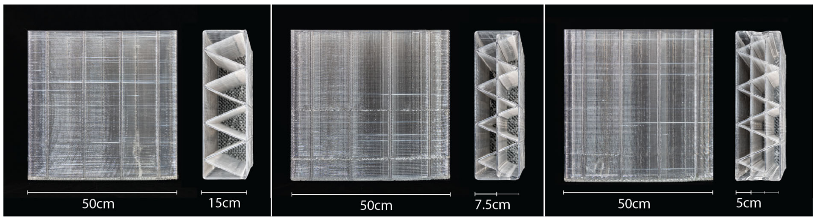

Figure B.1: Overview of the specimen 3D printed through ME and tested with calorimetric experiment in [45]. The first sample from the left (ME-2-R1-150) has the same dimensions and infill geometry as HC-6-O-150, HC-24-O-150, and HC-24-X-150 and is used for benchmarking.

Acknowledgements

This research is financially supported by the National Centre for Competence in Research in Digital Fabrication, funded by the Swiss National Science Foundation (NCCR Digital Fabrication Agreement number 51NF40141853).

Material Characterization and Structural Behaviour of H3DP Elements for Lightweight Facades

8

8.1 Overview of Paper G . . . 161
8.2 Introduction 164
8.3 Methods and materials . 165
8.4 Results 171
8.5 Discussion 177
8.6 Conclusion 178

8.1 Overview of Paper G

8.1.1 Content

Paper G examines the material properties and structural performance of both solid and hollow-core 3D printed polymer beads. It explores various factors, including temperature and print orientation. The paper details four distinct experimental test procedures, offering a comprehensive understanding of both material extrusion and hollow-core 3D printing specimens. Additionally, the study underscores the importance of further research into construction-related aspects of facades, such as creep behavior, impact resistance, and the connection details in low-resolution 3D printing. Overall, this manuscript provides significant insights into the mechanical characteristics and structural behavior of large-scale hollow-core 3D printed elements, underlining the potential of this 3D printing technology in construction applications.

8.1.2 Method

This manuscript uses different 3D printing methods and testing procedures to investigate the material characteristics, and mechanical behaviour of ME and HC3DP specimen. The printing methods used include off-the-shelf large-scale ME, using a pellet extruder mounted on a robotic arm. Furthermore, the novel concept of Hollow-Core 3D printing is investigated. The material characterization of ME is performed using tensile testing in accordance to ISO ISO 527-1. Then, for a series of ME and HC3DP specimen, featuring an identical extrusion width, 3PT bending tests are performed to compare both methods. These 3PT bending tests are followed by 3PT bending tests on large cross-section of HC3DP, featuring different wall-thicknesses and internal reinforcements. Both 3PT bending testing campaigns shift the focus from material characterization towards gathering information regarding the components shape. As a final set of experiments, large-scale beams with a length of 1.2m meters are tested to failure. This series features beams with different structural height, ranging from 150 to 75mm, and different printing orientation. Finally, these findings are used to calculate a preliminary maximum spanning distance for different 3DP facade systems.

8.1.3 Results

The tensile testing, performed with specimen conditioned at three different temperatures, shows that the outdoor temperature has a significant influence on the ultimate tensile strength of the material. It was found that the material's tensile strength is the highest in cold environment and reduces at increased temperatures. This leads to the conclusion that future research must investigate in more depth moderate and hot conditioned specimen. However, the reduction in temperature might affect other mechanical aspects, such as impact resistance of the 3DP element. The large-scale 3PT bending tests on different bead cross-sections indicate that an internal reinforcement of the tubular bead does not improve the bending resistance, but influences the ductility of the specimen. The highest force resistance was achieved with specimen features the 2mm wall thickness. The results of the large-scale beams revealed that shifting the infill and outline print-path in z-direction, by half a layer against each other, increased the maximum load capacity. This shift causes the infill lines to have more contact area to the 3DP printed lines that form the shell of the object. Finally, the height estimations for 3DP facades show that 3DP elements, depending on the printing method, chosen cross-section, and structural height, can be applied as free spanning facades at heights ranging from 2.9m to over 12m.

8.1.4 Authors contribution to the paper

Matthias Leschok - Conceptualization, Methodology, Investigation, Formal analysis, Writing – Original Draft Preparation, Visualization.
Thomas Wuest Investigation, Formal analysis, Methodology,Writing – Review & Editing.
Valeria Piccioni - Writing – Review & Editing.
Matthias Kohler - Supervision, Writing – Review & Editing.
Fabio Gramazio - Supervision, Writing – Review & Editing.
Arno Schlueter - Supervision, Writing – Review & Editing.
Benjamin Dillenburger - Supervision, Writing – Review & Editing

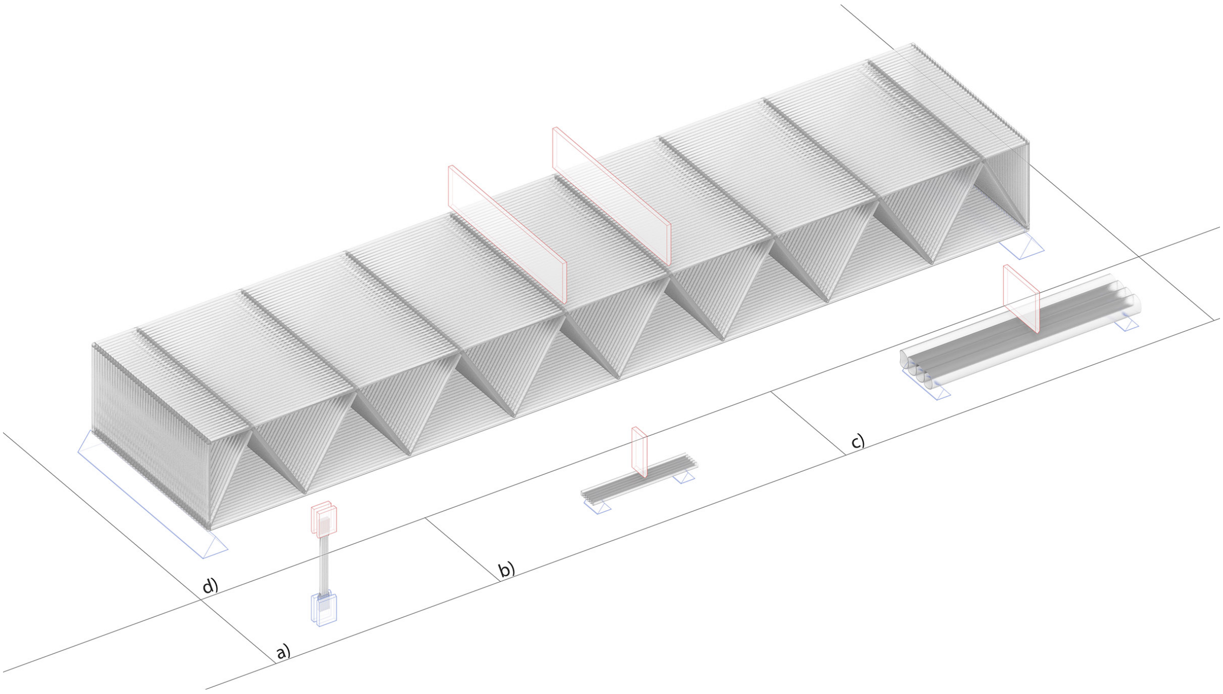

Figure 8.1: Overview of mechanical testing campaigns on ME and HC3DP specimens.

Abstract This paper investigates the structural behavior and material characteristics of Hollow-Core 3D Printing (HC3DP) for large-spanning facades. The study compares HC3DP with conventional large-scale Material Extrusion (ME) methods and explores the influence of varying temperatures on the mechanical properties the 3D printed polymer. In total three types of experimental procedures are presented. Tensile experiments, 3PT bending tests, and finally, 4PT bending tests of large-scale beams. The research highlights the potential of HC3DP in architectural applications, particularly in the construction of high-performance, site-specific facades. The findings underscore the importance of planning and design in the 3D printing process, emphasizing the critical role of printing direction in determining the structural behavior and performance of 3D printed facade elements. Additionally, the paper presents theoretical calculations for the maximum spanning distance of 3D printed facades, based on the results obtained from the experiments presented. The results demonstrate that HC3DP is a promising technology for facade construction, enabling the fabrication of aesthetically unique and material efficient 3DP facades with good structural capacity.

8.2 Introduction

The use of 3D printing (3DP) in the construction of facades presents a transformative approach to architectural design and fabrication. This technology allows for the creation of site-specific facades, tailored precisely to the unique environmental and structural requirements of each location. By leveraging 3DP, architects and engineers can design facades that are not only aesthetically unique but also optimised for high-performance in regard to energy efficiency, material usage, and environmental impact. Such customization enables the integration of complex geometries and materials savings, which can increase thermal performance, control light distribution, or acoustic properties, and therefore, significantly contribute to the overall sustainability of the building. This approach to bespoke facade construction is pivotal in the pursuit of net-zero emissions [3], as it facilitates the creation of buildings that are both environmentally responsible and adapt to their surroundings in the best possible way.

Therefore 3D printing of facades has become a research topic of great interest over the last years [33, 44]. One of the most investigated 3DP methods for facade applications is Material Extrusion (ME). In ME thermoplastic polymers are used to fabricate bespoke elements by adding material in a layered fashion [7]. Reasons for this interest in ME could be that with recent advances in the fabrication process, ME has been scaled up to an architectural relevant scale. In addition, ME is one of the few 3DP methods that enables the fabrication of large-scale translucent elements. Hollow-Core 3D printing (HC3DP) has been recently introduced as a novel alternative for large-scale ME, specifically designed for facade applications. HC3DP has already proven its viability in regards to increased fabrication speed [46], variability in cross sections [47], and its increased thermal performance [49] compared to ME. HC3DP improves these aspects by facilitating the 3D printing of large-scale tubular beads with or without internal reinforcements, see fig. 8.2. Prior research shows that HC3DP can produce facade elements with a u-value of 0.85 W/m2K in just under 1.5 h/m2.

A large body of research has investigated the different aspects of Material Extrusion (ME) for 3DP facades (3DPF), such as proving the feasibility of production large-scale translucent elements [40, 43, 111, 116], or investigations of bespoke shading panels [105, 108]. Further research investigated ME facade prototypes that contain PCM, or transfer fluids to account for annual seasonal climatic variations [106, 107]. The thermo-optical properties of ME and HC3DP 3DP facades have been investigated [45, 49, 197]. However, to the best of the author's knowledge, there is only one prior investigation into the structural behaviour of such large-scale 3D printed elements for the application of facades. Mungegnast [40] showcased a maximum of 600 kN for a prototype with a structural height of approximately 60 mm.

For large-scale ME, not specifically focusing on facade applications, the mechanical behaviour of different compounds has been investigated. Those mostly focus on comparisons on added fibre and neat polymers and influence of printing direction [30, 309], or the difference from virgin to recycled material [24]. Further research investigates improving the mechanical properties of large-scale ME by improving the layer bonding [29, 310]. Most studies focus on material characterization and

[3]: Delmastro et al. (2022), *Building Envelopes – Technology deep dive*

[33]: Naboni et al. (2022), 'Additive manufacturing in skin systems'

[44]: Leschok et al. (2023), '3D printing facades'

[7]: ISO/ASTM (2020), *ISO/ASTM 52903-1:2020 - Additive manufacturing. Material extrusion-based additive manufacturing of plastic materials*

[46]: Leschok et al. (2023), 'Large-scale hollow-core 3D printing (HC3DP)'

[47]: Leschok et al. (), 'Large-Scale Hollow-Core 3D Printing'

[49]: Leschok et al. (2024), 'Thermal and Manufacturing Properties of HC3D Elements for Lightweight Facades'

[40]: Moritz Basil Mungenast (2019), '3D-Printed Future Facade'

[43]: Cheibas et al. (2023), 'Thermoplastic large-scale 3D printing of a light-distribution and fabrication-informed facade panel'

[111]: Taseva et al. (2020), 'Large-Scale 3D Printing for Functionally-Graded Facade'

[116]: Snooks et al. (2020), 'Fabricate 2020'

[105]: Karagianni et al. (2016), 'Additive Manufacturing for daylight: Towards a customized shading device'

[108]: Grassi et al. (2019), 'Fabrication and durability testing of a 3D printed façade for desert climates'

[106]: Sarakinioti et al. (2018), 'Developing an integrated 3D-printed façade with complex geometries for active temperature control'

[107]: Tenpierik et al. (2018), 'Double Face 2.0'

[45]: Piccioni et al. (2023), 'Printing thermal performance'

[49]: Leschok et al. (2024), 'Thermal and Manufacturing Properties of HC3D Elements for Lightweight Facades'

[197]: Piccioni et al. (2023), 'Tuning the Solar Performance of Building Facades through Polymer 3D Printing'

[40]: Moritz Basil Mungenast (2019), '3D-Printed Future Facade'

[30]: Duty et al. (2017), 'Structure and mechanical behavior of Big Area Additive Manufacturing (BAAM) materials'

[309]: Duty et al. (2015), *Material Development for Tooling Applications Using Big Area Additive Manufacturing (BAAM)*

[24]: Anderson (2017), 'Mechanical Properties of Specimens 3D Printed with Virgin and Recycled Polylactic Acid'

[29]: Kishore et al. (2017), 'Infrared preheating to improve interlayer strength of big area additive manufacturing (BAAM) components'

[310]: Lind et al. (2018), 'Enhanced additive manufacturing with a reciprocating platen'

the effects related to fabrication, but not on the effects of geometry and component-scale design.

To the best of the author's knowledge, only one prior manuscript has investigated the behaviour of 3D printed tubular beads on a small scale [264]. However, there is a notable gap in research on large-scale extruded beads, which are proposed for facade applications. Moreover, investigations that extend beyond material characterization to explore the structural systems of 3D printed (3DP) facades are missing. Therefore, this manuscript delves into the structural performance of HC3DP at various resolutions. It includes the development and analysis of large-scale prototypes, showcasing the structural capacity of large-scale HC3DP. The results are then compared with those of conventional large-scale ME methods, highlighting the advantages of HC3DP in the application of 3DP facades.

[264]: Hopkins et al. (2020), 'Additive manufacturing via tube extrusion (AMTEx)'

8.3 Methods and materials

8.3.1 Material Extrusion and HC3DP

In this manuscript two robotic 3D printing methods are used to fabricate specimens for mechanical testing. Material extrusion (ME) describes the process of extruding a thermoplastic material to 3D print three dimensional objects in a layered manner. A layer usually consists of multiple printing lines, the extrudate following such line is often referred to as bead or road. The second 3DP approach used falls in the category of ME, but extrudes tubular, hollow beads, as shown in Figure 8.2. This process is called Hollow-Core 3D printing (HC3DP) and was recently established as an alternative ME approach to 3D print lightweight elements, with minimal material consumption at large dimensions.

The specimens tested in this manuscript are 3D printed using a pellet extruder, capable of extruding up to 10 kg/h of material, mounted on a six-axis robotic arm. A material drying and conveying system conditions the granular feedstock prior to printing, delivering granules to the extruder during operation. The extruder features three heating zones within the barrel that progressively heat the feedstock to its melting point. A screw, driven by a servo motor and gearbox, moves the feedstock through the barrel. The melted thermoplastic exits through an interchangeable nozzle at the extruder's tip, determining the extrudate's shape and size, thus allowing for various printing resolutions. For HC3DP, a bespoke nozzle, positive air pressure, and a pressure regulator are needed. Detailed information about the HC fabrication setup can be found in [46]. The different printing resolutions used in this manuscript are depicted in Figure 8.2.

[46]: Leschok et al. (2023), 'Large-scale hollow-core 3D printing (HC3DP)'

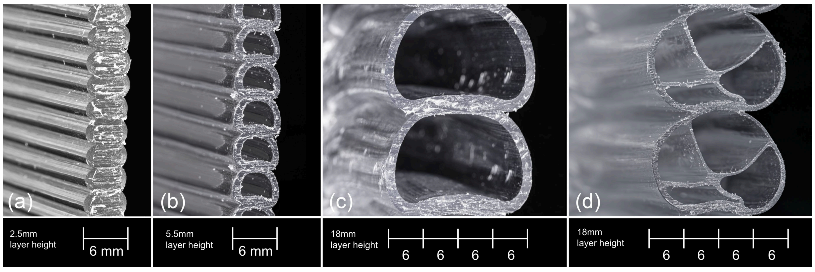

Figure 8.2: Different cross-sections tested. (a) ME 6mm width, 2.5mm height. (b) HC3DP 6mm width, 5.5mm height. (c) HC3DP 24mm width, 18mm height. (d) H3CDP 24mm width, 18mm height with internal reinforcement.

8.3.2 Material

The granular material used in these experiments is PETG, sourced from Extrudr GmbH [270]. Before printing, this material undergoes conditioning at 60°C for four hours. Due to its granular form, the pellets require drying to ensure optimal printing quality. PETG, a modified variant of PET, is selected for its properties that enhance 3D printing capabilities. The inclusion of glycol in PETG limits crystallisation, which aids in better moldability and preserves high transparency [231].

PET, the base polymer in PETG, ranks as the fourth most-produced polymer worldwide. It is primarily used in the production of fabrics and as containers for liquids and foods, [295]. Its widespread use is attributed to its excellent transparency, along with good chemical and structural properties [232].

[270]: Extrudr (), *PETG transparent - High Quality Filament*

[231]: Sepahi et al. (2021), 'Mechanical Properties of 3D-Printed Parts Made of Polyethylene Terephthalate Glycol'

[295]: Ji (2013), 'Study on Preparation Process and Properties of Polyethylene Terephthalate (PET)'

[232]: Petrov et al. (2021), 'Research into the effect of the 3D-printing mode on changing the properties of PETG transparent plastic'

8.3.3 Mechanical testing and specimens

This manuscript provides an in-depth investigation of the mechanical properties of ME and HC3DP at different resolutions. First tensile tests are conducted on ME specimens in line with DIN EN ISO 527-1, at three different temperatures. Then, three-point (3PT) bendings tests on ME and HC, featuring identical bead width, are conducted to compare off-the-shelf large-scale ME to HC3DP. As a next step, a series of 3PT tests investigate three types of large-scale HC specimen, featuring different wall thicknesses and internal reinforcements. As a last step, several 1250 mm long beams are tested to compare ME against HC3DP at an architectural relevant scale.

The goal of these investigations is not to provide extensive testing campaigns but rather to provide a broader understanding of the different scales that affect the mechanical properties of 3DP specimens. Finally, these can then be used to guide future, more extensive investigations based on the findings presented here.

Tensile testing- ISO 527-1

This section describes the procedure for performing tensile tests on ME 3DP specimens in line with the DIN EN ISO 527-1 standard. The goal is to determine the material characteristics of the 3D-printed specimen, including its tensile strength and modulus of elasticity.

To understand if Material Extrusion is a viable option for facade applications, the tensile testing of 3DP specimens is conducted at three different

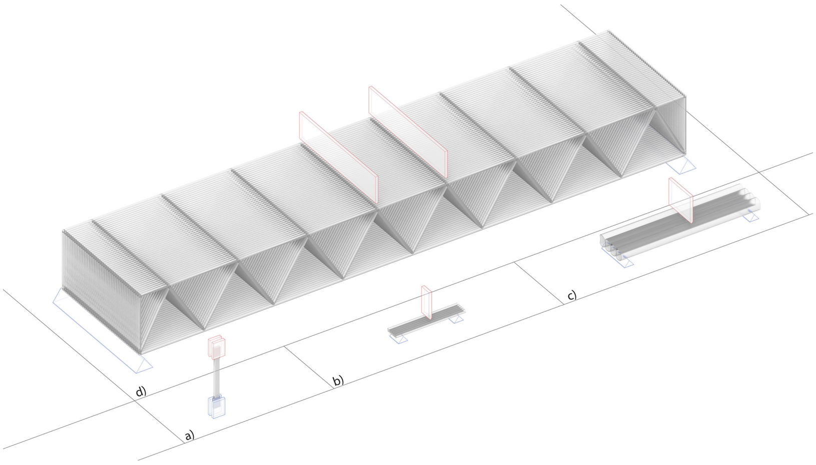

Figure 8.3: Four different types of mechanical testing performed in the manuscript. a) tensile testing with regular ME 3DP specimens. b) 3PT bending tests with ME and HC3DP at high resolution. d) 3PT bending test with HC3DP specimen featuring large cross-sections. d) 4PT bending test with large-scale beams, both ME and HC3DP.

temperatures. As facades are the barrier between in and outdoor environment they must withstand annual season variations in temperature. Therefore, we choose to perform the experiments for winter, spring and summer seasons, which are reflected in conditioning temperatures of -10, 20, and 50°C. The samples are pre-conditioned for each temperature over >17h in a climate chamber with additional 5 K (-15°C / 55°C). The tensile tests are conducted sequentially within less than two minutes from the climate chamber to test.

Standard test specimens are cut from a 3D printed cube and for each temperature six specimens are tested, the specimen have a testing cross section of 12x4mm at a parallel testing length of 80mm.Three samples have the 3DP layers parallel to the pulling direction, and the other three have the 3DP layer perpendicular to the tensile force applied. The experiments are conducted on a universal testing machine (Zwick/Roell Z010). The testing speed was increased from 10 mm/min to 50 mm, as it otherwise results in extreme elongation of the 3DP element, see Figure 8.10 (specimen 1).

To estimate the facade temperature under summer conditions, a simplified absorption model was derived based on preliminary goniophotometer measurements on 3D-printed samples, according to the procedure reported in [197]. The absorption model shown in Figure 8.4 ignores multiple reflections within the component and the angle-dependent optical properties of the 3D-printed material. Therefore, it is to be understood as an initial guide for the tensile experiments, assuming conservative conditions for a worst-case scenario. The thermal boundary conditions on the facade were determined by SIA 2057 with an incident solar radiation of 840 W/m2 as well as a temperature of 32°C outside and 20°C inside. The heat transfer coefficients also correspond to summer conditions with 12 W/(m2K) outside and 7.7 W/(m2K) inside.

[197]: Piccioni et al. (2023), 'Tuning the Solar Performance of Building Facades through Polymer 3D Printing'

The thermal analysis was carried out using the 2D thermal bridge software Flixo (pro, V 8.0). The absorbed solar energy was modeled as an internal heat source applied to the different surfaces of the component. With these boundary conditions, the steady-state temperature distribution was calculated. The maximum surface temperature was found to be approximately 51.5°C, see Figure 8.4, which is below the Vicat temperature of the material.

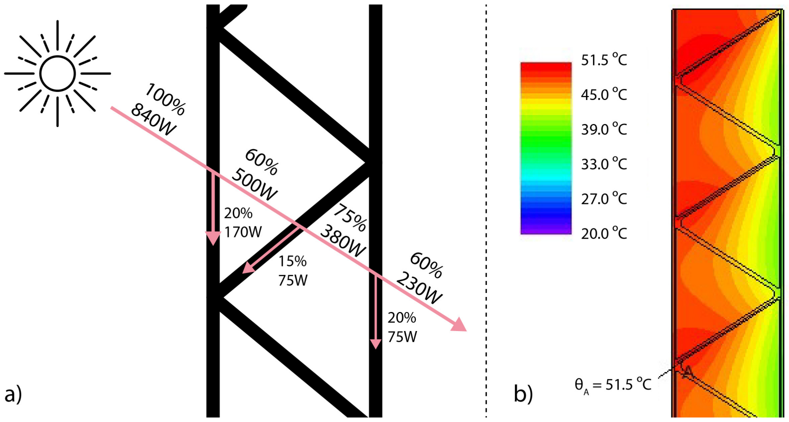

Figure 8.4: (a) Diagram of thermal boundary conditions. (b) Results of thermal analysis using Flixo..

3PT Bending - 6mm width ME and HC

The following section describes a first series of experiments that focuses on the components shape, as tubular 3D printed specimens are compared against full extruded beads. The tests aim to investigate the behaviour and material efficiency of H3DP, printed at a high resolution.

The 3PT bending tests were carried out on an universal testing machine (Zwick/Roell 150kN) according to ISO 178. Both sample types have a bead width of 6mm, the layer height for ME is 2.5mm and for HC 5.5mm. The HC3DP specimens have half the weight to their ME equivalents. Similar to the tensile experiments, the specimens were cut from a larger cube, but this time only parallel to the printing direction. In total five specimens of each type are tested. Each specimen is tested twice, as seen in Figure 8.13. The distance between supports is 110mm and the testing speed 10mm/min.

3PT Bending - 24mm width HC3DP

The following section describes 3PT bending tests on large-scale HC3DP specimens that investigates different cross sectional profiles, see Figure 8.5. These experiments have been published previously [46] but are presented here again in a shortened version, as their results complete a broader overview of mechanical properties of HC3DP.

[46]: Leschok et al. (2023), 'Large-scale hollow-core 3D printing (HC3DP)'

The specimen consists of three undisturbed layers, at a layer-height of 19mm and a layer-width of 24mm. This experimental campaign features three different types of extruded cross-section, a) a 24mm width with a 2mm wall-thickness, b) a 24mm width with a 1mm wall-thickness, and c) a 24mm width with a 1mm wall-thickness including a reinforcement cross inside the bead. Three samples are tested for each type on a universal testing machine (Zwick 1484) at a speed of 6mm/s. The distance between the supports is 270mm. Both ends of the specimens have been cast into epoxy resin to prevent a material failure at the supports.

4PT Bending tests of large-scale beams

After providing insights on the material characteristics and cross-section related behaviour, the following section describes large-scale experiments

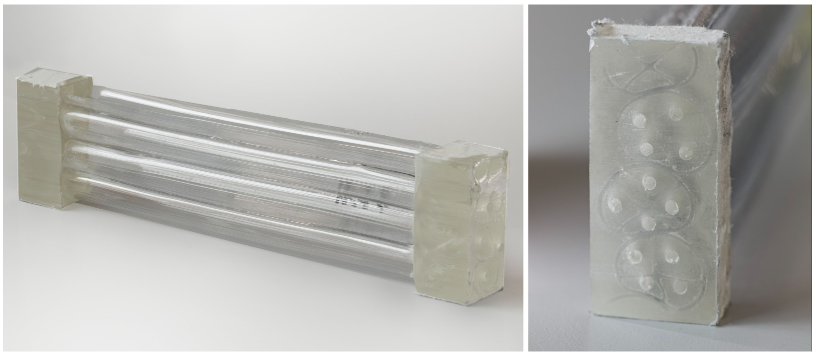

Figure 8.5: HC3DP specimen with a wall-thickness of 1mm and a reinforcement cross in the centre of the bead.

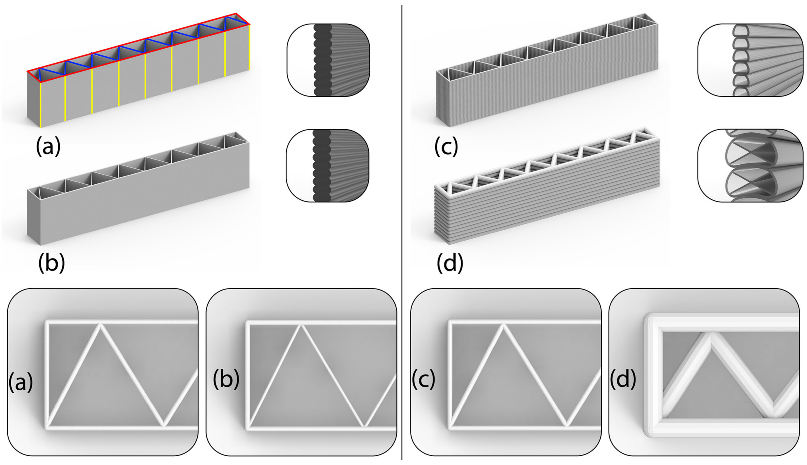

Figure 8.6: Printed specimen displayed in printing orientation a) ME, 6mm width shell and infill. b) ME, 6mm width shell, 4mm infill. c) HC3DP, 6mm width. d) HC3DP, 24mm width.

to evaluate the systemic behaviour of 3DP elements in the use-case of facade application. This section does not provide extensive testing campaigns with identical specimens, but rather a broad range of 3D printed geometries, featuring different printing resolutions, cross-sections and printing directions. The goal is to provide a first point of reference regarding the structural capacity of HC3DP and identify future research trajectories.

The last testing campaign presented in this manuscript consists of 12 different large beams. Their length and width are constant at 1250 x 250mm, and the structural height is varying from 150 to 50 mm. The structural height is chosen to be consistent with experiments on the thermal performance of such 3D printed elements [49]. Similar to the tensile tests in chapter 8.3.3, two types of ME are investigated, large-scale pellet-based ME and HC3DP. Furthermore, the specimens are categorised by their printing direction and are labelled as “upright” and “rotated”.

[49]: Leschok et al. (2024), ‘Thermal and Manufacturing Properties of HC3D Elements for Lightweight Facades’

All specimens are designed as continuous single outline prints, irrespectively of the printing method. As shown in Figure 8.6.a, the geometry consists of a shell (red) and infill lines (blue) with a distance of 150 mm between each other (yellow). The ME samples have a 2.5mm layer-height and a 6 mm layer-width. For ME two samples are tested, one with constant bead width 8.6.a and the other with a reduced bead width for the infill lines, see Figure 8.6.b. The reduction in bead-width from 6 to 4mm goes hand in hand with a reduction in weight of approximately 30 %. To mimic the identical printing width of off-the-shelf ME, a high-resolution HC3DP specimen is printed with 6mm layer width, however, featuring only half the weight of regular ME, see Figure 8.6.c.

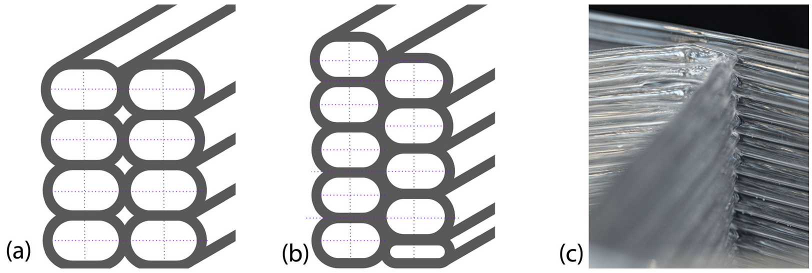

Figure 8.7: a) Section of regular ME bead arrangement. b) Diagram of section with layer-shift. c) Close-up of printed element showing the connection between shell and infill lines, offset by half a layer against each other.

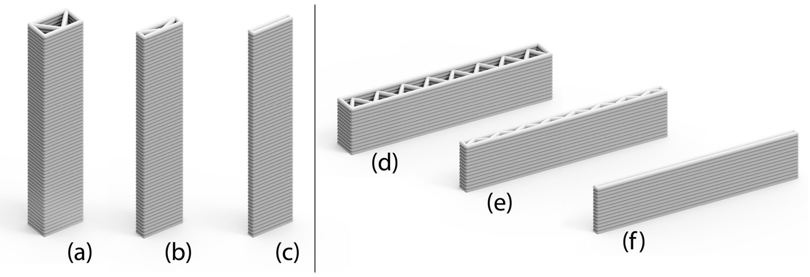

Figure 8.8: Printed specimen displayed in printing orientation a) HC3DP, 24mm width, 150mm depth, updstanding. b) HC3DP, 24mm width, 75mm depth, upstanding. c) HC3DP, 24mm width, 50mm depth, upstanding. d) HC3DP, 24mm width, 150mm depth, shifted layers. e) HC3DP, 24mm width, 75mm depth. f) HC3DP, 24mm width, 50mm depth.

For the HC specimen no distinction is made between the shell and infill lines, both are printed at constant bead widths. However, due to the round bead structure of HC3DP, two types of specimen are tested. Type |R| is printed regular with the shell and infill being at the same height (or layer), and type |S| where the shell and infill line are shifted in Z-direction against each other. Like this, as shown in Figure 8.7, the contact area between the beads increases and the air gaps between single beads are reduced. This gap is particularly large for HC3DP due to the large-bead size and their width to height ratio, compared to regular ME. Two samples are printed with a depth of 150 mm, with and without layer-shifting. Then, due to the extreme load capacity, a second batch of 3DP specimens with reduced depth are investigated, namely 75 mm and 50 mm, see Figure 8.8 e, f.

Finally, a series of "up-standing" prints, with the layer direction being parallel to the supports during testing, is investigated. It is important to understand the influence of the printing direction on the behaviour of large-scale 3DP facade elements.The testing setup consists of a Universal Testing machine (150kN Zwick/Roell) with the supports being 1200 mm spaced and the load is induced in the centre of the beam using a wooden beam with a footprint of 200 x 250 mm. The speed is set to 20 mm/s, Figure 8.17 documents the testing procedure.

8.3.4 Facade height estimation

In order to provide a first estimate of the maximum spanning distance of a 3D printed facade the following simplified calculation is suggested. This calculation assumes that the facade is linearly supported at the top and bottom, freely spanning between the two slabs as a single span beam. The calculations are based on the geometry tested, featuring an infill support span of 150mm. The assumptions for loads and safety factors are estimations with no specific use-case requirements. For high-rise building, or alpine region the wind force applied, or safety factors required would change from the example provided.

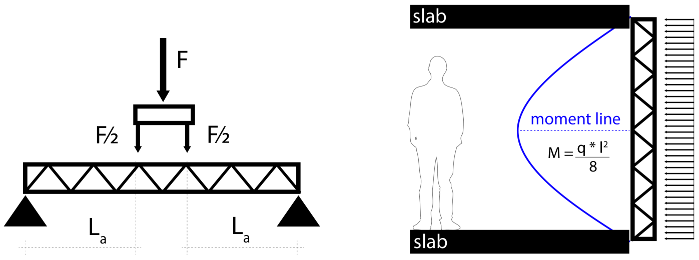

Figure 8.9: Left: Diagram of testing setup with labels for calculating the bending resistance. Right: Assumptions for wind load and maximum span calculation based on the moment line.

First, based on the measurement results the maximum bending resistance M_{Rd} is calculated for each sample, incorporating a safety factor of the material assuming 1.5:

$$M_{Rd} = \frac{F/_2 \times l_a}{Y_M} \tag{8.1}$$

Then we estimate the force applied to a building facade q_w, assuming a 1kN/m2 wind load with a safety factor of 1.5 for variable loads:

$$q_w = F_W \times b_{eff} \times Y_Q \tag{8.2}$$

Finally, l_max is calculated in a simplified manner as a single span beam with uniform load, based on the bending resistance and the load assumed.

$$l_{max} = \sqrt{\frac{8 \times M_{Rd}}{q_w}} \tag{8.3}$$

- F : the maximum force in N
- b_{eff} : width of the specimen tested
- F_W : force wind kN/m^2
- L_a : distance between the two linear loading spots
- Y_M : safety factor of 1.5, material
- Y_Q : safety factor of 1.5, load

8.4 Results

8.4.1 Tensile testing results

Figure 8.10 shows a strong difference between tensile strength for different printing orientations irrespective of the conditioned temperature. Tensile strength decreases by 55-62% according to the printing orientation. If the force direction is parallel to the printed beads, the tensile force is close to the ultimate tensile strength of the material provided by the manufacturers datasheet [270], and therefore can be considered a material failure. If the forces applied are perpendicular to the printing direction, the failure occurs at the layer bonding, leading to a different mode of structural failure. These observations are in line with existing literature

[30]: Duty et al. (2017), 'Structure and mechanical behavior of Big Area Additive Manufacturing (BAAM) materials'

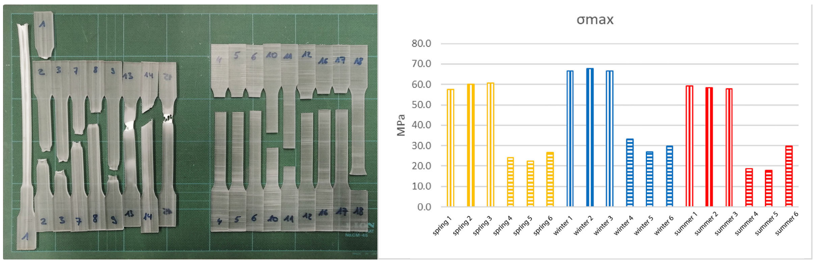

Figure 8.10: (a) Specimen after tensile testing. (b) Results of tensile testing, color-coded. Yellow: spring. Blue: winter. Red: summer.

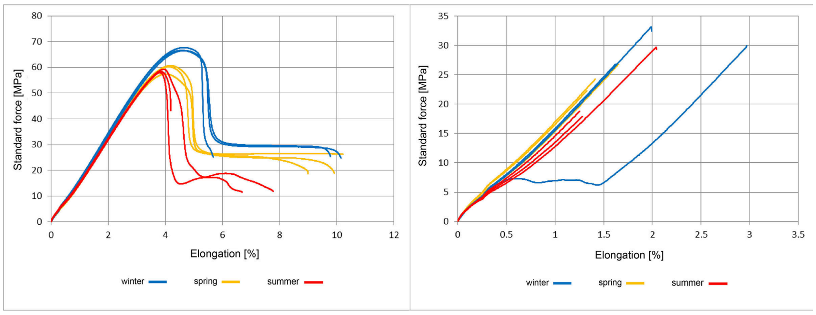

Figure 8.11: (a) Specimen with printing lines in parallel to tensile force. (b) Specimen with printing lines perpendicular to the tensile force.

on the subject [30], highlighting the critical role of printing orientation in 3D printing applications.

Altering the temperature of the specimen results in a moderate deviation in performance of up to approx. 14%. The ultimate tensile strength changes depending on the temperature and drops from avg. 66.9 MPa for winter to 59.4 MPa for spring, and 58.5 MPa for summer. However, for the specimens printed in parallel to the testing direction the variation within a series is limited to a maximum of 3%. These findings are in line with other investigations on the tensile properties of thermoplastics at different temperatures [311].

[311]: Lou et al. (2020), 'Effect of temperature on tensile properties of reinforced thermoplastic pipes'

The testing speed plays a role in influencing the failure behaviour of the materials, as demonstrated in Figure 8.10, particularly in sample 1. The specimen conditioned at 50°C showed a stronger white break than all other specimens, samples 13 did not break into two separate parts but stayed connected, see Figure 8.10.

The specimen with print lines in parallel to the force applied behave slightly ductile, the elongation stiffness stays identical for all temperatures until 3%, then the constriction in the flow area is longer for the winter case, and the shortest for the summer scenario. The perpendicular specimens fail brittle with no indication of impending fracture. There are minor differences in the stiffness of the specimen depending on the conditioned temperature.

8.4.2 Results of 3PT Bending - 6mm width ME and HC

The results show that all specimens failed due to buckling at an average maximum force of 277 N for the HC3DP specimen, and 615 N for ME. We use the averaged E-Module, obtained from the tensile experiments from chapter 8.4.1 to calculate the theoretical deformation of the specimens. Those values, depending on the printing method, align well with the measured results. We propose to use a mixed method to describe the geometric characteristics of the tubular beads with their disco-rectangular

Table 8.1: Comparison of deflection, measured and estimated values.

Type	layer width	layer height	s [mm] 3PT bending	s [mm] rectangle	s [mm] oval	s [mm] mixed
ME	7	2.5	14.8	13.63	23.14	17.16
HC3DP	6.5	5.5	12.1	9.54	16.01	11.96

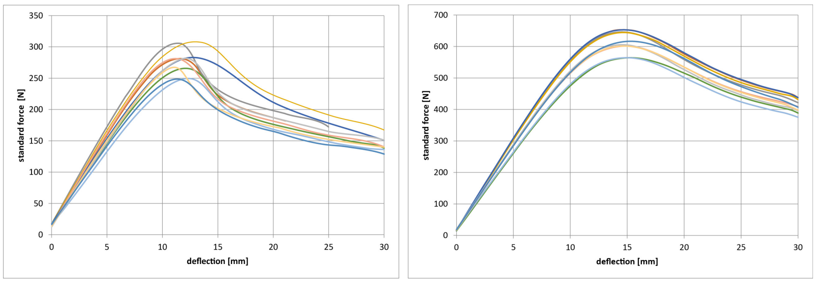

Figure 8.12: Results of 3PT bending tests, (a) HC3DP (b) ME.

shape, as shown in table 8.1. Using the average of a rectangular and oval tube aligns well with the measured results for HC3DP. For the regular printed specimen, featuring full material, this model does not align as well and is probably related to uncertainties of the cross-sectional geometry. More detailed analyses of the cross-sectional geometry of regular ME will provide a better approximation to the measured values.

8.4.3 Results 3PT Bending - 24mm width

The results show that the wall-thickness has a large influence on the bending resistance of the HC3DP elements. The specimens with the 2mm thick walls (w.2.) withstand 74 % more load than an equivalent specimen with a 1mm thick wall (w.1). This is in line with the theoretical increase in moment of inertia of 78%, calculated as suggested in [46]. The reinforcement cross inside the bead (specimen q.), although increasing material consumption, does not directly improve the maximum bending resistance. However, it should be noted that for the given specimen type, size, and wall-thickness it changes the ductility of the specimens. Overall two different failure modes are observed. Nearly all specimens failed due to buckling. Only two of the 2mm wall-thickness specimens (w.2.2 and w.2.4) failed brittle, after reaching their maximum load and continued to deform while their bending resistance decreased. It is not clear yet whether the scale of the bead, its wall-thickness, or other factors such as the width to height ratio leads to catastrophic failure.

[46]: Leschok et al. (2023), 'Large-scale hollow-core 3D printing (HC3DP)'

8.4.4 Results large-scale beams

For off-the-shelf pellet-based ME it was found that reducing the infill bead thickness reduces the max. F. significantly. A 30% reduction of material results in 60% less load capacity. The ME - specimen with reduced infill width and the HC - 150 - 6 - S have a similar max F. However, the HC specimen, although saving 40% of material, performs better (104%) than the ME-150-reduced.

The increase in Fmax for the HC3DP with large-bead sizes is extreme. Although the beams have an identical structural height of 150mm, the

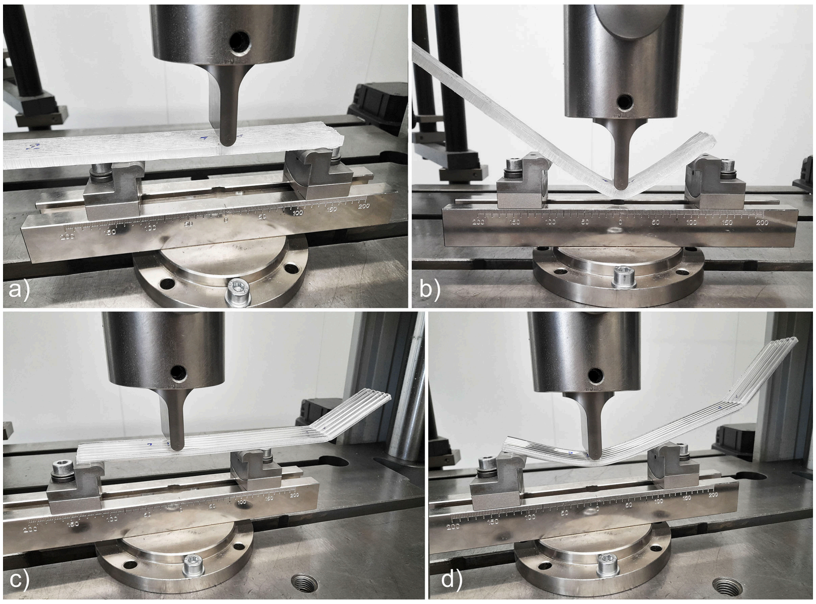

Figure 8.13: a-b) Testing procedure of ME specimen. c-d) HC3DP specimen.

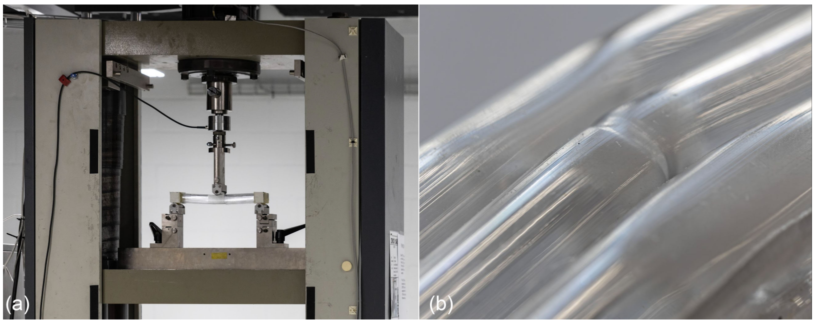

Figure 8.14: a) HC3DP specimen during 3PT testing. b) Close-up of constriction and whitening of the lower (tension) zone.

cross-sectional area of the extruded beads increases the thickness of the beam's walls by factor 4, from 6 to 24mm. A maximum max.F. of 45800 N is achieved when the shifted slicing method, shown in Figure 8.7 is used. For both specimen types, 150 and 75mm height, the shifted layer slicing method (specimen - S) performs better than their regular equivalents (60 to 98%).

The horizontal (HC-x-UP) printed specimens have a significantly lower resistance to load, see Figure 8.16 (yellow). These findings go hand in hand with observation from the tensile testing in chapter 8.4.1. However, the difference between large-scale elements printed in different orientations appears to be greater. If both specimens with a 150mm structural height are compared, the element with the layers oriented spanning from support to support withstands a 20 times higher force than the specimen with the layers oriented in parallel to the supports. For the small scale specimens in chapter 8.4.1, this difference is between factor 2.5 - 3.

Figure 8.17 documents the testing procedure and the failure mode for beam ME-150, HC-6-150, and HC-24-150-S. Different failure modes are observed, Fig. 8.17.a showcases a clean break tangential to the printing direction, exactly before or after the infill lines are merged with the shell. The infill lines stay connected and only the shell is broken. The HC-6-150 specimen, featuring high-resolution HC3DP, deforms under load until it buckles and the tubes bend. However, when the force is released the specimen moves back into its original shape. Finally, the HC3DP

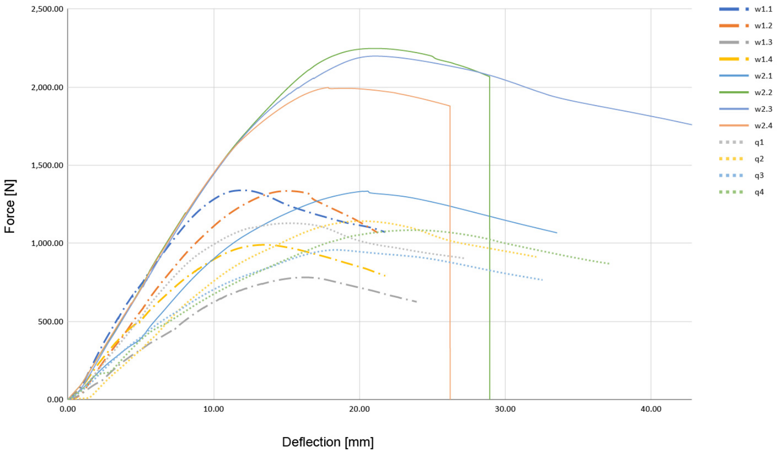

Figure 8.15: Results of 3PT bending tests.

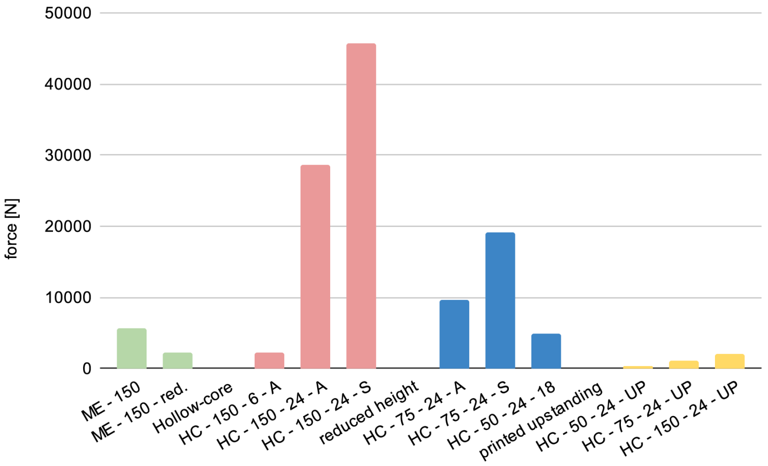

Figure 8.16: Results of 4PT bending tests. Green, regular ME 3DP with 6mm width. Red HC3DP with 6 and 24mm width. Blue, HC3DP 24mm with reduced specimen height in testing direction. Yellow, specimen fabricated in "upstanding" position.

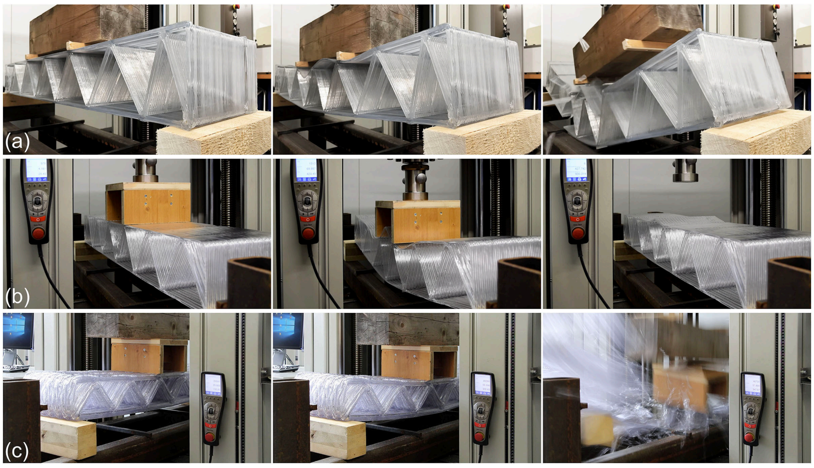

Figure 8.17: Different failure mode, depending on the chosen ME method and scale. a) ME, 6mm width, clean break tangential to the printing direction. Max. F. 5620N. b) HC3DP, 6mm width, the element buckles and moves back into its original position. Max. F. 2350N. c) HC3DP, 24mm width, elements shatters "catastrophic failure" after reaching a max. F. of 45800N.

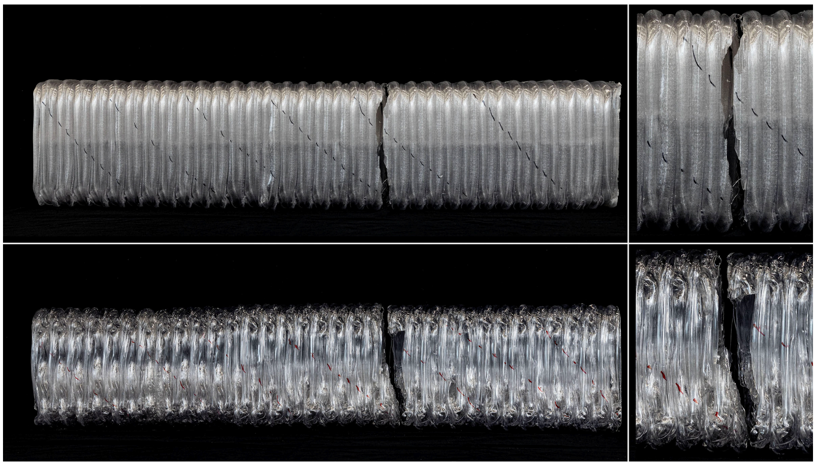

Figure 8.18: Failure mode of upstanding printed specimen. The failure does not occur as expected in between the layers, as known from small scale ME tensile testing.

specimen with a large cross-section fails catastrophically after reaching its maximum force load of 45800 N. This failure type is also observed for the large-scale 3PT bending test of HC3DP specimen, chapter 8.4.3. The influence of bead structure and sample geometry must be further investigated, as the reason for such failure remains unclear. For all HC specimens it is observed that the failures do not occur between single layers, and cracks do not propagate in between them. The failures rather occur in the thin walls, where material is not doubled up due to layer interfaces. This behaviour can be best observed in Figure 8.18, which shows the upstanding elements after testing.

8.4.5 Results facade height estimation

Figure 8.19 shows the results of the facade height estimations, with three zones indicating the amount of floor a 3DP facade can span, assuming a storey height of 3.5m. The results show that depending on the print strategy ME can be utilised for facades spanning a single storey. HC3DP at high resolution (6mm width) provides, as tested, only a maximum span of approximately 2.9m. For all "rotated" printed HC specimens with large-bead dimensions all specimens are sufficiently strong for a single floor application. With two types even reaching a three storey high element, based on the assumptions made. It is interesting to note that the specimens with a reduced structural height of 50mm are still sufficient to be applied as single storey tall facades. Upstanding prints represent the lowest possible span, and therefore could be only considered as elements that fit inside an existing structural system, like curtain walls. For both, ME-150 and ME-150-reduced a L_a of 0.4m is used for calculating the maximum span, for all other specimens L_a is 0.5m.walls

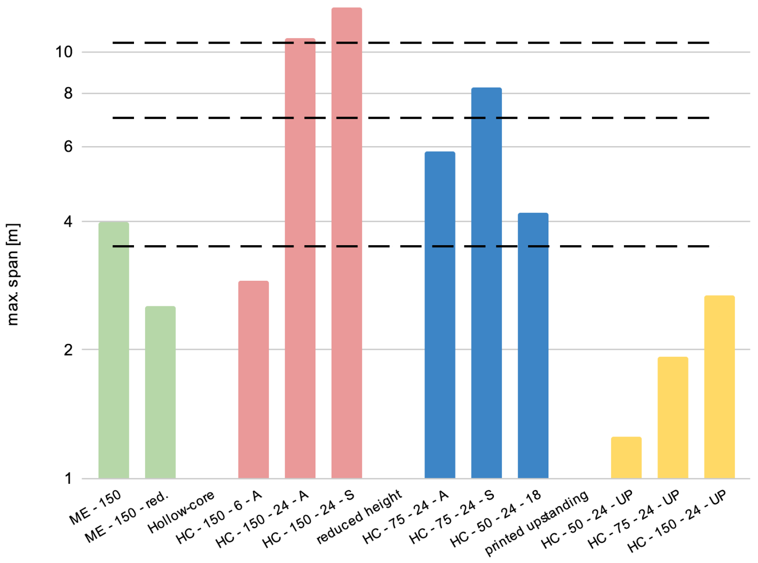

Figure 8.19: Results of the height estimation for a 3DP facade, color coded. Green: regular ME. Red: HC3DP at 6 or 24mm width and a structural height of 150mm. Blue: HC3DP at a width of 24mm and reduced structural heights. Yellow: HC3DP at a width of 24mm, printed upstanding.

8.5 Discussion

The material characteristic of 3DP specimens has to be examined in more detail in the future, which goes hand in hand with a more accurate calculation of the solar absorption rate and resulting maximum facade temperatures. New research on 3DP facades should focus on the spring as summer conditions, as those show the lowest tensile strength. It should be investigated how the material behaves at hotter climatic conditions, and if reaching temperatures that are close to the Vicat softening temperature of the 3DP material (79 °C), how to mitigate the heat build-up in a 3D facade system. Lastly, the tensile experiments should be repeated with thin wall HC prints, as the effects of warm, and cold environments might be more significant than for full cross-section prints.

In the context of 3D printed facades, the printing direction emerges as a critical factor in determining their structural behavior. The choice of whether to print the facade elements standing up or laying down depends largely on the mounting technique (whether it's top and bottom or side to side), but also on the feasibility of 3D printing the designed geometry in regard to printing features such as overhangs, or bridges. This decision is key to optimising the structural integrity and performance of 3DPFs, underlining the importance of careful planning and design in the 3D printing process of architectural elements.

The results obtained from the 4PT bending tests of the beams indicate that the structural requirements for facade application can be easily met by HC3DP. Regular ME, at a depth of 150mm, provides enough resistance to build elements of over four metres height. Especially for HC3DP, the panel depth, or infill density can be chosen by other requirements such as the thermo-optical properties. For larger projects where great spans must be reached, such as public buildings or event halls, HC3DP can provide sufficient structural capacity. To control the structural performance of a 3DP facade element, the structural height, the printing cross-section, as well as the infill density, can be varied. To improve, for instance, the mechanical behaviour of high-resolution HC3DP, the structural height of the element can be increased, or the infill density increased. Although the aspect of infill density has not been investigated in this manuscript, it most likely results in an increase in bending resistance. In addition, the catastrophic failure mode of the large-scale HC beams must be investigated and strategies to mitigate such failure mode. The high-resolution HC3DP beams failed due to buckling, and an ideal cross-section for HC3DP that allows for high load capacity and non-catastrophic failure must be investigated.

Although HC3DP showcased high maximum loading capacity, other construction related aspects of facades must be investigated, such as the creeping behaviour or impact testing. Also connection details for these low-resolution 3D printed objects with their undulated surface finish requires more investigations. In regards to connections, three main topics must be addressed, the connection to the built structure, the connection between single 3DP elements, as well as securing weather tightness. Finally, more research on HC3DP is necessary to investigate other facade relevant aspects, such as the airborne sound insulation, or the optical properties of HC3DP. Only if those structural and functional aspects are successfully investigated can HC3DP be applied in facade construction in the future.

In the absence of data on the structural properties of HC3DP elements, the cross-sectional dimensions and wall-thicknesses of the tested beads should be considered as an initial experimental set that must be refined based on the findings of this manuscript. With the extreme loading capacity tested, other cross-sectional dimensions that reduce material consumption, and improve maximum printing speed should be investigated.

In this manuscript the calculations regarding the maximum height for a 3DP facades system assume a linear support at the top and bottom. However, there are other common constructive methods to support facades, such as point supports. For such systems, new research must investigate if and how the behaviour of the 3D printed elements change under loading and whether there are other critical factors determining the performance of 3DPF such as peak stress at the connections.

8.6 Conclusion

This manuscript provides insight into the material characteristics of Hollow-Core 3D Printing and the structural behaviour of such elements, in comparison to large-scale pellet-based ME. The influence of varying temperatures is investigated and provides crucial insights on its influence on the mechanical properties of 3DP facades. Furthermore, experiments on different cross-sections for HC3DP indicate that the wall-thickness is the most important factor to influence the structural performance.

This manuscript provides insight into the material characteristics of Hollow-Core 3D Printing and the structural behaviour of such elements, in comparison to large-scale pellet-based ME. It can be concluded that off-the-shelf ME can be used to fabricate 3DP facades. However, their design and fabrication must adhere to certain minimal design guidelines like infill density, pattern, and panel depth. For HC3DP the design is less constrained, as even a panel with minimal depth (50 mm), without infill, is able to withstand sufficient load. The influence of varying temperatures is investigated and provides crucial insights on its influence on the mechanical properties of 3DP facades. Furthermore, experiments on different cross-sections for HC3DP indicate that the wall-thickness is the most important factor to influence the structural performance.

This manuscript furthermore emphasises the potential of large-scale HC3DP in architectural applications, particularly in the construction of facades. The experiments revealed an extreme loading capacity of HC3DP, making it suitable for applications with large spans. Besides the sufficient structural capacity for facade applications, further research trajectories such as weather-tight connection details, optical properties, and other facade-relevant properties are highlighted. The findings underscore the importance of planning and design for the 3D printing process, indicating that the choice of printing direction is critical in determining the structural behavior and performance of 3DP facade elements. Overall, the research presents HC3DP as a promising technology with the potential to improve current ME methods for facade application, enabling high-performance, site-specific facades that are both aesthetically unique and environmentally sustainable.

Acknowledgements

This research is financially supported by the National Centre for Competence in Research in Digital Fabrication, funded by the Swiss National Science Foundation (NCCR Digital Fabrication Agreement number 51NF40141853).

CONCLUSIONS AND FUTURE WORK

Contribution and discussion 9

9.1 Potentials of 3DP facades 183
9.2 ME and HC3DP for facade application 186

This thesis contributes to the growing field of AM for building envelopes by investigating how the 3D printing process of ME can be altered, overcoming current limitations of current ME processes for large-scale applications. Printing speed and material efficiency are key aspects when it comes to the production viability of 3D printing for construction. The presented work innovates the 3DP printing process of thermoplastics enabling the production of high-performance, material-efficient elements, at increased fabrication rates. It does so by introducing large-scale hollow, tubular beads that lead to improved cooling behaviour and, therefore, to significant increase in fabrication speed. The extrusion rate of HC3DP is competitive to state-of-the-art high-resolution 3D concrete printing methods.

The work presented in this dissertation furthermore demonstrates that the tubular bead structure improves facade related performances, such as thermal resistance, strength-to-weight ratio, and acoustic airborne insulation, compared to established ME methods. These aspects are of great relevance for high-performance designs.

HC3DP of high-performance and site-specific facade designs can be directly fabricated through the automated process of 3D printing, where customization is not directly related to increasing costs. With the introduction of large-scale HC3DP, the 3D printed element can be once again be designed by functional requirements, and not dictated by process limitations, as wall thicknesses can be varied and adapted.

The contributions of this thesis are categorized as follows :

- Investigating the potentials of 3DP facades and highlighting research gaps
- Developing a novel 3DP method tailored to facade construction.
- Understanding and evaluating the fundamental performances of 3DP for facades (ME and HC3DP)
- Evaluating the production viability of 3DP facades

The following chapter presents the contributions in more detail and discusses them through the lens of facade construction and architecture.

9.1 Potentials of 3DP facades

This thesis contributes to the field of 3D printing facades by offering a comprehensive overview of their design, fabrication, and assessment methods. It explores the challenges and advancements in computational design, fabrication processes, and performance assessment specific to 3D printed facades. The need for standardized design software, printing, and assessment tools is highlighted by the thesis, as well as the potential for new modeling approaches. Furthermore, it discusses the maturity and potential commercialization of 3D printing technologies for facades, emphasizing the shift towards commercially available systems and the potential for increased research activities and data sharing. With that, PAPER A provides a fundamental understanding on the potentials, limitations, and challenges of 3DP facades. However, this contribution must be understood as a *minor contribution*, as the main body of work of this thesis revolves around the conceptualization and development of HC3DP. Nevertheless, it lays the foundation for the interdisciplinary collaboration as research questions are identified based on the research gaps presented in this review. As the facade is understood as one of the most complex building systems, it is best addressed in an interdisciplinary research stream with different expertises involved.

3DP of facade elements using Material Extrusion has been identified as a field of interest opposed to earlier investigations [60]. The main reason for this opposition might be that ME did not have the sufficient scale to provide a viable solution for 3DPF before 2015. As elaborated in the introduction, the upscaling of ME to construction scale in an ongoing endeavour with major improvements over the last five years. Today, ME provides to opportunity to 3D print large-scale elements, using different materials, at increasing speed. This up-scaled ME method has been used to create facade prototypes at different scales. However, for the complexity of facade construction, state of the art research does not provide enough data to design and fabricate site-specific, and high-performance 3DP building envelopes. Although there is a great potential to fabricate facades through 3D printing, state of the art ME methods as shown in this thesis, result in material intense components, with mediocre performance, at relatively high printing times (Paper B).

The need for site-specific and high-performance facade systems is immanent and 3DP has been identified as a fabrication method that allows for the fabrication of multi-functional mono-materials elements. Thermoplastics can be seen as an abundant resource available anywhere on the planet. There is an untouched potential to create 3DP facade elements from locally sourced waste-streams. Thermoplastics need to be understood as a resource and not as a problem in themselves. The material's inherent properties, such as its versatility, durability, and recyclability, present significant opportunities for sustainable construction practices. However, the challenge lies in the way the material is managed and utilized at the end of life. Improper disposal and overuse have led to environmental concerns. By focusing on responsible production, usage, and recycling of thermoplastics, especially in 3D printing applications, their potential can be harnessed without exacerbating ecological issues. This approach transforms the perception of thermoplastics from being merely waste to a valuable, circular economy material, especially in the context of customized facade systems.

The potential of 3DP facades in terms of customization, complexity, and site-specificity has been outlined in the introduction. However, these aspects have not yet been sufficiently explored as research so far mostly focuses on the morphogenetic aspects of 3DP facades. The research conducted here is crucial for fully realizing the potential of 3DP facades by merging architectural vision with high performance. Design intentions can now be integrated with distinct functionalities, enabling designs that are not only novel in appearance but also high-performing and tailored to specific locations.

9.1.1 HC3DP development

This thesis makes several significant contributions to the state of the art in 3D printing technology. It introduces the innovative concept of hollow-core 3D printing (HC3DP) as a method specifically designed for large-scale 3D printing applications (PAPER C and D). HC3DP addresses the limitations of traditional ME approaches, such as scalability, material consumption, and extrusion rate, and offers a new dimension to large-scale 3D printing by using hollow, tubular beads. The system is based on off-the-shelf printing materials and off-the-shelf large-scale extrusion systems, often found in robotic large-scale 3D printing. This enables an easy adaptation of HC3DP at other research institutions to continue research on future research trajectories outlined in Chapter 10.

The thesis provides a comprehensive comparison of the extrusion rates for different printing setups, including off-the-shelf large-scale filament based ME, large-scale pellet-based ME, and HC3DP. This comparison highlights the competitive advantage of HC3DP in terms of extrusion rate and printing speed, demonstrating its potential to significantly enhance the efficiency of large-scale 3D printing processes (PAPER C). The fabrication method is validated for different materials showing the versatility of the printing method (PAPER C and F). This variety demonstrates that HC can be adapted to a large variety of polymers, including fibre-reinforced, as well as recycled materials.The manuscript additionally establishes a thermal cool-down model for large-scale ME and HC3DP (PAPER C), showcasing the superior cool-down rate of HC3DP. This analysis provides essential information on the thermal characteristics of HC3DP to clarify the physical phenomena of the improved cooling behaviour. This model can be used to calculate the minimal layer time, an essential factor for printing large-scale elements.

The manuscript describes the hardware and process development of HC3DP. The fabrication method is validated for different die geometries (PAPER C and D) for pellet extrusion, as well as small-scale filament-based 3D printing (appendix B). The introduction of geometry dependant air pressure values increases fabrication stability, allows for 3DP of non-tubular cross section (PAPER C and D), allows printing tight turns, and finally, enables the active control of the size of the printed cross-section. The introduction of dies with purpose-made cross sections creates a new research trajectory for large-scale HC3DP, expanding the design possibilities and functionality of 3D printed components. Furthermore, it was demonstrated that the cross-section of the hollow bead can be significantly varied during the printing process, from 16 to 32 mm (PAPER D). The research reveals the possibility of achieving multi-resolution 3DP without the need for a second extruder or additional hardware, expanding the capabilities of HC3DP technology.

Based on these developments, printing guidelines are proposed as well as process specific printing phenomena described. PAPER D demonstrates improved bridging behaviour for large-scale HC beads, due to increased cool-down. Another contribution of the research is the investigation of the post-inflation behavior of HC3DP beads, which is different from that of traditional ME. The research shows that although HC3DP layers can be squeezed down during the printing process, the inflation of the bead continues once the extruder moves along the printing path, resulting in strong deviation from the desired shape and remaining a challenge for non-planar HC3DP. This observation highlights the need for further research to fully understand the post-print inflation and achieve controlled results. Finally, this thesis offers valuable insights into the mechanical behavior of 3D-printed hollow beads with different die geometries, contributing to a deeper understanding of their structural performance. This aspect is discussed in more detail in Section 9.2.2.

Overall, these contributions significantly advance the state of the art in 3D printing technology by introducing a novel method for large-scale 3D printing, providing insights into its potential benefits, offering a comprehensive analysis on different aspects, and providing process guidelines to successfully HC3DP.

9.2 ME and HC3DP for facade application

In parallel to the print process developments, several key aspects for 3D printed facades are investigated, and contributions are made by investigating thermal resistance, structural capacity, and acoustic dampening effects. The investigations cover experiments featuring desktop 3D printing (FDM), large-scale pellet-based ME, and HC3DP. This methodology allows to compare HC3DP against other established ME methods.

9.2.1 Highly insulating 3D printed facades

This thesis provides a holistic overview on different ME methods and their thermal performance in relation to print time and weight/m2. The research on the thermal performance of polymer 3D printed facades was conducted on several scales, using different printing technologies. Starting with desktop scale ME, often referred to as FDM, then using large-scale pellet based extrusion, and finally, high-and low-resolution HC3DP (Paper B and Paper F). Large-scale experiments offer a deeper understanding of the thermal insulation properties of 3D printed objects with bespoke internal structures. The results show that HC3DP provides the best print time to u-value ratio, making it the fastest ME method to create highly insulating 3DP facades. FDM results due to the high printing resolution commonly in smaller infill cells. Those small cells sizes correlate to good u-values, but when printing objects at large dimensions, result in long print times per square meter (<190h). Pellet-based ME results in elements with a moderate u-value at reduced fabrication time. This is explained with the increased maximum extrusion rate of the extruder compared to FDM, 10kg/h instead of 0.25kg/h. This increase in material deposition rate comes with the reduction in print resolution as the layer height changes from 0.25mm to 2.5mm. Nevertheless, it was shown that in order to reach a moderate u-value (1.6- 1.1 W/m2K), elements with small cavity sizes need to be printed. Facade elements with a best u-value investigated in this research (ME - R3) needs 12 h/ m^2 to print and have a weight of 50 kg/m2. The results of PAPER B brought into question the production viability, and material efficiency of regular ME for facade construction.

Building upon these insights, HC3DP is proposed as a method to improve the thermal performance of ME for 3DPF. The results show improvements compared to regular ME for thermal performance, and print time reduction by up to factor 8. Furthermore, the thesis explores the combination of HC3DP with aerogel to create ultra-lightweight and highly insulating 3D-printed facade elements (Paper F). This composite does not permanently bond the material but promotes recycling of the polymer and reuse of the aerogel. This type of facade provides a u-value comparable to a triple-glazed window, but does not provide the same transparency. Nevertheless, compared to all other samples 3D printed samples, the aerogel HC prototype reduces the thickness of the panels by 50% (to 7cm) while maintaining high thermal resistance (<0.9W/m2K). It is shown that a square meter of such a facade can be 3D printed within under 2 hours and only weighs 12.6 kg/m2.

Overall, the thesis makes several significant contributions to the state of the art in the field of 3D printed facades and building envelope in regards to their thermal performance. Paper's C and F contributions advance the understanding of thermal performance in 3D printing for architectural applications and provide practical guidelines for designing energy-efficient 3D printed facade elements, with potential applications in sustainable architecture.

9.2.2 ME and HC3DP structural performance

This thesis provides a holistic overview on different ME methods and their structural performance in relation to print time and weight/m2. It contributes with a broad range of experimental data covering ME, HC3DP at high and at low resolution.

Tensile tests of ME samples are performed at different temperatures (-10, 20, 50 C) simulating different seasonal outdoor conditions. These experiments examine significant difference in maximum force taken (up to 14%) which is especially relevant for facade applications, as 3DP facades acts as the barrier between the in- and outside in changing environmental conditions. Furthermore, the temperature changes potentially influence other behaviours such as impact resistance in cold, or creeping for hot climate. In addition, the experiments prove that the layer orientation, respectively the printing orientations, plays a significant role for the structural behaviour of the elements. Depending on the chosen constructive system, either printing orientation, standing up or rotated, can result in preferred behaviour. These results are true for both, regular ME and HC3DP. 3PT bending tests of HC3DP speciment with large cross sections demonstrate that the internal bead reinforcements introduced in Paper C and D do not increase the maximum load but influence the ductility of the specimen. There was not significant difference in the maximum load taken between a neat and a reinforced bead. The wall-thickness of the tubular bead and the shape is found to play a more significant role.

The testing of large-scale beams revealed significant differences between ME and HC3DP in regards to their maximum load capacity. ME at a facade depth of 150mm, and an infill raster distance of 150mm, can take a maximum load of 5620 N, HC reaches 45800N with only 25 % more material, 12.5 instead of 8.9kg. HC3DP enhances the strength to weight ratio of ME 3DP elements as it increases the cross-section without increasing the material consumption significantly. The feature implemented in the specimen that exhibited the highest maximum force involves shifting the infill layers half a layer upwards relative to the contours (skin) of the 3D-printed element. Consequently, the round bead cross-sections of the infill lines consistently connect to two outline layers. This feature significantly increases the structural capacity of the beams, approximately by a factor of 1.8 compared to specimens without this layer shift. The experiments identified different failure modes of the large-scale beams, depending on the chosen printing process and scale. Both ME specimen failed brittle, the specimen with reduced infill bead width behaved more ductile than its regular printed equivalent. For HC3DP it was found that thin bead cross-sections (6mm) do not fail brittle, but buckle under load, which is potentially beneficial for facade applications. It was observed that the buckled element was just temporarily deformed and bend back into shape while the load was released. The HC specimen with larger cross-sections fail brittle, and as they take a significant amount of load, and shatter once the maximum force has been applied.

The development of HC3DP and the implementation of layer shifting makes 3DP facade elements possible without the need of supporting substructures. However, depending on the chosen constructive system, a different HC approach can be chosen, by using a medium bead cross section e.g. 15mm, or thinner panels (<150mm). PAPER E investigates HC3DP columns acting as load-bearing elements, supporting 3 meter cantilevering space frame structures. Although being detached from the research focus of 3DP facade, this demonstrator project pushed the technological readiness of HC3DP and acted as a stress test of the novel 3DP method. For the first time, elements of architectural scale are HC3DP and proved the viability of the method for large-scale applications.

9.2.3 ME and HC3DP acoustic performance

The specimen described in PAPER B and PAPER F are reused for measuring the airborne sound insulation and calculating the R_w value for each sample, see appendix A. For regular pellet-based ME it was shown that the cavity number and size, although influencing the thermal insulation, has no effect on R_w and frequency-dependent insulation. The HC3DP specimen show, depending on the chosen cross-section and panel depth, a better sound insulation, with R_w values of up to 42 compared to 37. Furthermore, the highly thermally insulating aerogel HC3DP panel was measured with and without aerogel filling. However, although improving the thermal resistance significantly, the airborne sound insulation is not influenced by the granular aerogel. This study is a first endeavour to asses the acoustic performance of ME and HC3DP facade elements. In general the results show similar R_w values to glazing, making them a viable alternative in such applications.

Table 9.1: Summary table stating the performative aspects of 3DP facades, based on the geometries tested. Please refer to PAPER F for visual representation of the samples. Values are either provided by sample type or m^2

type	panel depth [mm]	weight [kg/m2]	print time [h/m2]	cost production [CHF/m2]	U-value [W/m²K]	R_w [dB]	max. span [m]
FDM	50	18.00	181.00	9,688	0.93	n.a.	4.64
ME-6-150	150	34.12	11.95	938	1.65	35	4.46
HC-6-150	150	17.84	2.57	307	1.43	33	2.9
HC-24-150	150	23.75	3.54	414	0.88	42	12.7
HC-24-75-AF	75	12.67	1.53	306	0.86	35	4.2

9.2.4 Production viability of 3DP translucent facade elements using ME

The production viability of 3D printed facades is determined by the production time, the cost associated to production, and the expenses of feedstock material. This thesis contributes by establishing an initial production viability matrix using these criteria. To do so, based on the findings on improved thermal cool down and the resulting theoretical cool-down model of PAPER C, PAPER F establishes a realistic maximum extrusion rate for regular large-scale ME and HC3DP. This model allows to calculate the print time per square-meter of a 3D printed facade using a upper and lower boundary for the maximum extrusion rate. The cost of material can be calculated based on the volume of such facades, and the performance of these 3DP elements can be associated to the specific ME method used (PAPER B, F, G, Appendix A).

It was shown that for filament-based ME (often referred to as FDM), even for large-scale 3D printers in this category, the print time for one square meter of facade requires approximately 190 h, to reach a meaningful structural performance. The ME specimen investigated in PAPER B, with u-values ranging from 1.65 to 1.1, the print time is approximately 12 h/m2. For these samples, printed with regular ME, the fabrication time is limited by the material cool-down and not the maximum extrusion rate of the extruder, therefore improved thermal insulation does not come at increased fabrication speed. However, the material consumption increases significantly. HC3DP shows significantly shorter production times, depending on the chosen cross-section of bead, and printed geometry ranging from 4 to 1.5h, due to the improved cooling behaviour. Being able to print one square-meter of insulating, structurally sound, and acoustic insulation facade element in under 2 hours can be seen as a game-changer when it come to 3DP facades and opens up new research trajectories, as elaborated in Chapter 10.

9.2.5 Design of future HC3DP facades

To revolutionise future facade design using 3DP, designers must shift from relying on predefined facade products or discrete building components. Instead, they should focus on how material-efficient designs can achieve optimal performance tailored to specific global climates, local conditions, building typologies, and use-cases. This approach requires considering various scales in 3DP facade design. Local climate conditions set initial design parameters, which are then refined by other factors like building orientation and surrounding structures. Additionally, variations in the building's vertical volume, such as connections to the ground or roof and material reduction on higher floors, should be considered.

While the benefits of adapting construction schemes to environmental conditions within a single building are recognized, they are seldom implemented. This is often due to the increased complexity and resulting need for more subcontractors, diverse material systems, and thus, heightened on-site complexity. However, 3DP offers a solution by enabling these adjustments through a single fabrication process, potentially using a unified, mono-material construction scheme. This not only simplifies the process but also opens up new possibilities for innovative, efficient, and context-sensitive facade design.

Finally, as 3D printing allows for the fabrication of bespoke elements without external moulds, or tooling, it is currently best employed for freeform architectural design, or non-repetitive elements within a building envelope. Compared to current ME methods, HC3DP allows for an even higher level of adaptability, as the hollow cross-section can be chosen and varied depending on the design or performance requirements. Furthermore, with its increased structural capacity HC3DP enables the fabrication of freestanding structures with large-spans, without the need for secondary substructures. This fact promotes two things: first, the design freedom increases, and secondly, the aspect of mono-materiality is strengthened. The design freedom is extended compared to off-the-shelf ME systems due to the increased layer variability (cross-section) and the possibility of using different extrusion profiles (shape). Furthermore, depending on the chosen cross-section, the achievable printable overhangs can be increased, or beads can even be printed in air. These aspects, especially when combined, provide a broad range of new design possibilities that must be investigated in the future.

For now, two conclusions can be drawn. First, HC3DP can directly supplement existing fabrication techniques if used at a resolution comparable to massive ME. Established overall design strategies, or connection details can be maintained if the bead cross section is not significantly changed from current standards, like a bead width of 6mm. In such cases HC3DP, can be understood as a replacement of an existing and established fabrication technique that simply increases fabrication viability and performance of the components. To what extent the increased cross-sectional diameter, also presented in this thesis, will influence the design of 3DP facades is still to be investigated. For now, the experiments of this thesis display a new language of low-resolution 3D prints, made from thermoplastics that are in line with the promise of synthetic materials in architecture, such as lightness and transparency, fabricated at a fast pace, finally rendering them affordable.

Future work 10

10.1 Category 1 191
10.2 Category 2 193
10.3 Category 3 194
10.4 Category 4 195

Multiple new research trajectories must be explored to develop a more reliable, performative, and sustainable production scheme based on the HC3DP. Future research topics, identified from this thesis, will facilitate the adaptation of HC3DP for real-world construction projects, such as 3D printed facades. These novel trajectories can be categorized as follows:

category 1
- increase technological readiness and promote industry transfer

category 2
- facade related research

category 3
- investigate the aspects of sustainability of HC3DP

category 4
- explore novel application of HC3DP

10.1 Category 1

The first research trajectory focuses on advancing the technological readiness of HC3DP, aiming to enhance process stability and ultimately facilitate its transfer to industry. Achieving this requires improvements in hardware, materials, and software.

10.1.1 HD nozzles

Changing the nozzle design and its manufacturing process, described in this thesis, can help improve the reliability of the 3D printing process and allow for the extrusion of high-performance polymers. Although 3D printing of aluminum is sufficient for creating a prototypical fabrication setup, CNC-machined corrosion-resistant, high-strength metal alloys will make the nozzle more robust and increase the maximum extrusion temperature of the HC printing setup. High-performance polymers like PSU, or PEI have high melting temperatures of approx. 350C, and the yield and ultimate strength of aluminum decreases significantly in the range from 200 – 350°C [312]. Therefore, to allow for the extrusion of high-performance polymers an e.g. cnc-machined steel nozzle is needed. In addition, a precisely machined nozzle will allow for more accurate control over the extrusion diameter. Now, with 3DP aluminum, the minimal feature size and wall thicknesses are dictated by fabrication limitations and not by the desired cross section of the 3DP bead. However, this requires multipart assemblies where sealing will be a challenge, as the 3DP process requires high temperature and pressure.

One limitation found in this research is the static tool orientation during the printing process. As the large-scale extrudate needs to twist around the center of its cross-section during a change in printing direction, there is risk of print inconsistencies. Sharp corners in the print path can cause a collapse of the internal geometry, which can lead to over-inflation, reduce print quality, or print failure. In traditional 3DP setups, the nozzle has a fixed position in relation to the extruder with no possibility of being adjusted. For the experimental setup used in this thesis, the orientation can only be controlled by changing the pose of the robotic arm, and therefore can only accommodate minor tolerances. For nearly all toolpaths, a free-rotating nozzle would improve the printing quality and reduce the risk of print failures. Furthermore, by controlling the rotation of the extrudate, the orientation of the internal reinforcements can be controlled as well and, therefore, continuous cavities of the printed object can be achieved.

10.1.2 Printing material

Another aspect of improving the stability of the HC3DP process is the 3DP feedstock. Currently, the materials used for the experiments are off-the-shelf compounds for large-scale ME. For HC3DP, new compounds need to be investigated that are specifically made for the thin-wall 3D printing process. Future research needs to investigate if blow-mold graded polymer blends are improving the printing process, allowing for thinner wall-thicknesses, or faster extrusion rates.

10.1.3 Fabrication-informed modeling

An integrated design tool which allows for optimization of HC3DP, and automation of the design-to-fabrication workflow must be developed. The tool should integrate the specific fabrication constraints and possibilities of HC3DP, like minimum features size, or overhang angles and provide optimal print-strategies. Furthermore, strategies to compensate the deformation of the large-scale 3DP elements must be investigated and integrated into the design tool. For instance, scaling factors for the 3D geometry, as known for other 3D printing technologies, must be determined and incorporated.

10.1.4 Advanced fabrication control/closed-loop

Strategies to actively control and monitor printing parameters during fabrication must be investigated. A closed-loop process control in manufacturing refers to a control system in which the output of a process is continuously measured and used to adjust the input to the process. This creates a feedback loop that allows for real-time adjustments to be made to the process in order to maintain optimal performance and improve efficiency. In closed-loop process control for HC3DP for instance, sensors to measure the output of the process, such as the temperature or shape of the extrudate can be integrated. This measurement is then compared to a set point or target value, and any deviations are used to adjust the input to the process, such as the flow rate of the material, external cooling, and the air pressure. Due to the delicate AM process, based on large-scale and thin-walled tubes, a close-loop manufacturing process will have a great impact on the process stability, enhance the quality, and finally extend the range of printable geometry.

10.2 Category 2

The second research trajectory tackles open questions related to facade construction. Here, two subcategories are identified: a) general research on using thermoplastics for facades, and b) HC3DP specific research for 3DPF.

10.2.1 Plastics in facade construction

The 2017 Grenfell Tower fire, which burned for 72 hours and marked the largest fire in the UK since World War II, highlighted the dangers of using plastic as thermal insulation [313]. This incident significantly altered the perception of plastic as a safe building material, partly due to the fire's rapid spread, exacerbated by a cladding system that failed to comply with standards and regulations. New research is imperative to explore methods for enhancing the fire resistance of 3DP thermoplastic facade elements. Three critical aspects of fire safety to be addressed are the development of smoke during a fire (which affects safety during evacuation), the dripping of burning plastic (contributing to fire propagation downwards), and the intensity of flames (affecting fire spread upwards). Different strategies need to be investigated to address these distinct challenges. Potential approaches include improving materials with additives or coatings, integrating sensing devices into panels for rapid fire detection and extinguishment, and employing constructive measures to hinder fire propagation.

To provide sufficient longevity, 3DP facades must resist degradation through weathering and UV light. A recycling scheme must provide a cradle to cradle approach for 3DP facade construction. Recycling should be tested for either elements that have been exposed to direct weathering or those which have been artificially aged. Today, most studies on recycling of polymers investigates the direct recycling after 3D printing, and does not account for the harsh environmental changes a 3DPF encounters throughout its lifetime.

10.2.2 HC3DP future facades

The research presented in this thesis encompasses a broad spectrum of facade performances. However, to be applicable for real-world facade construction, other relevant topics must be addressed additionally.

Although it was shown that HC3DP creates elements with increased structural performance, the impact resistance of HC3DP elements needs further investigation. Depending on the wall thickness of the 3DP bead, the impact resistance might not be sufficient for facade applications and should therefore be considered when choosing the wall thickness for printing. HC3DP offers enhanced visual clarity compared to conventional ME because it reduces the number of layer interfaces. However, this increased clarity is not comparable to that of float glass windows. Visual comfort is crucial in our built environment, yet the extent to which the two systems can be combined remains unexplored.

The typology in which HC3DP facades can be deployed is not investigated yet. Either HC3DP elements are inserted into existing stick facade systems, or the elements are designed to perform as long-spanning self-supporting facades. The choice of constructive system has further implications on the design, print strategy, and connection details of the HC3DP facade elements. As showcased in this thesis, the structural performance of HC3DP is sufficient for both application scenarios and therefore both typologies require further investigations. The thesis has yet to explore the connection systems of either typology, which is crucial for the air and water tightness of 3DPF systems. The challenge lies in the low printing resolution, characterized by a round bead structure that is difficult to seal effectively against air and water. Investigating the extent to which traditional gaskets can seal the undulating sections of HC elements is necessary, along with strategies to flatten the inflated beads. The chosen facade typology and connection details will significantly influence the overall design strategy of the HC3DP facades system. There is a need for design research to investigate the low-resolution polymer 3D printing approach and its associated design possibilities. To date, besides the columns presented in Chapter **??**, only basic shapes have been printed. This research should expand the design space, not only in terms of design freedom but also in regard to creating site-specific designs, including the design of opaque and translucent facades.

10.3 Category 3

Category 3 summarizes future research activities related to the sustainability of HC3DP, driven by Life Cycle Assessment (LCA), recycling, and cradle-to-cradle principles. Additionally, it encompasses the design and fabrication of performative building elements. These components must work together to provide a holistic sustainable fabrication method.

The benefits presented in this thesis in regards to material savings, increased printing speed and improved thermal resistance have positive impacts on the energy consumption during fabrication (grey energy) but can also potentially reduce the energy consumption during the life-time of a building (operational energy). These aspects need to be investigated to quantify the actual benefits, in comparison to ME and traditional thermoplastic facades.

In general, the integration of circularity aspects of 3DP materials in construction is missing. For now, insufficient data of LCA of large-scale 3DP polymer elements in real-world environments is identified as a big research gap. Without this knowledge, arguing about potential benefits of lightweight, bespoke, and site-specific designs are overshadowed by the negative perception of plastics in construction. Similarly, the topic of sustainability is not fully understood and addressed yet. Although there is research on alternative bio-plastics and polymer recycling these researches are not tailored to facade elements that are exposed to outdoor changing environments for a longer period and therefore material degradation is unknown. The possible recyclability of 3DP plastic facades need to be investigated thoroughly by either using element that have been exposed to weathering for a longer period of time, or have been artificially aged.

10.4 Category 4

The fourth category revolves around fundamental research with exploration of different scales of HC3DP, spatial 3DP approaches, or multimaterial extrusion. The goal is to find new applications for HC3DP, not strictly related to the construction sector, or other than building envelopes.

To extend the possibilities of HC3DP a range of new extrusion profiles must be tested to understand limitations in size, and the potential of complex profiles. The implications of printing large-scale (over 50 mm diameter), asymmetric, or thin-wall extrusion profiles must be understood. The extruded wall thickness has a direct impact on the extrusion speed, cooling rate, and material usage and can therefore have a positive effect on the final component. Furthermore, explorations with non-round orifices has not been conducted yet. These efforts will extend the design possibilities and functionalities of HC3DP, that might bring this technology beyond the possible application for 3DP facades. In this manuscript the focus lies on scaling up the 3DP process for construction application. However, other disciplines like the medical technology industry might benefit from tubular 3D printing with watertight channels for instance for fluid transport. This requires investigation on 3DP with other feedstock materials that are bio-compatible or biodegradable. Furthermore, for this application the focus must shift to small-scale 3D printing.

Spatial extrusion has been investigated by different researchers and is also used by the startup Branch Technology to create bespoke concrete formworks. The printing speed of spatial extrusion is limited by the cooling rate of the free standing/spanning beads and could be dramatically sped up using HC3DP. Furthermore, HC3DP holds the potential for multi material extrusion. Two scenarios can be imagined, where either the hollow-sections of the bead are filled with e.g. an insulating material during the printing process, or that different sections of the extruded plastic are extruded using two different, but compatible polymers. The differentiation, as well as co-extrusion of materials will required new tool and control system developments.

APPENDIX

A

Sound insulation of HC3DP and ME

A.1 Method 200
A.2 Results 200
A.3 Discussion 201

Facades are the primary barrier between the internal environment of a building and the external world. Effective sound insulation in facades helps to reduce the amount of external noise, such as traffic, construction, aircraft, and urban activity, that enters the building. This is particularly important in densely populated or urban areas. Appendix A documents the current state of a journal paper in preparation investigating the sound borne insulation of ME and HC3DP elements. The specimen described in PAPER B and PAPER F are used for measuring sound insulation and calculating the R_w value for each sample. The term R_w in sound insulation refers to the *Weighted Sound Reduction Index*. It is a single number value used to rate the effectiveness of a material or construction assembly (like a wall, door, or window) at reducing sound transmission. The R_w rating is determined through laboratory testing where a material or assembly is subjected to a range of frequencies typically found in speech (125 Hz to 4000 Hz). The experiments of this paper are conducted a in an airborne sound test facilities, located am EMPA, Switzerland. The testing facility consists of two rooms separated with a replaceable framework for inserting specimens, see Figure C.2 and Figure A.3. The R_w rating simplifies comparing specimens as materials perform differently across various frequencies, by providing a single averaged number. A higher R_w rating indicates better sound insulation. For example, a wall with an R_w of 50 dB will be more effective at blocking sound than a wall with an R_w of 30 dB. To understand the R_w rating better, it's important to consider how sound reduction is measured and perceived. The R_w rating is measured in decibels (dB), which is a logarithmic unit used to describe a ratio of sound intensity. An increase of 10 dB in sound intensity represents a tenfold increase in sound energy, but is perceived by the human ear as roughly a doubling of the loudness.

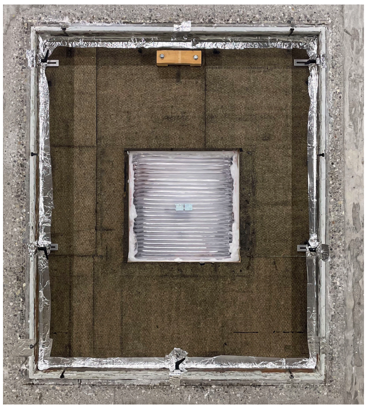

Figure A.1: 3D printed element installed in wooden frame. Element size 500x500x150mm.

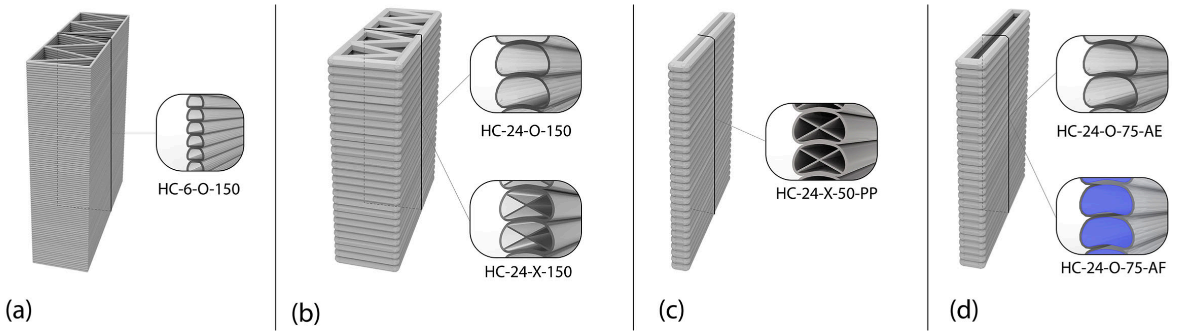

Figure A.2: HC3DP specimen. (a) HC-6-O-150, panel with 150mm thickness and identical toolpath to R1. (b) HC-24-O/X-150, panel with 150mm thickness, printed with tubular section and with internal reinforcement. Wall thickness HC-24-O-150 2mm, HC-24-X-150 1mm. (c) HC-24-x-50, panel with 50mm thickness, no air cavity. (d) HC-24-O-AE/AF, panel with 150mm thickness, empty and filled with aerogel.

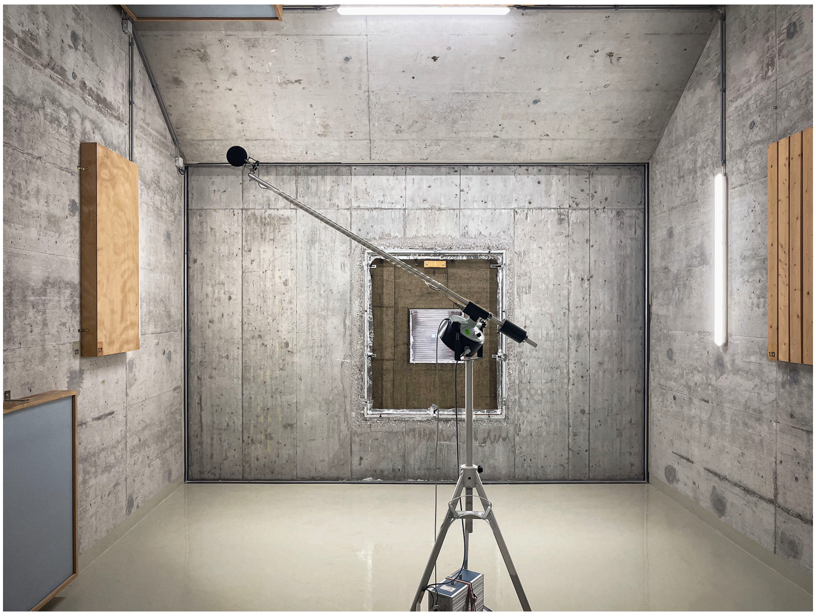

Figure A.3: Testing facility with specimen installed.

A.1 Method

The 3D printed specimen are placed frame within an opening between two rooms, the source room where sound is generated and the receiving room where the sound level is measured. After a first measurement, a second measurement is conducted with the rooms switching function; the source room becoming the receiver and vice versa. A range of sounds at different frequencies, typically between 125 Hz to 4000 Hz (covering the range of human speech), is produced in the source room. The sound level (intensity) is measured in both rooms. In the source room, the sound level is measured to know how much sound is being generated. In the receiving room, the sound level is measured to determine how much sound is passing through the test material. The difference in sound levels between the source and receiving rooms is calculated across the range of frequencies. This difference indicates how much sound is being reduced by the material or construction element. In total nine specimen have been tested, three ME specimen, and six HC3DP specimen including the aerogel filled one. Figure C.5 provides a diagrammatic overview of all samples printed with ME, and Figure C.1 for HC3DP.

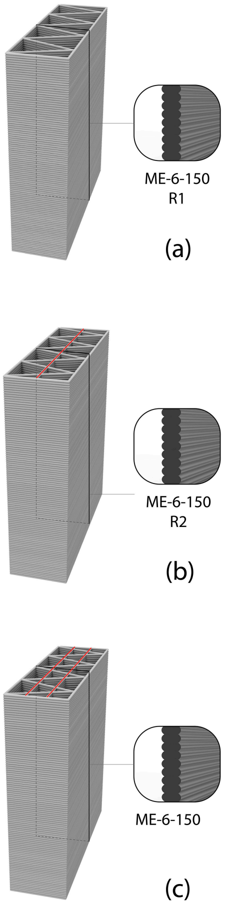

Figure A.4: ME specimens with 150mm thickness. (a) R1 with ones cavity, depth 150mm .(b) R2 with two cavities, depth 75mm each.(c) R3 with three cavities, depth 50mm each.

A.2 Results

For regular pellet-based ME it was shown that the cavity number and size, although influencing the thermal insulation, has no effect on R_w and frequency-dependent insulation. The specimens (R1, R2, R3) with increasing infill density, perform nearly identical. The decrease in cavity size does not influence the R_w, nor the increasing material consumption, Figure A.5. The HC specimen with 6mm extrusion width (HC-6-O-150) and identical geometry to R1, performs nearly identical to R1, with the sound insulation curve being slightly shifted to higher frequencies. Although, HC-6-O-150 show similar performance as R1, it has half the weight of it.

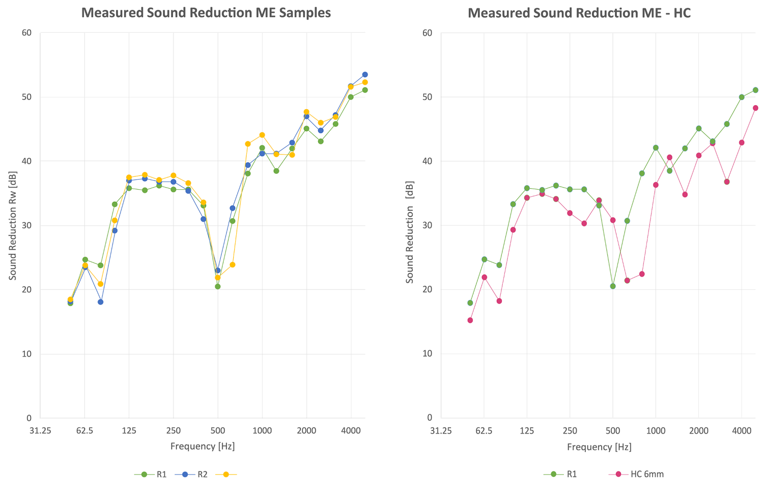

Figure A.5: Left: measured sound reduction for all ME samples. Right: measure sound reduction for ME and HC specimen with 6mm bead width.

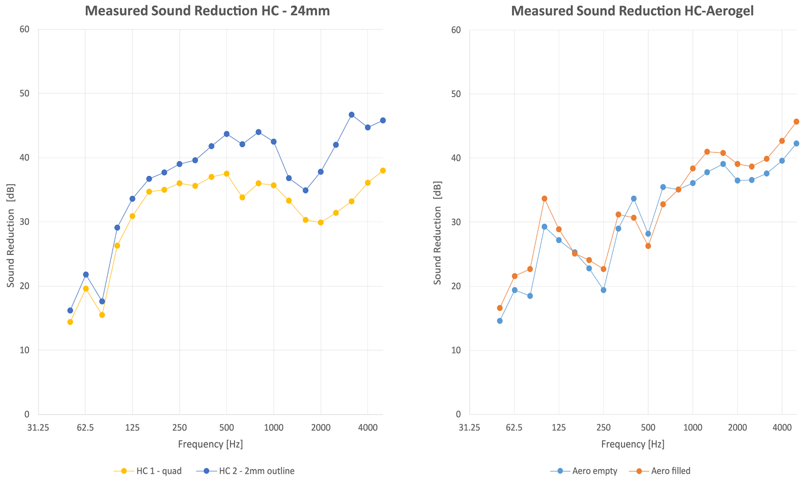

Figure A.6: Left: measured sound reduction for 24mm bead width, HC3DP. Right: measure sound reduction for aerogel filled and empty specimen.

The HC3DP specimen show, depending on the chosen cross-section and panel depth a better sound insulation, with R_w values up to 42 compared to 37. For HC with printed with large cross-section (24mm) the one with the 2mm wall thickness has a higher R_w value than then one with internal reinforcements. Furthermore, the highly thermally insulating aerogel HC3DP panel was measured with and without aerogel filling. Although improving the thermal resistance significantly, the airborne sound insulation is not influenced by the granular aerogel Figure A.6.

A.3 Discussion

Figure Figure A.8 compares all 3D printed specimen, ME and HC, in regards to their R_w value and $weight/m^2$. In addition, the graph states several triple-glazed windows with a broad range of R_w values and $weight/m^2$. Overall, HC3DP provides a moderate airborne sound insulation of 35 R_w for lightweight facade systems ($< 15kg/m^2$), which is approximately half the weight of triple-glazed windows. Higher R_w values for HC can be achieved with larger cross-sections at a comparable weight to current methods ($>45kg/m^2$). Figure Figure A.7 provides the

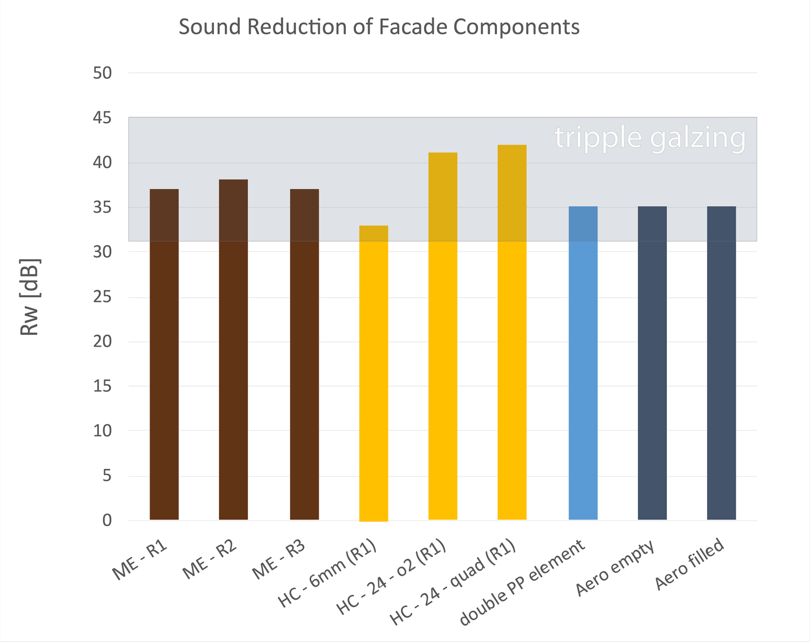

Figure A.7: Comparison of all tested specimen (ME and HC3DP) in relation to the sound insulation range of tripple glazed windows.

R_w values for all printed specimen, ME and HC3DP. HC3DP with large-cross section are the best performing. However, all 3DP samples fall within the range of current, non-specialized, triple-glazed windows.

To conclude, the printing method, design of the facade, and cross-section of the 3DP bead define the range of possible R_w values and can be therefore tailored to local boundary conditions. High-resolution HC3DP provides good sound insulation at minimal weight, larger cross-section allow for higher insulation but result in heavier components. How HC3DP can be tailored to improve airborne sound insulation without increasing the material consumption significantly is still to be investigated. This study is a first endeavour to asses the acoustic performance of ME and HC3DP facade elements. In general the results show similar R_w values to glazing, making them a viable alternative in such applications.

Contributions This research has been conducted in collaboration with Valeria Piccioni (Architecture Building Systems, ETH), Nino Blumer and Stefan Schoenwald from the Laboratory for Acoustics / Noise Control, EMPA.

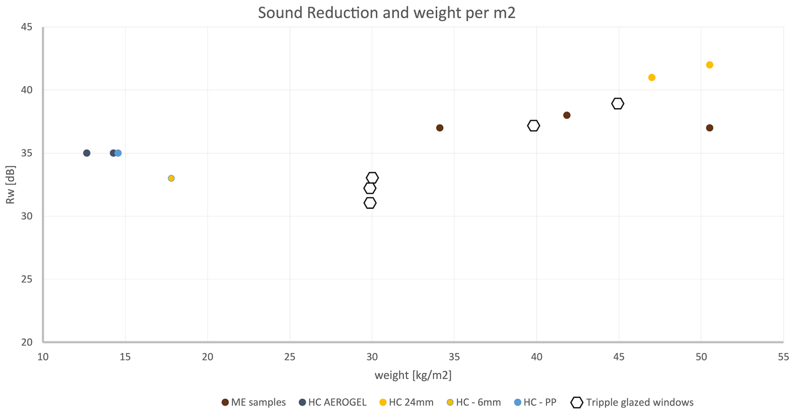

Figure A.8: The graph displays the sound insulation in relation to the weight per square meter.

B

Filament-based HC3DP

The following appendix documents explorations that have in conducted during the preparations for the semester project of the Master of Advanced Studies ETH in Architecture and Digital fabrication (SS 2023). The course introduces the students to the process of HC3DP and teaches bespoke tool-path design for robotic 3DP. The fabrication setup described in PAPER C and PAPER D, has been scaled down to be compatible with filament-based extruders, mounted on collaborative robots (UR5 and UR10). The goal of the course is to familiarize the students with the concept of robotic ME, in particular HC3DP, and explore the design potential of low-resolution HC3DP. The change in resolution, and increased cool-down behaviour is explored through a series of physical prototypes. Different concepts are investigated such as add-on 3D printing, large-scale interlocking elements, patterns and ornaments.

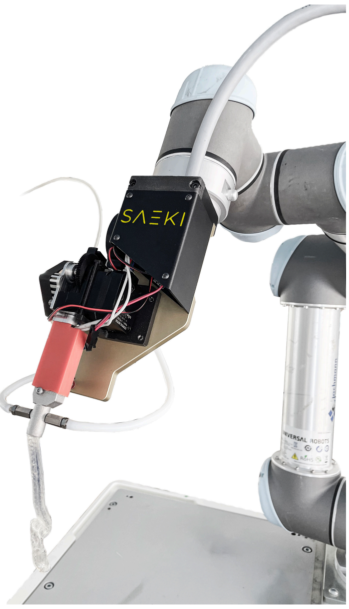

Figure B.1: UR-5 co-bot with a filament-based HC3DP system attachted.

The HC3DP filament extruder consits of off-the-shelf components, such as an E3D Titan AERO extruder and a E3D super volcano hotend. Futhermore, bespoke elements such as a 3D printed nozzle made from aluminum with an orifice of 10mm and a wall-thickness of 1mm. The internal air pressure is facilitated using a 24v fan. These extruders are mounted on collaborative robots with a reach of up to 1.3 m. The figures document initial design explorations conducted during the preparation of the MAS T2 semester project that resulted in the exhibition Protoplasto, see section 6.

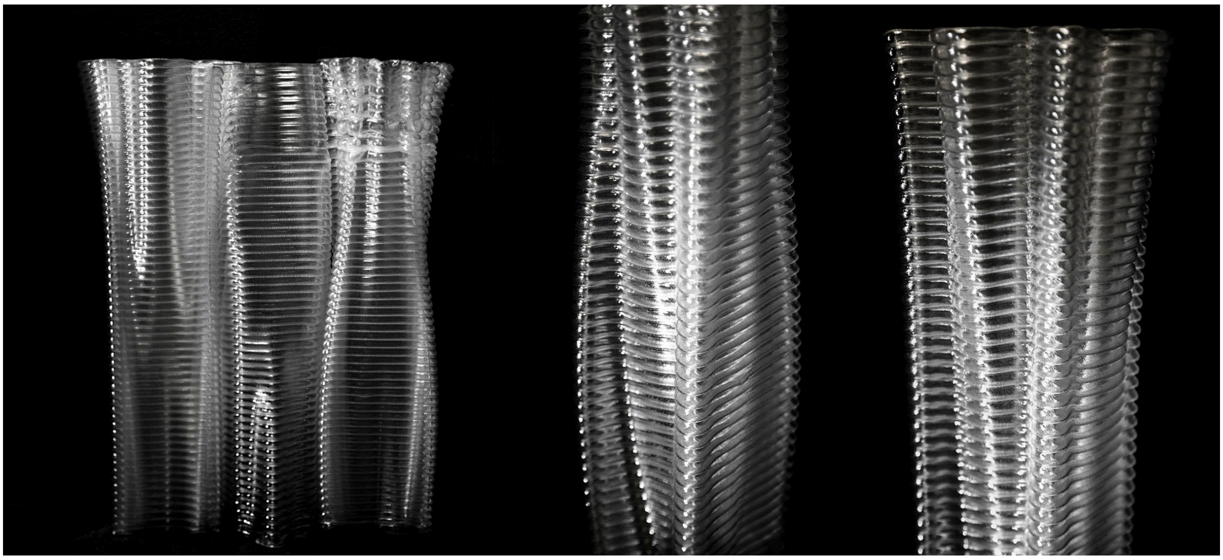

Figure B.2: documents an array of vertical elements that interlock through their geometrical articulation and creates a wall-like elements. These single elements are approx. 1.2 m high.

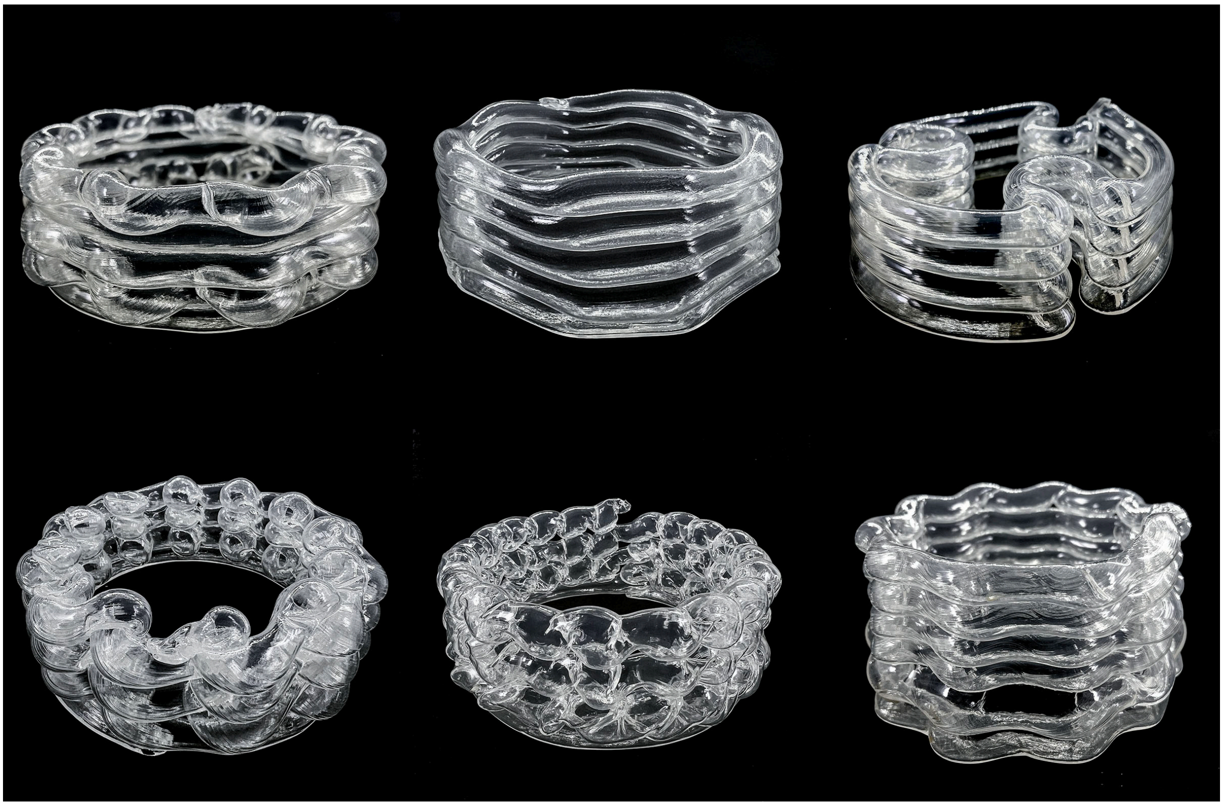

Figure B.3: Studies on different print patterns evoked through direct toolpath-planing. Incorporating pausing, differentiated speeds and extruder velocities.

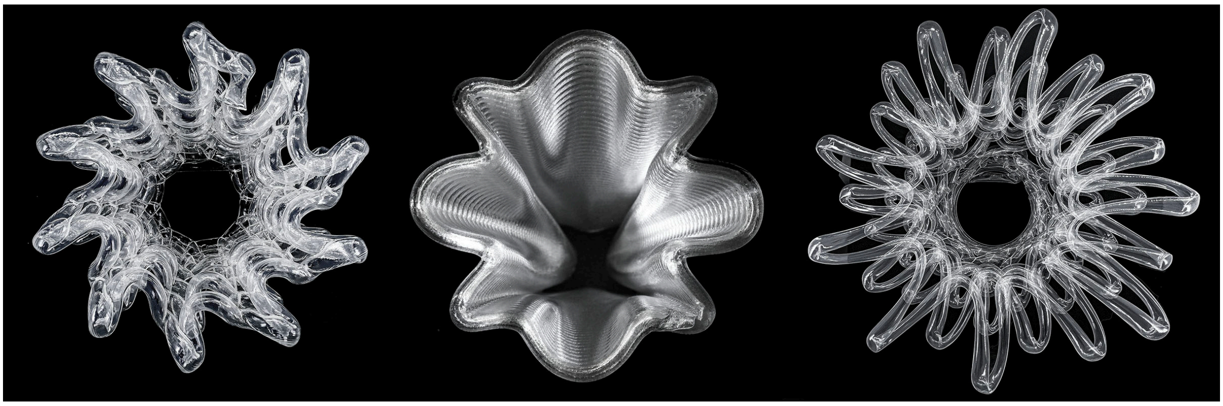

Figure B.4: Studies on cantilvering structures and extreme overhangs.

Credits

Digital Building Technologies, ETH Zurich

Tutors: Matthias Leschok (Project lead), Marirena Kladeftira, Nik Eftekhar

Design Development: MAS ETH DFAB 22-23 STUDENTS: Eleni Alexi, Adam Anouar, Ana Ascic, Keng Chia Chang, Xue Chen, Po Yen Chen, Ahmed Elmeraghy, Caitlin Emily Gallagher, Yixiao Huang, Yi Hsiu Hung, Chenming Jiang, Lihin Karunadhipathi, Joseph Kenny, Man Ki Ian Law, Ramon Lopez Moldano, Nijat Mahamaliyev, Abhipsa Pal, Carl Pantos Conquilla, Etienne Pavoncello, Huang Su, Lee Yo Cheng, Zhuo Zhang

C

HC3DP formwork for concrete

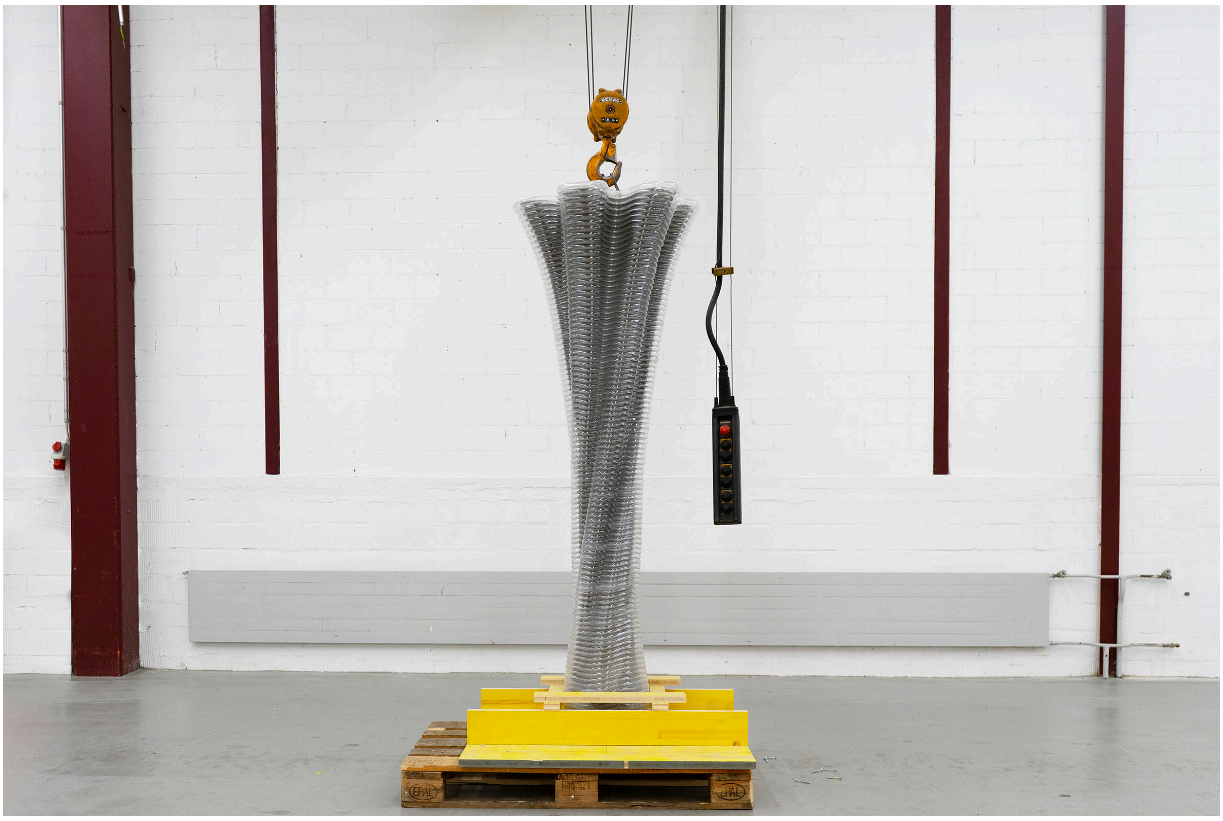

Figure C.1: 2.1 m tall concrete column cast into HC3DP formwork.

3D printed formwork facilitates the creation of complex, customized elements that would be challenging, time-consuming, and costly to produce using traditional methods. The benefits of 3D printed (3DP) formwork are manifold, it can potentially reduce waste during production, significantly lower labor costs, and shorten construction time. Additionally, it enables architects and engineers to pursue innovative designs and material-efficient structures. The adoption of 3D printed formwork exemplifies the integration of digital fabrication technologies into the traditionally conservative construction industry.

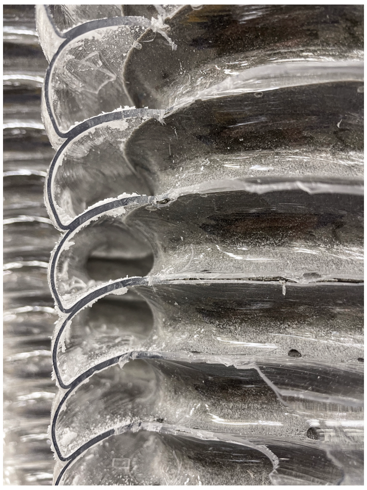

Figure C.2: Close-up during demolding of HC3DP formwork.

HC3DP formwork for concrete shares similar advantages to those highlighted in earlier chapters when compared to off-the-shelf ME methods. Improvements in printing speed and material efficiency potentially allow for the fabrication of HC3DP formworks at competitive prices. The price-driven construction sector, in particular, stands to benefit from the availability of large-scale lightweight elements. Due to its excellent weight-to-strength ratio, HC3DP formwork could potentially be easily managed on-site, reducing the need for extensive falsework.

In contrast to prior research, either a set-on-demand concrete must be employed for the thin-walled 3D formwork to be adequately stable [314], or, as in the case of thin-shell water-dissolvable 3D printed formwork, the formwork was temporarily reinforced during casting, especially at the bottom where hydrostatic pressure is highest [315]. HC3DP formwork combines the advantages of both systems: the material-efficient 3DP formwork system with wall thicknesses of 1mm and below, and the ability to use standard concrete mixes without the need for additional reinforcements.

[314]: Burger et al. (2020), 'Design and Fabrication of a Non-standard, Structural Concrete Column Using Eggshell'

[315]: Leschok et al. (2019), 'Dissolvable 3DP Formwork Water-Dissolvable 3D Printed Thin-Shell Formwork for Complex Concrete Components'

C.1 Results

Figure C.4 displays the successfully casting of a 2.1 m tall column using self-compacting concrete into a HC3DP formwork. The formwork was printed from PETG in 4.5 h and weighs only 9.6kg. The cross section of the bead is 24x19 mm at a wall thickness of 1 mm. Despite the thin wall bead cross-section, the HC3DP formwork was able to widthstand the hydrostatic pressure during the casting process. The volumne of concrete cast is 200 l, resulting in approximately 500 kg of concrete. As the formwork was printed a single element, the formwork needed to be cut and broken and could not be reused. The HC3DP formwork results in a unique surface texture with shiny surface finish. The texture resembles the negative imprint of a concrete 3D printed structure.

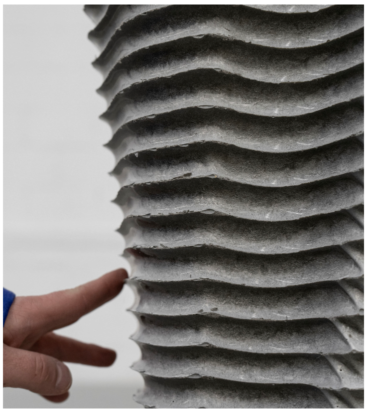

Figure C.3: Close-up of sharp concrete details.

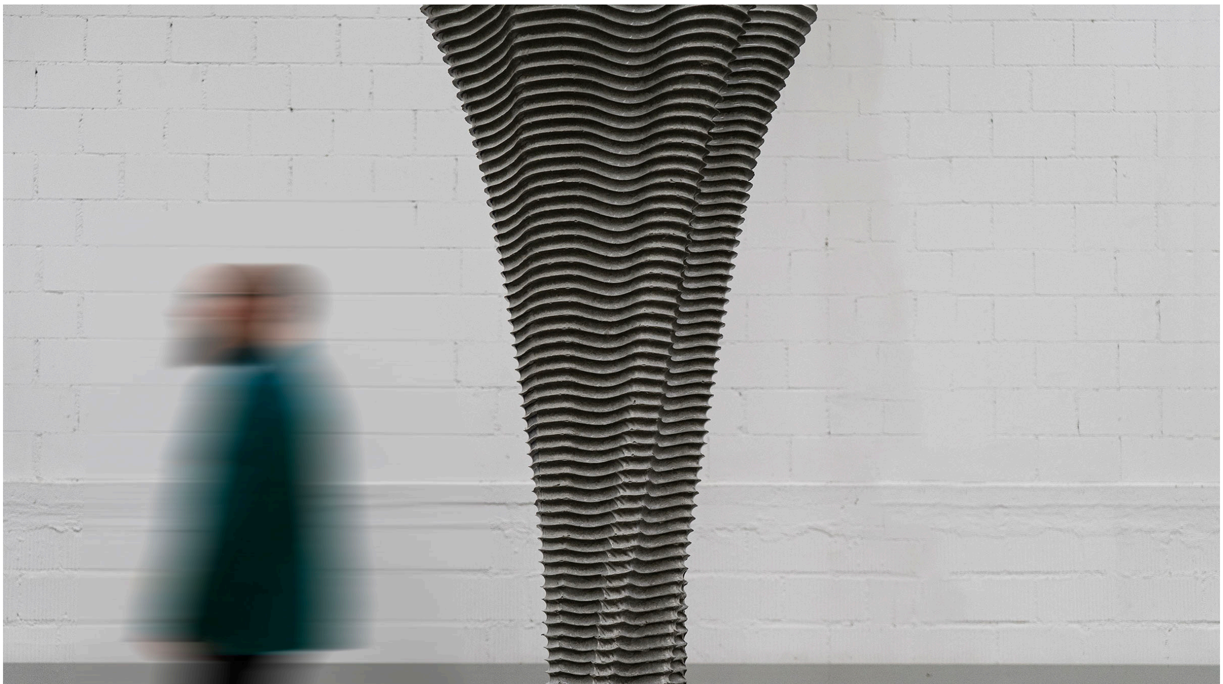

Figure C.4: Testing facility with specimen installed.

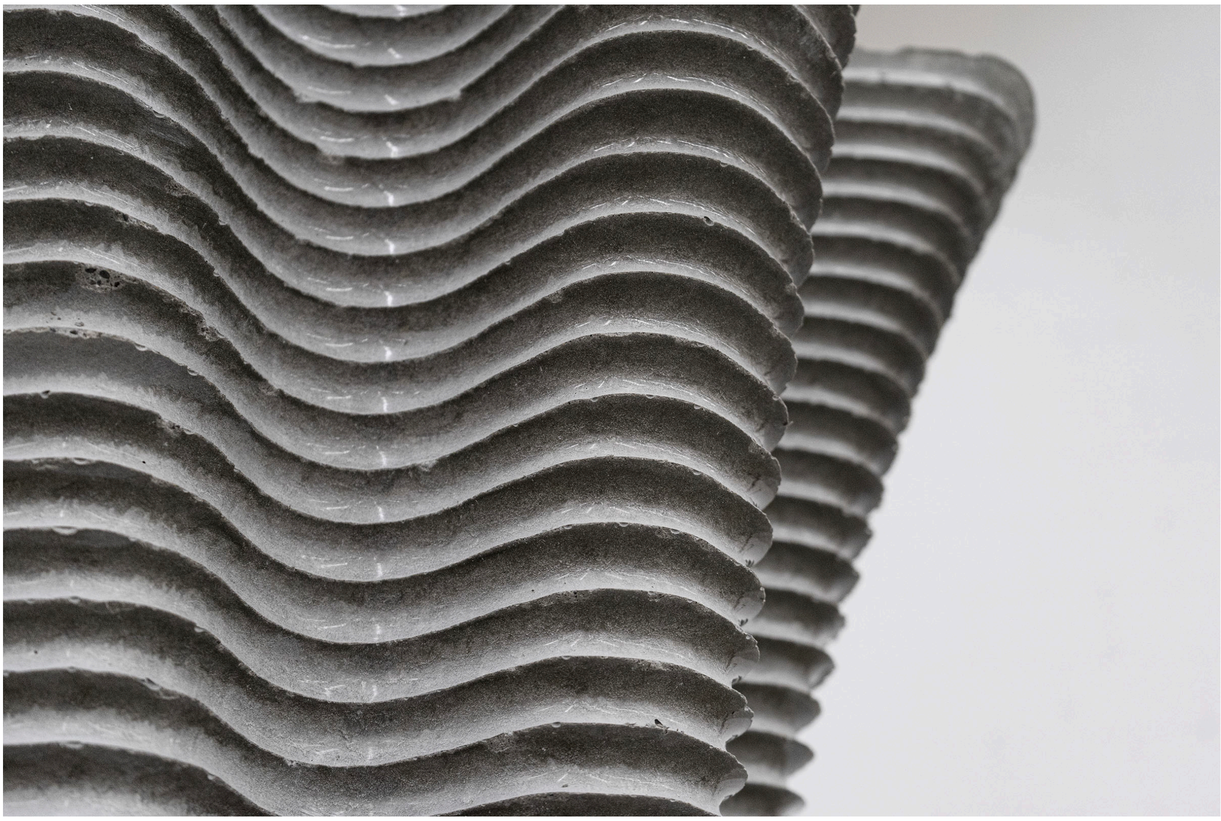

Figure C.5: Close-up of the capital. Undulating HC3DP resulting in a concrete texture with dramatic shadow effects.

C.2 Next steps

To fully understand the material behavior of the thin-walled HC3DP formwork system, it is essential to conduct new research that quantifies the system's resistance to hydrostatic pressure and its stress-corrosion cracking behaviour. Additionally, the reusability of HC3DP formwork must be investigated, particularly considering how the undulated surface finish of HC 3D prints might influence the separation of concrete from the formwork. Alongside the issue of reusability, the question of how to connect multiple low-resolution 3D printed elements arises, a challenge comparable to ensuring water tightness in 3DP facade systems.

The texture of the concrete is defined by the shape of the 3D printed bead. The unique texture of the round die geometries, used in this thesis, creates concrete finishes with sharp detailing, resulting in a unique texture and dramatic shadow effects. The potential impact of new nozzle designs, such as those with non-round orifices, on the concrete texture is another area that requires exploration.

Contributions:

This prototype was cast in collaboration with K. Studer AG, Frick Switzerland

Bibliography

Here are the references in citation order.

[1] Hylke E. Beck et al. 'Present and future Köppen-Geiger climate classification maps at 1-km resolution'. en. In: *Scientific Data* 5.1 (Oct. 2018). Number: 1 Publisher: Nature Publishing Group, p. 180214. DOI: `10.1038/sdata.2018.214` (cited on page 4).

[2] Zak Cutler et al. *Reducing embodied carbon in new construction*. en. Tech. rep. 2022 (cited on page 5).

[3] Chiara Delmastro and IEA. *Building Envelopes – Technology deep dive*. en-GB. Tech. rep. Paris: IEA, 2022. (Visited on 10/08/2022) (cited on pages 6, 24, 59, 134, 164).

[4] Rebecca Hartwell, Sebastian Macmillan, and Mauro Overend. 'Circular economy of façades: Real-world challenges and opportunities'. In: *Resources, Conservation and Recycling* 175 (Dec. 2021), p. 105827. DOI: `10.1016/j.resconrec.2021.105827` (cited on pages 6, 134).

[5] Mike Davies and Richard Rogers. 'A wall for all seasons'. en. In: *The Royal Institute of British Architects Journal (RIBAJ)* 88.2 (1981), pp. 55–57 (cited on pages 6, 25, 134).

[6] Isolda Agustí-Juan and Guillaume Habert. 'Environmental design guidelines for digital fabrication'. en. In: *Journal of Cleaner Production* 142.4 (Jan. 2017), pp. 2780–2791. DOI: `10.1016/j.jclepro.2016.10.190` (cited on pages 6, 26, 50).

[7] ISO/ASTM. *ISO/ASTM 52903-1:2020 - Additive manufacturing. Material extrusion-based additive manufacturing of plastic materials*. 2020 (cited on pages 6, 134, 164).

[8] S. Scott Crump. 'Modeling apparatus for three-dimensional objects'. US5340433A. Aug. 1994. (Visited on 03/01/2023) (cited on pages 6, 77, 104).

[9] Charles Koehler, ed. *Plastics in Building*. Washington DC: Building Reserach Insitute, Apr. 1955 (cited on page 6).

[10] Tarja Häkkinen, Matti Kuittinen, and Sirje Vares. *Plastic in Buildings, A Study of Finnish Blocks of Flats and Daycare Centers*. The Ministry of the Environment Finnland, 2018 (cited on page 6).

[11] J Baldwin and Richard Buckminster Fuller. *Bucky works : Buckminster Fuller's ideas for today*. eng. Publication Title: Bucky works Buckminster Fuller's ideas for today. New York [etc: Wiley, 1996 (cited on page 7).

[12] Jung Yun Chi. 'An outline of the evolution of pneumatic structures'. en. In: (2014) (cited on page 7).

[13] Simone Jeska. 'A Brief History of Plastic Buildings'. In: *Transparent Plastics: Design and Technology*. Basel: Birkhäuser Basel, 2008, pp. 8–23. DOI: `10.1007/978-3-7643-8287-2_1` (cited on pages 7, 121, 155).

[14] Stefan Helmcke et al. *Climate impact of plastics*. Tech. rep. McKinsey & Company, 2022 (cited on page 8).

[15] Rakesh Kumar et al. 'Impacts of Plastic Pollution on Ecosystem Services, Sustainable Development Goals, and Need to Focus on Circular Economy and Policy Interventions'. en. In: *Sustainability* 13.17 (Sept. 2021), p. 9963. DOI: `10.3390/su13179963` (cited on page 8).

[16] Venkata Siva Naga Sai Goli, Arif Mohammad, and Devendra Narain Singh. 'Application of Municipal Plastic Waste as a Manmade Neo-construction Material: Issues & Wayforward'. en. In: *Resources, Conservation and Recycling* 161 (Oct. 2020), p. 105008. DOI: `10.1016/j.resconrec.2020.105008` (cited on page 9).

[17] K.S. Rebeiz and A.P. Craft. 'Plastic waste management in construction: technological and institutional issues'. en. In: *Resources, Conservation and Recycling* 15.3-4 (Dec. 1995), pp. 245–257. DOI: `10.1016/0921-3449(95)00034-8` (cited on page 9).

[18] Nur Hanis Zulkernain et al. 'Utilisation of plastic waste as aggregate in construction materials: A review'. en. In: *Construction and Building Materials* 296 (Aug. 2021), p. 123669. DOI: `10.1016/j.conbuildmat.2021.123669` (cited on page 9).

[19] Esen Gökçe. 'Rethinking sustainability: A research on starch based bioplastic'. en. In: *Journal of Sustainable Construction Materials and Technologies* 3.3 (Oct. 2018), pp. 249–260. DOI: `10.29187/jscmt.2018.28` (cited on page 9).

[20] Ilaria Oberti and Alessia Paciello. 'Bioplastic as a Substitute for Plastic in Construction Industry'. en. In: *Encyclopedia* 2.3 (July 2022), pp. 1408–1420. DOI: `10.3390/encyclopedia2030095` (cited on page 9).

[21] Center for International Environmental Law. *Fueling Plastics: Plastic Industry Awareness of the Ocean Plastics Problem*. Tech. rep. 3. Washington: CIEL Center for International Environmental Law, 2017 (cited on page 9).

[22] Dominic Charles, Laurent Kimman, and Leschok Matthias. *Plastic Waste Makers Index 2023*. Tech. rep. The Minderoo Foundation, 2023 (cited on page 9).

[23] Paulina Latko-Durałek, Kamil Dydek, and Anna Boczkowska. 'Thermal, Rheological and Mechanical Properties of PETG/rPETG Blends'. en. In: *Journal of Polymers and the Environment* 27.11 (Nov. 2019), pp. 2600–2606. DOI: `10.1007/s10924-019-01544-6` (cited on pages 9, 37).

[24] Isabelle Anderson. 'Mechanical Properties of Specimens 3D Printed with Virgin and Recycled Polylactic Acid'. en. In: *3D Printing and Additive Manufacturing* 4.2 (June 2017), pp. 110–115. DOI: `10.1089/3dp.2016.0054` (cited on pages 9, 37, 164).

[25] Nectarios Vidakis et al. 'Sustainable Additive Manufacturing: Mechanical Response of Polyethylene Terephthalate Glycol over Multiple Recycling Processes'. en. In: *Materials* 14.5 (Mar. 2021), p. 1162. DOI: `10.3390/ma14051162` (cited on pages 9, 37, 145).

[26] Dirk van der Kooij. *Endless Chair - Kooij*. 2011. URL: `https://dirkvanderkooij.com/endless-chair` (visited on 02/01/2023) (cited on pages 10, 78, 104).

[27] DUS Architects. *XL 3D Printer – DUS Architects*. (accessed 2023-02-01). 2013. URL: `https://houseofdus.com/project/kamermaker/` (cited on pages 11, 78).

[28] Lonnie J Love et al. 'Breaking barriers in polymer additive manufacturing'. en. In: (2015) (cited on pages 11, 78).

[29] Vidya Kishore et al. 'Infrared preheating to improve interlayer strength of big area additive manufacturing (BAAM) components'. en. In: *Additive Manufacturing* 14 (Mar. 2017), pp. 7–12. DOI: `10.1016/j.addma.2016.11.008` (cited on pages 11, 78, 94, 104, 164).

[30] Chad E. Duty et al. 'Structure and mechanical behavior of Big Area Additive Manufacturing (BAAM) materials'. In: *Rapid Prototyping Journal* 23.1 (Jan. 2017). Publisher: Emerald Publishing Limited, pp. 181–189. DOI: `10.1108/RPJ-12-2015-0183` (cited on pages 11, 31, 35, 76–78, 104, 122, 135, 139, 164, 171, 172).

[31] Francesco Pignatelli and Gianluca Percoco. 'An application- and market-oriented review on large format additive manufacturing, focusing on polymer pellet-based 3D printing'. en. In: *Progress in Additive Manufacturing* 7.6 (Dec. 2022), pp. 1363–1377. DOI: `10.1007/s40964-022-00309-3` (cited on pages 11, 76, 78).

[32] Andrei Jipa and Benjamin Dillenburger. '3D Printed Formwork for Concrete: State-of-the-Art, Opportunities, Challenges, and Applications'. In: *3D Printing and Additive Manufacturing* 9.2 (Apr. 2022). Publisher: Mary Ann Liebert, Inc., publishers, pp. 84–107. DOI: `10.1089/3dp.2021.0024` (cited on pages 11, 78).

[33] Roberto Naboni and Nebojša Jakica. 'Additive manufacturing in skin systems: trends and future perspectives'. en. In: *Rethinking Building Skins*. Ed. by Eugenia Gasparri et al. Woodhead Publishing Series in Civil and Structural Engineering. Woodhead Publishing, 2022, pp. 425–451. DOI: `10.1016/B978-0-12-822477-9.00004-8` (cited on pages 11, 27, 78, 135, 164).

[34] Branch Technology. *Branch Technology*. en-US. 2022. URL: `https://branchtechnology.com/products/` (visited on 05/04/2022) (cited on pages 11, 78, 79).

[35] Branch Technology. *oneCITY Pavilion*. URL: https://branchtechnology.com/one-city-pavilion/ (visited on 02/01/2023) (cited on pages 11, 78).

[36] The New Raw. *Crafting plasitc waste with robots*. en. Company website. (accessed October 8, 2022). 2015. URL: https://thenewraw.org/Work (visited on 10/08/2022) (cited on pages 11, 50, 78).

[37] Daniel Moreno Nieto and Sergio I. Molina. 'Large-format fused deposition additive manufacturing: a review'. In: *Rapid Prototyping Journal* 26.5 (Jan. 2020). Publisher: Emerald Publishing Limited, pp. 793–799. DOI: 10.1108/RPJ-05-2018-0126 (cited on pages 11, 78, 103).

[38] Alex Roschli et al. 'Designing for Big Area Additive Manufacturing'. en. In: *Additive Manufacturing* 25 (Jan. 2019), pp. 275–285. DOI: 10.1016/j.addma.2018.11.006 (cited on pages 12, 78, 81, 85, 103, 105, 135, 144, 149, 157).

[39] Daniel Aelenei, Laura Aelenei, and Catarina Pacheco Vieira. 'Adaptive Façade: Concept, Applications, Research Questions'. en. In: *Energy Procedia* 91 (June 2016), pp. 269–275. DOI: 10.1016/j.egypro.2016.06.218 (cited on pages 12, 25, 134).

[40] Moritz Basil Mungenast. '3D-Printed Future Facade'. German. PhD thesis. Munich, Germany: Technical University of Munich, Sept. 2019 (cited on pages 12, 33, 36, 49, 50, 60, 104, 105, 134–136, 147, 164).

[41] Helena Coch. 'Chapter 4—Bioclimatism in vernacular architecture'. en. In: *Renewable and Sustainable Energy Reviews* 2.1-2 (June 1998), pp. 67–87. DOI: 10.1016/S1364-0321(98)00012-4 (cited on page 12).

[42] Rebecca Hartwell and Dr Mauro Overend. 'Unlocking the Re-use Potential of Glass Façade Systems'. en. In: (2019) (cited on pages 12, 134).

[43] Ina Cheibas et al. 'Thermoplastic large-scale 3D printing of a light-distribution and fabrication-informed facade panel'. In: (Oct. 2023), 18 p. DOI: 10.3929/ETHZ-B-000639445 (cited on pages 15, 136, 164).

[44] Matthias Leschok et al. '3D printing facades: Design, fabrication, and assessment methods'. en. In: *Automation in Construction* 152 (Aug. 2023), p. 104918. DOI: 10.1016/j.autcon.2023.104918 (cited on pages 16, 78, 134, 135, 164).

[45] Valeria Piccioni et al. 'Printing thermal performance: an experimental exploration of 3DP polymers for facade applications'. en. In: *IOP Conference Series: Earth and Environmental Science* 1196.1 (June 2023), p. 012063. DOI: 10.1088/1755-1315/1196/1/012063 (cited on pages 16, 134, 137, 138, 144, 147, 148, 150, 159, 164).

[46] Matthias Leschok, Lex Reiter, and Benjamin Dillenburger. 'Large-scale hollow-core 3D printing (HC3DP): A polymer 3D printing technology for large-scale ultralightweight components'. In: *Additive Manufacturing* 78 (Sept. 2023), p. 103874. DOI: 10.1016/j.addma.2023.103874 (cited on pages 17, 103, 105, 106, 115, 123, 135, 136, 139, 145, 148, 158, 164, 165, 168, 173).

[47] Matthias Leschok et al. 'Large-Scale Hollow-Core 3D Printing: Variable Cross-Section and Printing Features for Lightweight Plastic Elements'. In: *3D Printing and Additive Manufacturing* (), 3dp.2023.0287. DOI: 10.1089/3dp.2023.0287 (cited on pages 17, 136, 164).

[48] Matthias Leschok et al. 'Prōtóplasto A Discrete Roof-Column System With Hollow-Core 3D Printing And Bespoke Space Frames'. In: *Fabricate 2024: Creating Resourceful Futures*. Fabricate 2024. Ed. by Phil Ayres et al. UCL Press. DOI: 10.2307/jj.11374766 (cited on page 17).

[49] Matthias Leschok et al. 'Thermal and Manufacturing Properties of HC3D Elements for Lightweight Facades'. en. In: (2024). in review (cited on pages 17, 164, 169).

[50] AmirHosein GhaffarianHoseini et al. 'Intelligent Facades in Low-Energy Buildings'. en. In: *International Journal of Environment and Climate Change* 2.4 (Jan. 2013), pp. 437–464. DOI: 10.9734/BJECC/2012/2912 (cited on pages 24, 134).

[51] Miren Juaristi, Tomás Gómez-Acebo, and Aurora Monge-Barrio. 'Qualitative analysis of promising materials and technologies for the design and evaluation of Climate Adaptive Opaque Façades'. en. In: *Building and Environment* 144 (Oct. 2018), pp. 482–501. DOI: 10.1016/j.buildenv.2018.08.028 (cited on pages 25, 134).

[52] Fabio Favoino, Mauro Overend, and Qian Jin. 'The optimal thermo-optical properties and energy saving potential of adaptive glazing technologies'. en. In: *Applied Energy* 156 (Oct. 2015), pp. 1–15. DOI: `10.1016/j.apenergy.2015.05.065` (cited on page 25).

[53] Wajiha Tariq Sheikh and Quratulain Asghar. 'Adaptive biomimetic facades: Enhancing energy efficiency of highly glazed buildings'. en. In: *Frontiers of Architectural Research* 8.3 (Sept. 2019), pp. 319–331. DOI: `10.1016/j.foar.2019.06.001` (cited on page 25).

[54] R.C.G.M. Loonen et al. 'Climate adaptive building shells: State-of-the-art and future challenges'. en. In: *Renewable and Sustainable Energy Reviews* 25 (Sept. 2013), pp. 483–493. DOI: `10.1016/j.rser.2013.04.016` (cited on page 25).

[55] Rosa Romano et al. 'What is an Adaptive Façade? Analysis of Recent Terms and Definitions from an International Perspective'. en. In: *Journal of Facade Design and Engineering* 6.3 (July 2018), pp. 65–76. DOI: `10.7480/JFDE.2018.3.2478` (cited on page 25).

[56] Donghua Zhao and Weizhong Guo. 'Shape and Performance Controlled Advanced Design for Additive Manufacturing: A Review of Slicing and Path Planning'. en. In: *Journal of Manufacturing Science and Engineering* 142.1 (2019), p. 010801. DOI: `10.1115/1.4045055` (cited on pages 25, 31, 32, 51).

[57] David W. Rosen et al. 'Special Issue: Design for Additive Manufacturing: A Paradigm Shift in Design, Fabrication, and Qualification'. en. In: *Journal of Mechanical Design* 137.11 (2015), p. 110301. DOI: `10.1115/1.4031470` (cited on pages 25, 28).

[58] Shady Attia et al. 'Current trends and future challenges in the performance assessment of adaptive façade systems'. en. In: *Energy and Buildings* 179 (Nov. 2018), pp. 165–182. DOI: `10.1016/j.enbuild.2018.09.017` (cited on page 25).

[59] Roel C.G.M. Loonen et al. 'Review of current status, requirements and opportunities for building performance simulation of adaptive facades'. en. In: *Journal of Building Performance Simulation* 10.2 (Mar. 2017), pp. 205–223. DOI: `10.1080/19401493.2016.1152303` (cited on pages 25, 52).

[60] Holger Strauß. 'AM Envelope: The potential of Additive Manufacturing for façade construction'. en. ISBN: 978-1-4812-1433-9 DOI https://doi.org/10.7480/abe.2013.1. Thesis. Delft: TU Delft, 2013 (cited on pages 25, 44, 45, 135, 184).

[61] Yuen-Shan Leung et al. 'Challenges and Status on Design and Computation for Emerging Additive Manufacturing Technologies'. en. In: *Journal of Computing and Information Science in Engineering* 19.2 (June 2019), p. 021013. DOI: `10.1115/1.4041913` (cited on pages 25, 32).

[62] Carolyn Conner Seepersad. 'Challenges and Opportunities in Design for Additive Manufacturing'. en. In: *3D Printing and Additive Manufacturing* 1.1 (Mar. 2014), pp. 10–13. DOI: `10.1089/3dp.2013.0006` (cited on pages 26, 28).

[63] Moritz Hauschild and Rüdiger Karzel. *Digital Processes Planning, Designing, Production*. DETAIL Practice. Birkhäuser, 2011 (cited on page 26).

[64] Ingrid Paoletti. 'Mass Customization with Additive Manufacturing: New Perspectives for Multi Performative Building Components in Architecture'. en. In: *Procedia Engineering* 180 (2017), pp. 1150–1159. DOI: `10.1016/j.proeng.2017.04.275` (cited on pages 26, 49).

[65] Isolda Agustí-Juan, Alexander Hollberg, and Guillaume Habert. 'Integration of environmental criteria in early stages of digital fabrication'. en. In: *Proceedings of the 35th Education and Research in Computer Aided Architectural Design in Europe Conference*. Vol. 2. Rome, Italy, 2017, pp. 185–192. DOI: `10.52842/conf.ecaade.2017.2.185` (cited on pages 26, 50).

[66] Daniel Delgado Camacho et al. 'Applications of additive manufacturing in the construction industry – A forward-looking review'. en. In: *Automation in Construction* 89 (May 2018), pp. 110–119. DOI: `10.1016/j.autcon.2017.12.031` (cited on pages 26, 30).

[67] Tuan D. Ngo et al. 'Additive manufacturing (3D printing): A review of materials, methods, applications and challenges'. en. In: *Composites Part B: Engineering* 143 (June 2018), pp. 172–196. DOI: `10.1016/j.compositesb.2018.02.012` (cited on pages 26, 44).

[68] Nathalie Labonnote et al. ‘Additive construction: State-of-the-art, challenges and opportunities’. en. In: *Automation in Construction* 72.3 (Dec. 2016), pp. 347–366. DOI: `10.1016/j.autcon.2016.08.026` (cited on pages 26, 31, 50).

[69] Amabel García-Dominguez, Juan Claver, and Miguel A. Sebastián. ‘Integration of Additive Manufacturing, Parametric Design, and Optimization of Parts Obtained by Fused Deposition Modeling (FDM). A Methodological Approach’. en. In: *Polymers* 12.9 (Sept. 2020), p. 1993. DOI: `10.3390/polym12091993` (cited on pages 28, 29).

[70] McNeel. *Grasshopper, Algorithmic Modeling for Rhino*. en. (accessed October 18, 2021). 2021. URL: `https://www.grasshopper3d.com/` (visited on 10/18/2021) (cited on page 28).

[71] *Dynamo*. en-US. (accessed October 18, 2021). 2021. URL: `https://dynamobim.org/` (visited on 10/18/2021) (cited on page 28).

[72] L. J. Gibson. ‘Cellular Solids’. en. In: *Materials Research Society (MRS) Bulletin* 28.4 (Apr. 2003), pp. 270–274. DOI: `10.1557/mrs2003.79` (cited on page 29).

[73] Flávio Craveiro et al. ‘An automated system for 3D printing functionally graded concrete-based materials’. en. In: *Additive Manufacturing* 33 (May 2020), p. 101146. DOI: `10.1016/j.addma.2020.101146` (cited on pages 29, 51, 52).

[74] Wenjin Tao and Ming C. Leu. ‘Design of lattice structure for additive manufacturing’. en. In: *2016 International Symposium on Flexible Automation (ISFA)*. Cleveland, USA: Institute of Electrical and Electronics Engineers (IEEE), Aug. 2016, pp. 325–332. DOI: `10.1109/ISFA.2016.7790182` (cited on page 29).

[75] Roberto Naboni and Anja Kunic. ‘Bone-inspired 3D printed structures for construction applications’. en. In: *Gestão & Tecnologia De Projetos (Design Management and Technology)* 14.1 (Sept. 2019), pp. 111–124. DOI: `10.11606/gtp.v14i1.148496` (cited on pages 29, 31).

[76] Materialise, Altair, and Renishaw. *The Spider Bracket: A Topology Optimization Project by Altair, Materialise and Renishaw*. en. (accessed June 16, 2021). 2021. URL: `https://www.materialise.com/en/cases/spider-bracket-a-topology-optimization-project-by-altair-materialise-and-renishaw` (visited on 06/16/2021) (cited on pages 29–31, 44, 45, 51, 52).

[77] Martti Mäntylä. *An introduction to solid modeling*. English. ISBN: 0-7167-8015-1. Rockville, Md.: Computer Science Press, 1988 (cited on page 29).

[78] Ian Gibson et al. ‘Design for Additive Manufacturing’. en. In: *Additive Manufacturing Technologies*. Cham: Springer International Publishing, 2021, pp. 555–607. DOI: `10.1007/978-3-030-56127-7_19` (cited on page 29).

[79] Mathias Bernhard, Michael Hansmeyer, and Benjamin Dillenburger. ‘Volumetric modelling for 3D printed architecture’. en. In: *AAG 2018: Advances in Architectural Geometry 2018*. Ed. by Lars Hesselgren et al. Klein Publishing, 2018, pp. 392–415 (cited on page 29).

[80] M Kladeftira et al. ‘Redefining Polyhedral Space Through 3D Printing’. en. In: *D Printing* (2020) (cited on pages 29, 140).

[81] ntopology. *nTopology. Next-Generation Engineering Design Software*. en-US. (accessed October 18, 2021). 2021. URL: `https://ntopology.com/` (visited on 10/18/2021) (cited on pages 29, 140).

[82] *Spherene AG*. (accessed August 5, 2022). 2022. URL: `https://spherene.ch/` (visited on 08/05/2022) (cited on page 29).

[83] DBT. *Axolotl*. en-US. (accessed October 18, 2021). 2021. URL: `https://dbt.arch.ethz.ch/project/axolotl/` (visited on 10/18/2021) (cited on pages 29, 140).

[84] Odysseas Kontovourkis, George Tryfonos, and Christos Georgiou. ‘Robotic additive manufacturing (RAM) with clay using topology optimization principles for toolpath planning: the example of a building element’. en. In: *Architectural Science Review* 63.2 (Mar. 2020), pp. 105–118. DOI: `10.1080/00038628.2019.1620170` (cited on pages 29–31, 37, 38, 49, 59).

[85] Sina Mostafavi and Henriette Bier. 'Materially Informed Design to Robotic Production: A Robotic 3D Printing System for Informed Material Deposition'. en. In: *Robotic Fabrication in Architecture, Art and Design 2016*. Ed. by Dagmar Reinhardt, Rob Saunders, and Jane Burry. Cham: Springer International Publishing, 2016, pp. 338–349. DOI: 10.1007/978-3-319-26378-6_27 (cited on pages 29, 31).

[86] Roberto Naboni, Luca Breseghello, and Anja Kunic. 'Multi-scale design and fabrication of the Trabeculae Pavilion'. en. In: *Additive Manufacturing* 27 (May 2019), pp. 305–317. DOI: 10.1016/j.addma.2019.03.005 (cited on pages 29, 104, 105).

[87] David J. Munk, Gareth A. Vio, and Grant P. Steven. 'Topology and shape optimization methods using evolutionary algorithms: a review'. en. In: *Structural and Multidisciplinary Optimization* 52.3 (Sept. 2015), pp. 613–631. DOI: 10.1007/s00158-015-1261-9 (cited on page 30).

[88] Ajit Panesar et al. 'Strategies for functionally graded lattice structures derived using topology optimisation for Additive Manufacturing'. en. In: *Additive Manufacturing* 19 (Jan. 2018), pp. 81–94. DOI: 10.1016/j.addma.2017.11.008 (cited on page 30).

[89] Vittoria Laghi et al. 'Computational design and manufacturing of a half-scaled 3D-printed stainless steel diagrid column'. en. In: *Additive Manufacturing* 36 (Dec. 2020), p. 101505. DOI: 10.1016/j.addma.2020.101505 (cited on page 30).

[90] C. Gosselin et al. 'Large-scale 3D printing of ultra-high performance concrete – a new processing route for architects and builders'. en. In: *Materials & Design* 100 (June 2016), pp. 102–109. DOI: 10.1016/j.matdes.2016.03.097 (cited on page 30).

[91] R.A. Buswell et al. 'Freeform Construction: Mega-scale Rapid Manufacturing for construction'. en. In: *Automation in Construction* 16.2 (Mar. 2007), pp. 224–231. DOI: 10.1016/j.autcon.2006.05.002 (cited on page 30).

[92] Vahid Hassani et al. 'Rationalization algorithm for a topologically-optimized multi-branch node for manufacturing by metal printing'. en. In: *Journal of Building Engineering* 29 (May 2020), p. 101146. DOI: 10.1016/j.jobe.2019.101146 (cited on page 30).

[93] *Optimization-enabled Structural Analysis - Altair OptiStruct*. (accessed October 19, 2022). 2021. URL: https://www.altair.com/optistruct/capabilities/ (visited on 10/19/2021) (cited on page 30).

[94] Marirena Kladeftira et al. 'Printing Whisper Dishes. Large-scale binder jetting for outdoor installations'. en. In: *Proceedings of the 38th Annual Conference of the Association for Computer Aided Design in Architecture (ACADIA)*. Ed. by Phillip Anzalone, Marcella Del Signore, and Andrew John Wit. Mexico City, Mexico, 2018, pp. 328–335. DOI: 10.52842/conf.acadia.2018.328 (cited on page 30).

[95] Ingrid Paoletti and Massimiliano Nastri. 'Adaptive Façades and Topology Optimization'. en. In: *Adaptive Facades Network Final Conference*. Ed. by Andreas Luible et al. Lucerne, Switzerland: TU Delft Open, 2018, pp. 473–484 (cited on page 30).

[96] Lucas A. Rodrigues da Silva, André J. Torii, and André T. Beck. 'Hyperstatic and redundancy thresholds in truss topology optimization considering progressive collapse due to aleatory and epistemic uncertainties'. en. In: *Probabilistic Engineering Mechanics* 71 (Jan. 2023), p. 103384. DOI: 10.1016/j.probengmech.2022.103384 (cited on page 30).

[97] Jikai Liu et al. 'Current and future trends in topology optimization for additive manufacturing'. en. In: *Structural and Multidisciplinary Optimization* 57.6 (June 2018), pp. 2457–2483. DOI: 10.1007/s00158-018-1994-3 (cited on page 31).

[98] Negar Ashrafi et al. 'Experimental prediction of material deformation in large-scale additive manufacturing of concrete'. en. In: *Additive Manufacturing* 37 (Jan. 2021), p. 101656. DOI: 10.1016/j.addma.2020.101656 (cited on page 31).

[99] *Silkworm*. en. (accessed October 19, 2021). Dec. 2012. URL: https://www.food4rhino.com/en/app/silkworm (visited on 10/19/2021) (cited on page 31).

[100] Isabella Molloy and Tim Miller. ‘Digital Dexterity. Freeform 3D Printing through Direct Toolpath Manipulation for Crafted Artifacts’. en. In: *Proceedings of the 38th Annual Conference of the Association for Computer Aided Design in Architecture (ACADIA)*. Ed. by Phillip Anzalone, Marcella Del Signore, and Andrew John Wit. Mexico City, Mexico, 2018, pp. 266–275. DOI: `10.52842/conf.acadia.2018.328` (cited on page 31).

[101] Ioanna Mitropoulou, Mathias Bernhard, and Benjamin Dillenburger. ‘Print Paths Key-framing: Design for non-planar layered robotic FDM printing’. In: *Proceedings of the 5th Annual ACM Symposium on Computational Fabrication*. SCF ’20. New York, NY, USA: Association for Computing Machinery, Nov. 2020, pp. 1–10. DOI: `10.1145/3424630.3425408` (cited on pages 32, 105).

[102] Luis Lisandro Lopez Taborda, Heriberto Maury, and Jovanny Pacheco. ‘Design for additive manufacturing: a comprehensive review of the tendencies and limitations of methodologies’. en. In: *Rapid Prototyping Journal* 27.5 (July 2021), pp. 918–966. DOI: `10.1108/RPJ-11-2019-0296` (cited on page 32).

[103] Amit M. E. Arefin et al. ‘Polymer 3D Printing Review: Materials, Process, and Design Strategies for Medical Applications’. en. In: *Polymers* 13.9 (May 2021), p. 1499. DOI: `10.3390/polym13091499` (cited on page 32).

[104] Thermwood. *Thermwood LSAM - Large Scale Additive Manufacturing*. 2023. URL: `https://www.thermwood.com/lsam_home.htm` (visited on 12/10/2023) (cited on pages 32, 60, 135).

[105] Lemonia Karagianni et al. ‘Additive Manufacturing for daylight: Towards a customized shading device’. en. In: *2016 Proceedings of the Symposium on Simulation for Architecture and Urban Design (SIMAUD)*. Ed. by Ramtin Attaran et al. Vol. 7. London, UK, 2016, pp. 69–76 (cited on pages 33, 36, 49, 50, 164).

[106] Maria Valentini Sarakinioti et al. ‘Developing an integrated 3D-printed façade with complex geometries for active temperature control’. en. In: *Materials Today Communications* 15 (June 2018), pp. 275–279. DOI: `10.1016/j.mtcomm.2018.02.027` (cited on pages 33, 35, 36, 49, 50, 60, 66, 134, 136, 137, 164).

[107] Martin Tenpierik et al. ‘Double Face 2.0: A lightweight translucent adaptable Trombe wall’. en. In: *Spool. Journal of Architecture and the Built Environment* 5.2 (2018). DOI: `10.7480/SPOOL.2018.2.2090` (cited on pages 33, 36, 60, 136, 164).

[108] Giulia Grassi, Sonia Lupica Spagnolo, and Ingrid Paoletti. ‘Fabrication and durability testing of a 3D printed façade for desert climates’. en. In: *Additive Manufacturing* 28 (2019), pp. 439–444. DOI: `10.1016/j.addma.2019.05.023` (cited on pages 33, 36, 50, 164).

[109] Hyunchul Kwon et al. ‘Digital Composites: Robotic 3D Printing of Continuous Carbon Fiber-Reinforced Plastics for Functionally-Graded Building Components’. en. In: *Robotic Fabrication in Architecture, Art and Design 2018*. Ed. by Jan Willmann et al. Zurich, Switzerland: Springer International Publishing, 2019, pp. 363–376. DOI: `10.1007/978-3-319-92294-2_28` (cited on pages 34, 35).

[110] Valeria Piccioni, Michela Turrin, and Martin J. Tenpierik. ‘A Performance-Driven Approach for the Design of Cellular Geometries with Low Thermal Conductivity for Application in 3D-Printed Façade Components’. en. In: *2020 Proceedings of the Symposium on Simulation for Architecture and Urban Design (SIMAUD)*. Ed. by Angelos Chronis et al. Vienna, Austria, 2020, pp. 327–334 (cited on pages 34, 35, 51, 52, 60, 66, 137).

[111] Yoana Taseva et al. ‘Large-Scale 3D Printing for Functionally-Graded Facade’. en. In: *RE: Anthropocene, Proceedings of the 25th International Conference of the Association for Computer-Aided Architectural Design Research in Asia (CAADRIA) 2020*. Ed. by I Holzer et al. Hong Kong, 2020, pp. 183–192 (cited on pages 34, 35, 51, 52, 104, 105, 136, 164).

[112] H. Mohamed, D. W. Bao, and R. Snooks. ‘Super Composite: Carbon Fibre Infused 3D Printed Tectonics’. en. In: *Proceedings of the 2020 DigitalFUTURES*. Ed. by Philip F. Yuan et al. Singapore: Springer Singapore, 2021, pp. 297–308. DOI: `10.1007/978-981-33-4400-6_28` (cited on pages 34, 35, 135).

[113] DUS. *Europe Building – DUS Architects*. en-US. (accessed June 23, 2021). 2015. URL: `https://houseofdus.com/project/europe-building/` (visited on 06/23/2021) (cited on pages 34, 36, 136).

[114] DUS Architects. *Urban Cabin*. en-US. (accessed June 23, 2021). 2015. URL: `https://houseofdus.com/project/urban-cabin/` (visited on 06/23/2021) (cited on pages 34, 36, 135, 136).

[115] Kaushik Biswas et al. 'Additive Manufacturing Integrated Energy - Enabling Innovative Solutions for Buildings of the Future'. en. In: *Journal of Solar Energy Engineering* 139.1 (Feb. 2017), p. 015001. DOI: `10.1115/1.4034980` (cited on pages 35, 36, 136).

[116] Roland Snooks and Laura Harper. 'Printed Assemblages: A Co-Evolution of Composite Tectonics and Additive Manufacturing Techniques'. en. In: *Fabricate 2020: Making Resilient Architecture*. Ed. by Jane Burry et al. UCL Press, Apr. 2020, pp. 202–209 (cited on pages 35, 36, 104, 105, 164).

[117] Angel R. Torrado et al. 'Characterizing the effect of additives to ABS on the mechanical property anisotropy of specimens fabricated by material extrusion 3D printing'. en. In: *Additive Manufacturing* 6 (Apr. 2015), pp. 16–29. DOI: `10.1016/j.addma.2015.02.001` (cited on pages 35, 51).

[118] Jeniffer Burke. *3D printing shapes building industry, creates rapid construction potential | ORNL*. (accessed June 21, 2022). 2019. URL: `https://www.ornl.gov/news/3d-printing-shapes-building-industry-creates-rapid-construction-potential-1` (visited on 06/21/2022) (cited on page 36).

[119] Mohamed Gomaa et al. 'Digital manufacturing for earth construction: A critical review'. en. In: *Journal of Cleaner Production* 338 (Mar. 2022), p. 130630. DOI: `10.1016/j.jclepro.2022.130630` (cited on page 37).

[120] A. Perrot, D. Rangeard, and E. Courteille. '3D printing of earth-based materials: Processing aspects'. en. In: *Construction and Building Materials* 172 (May 2018), pp. 670–676. DOI: `10.1016/j.conbuildmat.2018.04.017` (cited on page 37).

[121] Alexander Wolf, Philipp Laurens Rosendahl, and Ulrich Knaack. 'Additive manufacturing of clay and ceramic building components'. en. In: *Automation in Construction* 133 (Jan. 2022), p. 103956. DOI: `10.1016/j.autcon.2021.103956` (cited on page 37).

[122] Yomna K. Abdallah and Alberto T. Estévez. '3D-Printed Biodigital Clay Bricks'. en. In: *Biomimetics* 6.4 (Dec. 2021). DOI: `10.3390/biomimetics6040059` (cited on pages 37, 39).

[123] Virginia San Fratello and Ronald Rael. 'Innovating materials for large scale additive manufacturing: Salt, soil, cement and chardonnay'. en. In: *Cement and Concrete Research* 134 (Aug. 2020), p. 106097. DOI: `10.1016/j.cemconres.2020.106097` (cited on pages 37, 39).

[124] Alexandre Dubor, Edouard Cabay, and Angelos Chronis. 'Energy Efficient Design for 3D Printed Earth Architecture'. en. In: *Humanizing Digital Reality: Design Modelling Symposium Paris 2017*. Ed. by Klaas De Rycke et al. Singapore: Springer, 2018, pp. 383–393. DOI: `10.1007/978-981-10-6611-5_33` (cited on pages 37, 38, 59).

[125] Mohamed Gomaa et al. '3D printing system for earth-based construction: Case study of cob'. en. In: *Automation in Construction* 124 (Apr. 2021), p. 103577. DOI: `10.1016/j.autcon.2021.103577` (cited on pages 37, 49).

[126] Nahum Travitzky et al. 'Additive Manufacturing of Ceramic-Based Materials'. en. In: *Advanced Engineering Materials* 16.6 (June 2014), pp. 729–754. DOI: `10.1002/adem.201400097` (cited on page 38).

[127] Y. Lakhdar et al. 'Additive manufacturing of advanced ceramic materials'. en. In: *Progress in Materials Science* 116 (Feb. 2021), p. 100736. DOI: `10.1016/j.pmatsci.2020.100736` (cited on page 38).

[128] Paulo J.S. Cruz et al. 'Additive Manufacturing of Ceramic Components for Façade Construction'. en. In: *Journal of Facade Design and Engineering* 8.1 (Oct. 2020), pp. 1–20. DOI: `10.7480/JFDE.2020.1.4725` (cited on page 38).

[129] Sulaiman AlOthman et al. 'Spatial Print Trajectory: Controlling Material Behavior with Print Speed, Feed Rate, and Complex Print Path'. en. In: *Robotic Fabrication in Architecture, Art and Design 2018*. Ed. by Jan Willmann et al. Cham: Springer, 2019, pp. 167–180. DOI: `10.1007/978-3-319-92294-2` (cited on page 38).

[130] Jared Friedman, Heamin Kim, and Olga Mesa. 'Experiments in Additive Clay Depositions'. en. In: *Robotic Fabrication in Architecture, Art and Design 2014*. Ed. by Wes McGee and Monica Ponce de Leon. Cham: Springer, 2014, pp. 261–272. DOI: `10.1007/978-3-319-04663-1_18` (cited on page 38).

[131] David Rosenwasser, Sonya Mantell, and Jenny Sabin. 'Clay Non-Wovens: Robotic Fabrication and Digital Ceramics'. en. In: *Proceedings of the 37th Annual Conference of the Association for Computer Aided Design in Architecture (ACADIA)*. Ed. by Takehiko Nagakura, Skylar Tibbits, and Caitlin Mueller. Cambridge, MA, 2017, pp. 502–511. DOI: `10.52842/conf.acadia.2017.502` (cited on page 38).

[132] IAAC. *CO-MIDA : Biophotovoltaic Vertical Gardens 3D Printed With Clay*. es. University. (accessed May 6, 2022). 2022. URL: `https://iaac.net/project/co-mida/` (visited on 05/06/2022) (cited on page 39).

[133] Studio RAP. *New Delft Blue - Studio RAP*. en. (accessed May 6, 2022). 2016. URL: `https://studiorap.nl/New-Delft-Blue` (visited on 05/06/2022) (cited on page 39).

[134] Mario Cucinella. *TECLA Technology and Clay 3D Printed House / Mario Cucinella Architects*. en-US. Architecture, Projects. (accessed May 6, 2022). Apr. 2021. URL: `https://www.archdaily.com/960714/tecla-technology-and-clay-3d-printed-house-mario-cucinella-architects` (cited on page 39).

[135] Zach Seibold, Saurabh Mhatre, and Suleiman Alhadidi. 'Janus Printing: Coextrusion based Multi-material Additive Manufacturing for Ceramics'. en. In: *Proceedings of the Annual Conference of the Association for Computer-Aided Design in Architecture (ACADIA)*. Ed. by Kory Bieg, Danelle Briscone, and Odom Clay. Austin, Texas, USA., 2019, pp. 576–585. DOI: `10.52842/conf.acadia.2019.576` (cited on page 40).

[136] Benoit Furet, Philippe Poullain, and Sébastien Garnier. '3D printing for construction based on a complex wall of polymer-foam and concrete'. en. In: *Additive Manufacturing* 28 (Aug. 2019), pp. 58–64. DOI: `10.1016/j.addma.2019.04.002` (cited on pages 40, 42, 43, 59).

[137] Timothy Wangler et al. 'Digital Concrete: A Review'. en. In: *Cement and Concrete Research* 123 (Sept. 2019), p. 105780. DOI: `10.1016/j.cemconres.2019.105780` (cited on page 40).

[138] Shantanu Bhattacherjee et al. 'Sustainable materials for 3D concrete printing'. en. In: *Cement and Concrete Composites* 122 (Sept. 2021), p. 104156. DOI: `10.1016/j.cemconcomp.2021.104156` (cited on page 40).

[139] Malek Mohammad, Eyad Masad, and Sami G. Al-Ghamdi. '3D Concrete Printing Sustainability: A Comparative Life Cycle Assessment of Four Construction Method Scenarios'. en. In: *Buildings* 10.12 (Dec. 2020), p. 245. DOI: `10.3390/buildings10120245` (cited on page 40).

[140] Jianzhuang Xiao et al. '3D recycled mortar printing: System development, process design, material properties and on-site printing'. en. In: *Journal of Building Engineering* 32 (Nov. 2020), p. 101779. DOI: `10.1016/j.jobe.2020.101779` (cited on page 40).

[141] Jianzhuang Xiao et al. 'Fiber-reinforced mortar with 100% recycled fine aggregates: A cleaner perspective on 3D printing'. en. In: *Journal of Cleaner Production* 319 (Oct. 2021), p. 128720. DOI: `10.1016/j.jclepro.2021.128720` (cited on page 40).

[142] Harald Kloft et al. 'Reinforcement strategies for 3D-concrete-printing'. en. In: *Civil Engineering Design* 2.4 (2020), pp. 131–139. DOI: `10.1002/cend.202000022` (cited on page 40).

[143] Domenico Asprone et al. 'Rethinking reinforcement for digital fabrication with concrete'. en. In: *Cement and Concrete Research* 112 (Oct. 2018), pp. 111–121. DOI: `10.1016/j.cemconres.2018.05.020` (cited on page 40).

[144] Viktor Mechtcherine et al. 'Integrating reinforcement in digital fabrication with concrete: A review and classification framework'. en. In: *Cement and Concrete Composites* 119 (May 2021), p. 103964. DOI: `10.1016/j.cemconcomp.2021.103964` (cited on page 40).

[145] Freek Bos et al. 'Experimental Exploration of Metal Cable as Reinforcement in 3D Printed Concrete'. en. In: *Materials* 10.11 (Nov. 2017), p. 1314. DOI: `10.3390/ma10111314` (cited on page 40).

[146] Omar Geneidy et al. 'Simultaneous Reinforcement of Concrete While 3D Printing'. en. In: *Second RILEM International Conference on Concrete and Digital Fabrication*. Ed. by Freek P. Bos et al. Vol. 28. Cham: Springer International Publishing, 2020, pp. 895–905. DOI: `10.1007/978-3-030-49916-7_87` (cited on page 40).

[147] F. P. Bos et al. 'The realities of additively manufactured concrete structures in practice'. en. In: *Cement and Concrete Research* 156 (June 2022), p. 106746. doi: `10.1016/j.cemconres.2022.106746` (cited on pages 40, 59).

[148] Steven J. Keating et al. 'Toward site-specific and self-sufficient robotic fabrication on architectural scales'. en. In: *Science Robotics* 2.5 (Apr. 2017), p. 15. doi: `10.1126/scirobotics.aam8986` (cited on pages 41, 43).

[149] Joshua Bard et al. 'Robotic concrete surface finishing: a moldless approach to creating thermally tuned surface geometry for architectural building components using Profile-3D-Printing'. en. In: *Construction Robotics* 2.1-4 (Dec. 2018), pp. 53–65. doi: `10.1007/s41693-018-0014-x` (cited on pages 41, 42).

[150] Thomas Adams et al. 'Ultra-lightweight foamed concrete for an automated facade application'. en. In: *Magazine of Concrete Research* 71.8 (Apr. 2019), pp. 424–436. doi: `10.1680/jmacr.18.00272` (cited on pages 41, 43).

[151] Klaudius Henke, Daniel Talke, and Carla Matthäus. 'Additive Manufacturing by Extrusion of Lightweight Concrete - Strand Geometry, Nozzle Design and Layer Layout'. en. In: *Second RILEM International Conference on Concrete and Digital Fabrication*. Ed. by Freek P. Bos et al. Vol. 28. Springer, Cham, 2020, pp. 906–915. doi: `10.1007/978-3-030-49916-7_88` (cited on pages 41, 43).

[152] Lapyote Prasittisopin et al. 'Thermal and Sound Insulation of Large-Scale 3D Extrusion Printing Wall Panel'. en. In: *Second RILEM International Conference on Concrete and Digital Fabrication*. Ed. by Freek P. Bos et al. Vol. 28. Springer, Cham, 2020, pp. 1174–1182. doi: `10.1007/978-3-030-49916-7_111` (cited on pages 41, 43, 51, 52).

[153] Norman Hack and Harald Kloft. 'Shotcrete 3D Printing Technology for the Fabrication of Slender Fully Reinforced Freeform Concrete Elements with High Surface Quality: A Real-Scale Demonstrator'. en. In: *Second RILEM International Conference on Concrete and Digital Fabrication*. Ed. by Freek P. Bos et al. Vol. 28. Springer, Cham, 2020, pp. 1128–1137. doi: `10.1007/978-3-030-49916-7_107` (cited on pages 42, 43).

[154] Gido Dielemans et al. 'Additive Manufacturing of Thermally Enhanced Lightweight Concrete Wall Elements with Closed Cellular Structures'. en. In: *Journal of Facade Design and Engineering* 9.1 (Apr. 2021), pp. 59–72. doi: `10.7480/JFDE.2021.1.5418` (cited on pages 42, 43, 49, 59, 137).

[155] Jolien Van Der Putten et al. '3D Concrete Printing on Site: A Novel Way of Building Houses?' en. In: *Second RILEM International Conference on Concrete and Digital Fabrication*. Ed. by Freek P. Bos et al. Vol. 28. Springer, Cham, 2020, pp. 712–719. doi: `10.1007/978-3-030-49916-7_71` (cited on page 42).

[156] Patrick Bedarf et al. 'Foam 3D printing for construction: A review of applications, materials, and processes'. en. In: *Automation in Construction* 130 (Oct. 2021), p. 103861. doi: `10.1016/j.autcon.2021.103861` (cited on page 43).

[157] W.V. Liu, D.B. Apel, and V.S. Bindiganavile. 'Thermal properties of lightweight dry-mix shotcrete containing expanded perlite aggregate'. en. In: *Cement and Concrete Composites* 53 (Oct. 2014), pp. 44–51. doi: `10.1016/j.cemconcomp.2014.06.003` (cited on page 43).

[158] S. Pessoa et al. '3D printing in the construction industry - A systematic review of the thermal performance in buildings'. en. In: *Renewable and Sustainable Energy Reviews* 141 (May 2021), p. 110794. doi: `10.1016/j.rser.2021.110794` (cited on pages 43, 50, 59, 137).

[159] C. Buchanan and L. Gardner. 'Metal 3D printing in construction: A review of methods, research, applications, opportunities and challenges'. en. In: *Engineering Structures* 180 (Feb. 2019), pp. 332–348. doi: `10.1016/j.engstruct.2018.11.045` (cited on page 43).

[160] Suman Das, David L. Bourell, and S. S. Babu. 'Metallic materials for 3D printing'. en. In: *Materials Research Society (MRS) Bulletin* 41.10 (Oct. 2016), pp. 729–741. doi: `10.1557/mrs.2016.217` (cited on page 44).

[161] Thomas Duda and L. Venkat Raghavan. '3D Metal Printing Technology'. en. In: *International Federation of Automatic Control-PapersOnLine* 49.29 (2016), pp. 103–110. doi: `10.1016/j.ifacol.2016.11.111` (cited on page 44).

[162] Eric Vitug. *Rapid Analysis and Manufacturing Propulsion Technology (RAMPT)*. en. News. (accessed May 2, 2022). July 2020. URL: `http://www.nasa.gov/directorates/spacetech/game_changing_development/projects/RAMPT` (visited on 05/02/2022) (cited on page 44).

[163] Leroy Gardner et al. 'Testing and initial verification of the world's first metal 3D printed bridge'. en. In: *Journal of Constructional Steel Research* 172 (Sept. 2020), p. 106233. DOI: `10.1016/j.jcsr.2020.106233` (cited on page 44).

[164] Sheida Shakeri. *Remnants of a Future Architecture, by Roland Snooks*. en. Architecture, Projects. (accessed May 2, 2022). Mar. 2022. URL: `https://parametric-architecture.com/remnants-of-a-future-architecture-by-roland-snooks/` (visited on 05/02/2022) (cited on page 44).

[165] William E. Frazier. 'Metal Additive Manufacturing: A Review'. en. In: *Journal of Materials Engineering and Performance* 23.6 (June 2014), pp. 1917–1928. DOI: `10.1007/s11665-014-0958-z` (cited on page 44).

[166] Felix Raspall, Felix Amtsberg, and Carlos Banon. '3D Printed Space Frames'. en. In: *Proceedings of International Association for Shell and Spatial Structures Annual Symposia*. MIT. Cambridge, Massachusetts, July 2018, pp. 1–8 (cited on pages 44, 45).

[167] Paul Kassabian et al. '3D Metal Printing as Structure for Architectural and Sculptural Projects'. en. In: *Fabricate 2017*. Ed. by Achim Menges et al. UCL Press, Apr. 2017, pp. 196–197 (cited on pages 44, 45).

[168] Alamir Mohsen. *Design to Manufacture of Complex Building Envelopes: Single Layer Envelopes: Mullion-Transom Systems + 3D printed Metal Nodes*. en. Vol. 56. Mechanik, Werkstoffe und Konstruktion im Bauwesen. Wiesbaden: Springer Fachmedien, 2020 (cited on pages 44, 46).

[169] Salomé Galjaard, Sander Hofman, and Shibo Ren. 'New Opportunities to Optimize Structural Designs in Metal by Using Additive Manufacturing'. en. In: *Advances in Architectural Geometry 2014*. Ed. by Philippe Block et al. Cham: Springer International Publishing, 2015, pp. 79–93. DOI: `10.1007/978-3-319-11418-7_6` (cited on pages 44, 45).

[170] Amit Bandyopadhyay, Yanning Zhang, and Susmita Bose. 'Recent developments in metal additive manufacturing'. en. In: *Current Opinion in Chemical Engineering* 28 (June 2020), pp. 96–104. DOI: `10.1016/j.coche.2020.03.001` (cited on page 44).

[171] Mania Aghaei Meibodi et al. 'Bespoke Cast Facade: Design and Additive Manufacturing for Aluminum Facade Elements'. en. In: *Proceedings of the 39th Annual Conference of the Association for Computer Aided Design in Architecture (ACADIA)*. Austin, Texas, 2019, pp. 100–109. DOI: `10.52842/conf.acadia.2019.100` (cited on pages 44, 46).

[172] Mohsen Attaran. 'The rise of 3-D printing: The advantages of additive manufacturing over traditional manufacturing'. en. In: *Business Horizons* 60.5 (Sept. 2017), pp. 677–688. DOI: `10.1016/j.bushor.2017.05.011` (cited on page 44).

[173] FIT AG. *Construction and architecture, FIT Additive Manufacturing Group*. en. (accessed October 28, 2022). 2022. URL: `https://fit.technology/sectors/architecture` (visited on 10/28/2022) (cited on page 46).

[174] Henry A. Colorado, Elkin I. Gutiérrez Velásquez, and Sergio Neves Monteiro. 'Sustainability of additive manufacturing: the circular economy of materials and environmental perspectives'. en. In: *Journal of Materials Research and Technology* 9.4 (July 2020), pp. 8221–8234. DOI: `10.1016/j.jmrt.2020.04.062` (cited on page 46).

[175] Eliot F. Gomez et al. '3D-Printed Self-Healing Elastomers for Modular Soft Robotics'. In: *American Chemical Society Applied Materials & Interfaces* 13.24 (June 2021), pp. 28870–28877. DOI: `10.1021/acsami.1c06419` (cited on page 46).

[176] Ajit Behera, Dipen Kumar Rajak, and K. Jeyasubramanian. 'Chapter 19 - Fabrication of nanostructures with excellent self-cleaning properties'. en. In: *Design, Fabrication, and Characterization of Multifunctional Nanomaterials*. Ed. by Sabu Thomas, Nandakumar Kalarikkal, and Ann Rose Abraham. Micro and Nano Technologies. Elsevier, Jan. 2022, pp. 449–478. DOI: `10.1016/B978-0-12-820558-7.00014-5` (cited on page 46).

[177] Dianne B. Gutierrez et al. 'The potential of additively manufactured membranes for selective separation and capture of CO2'. en. In: *Materials Research Society Communications* 11.4 (Aug. 2021), pp. 391–401. DOI: `10.1557/s43579-021-00062-8` (cited on page 46).

[178] Asterios Agkathidis, Yorgos Berdos, and Andre Brown. 'Active membranes: 3D printing of elastic fibre patterns on pre-stretched textiles'. In: *International Journal of Architectural Computing* 17.1 (Mar. 2019), pp. 74–87. DOI: `10.1177/1478077118800890` (cited on page 47).

[179] Elena Vazquez, Benay Gursoy, and Jose Duarte. 'Designing for shape change'. en. In: *Proceedings of the 24th International Conference of the Association for Computer-Aided Architectural Design Research in Asia (CAADRIA)*. Vol. 2. Wellington, New Zealand, 2019, pp. 391–400. DOI: `10.52842/conf.caadria.2019.2.391` (cited on page 47).

[180] Amira Abdel-Rahman and Elnaz Tafrihi. 'Heat-actuated auxetic facades'. en. In: *Proceedings of Facade Tectonics 2018 World Congress*. Vol. 1. Los Angeles, USA, 2018, pp. 435–45 (cited on pages 47, 48).

[181] Aamir Ahmed et al. '4D printing: Fundamentals, materials, applications and challenges'. en. In: *Polymer* 228 (July 2021), p. 123926. DOI: `10.1016/j.polymer.2021.123926` (cited on page 47).

[182] Elena Vazquez, Clive Randall, and Jose Pinto Duarte. 'Shape-changing architectural skins: a review on materials, design and fabrication strategies and performance analysis'. en. In: *Journal of Facade Design and Engineering* (2019), pp. 91–102. DOI: `10.7480/JFDE.2019.2.3877` (cited on page 47).

[183] Hwang Yi and Yuri Kim. 'Prototyping of 4D-printed self-shaping building skin in architecture: Design, fabrication, and investigation of a two-way shape memory composite (TWSMC) façade panel'. en. In: *Journal of Building Engineering* 43 (2021), p. 103076. DOI: `10.1016/j.jobe.2021.103076` (cited on pages 47, 48).

[184] Rana El-Dabaa and Islam Salem. '4D printing of wooden actuators: encoding FDM wooden filaments for architectural responsive skins'. In: *Open House International* 46.3 (Jan. 2021), pp. 376–390. DOI: `10.1108/OHI-02-2021-0028` (cited on pages 47, 48).

[185] David Correa et al. '3D-Printed Wood: Programming Hygroscopic Material Transformations'. en. In: *3D Printing and Additive Manufacturing* 2.3 (Sept. 2015), pp. 106–116. DOI: `10.1089/3dp.2015.0022` (cited on pages 47, 49).

[186] Shadpour Mallakpour, Farbod Tabesh, and Chaudhery Mustansar Hussain. '3D and 4D printing: From innovation to evolution'. en. In: *Advances in Colloid and Interface Science* 294 (Aug. 2021), p. 102482. DOI: `10.1016/j.cis.2021.102482` (cited on page 47).

[187] Hassan A. Alshahrani. 'Review of 4D printing materials and reinforced composites: Behaviors, applications and challenges'. en. In: *Journal of Science: Advanced Materials and Devices* 6.2 (June 2021), pp. 167–185. DOI: `10.1016/j.jsamd.2021.03.006` (cited on page 47).

[188] Frederik Kotz et al. 'Three-dimensional printing of transparent fused silica glass'. en. In: *Nature* 544.7650 (Apr. 2017), pp. 337–339. DOI: `10.1038/nature22061` (cited on page 47).

[189] Dao Zhang, Xiaofeng Liu, and Jianrong Qiu. '3D printing of glass by additive manufacturing techniques: a review'. en. In: *Frontiers of Optoelectronics* 14.3 (Sept. 2021), pp. 263–277. DOI: `10.1007/s12200-020-1009-z` (cited on page 47).

[190] Chikara Inamura et al. 'Additive Manufacturing of Transparent Glass Structures'. en. In: *3D Printing and Additive Manufacturing* 5.4 (Dec. 2018), pp. 269–283. DOI: `10.1089/3dp.2018.0157` (cited on pages 47, 48).

[191] Maple Glass Printing Ltd. (accessed October 14, 2022). 2021. URL: `https://www.mapleglassprinting.com/` (visited on 10/14/2022) (cited on pages 47, 49).

[192] Jungwon Yoon. 'SMP Prototype Design and Fabrication for Thermo-responsive Façade Elements'. en. In: *Journal of Facade Design and Engineering* (Nov. 2018), pp. 41–62. DOI: `10.7480/JFDE.2019.1.2662` (cited on page 48).

[193] Dennis De Witte et al. 'Convective Concrete: Additive Manufacturing to facilitate activation of thermal mass'. en. In: *Journal of Facade Design and Engineering* 5.1 (2017), pp. 107–117. DOI: `10.7480/JFDE.2017.1.1430` (cited on page 49).

[194] Bharath Seshadri et al. 'Parametric design of an additively manufactured building facade for bespoke response to solar radiation'. en. In: *Journal of Physics: Conference Series* 2042.1 (Nov. 2021), p. 012180. DOI: `10.1088/1742-6596/2042/1/012180` (cited on pages 49, 50).

[195] David Briels et al. 'Thermal Optimization of Additively Manufactured Lightweight Concrete Wall Elements with Internal Cellular Structure through Simulations and Measurements'. en. In: *Buildings* 12.7 (July 2022). Number: 7 Publisher: Multidisciplinary Digital Publishing Institute, p. 1023. DOI: `10.3390/buildings12071023` (cited on pages 50–52, 59).

[196] Giuseppe De Michele et al. 'Opportunities and Challenges for Performance Prediction of Dynamic Complex Fenestration Systems (CFS)'. In: *Journal of Facade Design and Engineering* 6.3 (Nov. 2018), pp. 101–115. DOI: `10.7480/jfde.2018.3.2531` (cited on page 50).

[197] Valeria Piccioni et al. 'Tuning the Solar Performance of Building Facades through Polymer 3D Printing: Toward Bespoke Thermo-Optical Properties'. en. In: *Advanced Materials Technologies* 8.6 (Mar. 2023), p. 2201200. DOI: `10.1002/admt.202201200` (cited on pages 50, 69, 89, 134, 164, 167).

[198] Fabio Favoino et al. *Building Performance Simulation and Characterisation of Adaptive Facades - Adaptive Facade Network*. en. Delft: TU Delft Open, 2018 (cited on page 50).

[199] Anton Wiberg, Johan Persson, and Johan Ölvander. 'Design for additive manufacturing – a review of available design methods and software'. en. In: *Rapid Prototyping Journal* 25.6 (July 2019), pp. 1080–1094. DOI: `10.1108/RPJ-10-2018-0262` (cited on page 50).

[200] Izhar Hussain Shah et al. 'Environmental life cycle assessment of wire arc additively manufactured steel structural components'. en. In: *Journal of Cleaner Production* 389 (Feb. 2023), p. 136071. DOI: `10.1016/j.jclepro.2023.136071` (cited on page 50).

[201] ArchiTech. *R-Iglo workspace. Rotterdam*. en-US. (accessed October 8, 2022). 2021. URL: `https://www.architechcompany.com/site/r-iglo-workspace-rotterdam/` (visited on 10/08/2022) (cited on page 50).

[202] Inês Ribeiro et al. 'Framework for Life Cycle Sustainability Assessment of Additive Manufacturing'. en. In: *Sustainability* 12.3 (Jan. 2020), p. 929. DOI: `10.3390/su12030929` (cited on page 51).

[203] Nima Zohdi and Richard (Chunhui) Yang. 'Material Anisotropy in Additively Manufactured Polymers and Polymer Composites: A Review'. en. In: *Polymers* 13.19 (Jan. 2021), p. 3368. DOI: `10.3390/polym13193368` (cited on page 51).

[204] Lavinia Tonelli et al. 'Influence of Interlayer Forced Air Cooling on Microstructure and Mechanical Properties of Wire Arc Additively Manufactured 304L Austenitic Stainless Steel'. en. In: *steel research international* 92.11 (2021), p. 2100175. DOI: `10.1002/srin.202100175` (cited on page 51).

[205] Vittoria Laghi et al. 'Mechanical response of dot-by-dot wire-and-arc additively manufactured 304L stainless steel bars under tensile loading'. en. In: *Construction and Building Materials* 318 (Feb. 2022), p. 125925. DOI: `10.1016/j.conbuildmat.2021.125925` (cited on page 51).

[206] Vittoria Laghi et al. 'On the influence of the geometrical irregularities in the mechanical response of Wire-and-Arc Additively Manufactured planar elements'. en. In: *Journal of Constructional Steel Research* 178 (Mar. 2021), p. 106490. DOI: `10.1016/j.jcsr.2020.106490` (cited on page 51).

[207] Marouene Zouaoui et al. 'Numerical Prediction of 3D Printed Specimens Based on a Strengthening Method of Fracture Toughness'. en. In: *Procedia International Academy for Production Engineering*. 52nd CIRP Conference on Manufacturing Systems (CMS), Ljubljana, Slovenia, June 12-14, 2019 81 (Jan. 2019), pp. 40–44. DOI: `10.1016/j.procir.2019.03.008` (cited on page 51).

[208] Pinelopi Kyvelou et al. 'Mechanical and microstructural testing of wire and arc additively manufactured sheet material'. en. In: *Materials & Design* 192 (July 2020), p. 108675. DOI: `10.1016/j.matdes.2020.108675` (cited on page 51).

[209] Hyunwoo Yuk et al. '3D printing of conducting polymers'. en. In: *Nature Communications* 11.1 (Mar. 2020), p. 1604. DOI: `10.1038/s41467-020-15316-7` (cited on page 51).

[210] Caterina Amendola et al. 'Optical characterization of 3D printed PLA and ABS filaments for diffuse optics applications'. en. In: *Public Library of Science ONE* 16.6 (June 2021), e0253181. DOI: `10.1371/journal.pone.0253181` (cited on page 51).

[211] Zijian Li et al. ‘Anisotropy on electrical insulation performance of 3D printed nylon 12’. In: *2017 Institute of Electrical and Electronics Engineers Conference on Electrical Insulation and Dielectric Phenomenon (CEIDP)*. Oct. 2017, pp. 42–45. DOI: `10.1109/CEIDP.2017.8257452` (cited on page 51).

[212] Lionel Auffray, Pierre-André Gouge, and Lamine Hattali. ‘Design of experiment analysis on tensile properties of PLA samples produced by fused filament fabrication’. en. In: *The International Journal of Advanced Manufacturing Technology* 118.11 (Feb. 2022), pp. 4123–4137. DOI: `10.1007/s00170-021-08216-7` (cited on page 51).

[213] T. J. Dodwell et al. ‘A data-centric approach to generative modelling for 3D-printed steel’. In: *Proceedings of the Royal Society A: Mathematical, Physical and Engineering Sciences* 477.2255 (Nov. 2021), p. 20210444. DOI: `10.1098/rspa.2021.0444` (cited on page 51).

[214] Anupam Pandit, Ravi Sekhar, and Ram K. Revanur. ‘Simulation Mechanism Development for Additive Manufacturing’. en. In: *Materials Today: Proceedings*. International Conference on Advancements in Aeromechanical Materials for Manufacturing (ICAAMM-2016): Organized by MLR Institute of Technology, Hyderabad, Telangana, India 4.8 (Jan. 2017), pp. 7270–7278. DOI: `10.1016/j.matpr.2017.07.056` (cited on page 51).

[215] Janis Reinold et al. ‘Extrusion process simulation and layer shape prediction during 3D-concrete-printing using the Particle Finite Element Method’. en. In: *Automation in Construction* 136 (Apr. 2022), p. 104173. DOI: `10.1016/j.autcon.2022.104173` (cited on page 51).

[216] Nicholas Lavery et al. ‘A Review of Computational Modelling of Additive Layer, Manufacturing - Multi-Scale and Multi-Physics’. English. In: *The Journal of Innovation Impact* 7 (Apr. 2014), pp. 651–673. DOI: `10.13140/RG.2.1.3103.0884` (cited on pages 51, 52).

[217] Mark Horstemeyer. ‘Multiscale Modeling: A Review’. In: *Practical Aspects of Computational Chemistry*. Oct. 2009, pp. 87–135. DOI: `10.1007/978-90-481-2687-3_4` (cited on pages 51, 52).

[218] M. M. Francois et al. ‘Modeling of additive manufacturing processes for metals: Challenges and opportunities’. en. In: *Current Opinion in Solid State and Materials Science* 21.4 (Aug. 2017), pp. 198–206. DOI: `10.1016/j.cossms.2016.12.001` (cited on pages 51, 52).

[219] MIT. *Office of Sustainability - Living Labs | MIT Sustainability*. (accessed October 8, 2022). 2021. URL: `https://sustainability.mit.edu/living-labs` (visited on 10/08/2022) (cited on page 52).

[220] NEST. *Next Evolution in Sustainable Building Technologies - HiLo*. (accessed October 8, 2022). 2021. URL: `https://www.empa.ch/web/nest/hilo` (visited on 10/08/2022) (cited on page 52).

[221] The Green Village - TU Delft. *The Green Village - Field lab for sustainable innovation*. en-US. (accessed October 8, 2022). 2022. URL: `https://www.thegreenvillage.org/en/` (visited on 10/08/2022) (cited on page 52).

[222] Judy Too et al. ‘Framework for standardising carbon neutrality in building projects’. en. In: *Journal of Cleaner Production* 373 (Nov. 2022), p. 133858. DOI: `10.1016/j.jclepro.2022.133858` (cited on page 59).

[223] Patrick Bischof, Jaime Mata-Falcón, and Walter Kaufmann. ‘Fostering innovative and sustainable mass-market construction using digital fabrication with concrete’. en. In: *Cement and Concrete Research* 161 (Nov. 2022), p. 106948. DOI: `10.1016/j.cemconres.2022.106948` (cited on page 59).

[224] Andrei Jipa et al. ‘3D-Printed Formwork for Integrated Funicular Concrete Slabs’. en. In: (2019), p. 10 (cited on pages 59, 104, 105).

[225] Odysseas Kontovourkis and George Tryfonos. ‘Robotic 3D clay printing of prefabricated non-conventional wall components based on a parametric-integrated design’. en. In: *Automation in Construction* 110 (Feb. 2020), p. 103005. DOI: `10.1016/j.autcon.2019.103005` (cited on page 59).

[226] Mohamed Gomaa et al. ‘Thermal performance exploration of 3D printed cob’. In: *Architectural Science Review* 62.3 (May 2019). Publisher: Taylor & Francis _eprint: https://doi.org/10.1080/00038628.2019.1606776, pp. 230–237. DOI: `10.1080/00038628.2019.1606776` (cited on page 59).

[227] Hannelie Marais et al. ‘Computational assessment of thermal performance of 3D printed concrete wall structures with cavities’. en. In: *Journal of Building Engineering* 41 (Sept. 2021), p. 102431. DOI: `10.1016/j.jobe.2021.102431` (cited on page 59).

[228] Jingting Sun et al. 'Experimental study on the thermal performance of a 3D printed concrete prototype building'. en. In: *Energy and Buildings* 241 (June 2021), p. 110965. DOI: 10.1016/j.enbuild.2021.110965 (cited on page 59).

[229] Saad Alqahtani et al. 'Thermal performance of additively manufactured polymer lattices'. en. In: *Journal of Building Engineering* 39 (July 2021), p. 102243. DOI: 10.1016/j.jobe.2021.102243 (cited on pages 60, 66).

[230] Beata Grabowska and Jacek Kasperski. 'The Thermal Conductivity of 3D Printed Plastic Insulation Materials—The Effect of Optimizing the Regular Structure of Closures'. In: *Materials* 13.19 (Oct. 2020), p. 4400. DOI: 10.3390/ma13194400 (cited on page 60).

[231] Mohammad Taregh Sepahi et al. 'Mechanical Properties of 3D-Printed Parts Made of Polyethylene Terephthalate Glycol'. In: *Journal of Materials Engineering and Performance* 30 (Sept. 2021). ADS Bibcode: 2021JMEP...30.6851S, pp. 6851–6861. DOI: 10.1007/s11665-021-06032-4 (cited on pages 60, 82, 141, 166).

[232] Pavel Petrov et al. 'Research into the effect of the 3D-printing mode on changing the properties of PETG transparent plastic'. en. In: *ESAFORM 2021* (Apr. 2021). DOI: 10.25518/esaform21.3763 (cited on pages 60, 82, 107, 141, 166).

[233] CEAD. *E25 printing head. for large-scale additive manufacturing*. 2022. URL: https://ceadgroup.com/solutions/technology-components/e25/ (visited on 10/18/2022) (cited on page 61).

[234] Omer Eyercioglu et al. 'Determination of the Maximum Bridging Distance in Large Scale Additive Manufacturing'. en. In: (2019) (cited on pages 61, 104, 110, 146).

[235] C. Amaral et al. 'Polyurethane foams with microencapsulated phase change material: Comparative analysis of thermal conductivity characterization approaches'. en. In: *Energy and Buildings* 153 (Oct. 2017), pp. 392–402. DOI: 10.1016/j.enbuild.2017.08.019 (cited on page 62).

[236] Xi Meng et al. 'Feasibility experiment on the simple hot box-heat flow meter method and the optimization based on simulation reproduction'. In: *Applied Thermal Engineering* 83 (May 2015), pp. 48–56. DOI: 10.1016/j.applthermaleng.2015.03.010 (cited on pages 62, 146).

[237] C. Buratti et al. 'Thermal Conductivity Measurements By Means of a New 'Small Hot-Box' Apparatus: Manufacturing, Calibration and Preliminary Experimental Tests on Different Materials'. en. In: *International Journal of Thermophysics* 37.5 (May 2016), p. 47. DOI: 10.1007/s10765-016-2052-2 (cited on page 62).

[238] C16 Committee ASTM International. *Practice for Calculating Thermal Transmission Properties Under Steady-State Conditions*. en. Tech. rep. ASTM International, 2019. DOI: 10.1520/C1045-07. (Visited on 01/21/2022) (cited on page 62).

[239] C16 Committee ASTM International. *Test Method for Thermal Performance of Building Materials and Envelope Assemblies by Means of a Hot Box Apparatus*. en. Tech. rep. ASTM International, 2019. DOI: 10.1520/C1363-19. (Visited on 01/21/2022) (cited on page 62).

[240] Nelson Soares et al. 'Laboratory and in-situ non-destructive methods to evaluate the thermal transmittance and behavior of walls, windows, and construction elements with innovative materials: A review'. en. In: *Energy and Buildings* 182 (Jan. 2019), pp. 88–110. DOI: 10.1016/j.enbuild.2018.10.021 (cited on page 62).

[241] G.P. Lydon et al. 'Coupled simulation of thermally active building systems to support a digital twin'. en. In: *Energy and Buildings* 202 (Nov. 2019), p. 109298. DOI: 10.1016/j.enbuild.2019.07.015 (cited on page 63).

[242] ISO Central Secretary. *ISO 9869-1:2014(en), Thermal insulation — Building elements — In-situ measurement of thermal resistance and thermal transmittance — Part 1: Heat flow meter method*. 2014. URL: https://www.iso.org/obp/ui/en/#iso:std:iso:9869:-1:ed-1:v1:en (visited on 11/17/2023) (cited on pages 64, 66, 139, 147).

[243] Ismael Sánchez-Calderón et al. 'Methodology for measuring the thermal conductivity of insulating samples with small dimensions by heat flow meter technique'. en. In: *Journal of Thermal Analysis and Calorimetry* 147.22 (Nov. 2022), pp. 12523–12533. DOI: `10.1007/s10973-022-11457-7` (cited on page 64).

[244] Yunus A. Çengel. *Heat Transfer: A Practical Approach*. en. Google-Books-ID: nrbfpSZTwskC. McGraw-Hill, 2003 (cited on page 64).

[245] COMSOL. *COMSOL: Multiphysics Software for Optimizing Designs*. en. URL: `https://www.comsol.com/` (visited on 12/10/2023) (cited on page 65).

[246] MatWeb, LLC. *MatWeb: Material Property Data. Overview of materials for PETG Copolyester*. URL: `https://www.matweb.com/search/datasheet_print.aspx?matguid=4de1c85bb946406a86c52b688e3810d0` (visited on 12/10/2023) (cited on page 65).

[247] Rakshith Badarinath and Vittaldas Prabhu. 'Real-Time Sensing of Output Polymer Flow Temperature and Volumetric Flowrate in Fused Filament Fabrication Process'. en. In: *Materials* 15.2 (Jan. 2022). Number: 2 Publisher: Multidisciplinary Digital Publishing Institute, p. 618. DOI: `10.3390/ma15020618` (cited on page 65).

[248] A. Mezrhab et al. 'Computation of combined natural-convection and radiation heat-transfer in a cavity having a square body at its center'. en. In: *Applied Energy* 83.9 (Sept. 2006), pp. 1004–1023. DOI: `10.1016/j.apenergy.2005.09.006` (cited on page 65).

[249] Clement Kleinstreuer. 'Engineering Fluid Dynamics: An Interdisciplinary Systems Approach'. en. In: *Cambridge University Press* (), p. 8 (cited on page 65).

[250] COMSOL. *Modeling Natural and Forced Convection in COMSOL Multiphysics®*. en. URL: `https://www.comsol.com/blogs/modeling-natural-and-forced-convection-in-comsol-multiphysics/` (visited on 12/10/2023) (cited on page 65).

[251] Jiayi Zhu and Guoqing He. 'Heat transfer coefficients of double skin facade windows'. en. In: *Science and Technology for the Built Environment* 25.9 (Oct. 2019), pp. 1143–1151. DOI: `10.1080/23744731.2019.1624447` (cited on page 66).

[252] Thadshajini Suntharalingam et al. 'Numerical Study of Fire and Energy Performance of Innovative Light-Weight 3D Printed Concrete Wall Configurations in Modular Building System'. en. In: *Sustainability* 13.4 (Feb. 2021), p. 2314. DOI: `10.3390/su13042314` (cited on page 66).

[253] Zhou Shengrong. *An Environmental Perspective on 3DPrinted Facade with Plastics*. Tech. rep. ETH Zurich, 2021 (cited on page 68).

[254] Jamison Go et al. 'Rate limits of additive manufacturing by fused filament fabrication and guidelines for high-throughput system design'. en. In: *Additive Manufacturing* 16 (Aug. 2017), pp. 1–11. DOI: `10.1016/j.addma.2017.03.007` (cited on page 76).

[255] Narendra Singh et al. 'Sustainable materials alternative to petrochemical plastics pollution: A review analysis'. en. In: *Sustainable Horizons* 2 (Mar. 2022), p. 100016. DOI: `10.1016/j.horiz.2022.100016` (cited on page 76).

[256] Brian N. Turner, Robert Strong, and Scott A. Gold. 'A review of melt extrusion additive manufacturing processes: I. Process design and modeling'. In: *Rapid Prototyping Journal* 20.3 (Jan. 2014). Publisher: Emerald Group Publishing Limited, pp. 192–204. DOI: `10.1108/RPJ-01-2013-0012` (cited on pages 77, 104, 140).

[257] Christopher Barnatt. *3D Printing: The Next Industrial Revolution*. en. Third edition. OCLC: 974652195. United States: ExplainingTheFuture.com, 2013 (cited on pages 77, 104).

[258] Phillip Chesser et al. 'Extrusion control for high quality printing on Big Area Additive Manufacturing (BAAM) systems'. en. In: *Additive Manufacturing* 28 (Aug. 2019), pp. 445–455. DOI: `10.1016/j.addma.2019.05.020` (cited on pages 78, 104, 105).

[259] Brett G. Compton et al. 'Thermal analysis of additive manufacturing of large-scale thermoplastic polymer composites'. en. In: *Additive Manufacturing* 17 (Oct. 2017), pp. 77–86. DOI: `10.1016/j.addma.2017.07.006` (cited on pages 78, 86, 158).

[260] Michael Borish et al. 'Real-Time Defect Correction in Large-Scale Polymer Additive Manufacturing via Thermal Imaging and Laser Profilometer'. en. In: *Procedia Manufacturing* 48 (2020), pp. 625–633. DOI: `10.1016/j.promfg.2020.05.091` (cited on pages 78, 81, 85).

[261] Philip F. Yuan et al. 'Robotic Multi-dimensional Printing Based on Structural Performance'. en. In: *Robotic Fabrication in Architecture, Art and Design 2016*. Ed. by Dagmar Reinhardt, Rob Saunders, and Jane Burry. Cham: Springer International Publishing, 2016, pp. 92–105. DOI: `10.1007/978-3-319-26378-6_7` (cited on page 79).

[262] Natalie M. Larson et al. 'Rotational multimaterial printing of filaments with subvoxel control'. en. In: *Nature* 613.7945 (Jan. 2023), pp. 682–688. DOI: `10.1038/s41586-022-05490-7` (cited on pages 79, 95).

[263] Brad Michael Bourgoyne. 'Method and apparatus for additive fabrication of three-dimensional objects utilizing vesiculated extrusions, and objects thereof'. US 2016/0096320 A1 (Baton Rouge, LA). 2015 (cited on pages 79, 80, 84, 96, 105).

[264] Nicholas Hopkins, Ruben Janse van Vuuren, and Hadley Brooks. 'Additive manufacturing via tube extrusion (AMTEx)'. en. In: *Additive Manufacturing* 36 (Dec. 2020), p. 101606. DOI: `10.1016/j.addma.2020.101606` (cited on pages 79, 80, 84, 96, 105, 110, 113, 136, 165).

[265] J. Vlachopoulos and D. Strutt. 'Polymer processing'. en. In: *Materials Science and Technology* 19.9 (Sept. 2003), pp. 1161–1169. DOI: `10.1179/026708303225004738` (cited on pages 80, 84, 105, 136).

[266] SAEKI Robotics. *SAEKI Robotics*. en. URL: `https://saeki.ch/` (visited on 05/13/2023) (cited on page 81).

[267] Stuart W. Churchill and Humbert H.S. Chu. 'Correlating equations for laminar and turbulent free convection from a vertical plate'. en. In: *International Journal of Heat and Mass Transfer* 18.11 (Nov. 1975), pp. 1323–1329. DOI: `10.1016/0017-9310(75)90243-4` (cited on page 87).

[268] Ana Anton et al. 'A 3D concrete printing prefabrication platform for bespoke columns'. en. In: *Automation in Construction* 122 (Feb. 2021), p. 103467. DOI: `10.1016/j.autcon.2020.103467` (cited on pages 91, 97).

[269] Massivit. *Massivit*. en-US. (accessed May 2023). 2022. URL: `https://www.massivit3d.com/` (visited on 05/13/2023) (cited on page 91).

[270] Extrudr. *PETG transparent - High Quality Filament*. URL: `https://www.extrudr.com/en/products/catalogue/petg-transparent_1803/` (visited on 11/05/2023) (cited on pages 93, 99, 141, 166, 171).

[271] Chad Duty and Lonnie Love. *Cincinnati Big Area Additive Manufacturing (BAAM)*. en. Tech. rep. ORNL/TM-2015/100, 1210140, CRADA/NFE-14-04957. Mar. 2015, ORNL/TM–2015/100, 1210140, CRADA/NFE–14–04957. DOI: `10.2172/1210140` (cited on pages 94, 105).

[272] Michael Wüthrich et al. 'Novel 4-Axis 3D Printing Process to Print Overhangs Without Support Material'. en. In: *Industrializing Additive Manufacturing*. Ed. by Mirko Meboldt and Christoph Klahn. Cham: Springer International Publishing, 2021, pp. 130–145. DOI: `10.1007/978-3-030-54334-1_10` (cited on page 95).

[273] Jordan R. Raney et al. 'Rotational 3D printing of damage-tolerant composites with programmable mechanics'. en. In: *Proceedings of the National Academy of Sciences* 115.6 (Feb. 2018), pp. 1198–1203. DOI: `10.1073/pnas.1715157115` (cited on page 95).

[274] Carlos M. S. Vicente et al. 'Large-format additive manufacturing of polymer extrusion-based deposition systems: review and applications'. en. In: *Progress in Additive Manufacturing* (Jan. 2023). DOI: `10.1007/s40964-023-00397-9` (cited on pages 103, 122).

[275] Leapfrog. *Leapfrog XceL | Large Scale Industrial 3D Printer*. en-US. URL: `https://www.lpfrg.com/products/leapfrog-xcel/` (visited on 10/23/2023) (cited on page 104).

[276] Prusa. *Max volumetric speed | Prusa Knowledge Base*. en. 2021. URL: `https://help.prusa3d.com/article/max-volumetric-speed_127176` (visited on 10/23/2023) (cited on pages 104, 139).

[277] E3D. *Product Specifications SuperVolcano*. 2018. URL: `https://e3d-online.zendesk.com/hc/en-us/article_attachments/360016249778` (visited on 10/23/2023) (cited on page 104).

[278] Huaying Wu, Xiao Wang, and Yuqiang Li. 'Study on Support-Free Printing of Large-Flow Material Extrusion Process'. en. In: *The International Journal of Advanced Manufacturing Technology* 126.1-2 (May 2023), pp. 603–613. DOI: `10.1007/s00170-023-11119-4` (cited on pages 104, 110).

[279] Matthias Leschok and Benjamin Dillenburger. 'Sustainable Thin-Shell 3D Printed Formwork for Concrete'. en. In: *Impact: Design With All Senses*. Ed. by Christoph Gengnagel et al. Cham: Springer International Publishing, 2020, pp. 487–501. DOI: `10.1007/978-3-030-29829-6_38` (cited on pages 104, 105).

[280] Yeo Jung Yoon et al. 'Development of Three-Nozzle Extrusion System for Conformal Multi-Resolution 3D Printing With a Robotic Manipulator'. en. In: *Volume 1: 39th Computers and Information in Engineering Conference*. Anaheim, California, USA: American Society of Mechanical Engineers, Aug. 2019, V001T02A024. DOI: `10.1115/DETC2019-98069` (cited on page 105).

[281] Prahar M. Bhatt et al. 'A Robotic Cell for Multi-Resolution Additive Manufacturing'. In: *2019 International Conference on Robotics and Automation (ICRA)*. ISSN: 2577-087X. May 2019, pp. 2800–2807. DOI: `10.1109/ICRA.2019.8793730` (cited on page 105).

[282] Donald G. Baird. 'Polymer Processing'. In: *Encyclopedia of Physical Science and Technology (Third Edition)*. Ed. by Robert A. Meyers. New York: Academic Press, Jan. 2003, pp. 611–643. DOI: `10.1016/B0-12-227410-5/00593-7` (cited on pages 105, 136).

[283] Fleischmann Philippe. *compas_rrc - COMPAS RRC*. URL: `https://compas-rrc.github.io/compas_rrc/latest/` (visited on 10/13/2023) (cited on page 107).

[284] Caroline A Schneider, Wayne S Rasband, and Kevin W Eliceiri. 'NIH Image to ImageJ: 25 years of image analysis'. en. In: *Nature Methods* 9.7 (July 2012), pp. 671–675. DOI: `10.1038/nmeth.2089` (cited on page 108).

[285] Center of International Environmental Law. *Fossils, Plastics, & Petrochemical Feedstocks*. Tech. rep. Washington DC: Center of International Environmental Law, 2017, p. 5. (Visited on 10/23/2009) (cited on page 122).

[286] Marirena Kladeftira et al. 'A Study on Bamboo, 3D Printed Joints, and Digitally Fabricated Building Components for Ultralight Architectures'. en. In: *ACADIA 2022*. Philadelphia, PA, Oct. 2022 (cited on page 123).

[287] Anton, Ana et al. 'Concrete Choreography Prefabrication of 3D Printed Columns'. en. In: *Fabricate 2020: Making Resilient Architecture*. Ed. by Jane Burry et al. UCL Press, Apr. 2020. DOI: `10.2307/j.ctv13xpsvw` (cited on page 125).

[288] Bratislav Svetozarevic et al. 'Dynamic photovoltaic building envelopes for adaptive energy and comfort management'. en. In: *Nature Energy* 4.8 (July 2019), pp. 671–682. DOI: `10.1038/s41560-019-0424-0` (cited on page 134).

[289] Kate Pelletier et al. 'The viability of double-skin façade systems in the 21st century: A systematic review and meta-analysis of the nexus of factors affecting ventilation and thermal performance, and building integration'. en. In: *Building and Environment* 228 (Jan. 2023), p. 109870. DOI: `10.1016/j.buildenv.2022.109870` (cited on page 134).

[290] Elena Catto Lucchino et al. 'Modelling and validation of a single-storey flexible double-skin façade system with a building energy simulation tool'. en. In: *Building and Environment* 226 (Dec. 2022), p. 109704. DOI: `10.1016/j.buildenv.2022.109704` (cited on page 135).

[291] Harshit K. Dave and J. Paulo Davim, eds. *Fused Deposition Modeling Based 3D Printing*. en. Materials Forming, Machining and Tribology. Cham: Springer International Publishing, 2021. (Visited on 01/17/2023) (cited on page 140).

[292] Michael Van den Eynde and Peter Van Puyvelde. '3D Printing of Poly(lactic acid)'. en. In: *Industrial Applications of Poly(lactic acid)*. Ed. by Maria Laura Di Lorenzo and René Androsch. Advances in Polymer Science. Cham: Springer International Publishing, 2018, pp. 139–158. DOI: `10.1007/12_2017_28` (cited on page 140).

[293] Ceresans. *Bioplastics Market Report: Industry Analysis, Forecast 2032*. en-US. Tech. rep. May 2023, p. 350. (Visited on 11/05/2023) (cited on page 140).

[294] Rafael Auras et al., eds. *Poly(Lactic Acid): Synthesis, Structures, Properties, Processing, and Applications*. en. 1st ed. Wiley, Sept. 2010 (cited on page 140).

[295] Li Na Ji. 'Study on Preparation Process and Properties of Polyethylene Terephthalate (PET)'. en. In: *Applied Mechanics and Materials* 312 (2013). Publisher: Trans Tech Publications Ltd, pp. 406–410. DOI: `10.4028/www.scientific.net/AMM.312.406` (cited on pages 141, 166).

[296] S. S. Kistler. 'Coherent Expanded Aerogels and Jellies'. en. In: *Nature* 127.3211 (May 1931). Number: 3211 Publisher: Nature Publishing Group, pp. 741–741. DOI: `10.1038/127741a0` (cited on page 141).

[297] Nicola Hüsing and Ulrich Schubert. 'Aerogels—Airy Materials: Chemistry, Structure, and Properties'. en. In: *Angewandte Chemie International Edition* 37.1-2 (1998), pp. 22–45. DOI: `10.1002/(SICI)1521-3773(19980202)37:1/2<22::AID-ANIE22>3.0.CO;2-I` (cited on page 141).

[298] Michal Ganobjak et al. 'Get the light & keep the warmth - A highly insulating, translucent aerogel glass brick for building envelopes'. In: *Journal of Building Engineering* 64 (Apr. 2023), p. 105600. DOI: `10.1016/j.jobe.2022.105600` (cited on page 141).

[299] Ruben Baetens, Bjørn Petter Jelle, and Arild Gustavsen. 'Aerogel insulation for building applications: A state-of-the-art review'. en. In: *Energy and Buildings* 43.4 (Apr. 2011), pp. 761–769. DOI: `10.1016/j.enbuild.2010.12.012` (cited on page 141).

[300] AGITEC. *Granular Aerogel Datasheet*. 2013 (cited on page 141).

[301] ASTM International. *ASTM C1113/C1113M-09(2019) - Standard Test Method for Thermal Conductivity of Refractories by Hot Wire*. Jan. 2019. DOI: `10.1520/C1113_C1113M-09R19`. URL: `https://www.techstreet.com/standards/astm-c1113-c1113m-09-2019?product_id=2032861` (cited on page 142).

[302] Rixing Hu, Aichun Ma, and Yahui Wang. 'Transient hot wire measures thermophysical properties of organic foam thermal insulation materials'. In: *Experimental Thermal and Fluid Science* 98 (Nov. 2018), pp. 674–682. DOI: `10.1016/j.expthermflusci.2018.07.005` (cited on page 142).

[303] Nancy Mathis. 'Transient thermal conductivity measurements: Comparison of destructive and nondestructive techniques'. In: *High Temperatures-High Pressures* 32 (Jan. 2000), pp. 321–327. DOI: `10.1068/htwu289` (cited on page 142).

[304] S M A Bekkouche et al. 'Thermal resistances of air in cavity walls and their effect upon the thermal insulation performance'. en. In: (2013) (cited on pages 142, 150).

[305] Bharath Seshadri et al. 'Three-dimensionally printed hierarchical sand structures for space heating applications'. In: *3D Printing and Additive Manufacturing* (2024). IN REVIEW (cited on pages 143, 149).

[306] G.P. Lydon and A. Schlueter. 'Small-scale experiments on the operational performance of a lightweight thermally active building system'. en. In: *Journal of Building Engineering* 78 (Nov. 2023), p. 107372. DOI: `10.1016/j.jobe.2023.107372` (cited on page 146).

[307] Christophe Preux and Iryna Malinouskaya. 'Thermal conductivity model function of porosity: review and fitting using experimental data'. en. In: *Oil & Gas Science and Technology – Revue d'IFP Energies nouvelles* 76 (2021), p. 66. DOI: `10.2516/ogst/2021047` (cited on page 149).

[308] Brian Friedrich and Kyosung Choo. *Thermal Simulation of Big Area Additive Manufacturing*. Nov. 2020 (cited on page 157).

[309] Chad E. Duty, Tom Drye, and Alan Franc. *Material Development for Tooling Applications Using Big Area Additive Manufacturing (BAAM)*. en. Tech. rep. ORNL/TM-2015/78, 1209207. Mar. 2015, ORNL/TM–2015/78, 1209207. DOI: `10.2172/1209207` (cited on page 164).

[310] Randall F. Lind et al. 'Enhanced additive manufacturing with a reciprocating platen'. US 9,884,444 B2. Feb. 2018 (cited on page 164).

[311] Min Lou et al. 'Effect of temperature on tensile properties of reinforced thermoplastic pipes'. In: *Composite Structures* 241 (June 2020), p. 112119. DOI: `10.1016/j.compstruct.2020.112119` (cited on page 172).

[312] Patrick T Summers et al. 'Overview of aluminum alloy mechanical properties during and after fires'. en. In: *Fire Science Reviews* 4.1 (Dec. 2015), p. 3. DOI: `10.1186/s40038-015-0007-5` (cited on page 191).

[313] Haroon Siddique. 'Grenfell Tower fire: police considering manslaughter charges'. en-GB. In: *The Guardian* (June 2017). (Visited on 01/18/2024) (cited on page 193).

[314] Joris Burger et al. 'Design and Fabrication of a Non-standard, Structural Concrete Column Using Eggshell: Ultra-Thin, 3D Printed Formwork'. en. In: *Second RILEM International Conference on Concrete and Digital Fabrication*. Ed. by Freek P. Bos et al. RILEM Bookseries. Cham: Springer International Publishing, 2020, pp. 1104–1115. DOI: `10.1007/978-3-030-49916-7_105` (cited on page 206).

[315] Matthias Leschok and Benjamin Dillenburger. 'Dissolvable 3DP Formwork Water-Dissolvable 3D Printed Thin-Shell Formwork for Complex Concrete Components'. en. In: *Ubiquity and Autonomy*. Association for Computer Aided Design in Architecture (ACADIA). Austin, Texas, US., 2019, pp. 188–197 (cited on page 206).

List of Figures

1.1 Predicted changed in climate zones due to climate change. (a) shows the present-day map (1980–2016) and (b) the future map (2071–2100). Figure adapted from ”Present and future Köppen-Geiger climate classification maps at 1-km resolution" [1]. 4
1.2 (1) Construction material procurement. Driven by carbon-intensive manufacturing processes for materials such as steel, concrete, aluminum, copper, and plastic. (2) On-site construction. Driven by fuel consumed by heavy construction vehicles and other emissions. (3) Operations. Driven by heating and water utilities and electricity consumption. (4) End of life. Driven by demolition, waste processing; can gain credits for reuse and recycling [2]. 5
1.3 Polyvalent wall 1981, Mike Davies and Richard Rogers [5] 6
1.4 Dymaxion Dwelling model, with Buckminster Fuller. 7
1.5 Monsanto House of the Future, 1957. 7
1.6 Fuji Group pavilion, osaka, 1970, Yutaka Murata. © yutaka murata. © photo courtesy of Osaka prefectural government. 7
1.7 Cellophone advertisement 1950s. "Better things for better living... though chemistry", Du Pont. 8
1.8 Dixie Cup advertisement, 1954. Single-use paper cups with polyethylene coating. 8
1.9 Plastic pollution in the ocean and mountains. Source: www.circular-solutions.eu, unsplash.com 9
1.10 Average lifespan of plastic elements per sector. Source: OECD Statista 2023. 10
1.11 Plastic consumption per sector. Building and construction is the second largest customer of plastic products. Source: plasticeurope.com 10
1.12 Example of large-scale thermoplastic extrusion in construction, 3D printed building envelope, interior wall elements , “urban cabin” from DUS architects , concrete formwork for facades, oneC1TY Pavilion Branch Technologies. 11
1.13 Diagram: From discrete building elements towards mono-material multi-functional elements, designed at millimetre scale. 12
1.14 Interdependencies in the methodology. 14
1.15 NCCR Facade research stream, internal and external collaborators and their function. 16

2.1 Conceptual diagram of manuscript strucutre, investigating different aspects of 3DP facades. . . 24
2.2 Bibliometric analysis on reviewed literature. a) Most sidecited journals: the reviewed articles cover a variety of disciplines from construction, to manufacturing up to specific material system (concrete and polymers). b) Publication year: the majority of reviewed articles were published in the last four years and represent a growing research interest. 27
2.3 DFAM methodologies for 3D printed facades. Topology Optimization, Infill Design, Toolpath Planning, and Performance informed workflows. 28

3.1 **a.** Robotic 3D printing setup, comprising a CEAD E25 extruder mounted on an ABB IRB4600. **b.** Close-up of the polymer printing process: PETG printed with 2.5mm layer height and 6mm layer width. 61
3.2 **a.** Studies on continuous print paths. Different arrangements of infill lines allow for differentiation within the 3DP component. **b.** Close-up of self-intersecting print path, crossing within the same layer forces the material to dwell and form a knot. 61
3.3 Boundary conditions for the numerical models. **a.** 3D model of sample R1 for the FE simulation. From this, 2D representation are derived based on the cross-section **b.** and the longitudinal section 62
3.4 3DP specimens for the experimental campaign. **a.** R1, one cavity approx. 15cm. Weight: 8.8kg. **b.** R2, two cavities approx. 7.5cm. Weight: 10.5kg. **c.** R3, three cavities approx. 5cm. Weight: 12.5kg. 62

3.5 **a.** Schematics of the hot-box setup. **b.** Front view of the experimental chamber with testing specimen. **c.** Example of RTD and heat-flux sensor placement on testing specimen. **d.** Thermographic images of a tested sample, guiding the sensors placement. 63
3.6 **a,b.** Schematics showing different testing directions for the 3DP samples. **c.** Schematics of thermal sensor placement, measuring the sample's surface temperatures at the connection of contour and infill and at the middle of an air cavity. 64
3.7 Recorded data during the 72h experiments. **a.** Measured temperatures inside the hot-box (red) and room temperature (blue); **b.** Measured heat flux (green) and calculated effective thermal conductivity (yellow). 65
3.8 Overview of experimental results: effective thermal conductivity for the six tested samples. Error bars represent the uncertainties of the measurements. 66
3.9 FE simulation results for sample R1. The joint effects of radiative, convective and conductive heat transfer influence the thermal stratification in the sample. 67
3.10 Comparison of results for experiments, 3D and 2D simulations. The error bars represent the measurement uncertainties. 67
3.11 Comparison of thermal performance of 3DP facade and traditional facade components. 68

4.1 Summary of printing strategies investigated. 76
4.2 Sections of 3D printed single wall samples. (a) regular 3DP using a pellet extruder (b) HC3DP with a 6mm bead width and 5.5mm layer height. (c) HC3DP 24mm bead width and 18mm layer height. Regular ME results in a disco-rectangular shape, HC3DP in sagging beads. 77
4.3 Schematic hardware setup for HC3DP. (a), HC3DP nozzle. (b), pellet extruder. (c), Robot, or gantry system. (d), the control unit for printing, including feedback processing. (e) robot controller. Right: Close-up of the closed-loop hollow core extrusion system and air inlet. 80
4.4 Different nozzles types, prototyped using 3DP of aluminum. 83
4.5 Sample preparation for 3PT bending tests. 83
4.6 (a) Initial experiments of HC3DP without air support, resulting in non-inflated beads. Only two out of 13 beads remain non-solid. (b-g) Series of test prints adjusting printing parameters to increase print quality. 84
4.7 Typical printing errors of HC3DP. (a) Sharp corners can result in overinflation of the extruded bead. (b) Crossing of printpaths often results in a collapsed bead. 85
4.8 Comparison of HC3DP, regular 3DP, and a PETG sheet of similar size. The material savings of HC compared to TE3DP are over 50%. Samples size 200×200×6mm. Measured results and normalized values for a plate of 200×200×6mm. 85
4.9 Printed samples 40cm diameter, 20cm height. (a) Regular large-scale 3D printing, buildup rate 5.97mm/min, resulting in print failure. (b) HC3DP, buildup-rate 9.19mm/min. Thermal images after 1min, 5min and 20min cooldown time. (c) Cut sample of collapsed regular ME due to overheating. 86
4.10 Qualitative temperature evolution for full walled filaments and HC (0.6min with 1mm, then 3mm.) 88
4.11 Comparison between experimental results. Model ME b=6mm, Model HC b=1mm for 0.6min, then b=3mm. Right: Diagram of equivalent wall thickness. 88
4.12 HC3DP nozzle with a 24mm orifice and a 2mm wall thickness. (b): Extruded PETG bead. (c): 3D printed sample, cut, with a hand to represent scale and transparency. 89
4.13 HC3DP cylinders. (a) PETG, (b) PP needed an increased printing speed to maintain layer adhesion, the print speed was increased from 6 mm/s to 10 mm/s. Lower row: 40cm diameter samples printed using different materials. (c) PETG, (d) PLA, (e) COC, and (f) PP. 89
4.14 Series of 40cm diameter cylinders printed at different layer heights. The final demonstrator (right) is 2 meters tall, and the print time is 1:54 hours, weight 10.3kg. 91
4.15 Differentiated air pressure per print point. Difference between a ME and HC toolpath. The increase in speed and reduction in air pressure and the distance (d) to the corner is influenced by the angle α. 92

4.16 (a): overinflation due to constant internal air pressure. (b) successful print due to active control of air pressure. Red indication overinflated bead. Yellow indicates the twisting of the bead due to constant tool orientation. 92
4.17 Results of the bending tests with different bead cross sections. 93
4.18 Testing setup. Close up of ductile failure behaviour. Thinning out before breaking. 93
4.19 Rectangular and elliptical cross section assumption. Actual section of 3DP specimen, and high-resolution 2D scan. The shape of the cross section can be described as non-symmetrical disco rectangular, with a sagging behaviour in the layer build up direction. 99

5.1 Large-scale HC3DP samples. Layer height 18mm, layer width 24mm. 104
5.2 The 3D printing setup includes ABB IRB6700, a pellet extruder, a control cabinet, and a material handling system. Right: Close-up of the printing process. 106
5.3 Closeup of a section, layer height 24 and diagram of measurement points. C: Center point, determined by ImageJ. H(c): height at point C. W(c): width at point C. W(max): maximum width, determined by ImageJ bounding box. R(x): wall thickness at point X. 109
5.4 Different nozzles types, prototyped using 3DP of aluminum. 109
5.5 Bespoke toolpath with strong undulations in XY direction. Red represents bridges with a distance of 60mm, blue indicates cantilevering areas. 110
5.6 A) bespoke toolpath design for large-scale elements, non-planar 3D printing with increasing amplitude in Z direction. B) Diagram for non-planar printing with fixed tool head orientation. . 111
5.7 Sections of specimen printed with the same nozzle, but increased layer height. 111
5.8 Left 16mm layer height, right 32mm layer height. 112
5.9 2D scan of the bead cross sections, printed with static tool orientation. Left and right wall printed with die at 0 respectively 180 degree. (a) Cross-hair die, different deformations inside the bead, probably caused by unequal air pressure distribution inside the individual air pockets. (b) Tube in tube die, non-symmetrical nozzle geometry causes different sections. 112
5.10 Section of 3D printed samples. A) Quad. B) Crosshair. C) Tube in tube. 112
5.11 Visualization of the material distribution in the HC3DP beads, the color gradient displays the distance from a pixel to the closest border. 113
5.12 3D printed specimen overlaid with actual toolpath. 113
5.13 Large-scale specimen with light source in background. 113
5.14 Bespoke toolpath design for large-scale elements. 114
5.15 Sagging behavior of HC3DP during bridging. 114
5.16 Non-planar HC3DP, the print failed after a height of 250mm. B) Non-planar HC3DP, printed to the end, as the undulations in Z directions are less strong. 114
5.17 Post inflation diagram. A) In ME the bead is squeezed down during the printing process and receives its typical rectangular shape with half circular ends. The extruded beads stay in place during the cool down process. B) In HC3DP the bead can be squeezed down during the printing process, but due to the positive air pressure within the bead, might inflate and stretch the bead after the extruder continues to print. 115
5.18 Close up of the bridging sample. Sample flipped. 116

6.1 Protoplasto exhibition. Credit: Andrei Jipa, DBT. 121
6.2 Transition between column and roof structure. Photo: Andrei Jipa, DBT. 123
6.3 Assembly scheme. Photo: Matthias Leschok. 124
6.4 Prototype of concrete feet, SCC cast into HC3DP formwork. Photo: Matthias Leschok, DBT. . . . 124
6.5 A series of design explorations conducted by the MAS DFAB students 2023. Filament based HC extrusion with a diameter of 10mm. Photo: Fen Chan, DBT. 125
6.6 Close-up of HC3DP process. Diameter of extrusion 24mm. Right: Section of HC3DP element. Photo: Girts Apskalns, girtsapskalns.com. Matthias Leschok, DBT. 125

6.7 All columns were 3D printed at the fabrication hall of SAEKI Robotics, using one ABB IRB 6700 industrial robot. Photo: Girts Apskalns, girtsapskalns.com. 126
6.8 Module-module connection details for support free assembly. Photo: Marirena Kladeftira, DBT. 126
6.9 Computational design framework. Photo: Matthias Leschok. 126
6.10 Assembly sequence. Photo: Nik Eftekhar. 127
6.11 Supportfree assembly, last element being placed. Photo: Girts Apskalns, girtsapskalns.com. . . 127
6.12 Top view of one mushroom column. Photo: Marirena Kladeftira, DBT. 127
6.13 Installation view showing the 2.2m tall HC3DP chandeliers surrounding the pavilion display. . 128
6.14 2.2m tall HC3DP chandeliers suspended from the ceiling are framing the exhibition. Photo: Girts Apskalns, girtsapskalns.com. 128
6.15 A series of 2.2m tall HC3DP elements aligned and alight. Photo: Nijat Mahamaliyev 128

7.1 Overview of different aspects investigated, part geomerty, bead cross sectiond, and materials. . 133
7.2 Approaches to improve thermal insulation: (a) geometry (b) bead cross-section and (c) material. For desktop 3DP only approach can be used; for HC3DP option a) b) and c) are possible. 138
7.3 Fig. 2. Different types of ME, scale relative to each other. (a) desktop 3DP. (b) Pellet Extrusion, width 6mm height 2.5. (c) HC3DP width 6mm, 5.5mm height, (d) HC3DP, 24mm width, 19mm height. (e) HC3DP with internal subdivision, 24mm width, 19mm height. 139
7.4 Different types of infill typology. A) Cubic. B) Gyroid. C) Random. 141
7.5 Left: Estimated heat transfer in closed air cavity bounded by ordinary material. Graphic from Bekkouche et al., 2013 [304]. Right: Transient Hot Wire Method, testing setup. 142
7.6 Different cross-sections tested. a) HC3DP with the nozzle o6w1, resulting in a 6mm layer width and a 5.8mm layer height. Wall thickness 1mm. b) HC3DP with the nozzle o24w1, resulting in a 24mm layer width and a 19mm layer height, at a 1mm wall thickness. c) HC3DP with the o24w1Quad nozzles, resulting in a 24mm layer width and a 19mm layer height, at a 1mm wall thickness. . . 143
7.7 Fig. 6. Different types of samples presented and discussed. (a) desktop 3DP cylinders. 100x100x50mm (b) High resolution HC3DP, 6mm layer width, 5.5mm layer height. (c) Low resolution HC3DP, sample size 500x500x150mm. Layer width 24mm, 19mm layer height, two different cross sections, empty and cross. (d) Low resolution HC3DP, sample size 500x500x50mm no infill. 24mm layer width, 19mm layer height, printed in PETG and PP. (e) Low resolution HC3DP with one continuous air pocket, 24mm layer width, 19mm layer height, tested empty and filled with aerogel. 144
7.8 Production steps and design of the HC3DP element filled with aerogel. A) Close-up of the specimen, focus on non-collapsed tight corners and opening to insert aerogel. 146
7.9 Hotbox testing setup. A) Schematics of the hot-box setup. B) installation of HC3DP sample, filled with aerogel. C) Door installed with sensors in place. 147
7.10 All 3D printed samples. Upper left, 10% infill to lower right 90%. Left cubic, middle gyroid, and right random infill. 149
7.11 reports the measured effective thermal conductivities for the 3DP samples. 150
7.12 Printed specimen. (a) ME-6-150 (b) HC-6-O-150 (c) HC-24-O-150. (d) HC-24-X-50-PETG (e) HC-24-O-75-AE (f) HC-24-O-75-AF. 151
7.13 Comparison matrix for investigated methods against off-the-shelf facade solutions. 152
7.14 Comparison of print time, production costs, and achieved u-value for 1m2 of 3DPF. 153
7.15 Comparison matrix for all tested samples, calculated for 1m2 of 3DPF. Weight, u-value and printing time provide insights about the production viability of a 3DF. 154
A.1 Thermal cool down behavior of regular ME (6x2.5mm) orange, and HC3D (6 diameter, 1mm wall thickness) blue. The violet horizontal lines describe the optimal printing time window. Lower boundary represents the glass transition temperature for the polymer, and the upper is estimated to be 391K 158
B.1 Overview of the specimen 3D printed through ME and tested with calorimetric experiment in [45]. The first sample from the left (ME-2-R1-150) has the same dimensions and infill geometry as HC-6-O-150, HC-24-O-150, and HC-24-X-150 and is used for benchmarking. 159

8.1 Overview of mechanical testing campaigns on ME and HC3DP specimens. 163
8.2 Different cross-sections tested. (a) ME 6mm width, 2.5mm height. (b) HC3DP 6mm width, 5.5mm height. (c) HC3DP 24mm width, 18mm height. (d) H3CDP 24mm width, 18mm height with internal reinforcement. 166
8.3 Four different types of mechanical testing performed in the manuscript. a) tensile testing with regular ME 3DP specimens. b) 3PT bending tests with ME and HC3DP at high resolution. d) 3PT bending test with HC3DP specimen featuring large cross-sections. d) 4PT bending test with large-scale beams, both ME and HC3DP. 167
8.4 (a) Diagram of thermal boundary conditions. (b) Results of thermal analysis using Flixo.. 168
8.5 HC3DP specimen with a wall-thickness of 1mm and a reinforcement cross in the centre of the bead. 169
8.6 Printed specimen displayed in printing orientation a) ME, 6mm width shell and infill. b) ME, 6mm width shell, 4mm infill. c) HC3DP, 6mm width. d) HC3DP, 24mm width. 169
8.7 a) Section of regular ME bead arrangement. b) Diagram of section with layer-shift. c) Close-up of printed element showing the connection between shell and infill lines, offset by half a layer against each other. 170
8.8 Printed specimen displayed in printing orientation a) HC3DP, 24mm width, 150mm depth, updstanding. b) HC3DP, 24mm width, 75mm depth, upstanding. c) HC3DP, 24mm width, 50mm depth, upstanding. d) HC3DP, 24mm width, 150mm depth, shifted layers. e) HC3DP, 24mm width, 75mm depth. f) HC3DP, 24mm width, 50mm depth. 170
8.9 Left: Diagram of testing setup with labels for calculating the bending resistance. Right: Assumptions for wind load and maximum span calculation based on the moment line. 171
8.10 (a) Specimen after tensile testing. (b) Results of tensile testing, color-coded. Yellow: spring. Blue: winter. Red: summer. 172
8.11 (a) Specimen with printing lines in parallel to tensile force. (b) Specimen with printing lines perpendicular to the tensile force. 172
8.12 Results of 3PT bending tests, (a) HC3DP (b) ME. 173
8.13 a-b) Testing procedure of ME specimen. c-d) HC3DP specimen. 174
8.14 a) HC3DP specimen during 3PT testing. b) Close-up of constriction and whitening of the lower (tension) zone. 174
8.15 Results of 3PT bending tests. 175
8.16 Results of 4PT bending tests. Green, regular ME 3DP with 6mm width. Red HC3DP with 6 and 24mm width. Blue, HC3DP 24mm with reduced specimen height in testing direction. Yellow, specimen fabricated in "upstanding" position. 175
8.17 Different failure mode, depending on the chosen ME method and scale. a) ME, 6mm width, clean break tangential to the printing direction. Max. F. 5620N. b) HC3DP, 6mm width, the element buckles and moves back into its original position. Max. F. 2350N. c) HC3DP, 24mm width, elements shatters "catastrophic failure" after reaching a max. F. of 45800N. 175
8.18 Failure mode of upstanding printed specimen. The failure does not occur as expected in between the layers, as known from small scale ME tensile testing. 176
8.19 Results of the height estimation for a 3DP facade, color coded. Green: regular ME. Red: HC3DP at 6 or 24mm width and a structural height of 150mm. Blue: HC3DP at a width of 24mm and reduced structural heights. Yellow: HC3DP at a width of 24mm, printed upstanding. 177

A.1 3D printed element installed in wooden frame. Element size 500x500x150mm. 199
A.2 HC3DP specimen. (a) HC-6-O-150, panel with 150mm thickness and identical toolpath to R1. (b) HC-24-O/X-150, panel with 150mm thickness, printed with tubular section and with internal reinforcement. Wall thickness HC-24-O-150 2mm, HC-24-X-150 1mm. (c) HC-24-x-50, panel with 50mm thickness, no air cavity. (d) HC-24-O-AE/AF, panel with 150mm thickness, empty and filled with aerogel. 199
A.3 Testing facility with specimen installed. 200

A.4 ME specimens with 150mm thickness. (a) R1 with ones cavity, depth 150mm .(b) R2 with two cavities, depth 75mm each.(c) R3 with three cavities, depth 50mm each. 200
A.5 Left: measured sound reduction for all ME samples. Right: measure sound reduction for ME and HC specimen with 6mm bead width. 201
A.6 Left: measured sound reduction for 24mm bead width, HC3DP. Right: measure sound reduction for aerogel filled and empty specimen. 201
A.7 Comparison of all tested specimen (ME and HC3DP) in relation to the sound insulation range of tripple glazed windows. 202
A.8 The graph displays the sound insulation in relation to the weight per square meter. 202

B.1 UR-5 co-bot with a filament-based HC3DP system attachted. 203
B.2 documents an array of vertical elements that interlock through their geometrical articulation and creates a wall-like elements. These single elements are approx. 1.2 m high. 203
B.3 Studies on different print patterns evoked through direct toolpath-planing. Incorporating pausing, differentiated speeds and extruder velocities. 204
B.4 Studies on cantilvering structures and extreme overhangs. 204
C.2 Close-up during demolding of HC3DP formwork. 205

C.1 2.1 m tall concrete column cast into HC3DP formwork. 205
C.3 Close-up of sharp concrete details. 206
C.4 Testing facility with specimen installed. 206
C.5 Close-up of the capital. Undulating HC3DP resulting in a concrete texture with dramatic shadow effects. 207

List of Tables

2.1 Thermoplastic 3DP for facade application. 33
2.2 Clay-based 3DP for facade application. 38
2.3 Concrete 3DP for facade application. 41
2.4 Metal 3DP for facade application. 45
2.5 Alternative 3DP processes for facade application. 48

4.1 Comparison of different nozzle geometries and wall thicknesses. Material savings are calculated in comparison to a full bead. 81
4.2 Comparison of different nozzles, showing area of extruded plastic and internal voids [mm2]. . 82
4.3 Maximum extrusion rate of traditional ME and HC3DP, assuming a symmetric disco rectangular shape. Ambient temperature 10.5°C. 86
4.4 Summary of printing parameters used during the material testing. For all experiments, two 24v 60mm fans with a flow rate of 40m3/h are used for cooling. 90
4.5 Comparison of extrusion rate [mm3/s] for different printing setups. Regular ME, HC3DP, BigRep pro.2 3D printer. The values represent a single outline print. 90

5.1 Comparison of different nozzles, showing area of extruded plastic and internal voids [mm2]. The nozzles are sorted by increasing the extrusion footprint. 109
5.2 Summary of changing printing resolution. All parameters are kept constant, only the layer height and pressure increase. 112

7.1 Die geometries and their specifications. 144

7.2 Summary of all samples. See figure 6 7.7 for visual reference. 145
7.3 Maximum print speed and minimal layer time on the cross sections printed during this research and a maximum extrusion rate of 1500 mm3/s. 148
7.4 Comparison of different ME methods for facade applications. 152

8.1 Comparison of deflection, measured and estimated values. 173

9.1 Summary table stating the performative aspects of 3DP facades, based on the geometries tested. Please refer to PAPER F for visual representation of the samples. Values are either provided by sample type or m^2 189

CURRICULUM VITAE

Curriculum Vitae

Personal Data

Name	Matthias Leschok	**Telephone**	+41 77 999 45 91
Day of Birth	12.01.1989	**Email**	leschok@arch.ethz.ch
Place of Birth	Mannheim		m.leschok@icloud.com

Education

Doctoral Studies **2018 - 2024**
Thesis: Hollow-Core-3D-Printing for Facades
Eidgenössische Technische Hochschule Zürich

Master of Advanced Studies in Architecture and Digital Fabrication **2016 - 2017**
Thesis: Living Column, 3DP Formwork for Growth-based Fabrication
Eidgenössische Technische Hochschule Zürich

Diploma in Architecture **2008 - 2015**
Grade: 1.0 with distinction.
Graduated top of the class year 2015, top 1%.
Karlsruhe Institute of Technology, Germany

Abitur - German School Examination Certificate **2000 - 2008**
Grade 2.0 - good - (600/840 pt) - top 10%
Karloninen Gymnasium Frankenthal, Germany.

Work Experience

Co-Founder and COO of SAEKI Robotics **2021 - present**
ETH Spin-off

Doctoral Researcher **2018 - 2024**
National Center of Competence in Digital Fabrication (NCCR Dfab)
Digital Building Technologies
Supervisor Prof. Dillenburger

Training Manager and Consultant for German RepRap GmbH **2013 - 2020**
Munich based 3D printing company
Germany

2017 - 2018

Research Assistant
Digital Building Technologies
Supervisor Prof. Dillenburger

2016 - 2017

Student Assistant
Digital Building Technologies
Supervisor Prof. Dillenburger

2015 - 2016

Head of the digital workshop
Faculty of Architecture, KIT
Karlsruhe, Germany

2015 - 2016

Freelance Architect
TAFKAL
Karlsruhe, Germany

2012 - 2015

Student Assistant
Building Lifecycle Management (BLM)
Faculty of Architecture, KIT
Karlsruhe, Germany

2011 - 2012

Internship Architecture
Buchner Bruendler Architects, BBArch
Basel, Switzerland

Patents

2022

Arrangement for Additive Manufacturing of a Structure
EP22201353.4
Dillenburger B., Leschok M.

2019

Computer-aided process for dimensioning a formwork arrangement to be manufactured additively as well as a device for carrying out the process
DE102019216341A1
Leschok M., Dillenburger B., Ismaila I.

Teaching

2023

Protoplasto
MAS in Digital Fabrication
Tutors: Leschok M., Kladeftira M., Eftekhar N.

2022

Computational Design II
2nd year Bachelor course
ETH Zurich

Computational Design I **2021**
1st year Bachelor course
ETH Zurich

Mini Facade **2020**
MAS in Digital Fabrication
Tutors: Leschok M., Cheibas I., Clemente R., Piccioni V.

PerSkin, Add-On 3D-Printing on Fabric **2020**
MAS in Digital Fabrication
Student: Sallin E.
Tutor: Leschok M.

Digital Bamboo **2020**
MAS in Digital Fabrication
Tutor: Kladeftira M., Leschok M., Skevaki E., Tanadini D.

Teaching courses on 3D printing for German RepRap **2013-2020**
Courses for industrial and reserach institutions
Fraunhofer Institut, FH Rosenheim, Leica, Toyota Motorsport, Adidas, Airbus, etc.

Large-Scale 3D Printing for Functionally-Graded Facade **2019**
MAS in Digital Fabrication
Students: Taseva Y., Eftekhar N.
Tutors: Leschok M. , Kwon H.

Fast From Work **2019**
Summer School: DBT ETH Zurich, GSAPP Columbia.
Tutors: Leschok M. , Kwon H., Anton A.

Non-Regular Freedom **2018**
MAS in Digital Fabrication
Student: Enz A. Tutors: Kladeftira M., Leschok M.

Frame Moebel **2018**
MAS in Digital Fabrication
Tutors: Kladeftira M., Leschok M.

Smart FDM Formwork **2017**
MAS in Digital Fabrication
Tutors: Jipa A., Leschok M.

Distinction and Awards

IBAM InnoBooster: Enhancing thermal insulation of building components through custom nozzle design for tubular 3D printing **2024**
20k CHF, with DBT ETH Zurich

2023
Feasibility Study: Coating free 3D Printed Formwork
20k CHF, DBT, ETH Zurich

2022
Venture Kick - Startup Competition - Stage 2
40k CHF, with SAEKI Robotics

2021
Venture Kick - Startup Competition - Stage 1
10k CHF, with SAEKI Robotics

2021
IBAM InnoBooster
10k CHF, with DBT ETH Zurich

2019
ACADIA Student Tavel Scholarship
Austin, Texas

2016
Award „Sparkassenumweltpreis“ for Diploma thesis “Myzel, responsive Architecture”
10K Euro
Karlsruhe, Germany

2016
Finalist „3D Pioneers Challenge“
Design-Competition for additive manufacturing
Erfurt, Germany

2015
Ruth and Erich Rossmann Foundation
scholarship for postgraduate research studies
Karlsruhe, Germany

2014
Goldbeck Scholarship
grant for undergraduate studies
Goldbeck, Germany

2014
Research Student Award
grant for academic performance
Karlsruhe, Germany

Exhibitions

2023
Protoplasto
Futurama, Lupfig
Switzerland

2021
Digital Bamboo
Venice Biennale
Italy

2020
Digital Bamboo
Zurich center for architecture
Switzerland

2017
Liquid Metal
SUSAS Shanghai Urban Space Art Season 2017
Shanghai

2016
Mycelium Chair
3D Pioneers Challenge, Rapid Tech + FabCon 3.D
Erfurt, Germany

Publications

2024 Leschok, Matthias, Marirena Kladeftira, Yen-Fen Chan, and Benjamin Dillenburger. 2024. “Large-Scale Hollow-Core 3D Printing: Variable Cross-Section and Printing Features for Lightweight Plastic Elements.” 3D Printing and Additive Manufacturing, April, 3dp.2023.0287. `https://doi.org/10.1089/3dp.2023.0287`

2024 Leschok, Matthias, Marirena Kladeftira, Nik Eftekhar, and Benjamin Dillenburger. 2024. “Prōtóplasto A Discrete Roof-Column System With Hollow-Core 3D Printing And Bespoke Space Frames.” In Fabricate 2024: Creating Resourceful Futures, edited by Phil Ayres, Mette Ramsgaard Thomsen, Bob Sheil, and Marilena Skavara. UCL Press. `https://doi.org/10.2307/jj.11374766.19`.

2023 Leschok, Matthias, Lex Reiter, and Benjamin Dillenburger. “Large-Scale Hollow-Core 3D Printing (HC3DP): A Polymer 3D Printing Technology for Large-Scale Ultralightweight Components.” Additive Manufacturing 78 (September 25, 2023): 103874. `https://doi.org/10.1016/j.addma.2023.103874`.

2023 Leschok, Matthias, Ina Cheibas, Valeria Piccioni, Bharath Seshadri, Arno Schlüter, Fabio Gramazio, Matthias Kohler, and Benjamin Dillenburger. “3D Printing Facades: Design, Fabrication, and Assessment Methods.” Automation in Construction 152 (August 2023): 104918. `https://doi.org/10.1016/j.autcon.2023.104918`.

2023 Piccioni, Valeria, Matthias Leschok, Lars O. Grobe, Stephen Wasilwski, Bharath Seshadri, Illias Hischier, and Arno Schlüter. “Tuning the Solar Performance of Building Facades through Polymer 3D Printing: Toward Bespoke Thermo-Optical Properties.” Advanced Materials Technologies 8, no. 6 (March 2023): 2201200. `https://doi.org/10.1002/admt.202201200`.

2023 Piccioni, Valeria, Matthias Leschok, Esther Borkowski, Illias Hischier, and Arno Schlueter. “Challenges in Modelling Thermo-Optical Performance of 3D-Printed Facades: A Cross-Domain Review.” Application/pdf, September 2023. `https://doi.org/10.3929/ETHZ-B-000635325`.

2023 Piccioni, V, M Leschok, G Lydon, I Cheibas, I Hischier, B Dillenburger, M Kohler, F Gramazio, and A Schlueter. “Printing Thermal Performance: An Experimental Exploration of 3DP Polymers for Facade Applications.” IOP Conference Series: Earth and Environmental Science 1196, no. 1 (June 1, 2023): 012063. `https://doi.org/10.1088/1755-1315/1196/1/012063`.

2022 Leschok, Matthias, and Benjamin Dillenburger. “3D Printed Formwork for Mycelium Bound Composites.” In Hybrids & Haecceities. University of Pennsylvania, Philadelphia, PA, 2022.

2022 Kladeftira, Marirena, Matthias Leschok, Eleni Skevaki, Davide Tanadini, Patrick Ole Ohlbrock, Pierluigi DÁcunto, and Benjamin Dillenburger. “A

Study on Bamboo, 3D Printed Joints, and Digitally Fabricated Building Components for Ultralight Architectures," 2022.

2022 Tanadini, Davide, Patrick Ole Ohlbrock, Marirena Kladeftira, Matthias Leschok, Eleni Skevaki, Benjamin Dillenburger, and Pierluigi DÁcunto, "Exploring the Potential of Equilibrium-Based Methods in Additive Manufacturing: The Digital Bamboo Pavilion," 2022.

2021 Seshadri, Bharath, Ina Cheibas, Matthias Leschok, Valeria Piccioni, Illias Hischier, and Arno Schlüter. "Parametric Design of an Additively Manufactured Building Facade for Bespoke Response to Solar Radiation." Journal of Physics: Conference Series 2042, no. 1 (November 1, 2021): 012180. https://doi.org/10.1088/1742-6596/2042/1/012180.

2020 Kladeftira, M, M Leschok, E Skevaki, and B Dillenburger. "Redefining Polyhedral Space Through 3D Printing." In Advances in Architectural Geometry 2020. Paris, 2020.

2020 Taseva, Yoana, Nik Eftekhar, Hyunchul Kwon, Matthias Leschok, and Benjamin Dillenburger. "Large-Scale 3D Printing for Functionally-Graded Facade." In *RE: Anthropocene, Proceedings of the 25th International Conference of the Association for Computer-Aided Architectural Design Research in Asia (CAADRIA) 2020*, edited by I Holzer, W Nakapan, A Globa, and I Koh, 183–92. Hong Kong, 2020. http://papers.cumincad.org/cgi-bin/works/paper/caadria2020_332.

2020 Leschok, Matthias, and Benjamin Dillenburger. "Sustainable Thin-Shell 3D Printed Formwork for Concrete." In *Impact: Design With All Senses*, edited by Christoph Gengnagel, Olivier Baverel, Jane Burry, Mette Ramsgaard Thomsen, and Stefan Weinzierl, 487–501. Cham: Springer International Publishing, 2020. https://doi.org/10.1007/978-3-030-29829-6_38.

2019 Leschok, Matthias, and Benjamin Dillenburger. "Dissolvable 3DP Formwork Water-Dissolvable 3D Printed Thin-Shell Formwork for Complex Concrete Components." In *Ubiquity and Autonomy*, 188–97. Association for Computer Aided Design in Architecture (ACADIA). Austin, Texas, US., 2019.

2019 Jipa, Andrei, Federico Giacomarra, Rena Giesecke, Georgia Chousou, Matteo Pacher, Benjamin Dillenburger, Matteo Lomaglio, and Matthias Leschok. "3D-Printed Formwork for Bespoke Concrete Stairs: From Computational Design to Digital Fabrication." In *Proceedings of the ACM Symposium on Computational Fabrication*, 1–12. Pittsburgh Pennsylvania: ACM, 2019. https://doi.org/10.1145/3328939.3329003.

2018 Jipa, Andrei, Mania Aghaei Meibodi, Rena Giesecke, Demetris Shammas, Matthias Leschok, Mathias Bernhard, and Benjamin Dillenburger. "3D-Printed Formwork for Prefabricated Concrete Slabs." November 28, 2018, 9 p. https://doi.org/10.3929/ETHZ-B-000507651.

2018 Meibodi, Mania Aghaei, Andrei Jipa, Rena Giesecke, Demetris Shammas, Mathias Bernhard, Matthias Leschok, Konrad Graser, and Benjamin Dillenburger. "Smart Slab. Computational Design and Digital Fabrication

of a Lightweight Concrete Slab," 434–43. Mexico City, Mexico, 2018. https://doi.org/10.52842/conf.acadia.2018.434.